A study of nitrogen isotopic systematics in lunar soils and breccias

Thesis

A STUDY OF NITROGEN ISOTOPIC SYSTEMATICS IN LUNAR SOILS AND BRECCIAS

A thesis submitted for the degree of

Doctor of Philosophy

by

Debra Brilliant B.Sc Hons (Hatfield, 1991)

January 1999,

Planetary Science Research Institute,

The Open University

Abstract

A variety of lunar soils (bulk soils, grain size fractions and mineral separates) and regolith breccias are studied for nitrogen abundance and isotopic composition, in order to investigate the isotopic variation in the lunar regolith, and to constrain the origin of the nitrogen. The lunar soils and breccias are analysed using a high sensitivity static-vacuum mass spectrometer, capable of measuring nanogram quantities of nitrogen with a $\delta^{15}N$ precision of $\pm 0.5‰$. In addition to nitrogen abundance measurements, conjoint carbon and argon abundances (allthough the latter are semi-quantitative) are also measured. Lunar soils and breccias are analysed by stepped combustion and pyrolysis extraction, typically employing temperature resolution of 25-50°C. However, some soils and breccias are analysed by high-resolution extraction using temperature increments of 10°C, constituting the highest resolution studies performed to date.

The high-resolution extractions of lunar soils and breccias has confirmed the existence of the heavy-light-heavy-light-heavy (W-shaped) isotopic profile observed by previous workers for pyrolysis extractions of lunar breccias. The current study has confirmed that the W-shaped profile is restricted to pyrolysis extractions, but is present in both soils and breccias. The well documented heavy-light-heavy (V-shaped) isotopic profile is observed in stepped combustion extractions.

The nitrogen in the lunar regolith has been shown to be of both solar and non-solar origin. The former is confirmed from the solar-like C/N ratios in lunar soils, and the latter is confirmed from the excess $N/^{36}Ar$ ratio, between 5 and 39 times the solar value. Although neither nitrogen source is believed to be a minor component, the solar wind is believed to contribute ~30% of the total nitrogen, although the relative proportions of solar and non-solar nitrogen are not well constrained.

The surface-correlation of the low temperature nitrogen release (LTN), from the <10 μm fraction from soil A12023, has enabled calculation of the isotopic composition of this component with $\delta^{15}N = +35.3 \pm 13.6‰$. It is believed that this value is representative of the isotopic composition of the recent solar wind. Furthermore, the absence of isotopically

light nitrogen in agglutinates separated from A12023, and the increasing contribution of high temperature nitrogen (HTN) with increasing grain size from the same soil, has suggested that the volume-correlated nitrogen is released at temperatures ≥1050°C. This is believed to be representative of the ancient solar wind, and has a mean $\delta^{15}N = +27.0 \pm 6.0‰$. This work has shown that the maximum secular variation of $^{15}N/^{14}N$ in the lunar regolith is ~2.8‰, significantly lower than previous estimates.

The low temperature, isotopically heavy nitrogen component, N_{LT}, and the isotopically light nitrogen components, N_{MT} and N_{HT} (although the latter is only observed during stepped pyrolysis extractions), display a $^{15}N/^{14}N$ variation of 38‰. This cannot be accounted for by a secular variation of $^{15}N/^{14}N$ in this work. The origin of N_{LT} is not well constrained, but may be due to re-implantation of atmospheric nitrogen, or fractionation of solar wind gases during the formation of amorphous rims around soils grains. A proportion (~3‰) of N_{HT} has been observed in soil A12023, with $\delta^{15}N = -186‰$, the lightest observed in a lunar soil. The similarity of this value with that obtained for lunar breccia A79035, has suggested the possibility of a relict component, implanted prior to breccia consolidation. No evidence of presolar grains could be identified in A79035, although there is some evidence for amorphous carbon. This may also be associated with the presence of fine-grained metallic iron, as a significant proportion of this in lunar soils is believed to originate from meteorite contamination.

Acknowledgements

There are many people who have been directly or indirectly involved with this project and I wish to offer my sincere thanks to all of them.

Firstly, many thanks to Professor C.T.Pillinger for his advice on sample selection and help with the initial data interpretation in an unfamiliar area of research. Similar thanks should also go to Ian Franchi for his technical expertise in the setting up and calibration of Finesse, for correcting the many drafts of this thesis, and his endless patience in attempting to teach me to glassblow! I would like to thank Ian Wright, and especially Rainer Wieler, for constructive criticisms and for advice on presentation of the argon data. Thanks should also go to Jim Ball and Jez Higgins for constructing the computer programs for Finesse, and to Jez for electronic maintenance thereafter. I would also like to acknowledge John Arden for acid residue preparations, Martin Lee for TEM analysis, and the OU's Science & Technology workshops for being able to decipher my technical designs! The OU are also thanked for funding this research and the security team are acknowledged for checking up on me whilst in the lab throughout the night, and for the occasional chat and cup of coffee.

I am indebted to my kindred spirits: Caroline, for her constant support and encouragement, for enrolling me in the cat ownership club, and for introducing me to Magnum; and Adele, for her support, crisps, chocolate jelly eggs (I think!) and being someone with a mutual interest in fast cars. Thanks also go to Andy, for a constant supply of coffee and alcohol when required; Jason and Josanne, for showing it can be done against the odds; Sara, Richard and Paul, for help and advice in the early days; and past and present members of the PSRI who I may have inadvertently forgotten.

Special thanks should also go to Terry "Tez" Durrant for keeping me supplied with some great music over the years, and for allowing me to tag along on his roller-coaster ride through the music business. Thanks should also go to Now & Then records for signing and promoting some great rock bands and giving them the opportunity to play at the music festival of the year, and to the bands themselves (Gary Hughes & Ten, Bob Catley & Hard Rain, Tyketto and Emerald Rain to name but a few) for providing some great live gigs.

Thanks also to all my friends in St. Albans and Hatfield, especially Kim Banham and Andy "Is it finished yet?" Jelfs, and to Claire, Martin and my godson Thomas for their support. Further thanks go to friends in London for their constant encouragement and understanding.

Thanks also go to Radio 5 Live (for football commentary and lively debates), Bob Harris on Radio 1 (for some great music at anti-social times of the night), my two favourite types of bean (coffee and cocoa), Woughton Tennis Club (for enabling me to remove any pent-up tension), MKCSL (for giving me the opportunity to play league snooker) and THFC (for giving me something else to get stressed about over the last few years!).

Final acknowledgement should go to those who are closest to me: my family (Mum, Dad and Raymond) for their encouragement, love and support, and knowing when not to ask too many questions; and to Clive for his constant companionship, support (both moral and financial), encouragement and having faith in my abilities. I never could have got there without you all.

Table of contents

Chapter 1. Lunar and solar processes

Chapter 2. Experimental techniques

Chapter 3. A detailed investigation of the yield and isotopic components in lunar soil A12023

Chapter 4. A study of the isotopically heaviest and lightest nitrogen components in lunar soils and breccias.

Chapter 5. Nitrogen isotope studies of the <10 μm grain size fraction of Apollo 16 soils

Appendix C. Stepped extraction data from the Apollo 17 site

Appendix D. Stepped extraction data from the Apollo 16 site

List of figures

Chapter 1. Lunar and solar processes

Chapter 2. Experimental techniques

Chapter 3. A detailed investigation of the yield and isotopic components in lunar soil A12023

Chapter 4. A study of the isotopically heaviest and lightest nitrogen components in lunar soils and breccias.

Chapter 5. Nitrogen isotope studies of the <10 μm grain size fraction of Apollo 16 soils.

List of tables

Chapter 1. Lunar and solar processes

Chapter 2. Experimental techniques

Chapter 3. A detailed investigation of the yield and isotopic components in lunar soil A12023

Chapter 4. A study of the isotopically heaviest and lightest nitrogen components in lunar soils and breccias.

Chapter 5. Nitrogen isotope studies of the <10 μm grain size fraction of Apollo 16 soils

Chapter 1
Lunar and solar processes

1.1. Introduction

The lunar samples returned by the US Apollo and USSR Luna missions constituted the first material to be collected directly from outside the Earth's atmosphere. The study of these samples (the majority of which are surface soils) have enabled the development of our current knowledge of the formation of the Moon and the subsequent events which have modified the lunar surface, *e.g.* meteorite bombardment. In addition, the lunar surface has also been subjected to implantation of solar wind and cosmic-ray radiation, in the absence of an appreciable atmosphere and magnetic field. The Apollo and Luna soils have therefore retained a record which is essential to our understanding of the exposure history of the lunar surface.

The study of the nitrogen inventory in lunar samples has proved to be one of the more challenging and contentious areas of lunar research. The origin of the nitrogen and the variation of its two isotopes, ^{15}N and ^{14}N, within lunar soils has been investigated extensively by many workers, *e.g.* Becker and Clayton 1975, and theories invoking both a solar and non-solar origin for the nitrogen have been proposed. However, many of the results are in contradiction with current solar models and the observations for other elements observed in lunar soils, and hence this issue remains unresolved.

Prior to discussing the nitrogen inventory of the lunar surface, it is necessary to have a basic understanding of solar and lunar processes (sections 1.4 and 1.5 respectively). Although these are not directly relevant to the analyses undertaken in this work, it is deemed necessary in order to aid interpretation of the data obtained. This also involves an understanding of the characteristics and implantation effects of solar and cosmic-ray radiation, which have modified the lunar surface (section 1.6). The remainder of the chapter discusses the major issues regarding the nitrogen inventory of the lunar surface and the explanations which have been invoked to account for the variation of ^{15}N and ^{14}N in lunar samples (section 1.7). The discussion of the current theories are crucial as it forms the basis

for the studies undertaken in this work. Although the bulk of this discussion centres around nitrogen abundances and isotopic compostions, a full account of lunar nitrogen is incomplete without a discussion of the noble gas inventory, as this is essential when assessing the solar radiation contribution to the lunar surface. In the light of the current theories surrounding lunar nitrogen, section 1.8 describes the aims and objectives of this research.

1.2. Early observations of the Sun and Moon

1.2.1. Advances in celestial and planetary mechanics

Early records show that observations of the Sun and Moon aided early civilisations in China, India, Babylonia, Egypt, Central America and Europe in their understanding of the changing seasons, tides and climate. This was essential for those involved in agriculture, as it provided them with a useful calender for sowing and harvesting crops. However, as the Sun, Moon and stars or "wanderers" were thought of as deities, their physical nature was never questioned.

The apparent lack of motion of the Earth when compared to other bodies led the ancient Greek scientist Pythagoras (6th century BC) to propose the geocentric theory of the universe, in which the Sun, Moon and planets revolved around a stationary Earth. Although this theory gained widespread support from other influential thinkers, such as Aristotle, Ptolemy and Eudoxus of Cnidus, not all scientists believed in a geocentric universe. Aristarchos of Samos (280 BC) proposed a heliocentric or Sun-centred universe, but the implication that the Earth was not the centre of the known universe led to strong opposition in ecclesiastical circles. It was not until the telescopic observations of Galileo Galilei and Tycho Brahe, Johannes Kepler's laws of planetary motions, and Isaac Newtons's law of universal gravitation (including mathematical verification of Kepler's work), that the heliocentric theory was accepted.

1.2.2. Observational background of the Sun

During the 16th century the suggestion that the Sun was an "ordinary" star began to emerge and this was followed by an intense period of solar study. Early telescopic observations of the Sun confirmed the presence of "sunspots", dark blemishes on the surface of the Sun (previously observed by Chinese astronomers since around 150 BC), the movement of which led to accurate calculation of the period of solar rotation, and detailed studies of other solar phenomena, *i.e.* prominences and flares.

The major advance in the field of solar physics was the invention of the spectroscope, by the German physicist Joseph von Fraunhofer in 1814. This measured the wavelengths of the dark lines observed in the solar spectrum produced by the absorption of light, and allowed the elemental composition of the solar atmosphere to be determined. The advent of solar photography in 1845 and the invention of the "spectroheliograph" by George Ellery Hale in 1892, enabled the Sun and features such as prominences and flares to be observed in any wavelength, previously only discernible during solar eclipses.

As our closest star, the Sun has been studied extensively by solar physicists and astronomers alike in order to understand the processes of stellar formation and evolution.

1.2.3. Pre-Apollo observations of the Moon

Earth-based telescopic observations of the Moon had revealed two distinct types of terrain: bright regions, known as highlands, and dark areas termed maria or "seas". The advent of spacecraft imaging techniques later confirmed the heavily cratered nature of the highlands and the absence of surface water at low latitudes. The first telescopic maps were produced in 1609 by Thomas Harriet and were closely followed by the more detailed maps of Galileo in 1610. Towards the end of the 19th century the first photographic atlasses were being produced, *e.g.* Loewy and Puiseux in the 1890's and W.H.Pickering in 1904.

Early lunar missions were used to obtain high resolution images of the lunar nearside in order to identify a suitable landing site, *e.g.* Luna, Zond, Ranger and Orbiter (1959-1966). From 1964 various soft landings and studies of the lunar surface were made (Surveyor and Luna) with no crew, as preparation for the sample return missions. A

description of the Apollo and Luna missions is given in section 1.3.1.

1.3. Recent observations of the Moon

1.3.1. The Apollo/Luna missions

From 1969-76, six Apollo crewed missions (US) and three uncrewed Luna missions (USSR) collected samples from the lunar nearside[1]. None were collected from the lunar farside. These missions returned a diverse range of geological specimens, including lunar rocks, drill cores (collected at all sites with the exception of Apollo 11) and surface soils from the geologically distinct highland and mare regions. These have enabled study of the chemistry, mineralogy and petrology of the Moon, and have led to investigations into the formation of the Moon and the modification processes which the surface has subsequently undergone.

The astronauts on the six Apollo missions (11 to 17, excluding 13) returned 382 kg of lunar material, the latter three missions employing a Lunar Roving Vehicle for traversing the lunar surface (referred to as extra-vehicular activity or EVA) to enable sample collection across a larger field area. This eliminated any potential contamination of the samples by the exhaust gases from the lunar module. The Luna missions (Luna 16, 20 and 24) returned 0.3 kg of material using robot landers but sampled three regions that were distinct to the Apollo landing sites. It should be noted, however, that the area encompassed by the Apollo and Luna missions constituted <5% of the total lunar surface (Warren and Kallemeyn, 1991). A description of the lunar terrain is given in sections 1.5.2 to 1.5.4 inclusive, and extensive descriptions of the geology of the landing sites are given elsewhere (Shoemaker *et al.*,

[1] Lunar samples are identified by a generic five digit sample number, *e.g.* 79035. The first digit(s) specify the Apollo or Luna mission as follows: 10 (Apollo 11), 12 (Apollo 12), 14 (Apollo 14), 15 (Apollo 15), 6 (Apollo 16), 7 (Apollo 17), 16 (Luna 16), 20 (Luna 20), and 24 (Luna 24).
For the samples collected during the Apollo 16 and 17 missions, the second digit denotes the station number of the collection site. For all the missions (Apollo and Luna) the third and fourth digits denotes the sampling site and collection bags respectively. The fifth digit identifies the sample as unsieved or sieved fines as follows: 0 (unsieved <10 mm fines), 1-4 (sieved <10 mm fraction) and 5-9 (>10 mm rocks and breccias).

1970a, b; Swann *et al.*, 1972, 1977; Schmitt and Cernan, 1973; Spudis, 1984). The location of the Apollo and Luna landing sites are given in Table 1.1 and are illustrated in Figure 1.1.

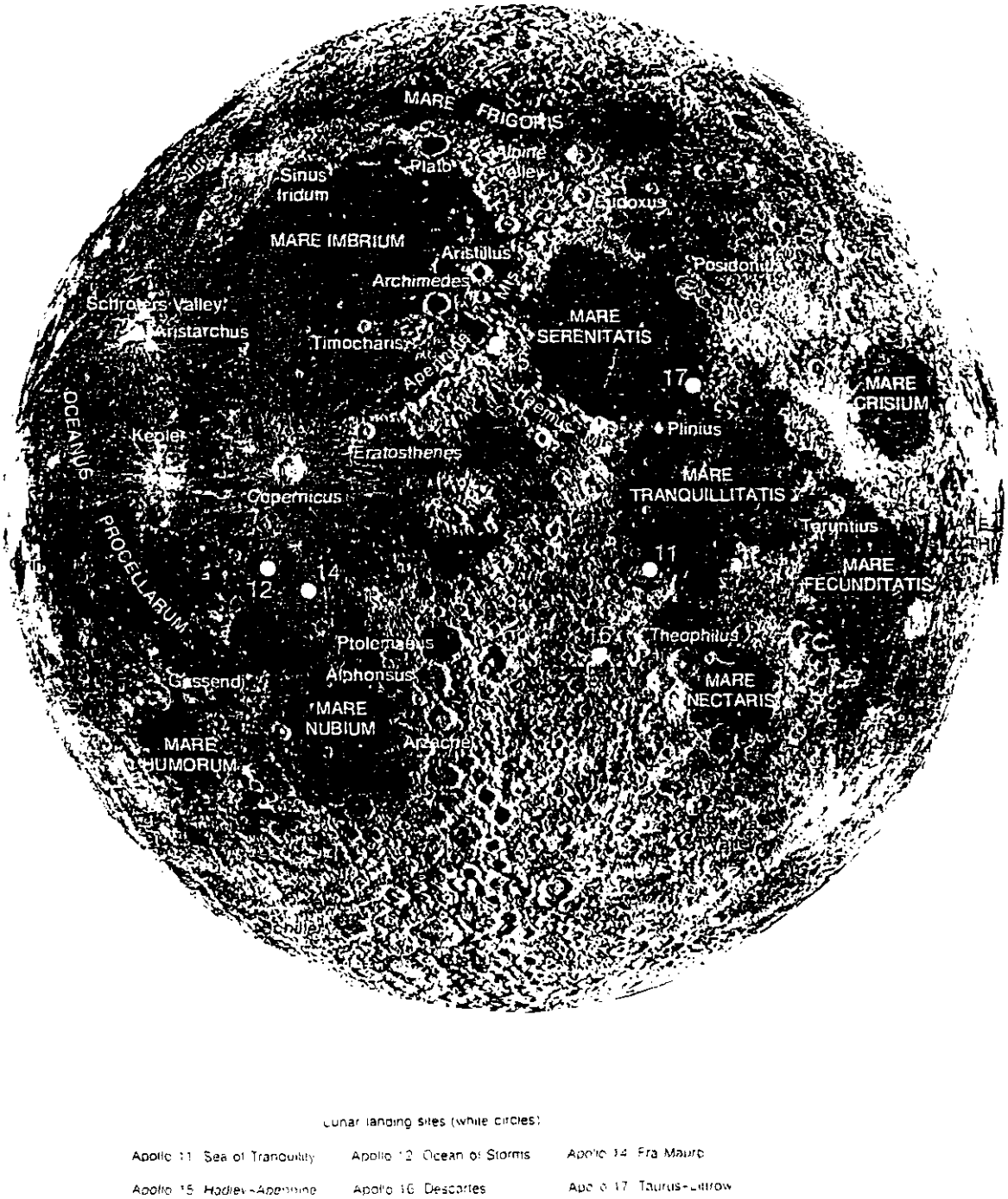

Figure 1.1. The major features of the lunar nearside, and location of the Apollo and Luna landing sites.

Mission	Landing Site	Description
Apollo 11	Mare Tranquillitatis	Mare
Apollo 12	Oceanus Procellarum	Mare
Apollo 14	Fra Mauro	Large-scale ejecta ridge
Apollo 15	Hadley-Apennine	Highland/mare boundary
Apollo 16	Cayley Plains/Descartes	Highland
Apollo 17	Taurus-Littrow	Highland/mare boundary
Luna 16	Mare Fecunditatis	Mare
Luna 20	south of the Crisium basin	Highland
Luna 24	Mare Crisium	Mare

Table 1.1. The landing sites for the Apollo and Luna missions.

1.3.2. Clementine observations of the Moon

The objective of the Clementine mission was to obtain high resolution images of a near-Earth asteroid. A lunar mapping project was used as the initial test phase for this mission to assess the performance of the instrumentation. However, the mission was aborted soon after the mapping project was complete. The Clementine images provided greater resolution on a number of lunar features including the Copernicus, Tycho and Giordano Bruno impact craters (Pieters *et al.*, 1994), Aristarchus crater (McEwen *et al.*, 1994) and the South Polar region (Shoemaker *et al.*, 1994). The results indicated that the range of topographical elevation was double that expected. The images also revealed the largest crater yet observed in the solar system, the South Pole-Aitken Basin. It has a diameter of 2500 km and depth of 12 km (Spudis *et al.*, 1994; Zuber *et al.*, 1994) but due to its high latitude at its deepest point, had not been observed by the Apollo and Orbiter spacecraft due to the low latitudes at which they operated. A further discovery was a region of permanent shadow near the south pole, ~300 km across and with a surface temperature of 40K. Preliminary results from radio wave scattering experiments have suggested the possible presence of water ice deposits. A summary of the Clementine results is given by Nozette *et al.* (1994).

1.4. The Sun

1.4.1. Structure of the Sun

The Sun has a radius of 6.96 x 10^5 km (1 $R_\odot$), a mass of 2 x 10^{30} kg (1 $M_\odot$) and lies at a distance of 1.5 x 10^8 km or 1 astronomical unit (1 AU) from the Earth. Figure 1.2 shows the layered structure of the sun and the corresponding densities and temperatures in each region.

The core extends out to 1.75 x 10^5 km (0.25 $R_\odot$) but contains half of the total solar mass (0.5 $M_\odot$). It has a central temperature of 1.5 x 10^7 K with a pressure of 2.5 x 10^{16} Pa. The principal nuclear reaction in the core is the proton-proton reaction, shown in Figure 1.3, whereby ^1H atoms are combined to form ^4He with an additional release of high frequency gamma rays (γ) and neutrinos (ν) to account for the mass difference. The ^4He is stable and will ultimately contribute to the production of heavier elements. The additional energy produced by this reaction is transported to the surface by three processes: conduction, radiation and convection, which are dependent on the density, pressure and temperature in each region.

Surrounding the core, is the radiative zone which extends from 0.25 to 0.86 $R_\odot$. In this layer, the temperature decreases from 8 x 10^6 K at the core boundary to 5 x 10^5 K at the base of the convective zone with a corresponding decrease in density (from 2 x 10^4 kgm^{-3} to 10 kgm^{-3}). Radiation and diffusion are the major modes of energy transport, whereby photons released during ^1H burning are repeatedly absorbed and scattered with a concomitant loss of energy, while journeying to the surface. The electromagnetic radiation initially emitted in the core as high frequency gamma rays would have lost sufficient energy by this process to be released as visible light at the photosphere.

The convective zone surrounds the radiative zone and extends to the base of the photosphere. The temperature and density continues to decrease in this layer and reaches values of 6600 K and 4 x 10^{-4} kgm^{-3} respectively at the base of the photosphere. The conditions allow convection to replace radiation as the dominant mechanism of energy transport, whereby gas bubbles form convective cells which rise to the solar surface and split apart radiating their energy.

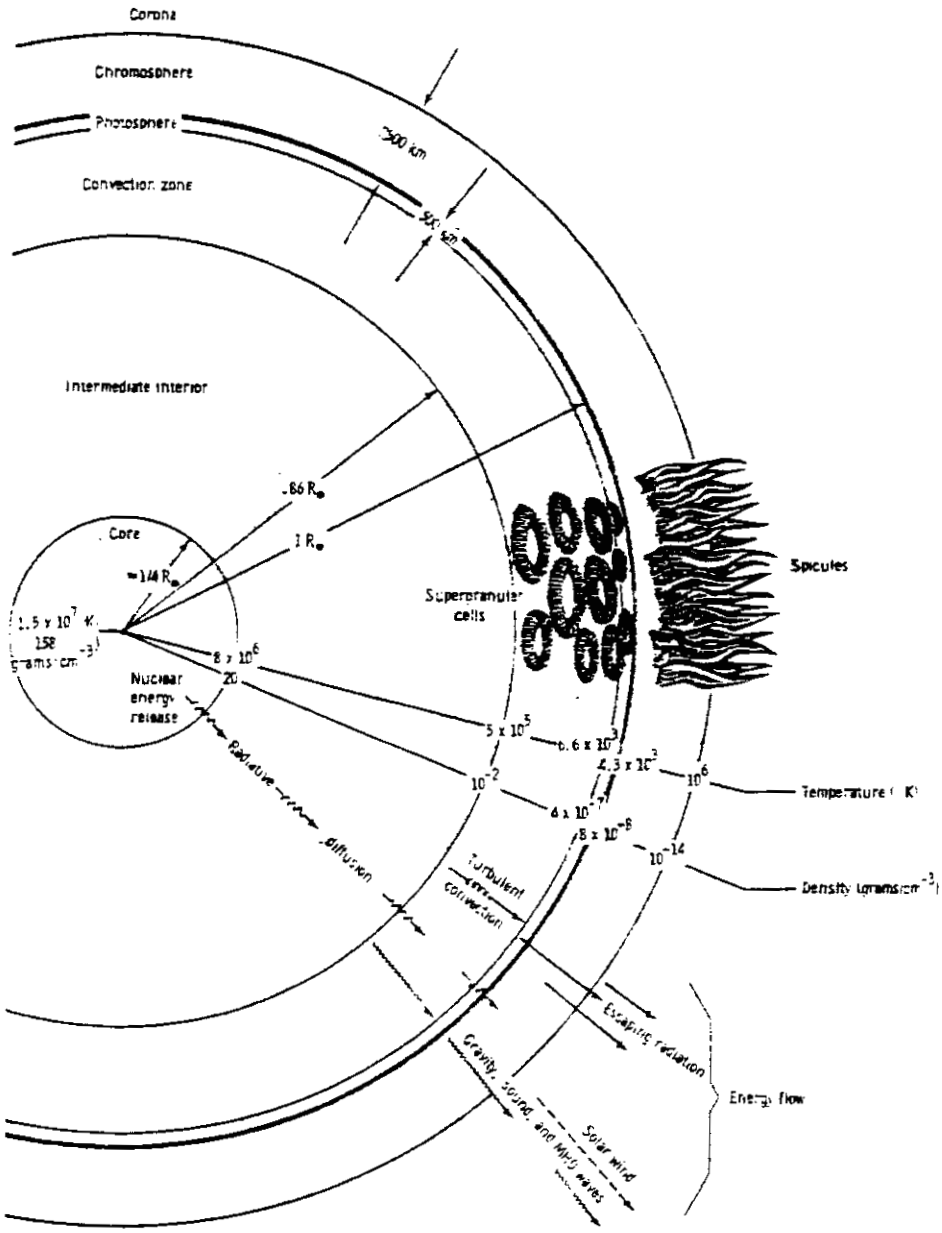

Figure 1.2. The structure of the Sun (after Gibson, 1973).

$$^1H + {}^1H \longrightarrow D + e^+ + \nu$$

$$D + {}^1H \longrightarrow {}^3He + \gamma$$

$$^3He + {}^3He \longrightarrow {}^4He + {}^1H + {}^1H + \gamma$$

Figure 1.3. The proton-proton reaction.

The photosphere, is a layer 500 km thick that consists of a thin shell of gas, from which the majority of the Sun's radiation is emitted at visible or near-visible wavelengths. At the outer regions of the photosphere (1 $R_\odot$) the temperature and density have decreased to values of 4300 K and 8.8 x 10^{-5} kgm^{-3} respectively. The visible surface of the Sun has a textured appearance, termed granulation, which is due to the rise and fall of turbulent convective cells from below the photosphere. These granules have a typical diameter of 1000 km but can also combine to form a larger network of "supergranules" with typical diameters of 3 x 10^4 km.

1.4.2. The solar atmosphere

Surrounding the photosphere is the chromosphere or lower layer of the solar atmosphere. This is a layer of rarefied gas, about 2500 km thick which has been studied by spectroscopic analyses using the absorption lines of hydrogen (Hα), neutral and ionised helium, Ca II (H and K) and Mg II (h and k).

The chromosphere is not homogeneous and displays large-scale structure known as the "chromospheric network", which coincides with the supergranular cells in the photosphere and is governed by the underlying magnetic field. In areas such as the polar regions where the network breaks up and the magnetic field lines are weaker, coronal holes appear through which solar wind particles can flow freely. A description of solar wind is given in section 1.4.4.

The density in the chromosphere decreases to 10^{-11} kgm^{-3} at the base of the upper solar atmosphere or solar corona with the temperature increasing rapidly to 10^6 K over the same region. This is believed to be due to the acceleration of low frequency sound and magnetohydrodynamic (MHD) waves by the low densities in the chromosphere.

The solar corona is an even more rarefied layer of gas surrounding the chromosphere which extends out to a distance of several solar radii. The temperature increases to several million degrees over this region, although the corona contains only a small amount of energy due to its low density. Beyond the corona extends the solar wind and magnetosphere.

1.4.3. The solar cycle

The most obvious feature on the solar disc are sunspots which appear as dark patches, with typical surface temperatures of 4200 K. These are thought to be the result of intense localised magnetic fields which impede convection from below the photosphere and create a region of lower temperature than the surroundings. R.Wolf in 1852 observed that the number of sunspots increased and decreased regularly over a period of 11 years. This was termed the solar cycle and can be characterised by the high numbers (up to 100 or more) and high latitudes (±15° approx.) of sunspots during period of high activity (solar maximum) and few sunspots at low latitudes (±5° approx.) when the Sun is less active (solar minimum).

Associated with sunspot activity and the solar cycle are phenomena such as flares which are also controlled by intense, localised magnetic fields. Solar flares are sudden and violent releases of energy from active regions often above areas of high sunspot activity. They occur when hot hydrogen gas suddenly brightens, and are commonly observed using monochromatic H_α (λ = 656 nm) light. They emit radiation across the entire electromagnetic spectrum and can result in disturbances in the Earth's ionosphere, including disruptions to long distance radio communications.

1.4.4. The solar wind

The solar wind is the continuous outflow of ionised particles from the corona due to the solar magnetic field or magnetosphere. The high temperatures and the low density in the corona ensures that the particles remain ionised due to the inefficiency of the recombination process. The radial outflow of the solar wind is strongly affected by the solar magnetic field, hence the particles travel outwards in a spiral motion which coincides with the direction of solar rotation. The dynamics of the solar wind and heliosphere is shown in Figure 1.4 (after Foukal, 1990), and are further described in Smith (1991).

Solar wind speeds, as measured by the Vela satellites (Strong *et al.*, 1967), vary from 200 - 900 kms^{-1} but are typically 400 - 500 kms^{-1}. During periods of low solar activity, velocities are reduced to 300 - 350 kms^{-1}. Solar particles take about 5 days to travel

1 AU by which time the particle density has decreased from 10^5 particles cm^{-3} to 5 particles cm^{-3} (Neugebauer and Snyder, 1966). In comparison, particles from solar flares take approximately 2 days to reach the Earth due to their higher velocities.

The presence of a protective magnetosphere shields the Earth against the influx of solar wind, solar flare and cosmic-ray radiation. The exceptions to this are at the polar regions from where the magnetic field lines emanate, allowing the solar and cosmic-ray particles to interact with the ionosphere producing auroral displays. Early evidence for a continuous emission of particles from the Sun resulted from the observation of these displays. The suggestion of a continous outflow of ionised particles from the Sun was first proposed by Biermann in the early 1950's and led to the first model of an expanding solar corona (Parker, 1958) from the study of cometary tails. Direct confirmation of a continuous solar wind was not obtained until the late 1960's and early 1970's by the US Mariner 2, Explorer 34 and the USSR Vela spacecraft and satellites. Further details of early spacecraft measurements are given in Pillinger (1979).

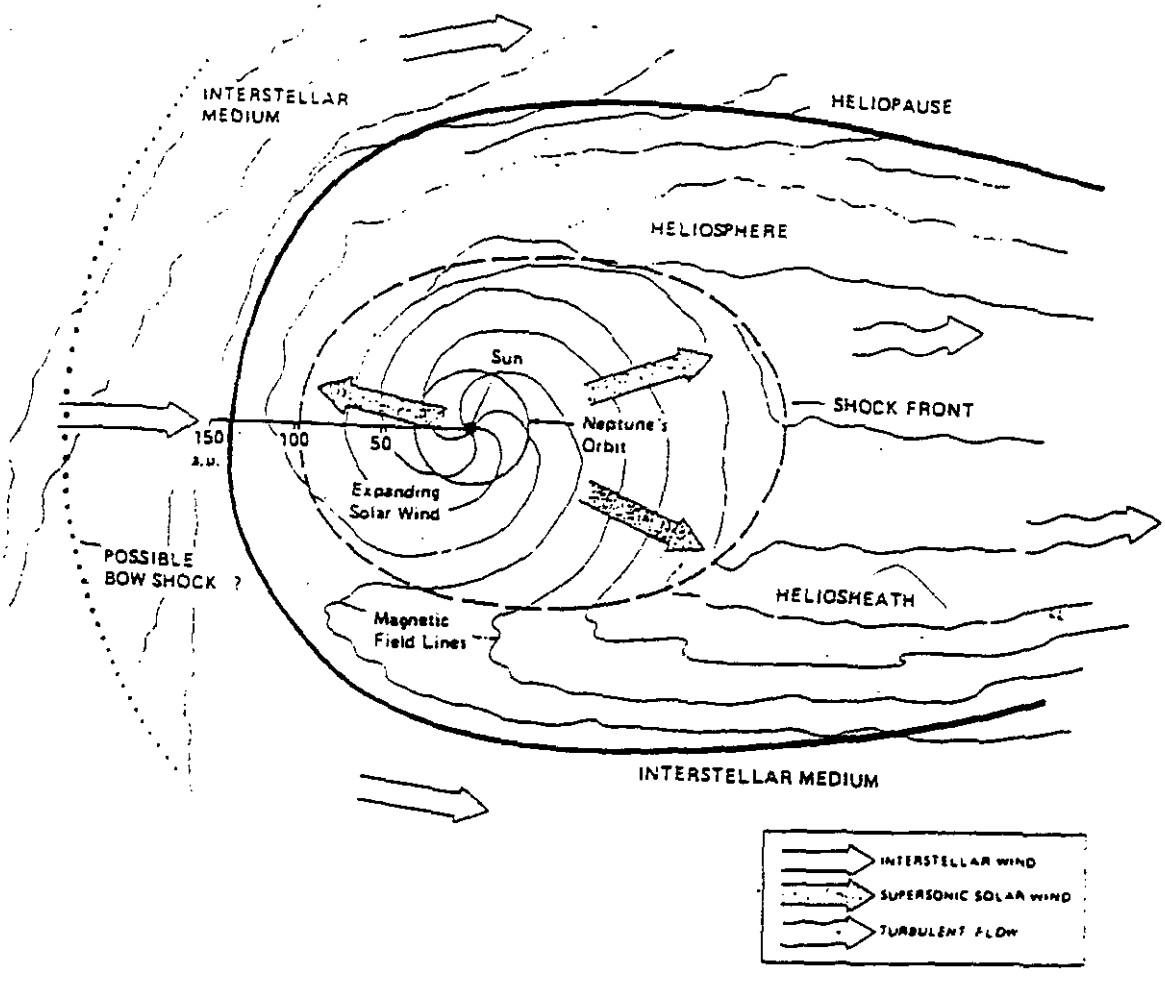

Figure 1.4. The solar wind and solar heliosphere (after Foukal, 1990).

In addition to the known source of protons and electrons in the solar wind, Explorer also confirmed the presence of a variable abundance of $^4He^{2+}$ (Neugebauer, 1981). The $^4He^{2+}/H^+$ ratio varied from 0.003 to 0.25 (Ogilvie and Wilkerson, 1969) which was thought to be associated with solar activity levels. An average value (over a 6 year period) was calculated at 0.045 (Hundhausen, 1970). Furthermore, Bame *et al.* (1968, 1970) also revealed the presence of $^3He^{2+}$, $^4He^+$ and the ionised species of O, N, Si and Fe. Also, small amounts of ionised ^{12}C and ^{20}Ne were believed to exist.

The most accurate measurements of solar wind elemental abundances and isotopic compositions were performed by the Solar Wind Composition Experiment. This experiment was devised (Signer *et al.*, 1965; Bühler *et al.*, 1966) to collect solar wind atoms from outside the Earth's magnetosphere for subsequent analysis on Earth. The solar wind atoms were collected using aluminium foils, located on the lunar surface. With the exception of Apollo 17, it was taken on all Apollo missions and has been detailed by Geiss *et al.* (1972a, b). A summary of the results obtained from the Apollo missions are given in Table 1.2 (after Geiss *et al.*, 1972b). Note that the weighted average value for $^{20}Ne/^{36}Ar$ of 45 ± 10, which has been quoted in this table, is modified from the original data and represents the best current value for this ratio (Cerutti, 1974).

Source	$^4He/^3He$	$^4He/^{20}Ne$	$^{20}Ne/^{22}Ne$	$^{22}Ne/^{21}Ne$	$^{20}Ne/^{36}Ar$
Terrestrial atmosphere	7×10^5	0.3	9.80 ± 0.08	35 ± 1	0.5
Apollo 11 [1]	1860 ± 140	430 ± 90	13.50 ± 1.00		
Apollo 12 [1]	2450 ± 100	620 ± 70	13.10 ± 0.60	26 ± 12	
Apollo 14 [2]	2230 ± 140	550 ± 70	13.65 ± 0.50		37^{+10}_{-5}
Apollo 15 [3]	2310 ± 100	550 ± 50	13.65 ± 0.30	31 ± 4	20^{+8}_{-5}
Apollo 16	2260 ± 100	570 ± 50	13.80 ± 0.40	31 ± 4	29 ± 6
Weighted average	2350 ± 120	570 ± 70	13.70 ± 0.30	30 ± 4	45 ± 10 [4]

Table 1.2. Noble gas isotopic ratios determined from the Solar Wind Composition Experiment (after Geiss *et al.*, 1972b).
References: (1) Geiss *et al.* (1970), (2) Geiss *et al.* (1971), (3) Geiss *et al.* (1972a), (4) Cerutti (1974).

1.4.5. Ulysses observations of the Sun

The Ulysses mission was a joint undertaking between the National Aeronautics and Space Administration (NASA) and the European Space Agency (ESA) to explore the polar regions of the Sun for the first time. The mission, launched in October 1990, passed the south pole between July and October 1994 at a latitude of -80° and a distance of 2.29 AU. The mission carried nine body-mounted hardware experiments, to provide information about solar magnetic fields and particle fluxes. A detailed review of results is given by Smith *et al.* (1995). The following is a brief summary of current findings.

The results from Ulysses showed that up to a latitude of -30°, the solar wind speed varied from ~400 to 750 kms^{-1} but above latitudes of -50°, the wind speed remained constant between 700 to 800 kms^{-1} due to a coronal hole over the south pole (Phillips *et al.*, 1995). Heavy ion composition experiments (Geiss *et al.*, 1995) observed a decrease in the Mg/O ratio between high wind speeds when compared to low wind speeds. In addition, the radial component of the solar magnetic field was confirmed not to vary with latitude (Balogh *et al.*, 1995) but remained essentially uniform. An unexpected observation was that there was only a slight increase in the cosmic-ray flux from the solar equator to the pole (Simpson *et al.*, 1995).

The observations from Ulysses were made during a period of minimal solar activity. The second pass of the south and north polar regions is scheduled for 2000 and 2001, during solar maximum and it will be interesting to compare the current results with those obtained from an active Sun.

1.5. The Moon

As the Earth's only natural satellite and the nearest astronomical object to our planet, the Moon has been studied extensively. It has a diameter of 3476 km (one-quarter that of the Earth), a mass of 7.35×10^{22} kg (81 times smaller than the Earth) and one-sixth the gravity. The Moon was believed to have formed 4.5 Gyr ago, when an impactor (probably Mars-sized) hit the Earth and expelled material into orbit, which was condensed together with some of the original impactor (Hartmann and Davis, 1975; Cameron and Ward, 1976).

In addition to the two distinct types of terrain (highland and mare), the most conspicuous features on the Moon are the abundance of craters, the absence of free water and the lack of an appreciable atmosphere. The combination of these factors have suggested that the Moon is not a primitive body and studies of lunar samples have indicated that at the beginning of its 4.5 Gyr history, the Moon underwent a 0.6 Gyr period of violent impacts and melting, followed by at least 1 Gyr of volcanic activity. In the last 2 Gyr, the Moon has been geologically quiet.

1.5.1. The lunar atmosphere

Due to the low gravity and low escape velocity (2.37 kms^{-1}) the Moon has been unable to retain an appreciable atmosphere. However, a tenuous atmosphere does exist with a density of 10^4 molecules cm^{-3}, 10^{-14} times that of the Earth (Hodges, 1975). The Apollo 12, 14 and 15 missions attempted to measure elemental abundances in the lunar atmosphere but results were heavily contaminated by the exhaust gases from the lunar module. The Lunar Atmospheric Composition Experiment (LACE) on the Apollo 17 mission had limited success and using a small mass spectrometer, was able to detect the presence of hydrogen, helium, neon and argon. The H, He and Ne are believed to originate from the solar wind, although up to 10% of He may be radiogenic, by the α-decay of heavy elements, and hence lunar in origin (Hodges, 1975). Argon is mainly ^{40}Ar, produced from the radioactive decay of ^{40}K and therefore of a lunar origin, but ~10% of argon is solar wind ^{36}Ar.

One consequence of the lack of atmosphere is the absence of free water on the lunar surface which implies that the effects of hydrous alteration and erosion by liquid water can be eliminated as surface modification processes. The Moon also has a negligible magnetic field, *i.e.* no protective magnetosphere, and hence the surface is subjected to constant bombardment by ionizing radiation such as solar wind particles and solar and galactic cosmic-rays (section 1.6). The lunar surface has therefore retained a record of solar and galactic implanted species since its formation, although much of the early record has been masked by intense meteorite bombardment and volcanism in its early history.

1.5.2. The lunar highlands

The lunar highlands formed more than 4.45 Gyr ago during an epoch of large-scale chemical segregation (differentiation). Some workers (Wood *et al.*, 1970) have suggested that the Moon was at least partially covered by a "magma ocean", whereby, during crystallisation lighter minerals such as plagioclase feldspar rose to the surface to form an anorthositic-rich crust, and denser minerals such as pyroxenes and olivines sank into the lunar mantle. A discussion of lunar highland formation is given by Warren (1985) and the major characteristics of the highlands is given in Table 1.3.

Subsequent impacts formed the highly cratered highland terrain now observed and this is reflected in the lunar samples returned from the Apollo/Luna missions. The majority of samples are polymict breccias, *i.e.* shock-melted fragments from a variety of sources, which are enriched in plagioclase but depleted in pyroxenes and olivines compared to the mare samples. A few pristine[1] highland rocks have been collected but as the highland samples analysed in this work were regolith soils, no review of these have been included in this work. However, a full description of highland rocks is given by Taylor *et al.* (1991).

Lunar highlands	Lunar maria
Appear bright when viewed from Earth	Appear dark when viewed from Earth
Heavily cratered	Less heavily cratered
Enriched in Ca, Al and Mg	Enriched in Fe and Ti
Plagioclase[1] dominant	Pyroxene[2] and olivine[3] dominant
Formed by chemical segregation followed by intense bombardment	Formed by basaltic lavas

Table 1.3. Summary of the major differences between the lunar highlands and maria. (1) $(Ca,Na)(Al,Si)_4O_8$, (2) $(Ca,Fe,Mg)_2Si_2O_6$, (3) $(Mg,Fe)_2SiO_4$.

[1] The term "pristine" is defined as "original" igneous rocks or monomict breccias, *i.e.* shattered fragments from a single source.

1.5.3. The lunar maria

The lunar maria are believed to have formed from the melting of the solid interior of the Moon at depths of 100-400 km followed by eruption at the surface. The volcanic activity, that filled many of the impact basins, continued for less than 1 Gyr after the cessation of intense bombardment ~3.9 Gyr ago and hence the maria are lightly cratered in comparison with the highland regions (Table 1.3).

Lunar mare rocks are primarily basaltic lavas enriched in Fe and Ti, the latter mainly present as ilmenite ($FeTiO_3$), with pyroxene as the dominant mineral (Taylor, 1975). Mare basalts display a wide variation in TiO_2 contents and hence have been divided into three major groups: high-Ti (>9 wt.% TiO_2), low-Ti (1.5-9 wt.% TiO_2) and very-low-Ti (<1.5 wt.% TiO_2). These are further subclassified based on their Al_2O_3 and K_2O contents (Shervais *et al.*, 1985). Full descriptions of mare basalt compositions are given in Papike *et al.* (1976) and Papike and Vaniman (1978).

Also present in the mare regions are two distinct types of glass droplets and fragments: pyroclastic deposits and impact produced glasses. The pyroclastic deposits are small glass beads formed by lava fountaining during volcanic activity, *e.g.* orange glass at the Apollo 17 site, and contain higher concentrations of Mg and Ni compared to mare basalts. They can also contain fine-grained crystals of ilmenite, olivine, spinel and metallic iron. Impact glasses, *e.g.* green glass at the Apollo 15 site, are formed during meteorite impacts, often as coatings around rocks and contain high contents of siderophile elements, *i.e.* Ni and Co, indicative of meteoritic contamination. Delano (1986) has described how to distinguish volcanic glasses from those of an impact melt origin, on the basis of their chemical composition, homogeneity and volatile element content.

1.5.4. The lunar regolith

The regolith, is the layer of fragmented and unconsolidated material that covers the entire lunar surface. Regolith samples, *i.e.* soils, breccias (conglomerates of rock and soil fragments), rocks and drill cores, constitute the entire Apollo and Luna sample collection as no bedrock material was located during these missions. The soils and breccias, especially,

are essential to our understanding of the exposure history of the regolith as they have retained a record of solar and cosmic-ray implanted radiation. As the samples analysed in this work are regolith soils and breccias, it is deemed necessary to give a detailed account of regolith processes.

1.5.4.1. Regolith formation and composition

The early lunar regolith was formed by the pulverisation, melting and dispersion of freshly excavated bedrock due to meteorite bombardment at the lunar surface. Subsequent impacts would expose fresh bedrock as well as pulverise the lunar surface in a continuous process resulting in the deepening of the regolith. Following the period of heavy bombardment (~3.9 Gyr ago), smaller micrometeorite impacts frequently re-worked or "gardened" the uppermost layer of the regolith while the underlying bedrock remained undisturbed. Regolith mixing calculations (Langevin and Arnold, 1977) have shown that in 10^6 years, regolith mixing occurs a few hundred times in the top 0.1 mm, an order of magnitude less in the upper 1 mm and only once (with 50% probability) in the upper 1 cm. Some deep regoliths are believed to have remained undisturbed for several million years, *e.g.* the deep-drill core base at the Apollo 15 site (~2.37 m) is thought to be 500 Myr old.

The thickness of the lunar regolith varies across the lunar surface, with depths rarely exceeding 10-20 m. Regolith thickness studies (McKay *et al.*, 1974; Langevin and Arnold, 1977; Taylor, 1982) have shown that, in general, the regolith is 4-5 m thick in mare regions and 10-15 m thick in older highland areas. The stratigraphy of the lunar regolith has been studied from drill cores returned from all Apollo sites (with the exception of Apollo 11), and consists of discrete layers of material ejected from impact craters. Each of these layers are well mixed, with a grain size which varies randomly between adjacent layers, but with an median diameter of 45-100 μm (Carrier, 1973). The soils are loosely packed in the upper few tens of centimetres of the regolith below which they are more compacted. McKay *et al.* (1980) has illustrated an inverse correlation between regolith thickness and mean grain size, *i.e.* thicker regoliths contain particles with finer grain sizes.

Studies of the samples returned by the Apollo and Luna missions have indicated that the lunar regolith mainly consists of particles of <1 cm diameter. Most of the Apollo regolith

samples have been separated into several size fractions at the Johnson Space Centre (herein abbreviated to JSC), Houston, Texas, USA; the most regularly studied fraction being the <1 mm fraction or "fines" as this fraction constitutes >90% of most regolith samples.

Lunar soils typically vary from light to dark grey in colour with compositions ranging from basaltic to anorthositic depending on the mare or highland origin, respectively, of the parent-rock. There are substantial variations in soil chemistry, both between landing sites and in geologically distinct areas within the same landing site. The regolith also consists of fragments of minerals and pristine crystalline rocks, which mainly originate from the local bedrock material, and breccia fragments, heterogeneous glasses and agglutinates (glass welded aggregates of soil and mineral fragments) which are derived by meteorite impact heating events. Trace element studies have also revealed that the regolith contains a contribution of carbonaceous chondrite debris (section 1.6.4) and a minor exotic, *i.e.* non-local component, believed to be ejecta material from the major basin forming events.

1.5.4.2. Regolith maturity

One of the problems encountered when attempting to determine the parent-rock compositions of the lunar regolith is the maturity of a lunar soil. Maturation is the process of modification to a lunar soil by micrometeorite bombardment and exposure to solar and galactic particle irradiation. A soil which has been exposed on the lunar surface for a longer duration is more mature than a recently exposed soil, and as a result has undergone higher levels of comminution and melting, which can obscure the composition of the parent-rock. A soil remains immature whilst buried beneath the lunar surface, until it is brought to the surface by gardening processes, and may undergo several periods of exposure interspersed with periods of burial. Immature soils generally tend to have coarser grain sizes than more mature soils due as they have not been fragmented by particle irradiation or bombardments for a sufficient time. The cumulative length of time that a sample is exposed in the upper few centimetres of the lunar surface is known as surface exposure age and can be estimated by the use of maturity indices such as grain size, agglutinate content, and the abundance of solar wind elements, *e.g.* ^{36}Ar. It should be noted that the maturity indices are at best semi-qualitative and no definitive measure of surface exposure has yet been established.

Agglutinates constitute on average between 25-30 vol.% of lunar soils, although some very mature soils may contain as much as 60 vol.%. Agglutinate particles are typically <1 mm in diameter, containing droplets of metallic Fe, mainly as fine grained (<10 nm), single domain Fe^0 (Morris, 1976) and also troilite (FeS). The metallic iron is formed either directly by preferential sputtering (Pillinger *et al.*, 1976), discussed in section 1.6.1.1, or by the reaction between FeO in the glass and solar wind H released from the soil during melting (Housley *et al.*, 1970). The agglutinates differ from other lunar impact glasses in the fine grain size of the Fe-metal, the lack of Ni and Co, indicative of meteoritic contamination, and the higher abundances of solar wind gases such as He and H (Housley *et al.*, 1973a; DesMarais *et al.*, 1974a, b). The agglutinate content of a soil increases with maturity and hence can be used as an indicator of its surface exposure age.

A further indicator of surface exposure history is the intensity of ferromagnetic resonance (I_S), normalised to the FeO content of the sample. The ratio I_S/FeO is a measurement of the reduction of ferrous iron Fe^{2+} to superparamagnetic Fe-metal (Fe^0) by solar wind hydrogen which is released from soil grain surfaces during micrometeorite bombardment. The abundance of Fe^0 was shown to correlate with increased exposure age (Tsay *et al.*, 1971; Cadogan *et al.*, 1973; Housley *et al.*, 1973a, b; Pillinger *et al.*, 1973, 1974) and hence the ratio I_S/FeO has been calculated for many lunar soils (Morris, 1976) and is regarded as a valuable maturity parameter.

Other useful indices of maturity are the abundance of solar wind elements, *e.g.* ^{36}Ar, ^{20}Ne and ^{22}Ne, densities of solar flare or cosmic-ray damage trails, mean grain size and depletion of volatile elements, *i.e.* Ga, Cd and Zn.

1.5.4.3. Measurement of antiquity

In addition to maturity, a further important parameter when discussing the exposure of lunar soils and breccias to solar and cosmic-ray radiation is a measurement of how long ago the exposure took place, termed the "antiquity" of the sample. As an individual sample is likely to consist of a variety of grains with differing exposure histories, it has proved difficult to determine a reliable measurement of antiquity.

One measurement of antiquity which has been used to determine correlations

between the time of exposure and the isotopic composition of lunar nitrogen is cosmogenic ^{21}Ne (Kerridge, 1975; Kerridge *et al.*, 1977). Cosmogenic ^{21}Ne is produced by the interaction between galactic cosmic-rays and target elements in the Moon, primarily Mg, Al and Si. The abundances of ^{21}Ne produced by this method outweighs the solar wind contribution of ^{21}Ne to the regolith, and hence can be converted, *via* known production rates into the duration of residence within ~2 m of the lunar surface. However, ^{21}Ne abundances have proved difficult to measure due to the loss of this isotope from lunar samples by thermal diffusion.

One of the more commonly used antiquity parameters is the measurement of parentless ^{40}Ar (Eugster *et al.*, 1980; McKay *et al.*, 1986) in the lunar regolith. This component is derived from the re-implantation of ^{40}Ar into the lunar surface, following the diffusive escape of the radioactive decay products (half-life 1.28 Gyr) of ^{40}K (Manka and Michel, 1971; Yaniv and Heymann, 1972). Lunar atmospheric species are re-implanted into the lunar regolith by UV-induced ionisation and acceleration by the solar wind electric field. Eugster *et al.* (1983) has shown that $^{40}Ar/^{36}Ar$ of trapped Ar in the lunar regolith decreases exponentially with time, similar to the radioactive decay of ^{40}K and hence parentless ^{40}Ar can be used as a chronometer of antiquity. This is discussed further in section 1.6.1.3 in conjunction with the re-implantation of lunar atmospheric species, and in section 1.7.4.1, relating to the isotopic variation in lunar soils and breccias of differing antiquities.

1.5.4.4. Regolith breccias

Another valuable source of lunar material are the regolith breccias. These are shock welded aggregates of rock, mineral and glass in a glassy matrix forming coarse-grained polymict rocks. Prior to breccia formation, the constituent particles may have been exposed on the lunar surface and therefore subjected to meteorite, solar and cosmic-ray bombardment. Although the solar wind can only penetrate the regolith to depths of a few nanometres, solar gases are present to depths of several metres due to the dispersion of these gases by continuous gardening of the regolith. Once breccia formation has occurred, the interior of the breccia is "closed" to external processes and hence these materials provide us with a sample of ancient regolith and solar and cosmic-ray radiation at the time of

consolidation (Hintenberger *et al.*, 1974; Thiemens and Clayton, 1980). The low content of agglutinates observed in regolith breccias has led McKay *et al.* (1986) to suggest that some breccias were formed ~4 Gyr ago during the period of intense bombardments, prior to agglutinate formation. Furthermore, magnetic field measurements (Runcorn *et al.*, 1970, 1977; Stephenson *et al.*, 1974) have suggested that some breccias become closed whilst the Moon was still active and had a molten core.

1.6. The lunar regolith as a collector of solar and cosmic-ray particles

The absence of an appreciable atmosphere or a protective magnetosphere allows solar wind particles, solar and galactic cosmic-ray radiation to interact freely with the lunar surface. Hence, the regolith retains a record of implanted radiation over the lifetime of the Moon (Wänke, 1965) and thus provides valuable information regarding the present and past flux, and the exposure histories of the individual soils and breccias. This section details the major characteristics and effects of implanted solar wind and cosmic-ray radiation on the regolith (Table 1.4).

Solar radiation is the major contributor of hydrogen and most of the noble gases, *i.e.* He, Ne, Ar, Kr and Xe, to the lunar surface (Eberhardt *et al.*, 1970, 1972; Heymann *et al.*, 1970; Hintenberger *et al.*, 1970, 1971, 1974; Hohenberg *et al.*, 1970; Kirsten *et al.*, 1970, 1972; Pepin *et al.*, 1970; Reynolds *et al.*, 1970; Hintenberger and Weber, 1973). However, the origin of nitrogen and carbon in the regolith is far less well constrained with much dispute as to the proportion of these elements that originate from the Sun and the possible non-solar sources which may also contribute carbon and nitrogen to the lunar surface. This is discussed fully in section 1.7, however, for the purpose of discussing exposure effects in the lunar soils, both nitrogen and carbon are assumed to be, at least in part, of solar wind origin.

Radiation source	Implantation Energy	Penetration depth	Major effects
Solar wind	10^3 eV/amu	≤150 nm	Direct implantation, *e.g.* surface correlated noble gases. Reimplantation of lunar atmospheric species, *e.g.* ^{40}Ar. Sputter erosion. Amorphous rims around dust grains.
Solar cosmic rays (associated with solar flares)	10^4-10^8 eV/amu	few mm's to cm's	Radionuclide production, *e.g.* ^{26}Al, ^{53}Mn. Particle track production.
Galactic cosmic rays	≥ 10^6 eV/amu	cm's to metres	Radionuclide production. High density track production. Stable nuclide production, *e.g.* ^{15}N, ^{21}Ne. Production of secondary particles due to nuclear reactions.

Table 1.4. Implantation energies, penetration depths and effects of ionising solar and galactic radiation on the lunar regolith (modified after Walker, 1980).

1.6.1. Effects of solar wind implantation in the lunar regolith

Solar wind particles are implanted into the surface of soil grains with typical energies of ~10^3 eV/amu and implantation depths of up to 150 nm (Table 1.4). Range and depth profiles (Jull and Pillinger, 1977) have indicated that penetration depth is dependent on the atomic number of the implanted species, *i.e.* Kr and Xe are implanted at greater depth than H and He. Other elements, *e.g.* C, N, O, ^{20}Ne and ^{36}Ar, have intermediate implantation depths (~25 nm). It should be noted that solar wind species have been found at depths which exceed their anticipated penetration depth. Although diffusion of the gases following implantation is known to occur (Müller *et al.*, 1976), this observation is due to regolith gardening processes which disperse the gases to depths of up to several metres.

In addition to the accumulation of implanted species in the lunar regolith, the other effects of solar wind implantation are destructive, *e.g.* sputter erosion. These are discussed

in some detail as they are essential in the understanding of the past and present implanted radiation inventory in the regolith.

1.6.1.1. Sputtering reactions on the lunar surface

Sputtering is the process whereby target nuclei are displaced from the host material by incident solar wind ions. With the exception of cometary, meteorite and micrometeorite bombardment, sputtering remains the major cause of erosion on the lunar surface. The upper limit for sputter erosion has been calculated at 0.5 Å yr^{-1} (Bibring *et al.*, 1975), but is more likely less than 0.03 Å yr^{-1} (McDonnell and Ashworth, 1972; McDonnell *et al.*, 1972; Zinner and Walker, 1975). Many workers have endeavoured to calculate sputter erosion rates for the lunar soils, but there has been much dispute over initial parameters for these models. Early workers (Crozaz *et al.*, 1970, 1971; Price and O'Sullivan, 1970) calculated erosion rates of 1-10 Å yr^{-1} but this was due to the combination of erosion by sputtering and micrometeorite bombardment effects. However, the current best values for erosion rates on the lunar surface are 0.043 Å yr^{-1} from simulation experiments (McDonnell and Flavil, 1974) and 0.025 Å yr^{-1} from ion microprobe depth profiling experiments (Zinner and Walker, 1975).

It should be noted that the accumulation of atoms on a grain surface is a net result of two competitive processes: solar wind implantation and sputter erosion. During ion bombardment, atoms are simultaneously gained at the depth of penetration and lost during sputtering as the instantaneous surface advances (Carter and Colligon, 1968; Carter *et al.*, 1972). This results in equilibrium saturation of the grain surface such that the accumulation and loss of implanted species occurs at an equivalent rate. Pillinger (1979) has estimated that for species heavier than He, equilibrium saturation would be reached in ~10^4 years. It should be noted that the high abundance of solar wind H and He is more likely to result in real saturation of soil grain surfaces, *i.e.* the surface is unable to accomodate any further implantation of these species.

One effect of sputter erosion in soil grains is the reduction of ferrous iron Fe^{2+} to superparamagnetic Fe-metal (Fe^0), due to solar wind hydrogen sputtering (Housley *et al.*, 1970; Cadogan *et al.*, 1973; Pillinger *et al.*, 1973, 1974). Although the exact mechanism of

the reduction process is unresolved (Pillinger, 1979), the abundance of Fe^0 is used as a valuable maturity index for exposure of a soil to the solar wind (section 1.5.4.2).

An important point to note is that the above discussion applies only for an individual soil grain and not for the regolith as a whole. The process of sputter erosion may remove an atom from a grain surface, however that atom is likely to be deposited elsewhere in the regolith. The significance of this is that species may not be lost from the bulk regolith.

1.6.1.2. Amorphous rims around lunar soil grains

The solar wind implantation/sputtering process combines to disrupt mineral structure leading to the formation of a rim, approximately 50 nm thick, around the surfaces of many lunar soil grains (Dran *et al.*, 1970; Bibring *et al.*, 1974), caused by the overlapping of non-crystalline particle tracks. A recent study (Keller and McKay, 1997) has revealed the presence of several types of rims, the two most common being amorphous and inclusion-rich. Although the origin of these rims are in debate, the amorphous rims have been identified (Bradley *et al.*, 1996) as due to solar wind radiation damage, while the inclusion-rich are believed to be formed from vapour-deposited material. The amorphous rims are between 20-100 nm thick and have been observed around minerals such as plagioclase, orthopyroxene and cristobalite. They also contain <5 nm Fe-metal grains and have similar major element chemistry to the host soil, although the relative proportions of these elements vary considerably.

1.6.1.3. Re-implantation of lunar atmospheric species

Once implantation of the solar wind has occurred, the atoms are able to diffuse in many directions within the grain. Some species are able to diffuse outward to the surface, and the presence of some of these atoms have been confirmed in the lunar atmosphere (Hodges, 1975). One such species is ^{40}Ar, which is produced in the Moon from the radioactive decay of ^{40}K (Heymann *et al.*, 1970).

A proportion of the atmospheric species are ionised by the solar wind and accelerated into space. The same process is also responsible for re-implanting some of these ions back

into the lunar regolith. The abundance of ^{40}Ar in lunar soil grains was found to far exceed that expected from solar wind implanted ^{36}Ar, *i.e.* $^{40}Ar/^{36}Ar < 10^{-4}$ (Clayton, 1968), or from the production of ^{40}Ar from ^{40}K, and hence the "excess" argon was suggested by Manka and Michel (1971) to be due to the re-implantation of ^{40}Ar from the lunar atmosphere. The $^{40}Ar/^{36}Ar$ obtained from a variety of lunar soils and breccias ranges from 0.4 to 14 (Kirsten *et al.*, 1973; Reynolds *et al.*, 1974).

However, the atmospheric species are re-implanted into lunar soil grains with a similar implantation energy to the solar wind ions (1-2 keV) but with a lower penetration depth, and hence it is difficult to distinguish between the two processes. Such a process, in addition to sputter erosion, the formation of amorphous rims and regolith gardening have complicated the solar wind inventory within lunar soil grains and masked the true exposure histories of the regolith soils.

1.6.2. Solar cosmic-rays

Solar cosmic-ray (SCR) particles are primarily high energy electrons and protons with the presence of a few percent of He and a trace of heavier nuclei (McGuire *et al.*, 1986). They are also known as solar flare (SF) particles as they are associated with the occurrence of solar flares events during periods of high solar activity. The term "solar energetic particles" has also been used by some workers, although this can be mistaken for a noble gas component of the same name (section 1.7.5.2), but of lower energy than solar cosmic-rays (Wieler *et al.*, 1986), hence the term solar cosmic-ray is adopted in this work.

Solar cosmic-ray particle fluxes vary in conjunction with the 11-year cycle of solar activity with an average flux of ~100 protons cm^{-2} sec^{-1} at solar maximum but a negligible flux at solar minimum. Note that the flux quoted is the average flux over ~1 Myr for solar protons with energy $>10^7$ eV. It can be compared to the solar wind proton flux of ~3 $x10^8$ protons cm^{-2} sec^{-1} over the same period (Table 1.4).

Solar cosmic-ray particles have energies ranging from 10^6 eV (electrons) and 10^7-10^8 eV (protons) and will reach the Earth in less than a day. The higher energy of these particles relative to solar wind particles allows a greater implantation depth into the lunar regolith ranging from millimetres for heavier nuclei to centimetres for solar protons and α-

particles.

The resultant effects of implantation of solar cosmic-rays into the lunar surface is to produce particle tracks in lunar soil grains. The particle tracks are damage trails caused by the rapid deceleration of heavy nuclei (Z>20) in the upper millimetres of the regolith. The densities of these tracks are used as an indicator of surface exposure age (Walker, 1975; Reedy *et al.*, 1983). A further effect, is the production of radionuclides, *e.g.* ^{26}Al and ^{53}Mn, as a result of nuclear reactions between solar protons and the target material, in this case Si, Al and Mg (for ^{26}Al) and Fe (for ^{53}Mn). However, the production of these radionuclides is only significant during prolonged periods of high solar cosmic-ray activity.

1.6.3. Galactic cosmic-rays

The galactic cosmic-rays (GCR) originate from outside the solar system, although the sources of these particles are not well known (Simpson, 1983). The cosmic-rays undergo spallation reactions with the interstellar medium resulting in an enrichment in the rare elements such as Li, Be and B and other minor elements (Z<56). The galactic cosmic-ray particles lose energy as a result of interaction with the magnetic fields associated with the solar wind and hence the cosmic-ray flux varies by a factor of 2 over the solar cycle with the highest fluxes occurring during solar minimum.

Galactic cosmic-rays have energies typically $<10^{15}$ eV and penetration depths that range from centimetres to metres in the lunar regolith (Table 1.4). The heavy nuclei are implantated into the lunar regolith at a depth of <10 cm, as they are rapidly stopped due to ionisation energy losses. The rapid slowing of these nuclei results in high densities of particle tracks in some lunar samples (Walker, 1975; Reedy *et al.*, 1983). In comparison, the protons and α-particles penetrate deeper into the regolith and are responsible for the neutron particle cascades, that can penetrate to depths of up to several metres. Neutrons are the dominant particle in the cascades as they are not decelerated by ionisation energy losses. They have typical energies of ~10^6 eV and can only be stopped by interaction with an element lighter than oxygen (Lingenfelter *et al.*, 1972). Reedy *et al.* (1983) calculated that the flux of the secondary neutrons (~13 neutrons cm^{-2} sec^{-1}) is far greater than the flux of the primary protons striking the lunar surface (~2 protons cm^{-2} sec^{-1}).

A further effect of galactic cosmic-rays in lunar soils is the production of radiogenic nuclides, *e.g.* ^{26}Al and ^{23}Mn and many others (discussed in 1.6.2). In addition, nuclear spallation reactions between cosmic-ray elements and target elements in the Moon can produce spallogenic isotopes, *e.g.* ^{15}N from ^{16}O, and ^{21}Ne from Mg, Al and Si. Note that many other stable and radioactive nuclides are also produced.

1.6.4. Meteorite contributions to the lunar regolith

In addition to the implantation of solar wind and cosmic-ray radiation, the lunar surface has also been subjected to meteorite bombardment (of varying intensity and projectile size) during its lifetime. Initial determinations of the meteoritic contribution to the lunar regolith was measured by the contents of Ni and Co in native Fe^0 in lunar soils (Goldstein and Yakowitz, 1971). Fe^0 is present in the form of kamacite (0-6 wt.% Ni), taenite (6-50 wt.% Ni) and tetrataenite (~50 wt.% Ni), with a mean content of 5.5 wt.% Ni (Goldstein and Axon, 1973). It is worth noting that these minerals are also formed by normal crystallisation processes and the reduction of FeO in impact produced silicate melts. However, the data of Goldstein and Yakowitz (1971) utilised only Ni and Co abundances from iron meteorites and hence their limited abundances for these elements were not deemed representative of meteoritic metal as a whole (Misra and Taylor, 1975).

A better method for determining meteorite contributions to the lunar regolith is the use of siderophile (readily soluble in molten Fe) elements, *e.g.* Au, Pt, Ir, Os and Ge (Ganapathy *et al.*, 1970; Wlotzka *et al.*, 1973; Reed and Taylor, 1974). These elements are rare in lunar rocks, compared to FeNi metal, and hence estimates can be made of the quantity of meteoritic material in a soil or breccia. Using this method, Ganapathy *et al.* (1970) and Wasson & Baedecker (1970) have calculated that impacting meteorites contribute 1-2% carbonaceous chondrite material into the lunar regolith.

1.7. Nitrogen and noble gas inventory in the lunar regolith

This section details the current knowledge surrounding the origin of the nitrogen in the lunar regolith, and the theories which have been proposed to account for the nitrogen isotopic variations observed in lunar samples. This is deemed crucial as it forms the basis for the analyses undertaken in this work. Furthermore, the noble gas record in lunar soils is also discussed as most noble gases (except ^{40}Ar and some Kr and Xe) are not indigenous to the Moon and have been shown to be of a solar origin, *e.g.* Eberhardt *et al.* (1972).

1.7.1. Analytical techniques employed for the study of nitrogen and noble gases in lunar samples

1.7.1.1. Stepped heating extraction

Nitrogen abundances and isotopic compositions in lunar soils and breccias have been measured by many workers using a stepped heating extraction technique (Becker and Clayton, 1975, 1977, 1978; Kerridge *et al.*, 1975b, 1992b, 1993; Becker *et al.*, 1976; Kaplan *et al.*, 1976; DesMarais, 1978, 1983; Becker, 1980b; Clayton and Thiemens, 1980; Norris *et al.*, 1983; Carr *et al.*, 1985a, b; Frick *et al.*, 1988; Becker and Pepin, 1989; Kim *et al.*, 1995a, b). Some noble gas measurements have also been obtained by this method (Frick *et al.*, 1988; Becker and Pepin, 1989; Pepin and Becker, 1990). A sample is heated in discrete temperature increments either under vacuum (pyrolysis) or in a pressure of a few torr of O_2 (combustion), and the gas extracted from each temperature step is purified and then admitted into a mass spectrometer for analysis. The isotopic composition of the nitrogen is measured from the $^{28}N_2/^{29}N_2$ ratio as given in Equation 1.1 (section 1.7.1.3). The advantage of the stepped heating technique is that it enables resolution of individual components within a sample, provided these components are liberated at different temperatures. Both the stepped pyrolysis and combustion techniques are used exclusively in this work and the gas extraction procedures are fully described in section 2.4.2.

1.7.1.2. Closed system stepwise etching (CSSE)

Noble gas abundances and isotopic ratios have also been measured using a technique termed closed system stepwise etching (CSSE), whereby the sample is etched in a series of steps using HNO_3 acid at room temperature. The gas released is purified and analysed by mass spectrometry, in accordance with the procedures detailed in Signer *et al.* (1977). The CSSE technique was devised (Wieler *et al.*, 1986) in order to obtain a depth profile of solar implanted noble gases within lunar soils, by increasing the severity of the etch. When compared to stepped pyrolysis, CSSE has the advantage that the effects of thermal redistribution (diffusion) of the gases can be eliminated, as the extraction is conducted at room temperature. Becker and Pepin (1994) suggested that stepped combustion was preferable to CSSE as oxidation of the soil grains in mineral separates can select against glassy contaminants which may contain fractionated solar gases. However, these workers have since utilised an on-line etching technique (Becker *et al.*, 1998). CSSE has been used by many workers for analysis of lunar soils and some gas-rich meteorites (Wieler *et al.*, 1986, 1993, 1996; Benkert *et al.*, 1993; Signer *et al.*, 1993; Pedroni and Begemann, 1994; Wieler and Baur, 1994, 1995; Murer *et al.*, 1997).

1.7.1.3. The delta notation

For nitrogen, all isotopes are expressed in the standard "delta notation" ($\delta^{15}N$) in parts per thousand or "per mil" (‰), and are compared to the universally accepted standard (Urey, 1948) of atmospheric nitrogen (AIR) with a δ-value of 0‰, defined by equation 1.1.

$$\delta^{15}N_{AIR} = \left(\frac{(^{15}N/^{14}N)sample}{(^{15}N/^{14}N)reference} - 1 \right) \times 1000\ ‰$$

which is equivalent to:

$$\delta^{15}N_{AIR} = \left(\frac{(^{28}N_2/^{29}N_2)reference}{(^{28}N_2/^{29}N_2)sample} - 1 \right) \times 1000\ ‰ \qquad \textbf{Equation 1.1.}$$

where $\delta^{15}N$ is in the range of -1000‰ to +∞ ‰.

1.7.2. Origin of nitrogen in lunar soils and breccias

The origin of the nitrogen in the lunar regolith has been the cause of much debate over many years (Becker and Clayton, 1975; Kerridge, 1975, 1980, 1989, 1993; Geiss and Bochsler, 1982, 1991; Ray and Heymann, 1982; Norris *et al.*, 1983; Signer *et al.*, 1986; Frick *et al.*, 1988; Becker and Pepin, 1989; 1994). In this section, the main evidence for a solar origin for the nitrogen is presented (section 1.7.2.1), together with the major observation against this hypothesis (section 1.7.2.2). Note that many other arguments exist, both for and against a solar origin, and these are discussed later in this chapter in conjunction with isotopic composition data (section 1.7.3.1) and noble gas and carbon abundances (section 1.7.5 and 1.7.6 respectively).

1.7.2.1. Evidence for a solar origin for the nitrogen in lunar soils and breccias

Several observations have led to the proposal that the majority of nitrogen in the lunar regolith originates from the solar wind (Müller, 1974; Kerridge *et al.*, 1975a; Clayton and Thiemens, 1980; Frick *et al.*, 1988; Kerridge, 1993). Firstly, the nitrogen yields liberated from lunar soils, typically 50-150 ppm, significantly exceeds the low abundances of nitrogen (typically <1 ppm) in lunar rocks of presumably indigenous origin (Müller, 1974; Petrowski *et al.*, 1974; Becker and Clayton, 1975; Kerridge *et al.*, 1975a). Secondly, correlations between the nitrogen content and grain size of separated soil fractions (Goel and Kothari, 1972; Holland *et al.*, 1972a; Müller, 1974) have revealed a surficial location for the nitrogen, with the highest abundances of nitrogen obtained for the finest grain size fractions. This has been confirmed by stepped heating extractions, whereby the lowest temperature release (<900°C) is attributed to the nitrogen residing on the surface of mineral grains (Becker and Clayton, 1975, 1977; Becker *et al.*, 1976). A similar grain size correlation has also been observed for the solar noble gases (Eberhardt *et al.*, 1970). In addition, Müller (1974) and Kerridge *et al.* (1975b) also observed a positive correlation between nitrogen content and solar wind implanted species, *e.g.* ^{36}Ar, which suggested a similar origin for both elements. Whether or not the surface location of the nitrogen and noble gases are sufficient evidence for a solar origin are discussed further in section 1.7.4.1.

1.7.2.2. "Excess" nitrogen in the lunar regolith

The major problem with advocating a solar origin for the nitrogen in the lunar regolith is the enrichment of nitrogen when compared to the solar noble gases. It has been shown (Kerridge, 1980, 1993; Becker and Pepin, 1989; Frick *et al.*, 1988) that the $^{14}N/^{36}Ar$ ratio (herein referred to as $N/^{36}Ar$) in the lunar regolith is a factor of 10 higher than the solar value of ~37 inferred by Cameron (1982) and Anders and Grevesse (1989), and $^{14}N/^{132}Xe$ is overabundant by a factor of three. A full review of the nitrogen enrichment problem is given in Becker (1995). In order to invoke a solar origin for lunar regolith nitrogen, one of the following conditions would have to apply:

1). The $N/^{36}Ar$ solar value has been underestimated, *i.e.* nitrogen is enhanced in the solar corpuscular radiation by a factor of 10 (Becker and Pepin, 1994). However, recent measurements of this ratio in solar energetic particles (Brenemann and Stone, 1985) of 45 ± 8, within error limits, are similar to the estimated solar abundances of Cameron (1982) and Anders and Grevesse (1989), and hence this is not a viable explanation.

2). Assuming a solar value for $N/^{36}Ar$, non-solar nitrogen has contributed to the lunar regolith (Geiss and Bochsler, 1982; Signer *et al.*, 1986; Bochsler, 1994; Wieler *et al.*, 1999). However, in order to produce the observed excess, at least 90-95% of the nitrogen must be of a non-solar origin, either as a single or multiple components. This contradicts the close correlation observed between nitrogen content and the solar noble gases (section 1.7.2.1). The suggested sources of non-solar nitrogen are discussed in section 1.7.4.2.

3). A significant abundance of ^{36}Ar and heavier noble gases has been lost from the lunar regolith by diffusion (Frick *et al.*, 1988). This has been suggested by proponents of a solar origin for lunar nitrogen and would require ^{36}Ar losses of 90%, assuming a solar value for $N/^{36}Ar$. If a combination of 1) and 3) were effective the ^{36}Ar losses required to produce the observed trends would be reduced. However, some recent noble gas data (Wieler and Baur, 1995; Wieler *et al.*, 1996) have shown that this scenario is unlikely and their observations are discussed in section 1.7.5.3.

1.7.3. Stepped heating extraction of lunar soils and breccias

The stepped heating (primarily pyrolysis) extractions of lunar soils and breccias by the aforementioned workers (section 1.7.1.1) have revealed a characteristic nitrogen release profile. Most lunar soils and breccias contain 50-150 ppm of nitrogen, which is liberated across two distinct temperature ranges, typically 600-900°C and 900-1200°C.

1.7.3.1. Isotopic components in lunar soils and breccias

Stepped pyrolysis extractions on a variety of lunar soils and breccias have revealed a complex isotopic profile, and resolution of four distinct nitrogen components. The component which is liberated at the lowest temperature (<600°C) has been attributed by all workers to terrestrial contamination with a $\delta^{15}N$ value of ~0‰. Most workers believe this component to be completely removed by 600°C and hence it is not discussed further in this work. Lunar soils have been shown to liberate an isotopically heavy (^{15}N-rich) nitrogen component at a temperature of 800°C with $\delta^{15}N$ = +120‰, followed by an isotopically light component (^{14}N-rich) at 900°C with $\delta^{15}N$ = -105‰ (Becker and Clayton, 1975, 1977; Becker *et al.*, 1976). The theories which have been proposed to account for the isotopic variation between these components are discussed in section 1.7.4. In addition, most lunar soils and breccias also liberate a second isotopically heavy component at high temperatures (>1000°C). This component is identified by high $\delta^{15}N$ values and an increase in cosmogenic ^{38}Ar. It is attributed by all workers to the production of spallogenic ^{15}N from the interaction between galactic cosmic-rays and ^{16}O in the regolith (section 1.6.3). Note that if this component was pure spallogenic nitrogen the $^{15}N/^{14}N$ ratio would be ~1. The resulting isotopic profile is illustrated in Figure 1.5a. It has been observed to resemble a V-shape and is termed the heavy-light-heavy profile (Becker and Clayton, 1975; Thiemens and Clayton, 1980).

The isotopic profile for lunar breccias display a similar shape to that obtained for lunar soils, although the isotopic compositions are markedly different. Previous analyses of regolith breccia A79035 (Clayton and Thiemens, 1980; Carr *et al.*, 1985a; Frick *et al.*, 1988) revealed that the low temperature, isotopically heavy component, was not present, with a

$\delta^{15}N$ value close to 0‰. Although the isotopically light nitrogen component was liberated at a similar temperature to the equivalent component in lunar soils, *i.e.* 900°C, it displayed a significantly lighter composition with a $\delta^{15}N$ value of ~-210‰. This result has also been confirmed for breccias from other sites (Thiemens and Clayton, 1980; Becker and Epstein, 1981; Carr *et al.*, 1985b).

The story is further complicated by the discovery that the isotopic profile is more complex than previously thought (Carr *et al.*, 1985a, b). A pyrolysis extraction of lunar breccia A79035 (Carr *et al.*, 1985a) revealed the presence of a second light component at a temperature of 1050°C, separated from the lower temperature light nitrogen (900°C) by an isotopic plateau. The isotopic profile follows a heavy-light-heavy-light-heavy trend which has been observed to resemble a W-shape and is illustrated in Figure 1.5b. The profile was identified due to the very high temperature resolution which was employed for the first time in the extraction and has provided the basis for the current study. It should be noted that further investigations by Carr *et al.* (1985b) also revealed the presence of the W-shaped profile during pyrolysis extractions of other lunar breccias, but no extractions were undertaken to determine whether a similar phenomenon occurred during stepped combustion extractions.

1.7.3.2. Definitions of the terminology used in this work

The stepped pyrolysis and combustion data obtained in this study are displayed by a stepped release profile, as shown in Figures 1.5a and b. The horizontal axis represents the extraction temperature (°C), and is displayed on a scale from 0-1200°C. The histogram plot denotes the nitrogen yield, in units of ppm $°C^{-1}$, between successive temperature steps, *e.g.* from 500-600°C, and is given on the left hand axis. The line plot denotes the isotopic composition of the nitrogen, expressed in ‰ as given in Equation 1.1, and is shown on the right hand axis.

Figures 1.5a and b also illustrate the terminology employed in this study to define the individual nitrogen components in lunar soils and breccias. These definitions differ slightly from the terminology adopted by previous workers as no consistent terminology was employed by these groups. It should be noted that no yields or isotopic compositions have

been included on the figures as these vary considerably between samples.

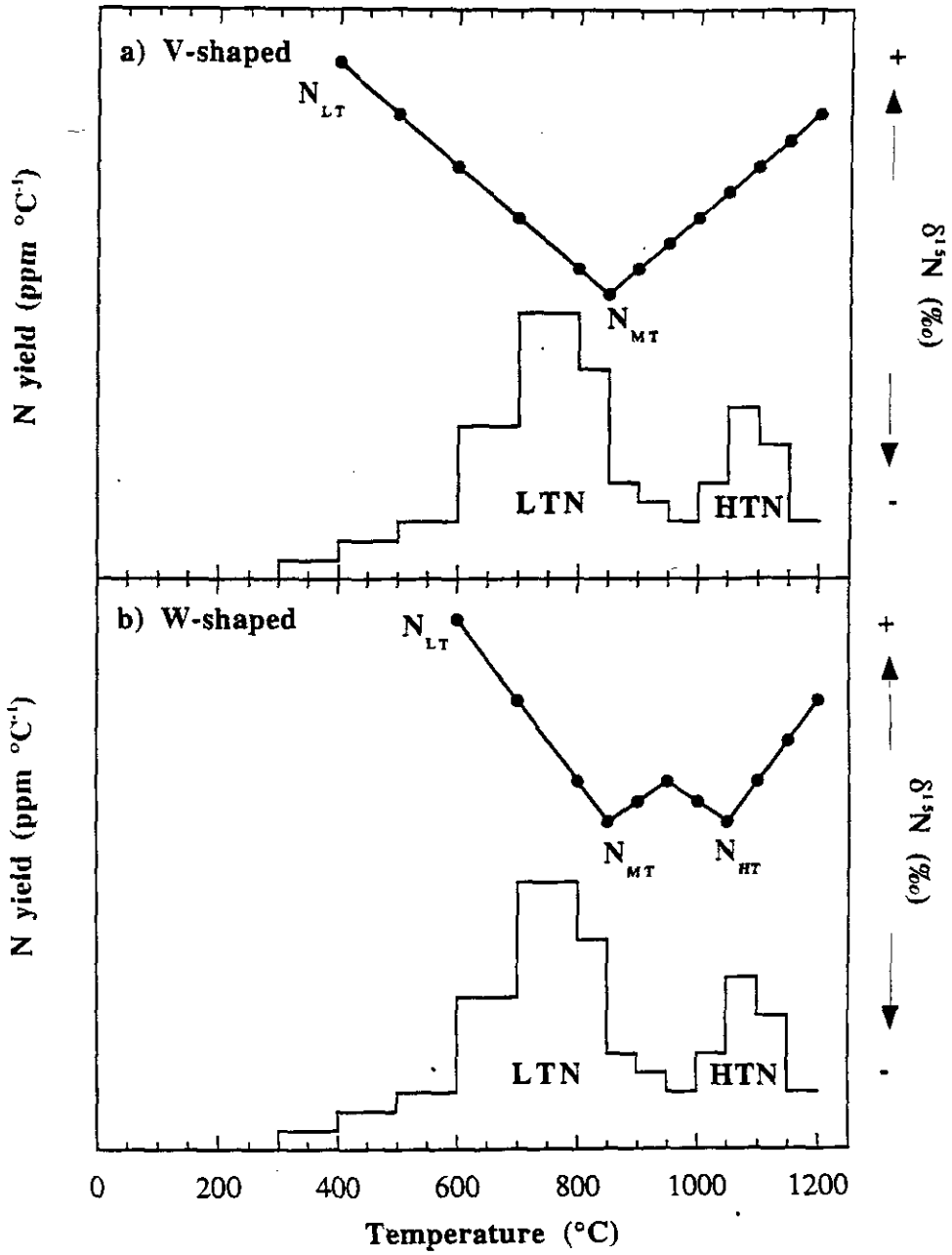

Figure 1.5. An illustration of the V-shaped (Figure 1.5a) and W-shaped (Figure 1.5b) isotopic profile obtained for lunar samples during stepped heating extraction, and a definition of the terminology used for nitrogen components obtained in this work.

For the purpose of this work, the nitrogen liberated from lunar samples across the temperature ranges 600-1000°C and 1000-1200°C are termed "low temperature nitrogen" (or LTN) and "high temperature nitrogen" (or HTN) respectively. Only the lowest temperature,

isotopically heavy component and the two light components (where resolved) are termed. These components, defined simply as the observed $\delta^{15}N$ maxima or minima, are termed N_x where x defines the low- (LT), mid- (MT) or high-temperature (HT) of the release, *i.e.* the low temperature, heavy component is termed N_{LT}. The low temperature (<600°C) component and the high temperature, isotopically heavy components (~1200°C) do not require redefinition as all workers currently agree on their origin.

1.7.4. The models proposed to account for the observed nitrogen isotopic variations in the lunar regolith

The bulk isotopic composition ($\Sigma\delta^{15}N$) liberated from lunar soils and breccias range from $\delta^{15}N$ = -170‰ (Clayton and Thiemens, 1980) to $\delta^{15}N$ = +100‰ (Kerridge, 1975), although individual nitrogen components within these samples may have isotopic compositions which exceed these extremes (section 1.7.3.1). The explanation for the isotopic variation of $^{15}N/^{14}N$ (~30%) has been the cause of much debate over the last 20 years and is currently unresolved. Two main schools of thought exist to account for the observed variations and the proposed models are discussed below.

1.7.4.1. Secular variation of the solar wind

Those workers who advocate a solar origin for the nitrogen in the lunar regolith (section 1.7.2.1) have proposed that the observed $\delta^{15}N$ variation is due to a secular variation of 20-50% of $^{15}N/^{14}N$ in the solar convective zone during the lifetime of the regolith (Becker and Clayton, 1975; Kerridge, 1975, 1980, 1989; Ray and Heymann, 1980). This model was based on the observation that the abundance of nitrogen, and solar wind noble gases, integrated over the depth of the regolith, exceeds by a factor of ~3, the abundance expected from implantation of the present solar-wind flux over the last 4 Gyr (Geiss, 1973; Clayton and Thiemens, 1980), and hence implied that the solar wind flux was greater in the past. Furthermore, the $^{15}N/^{14}N$ ratio of a lunar soil was shown to decrease with increasing antiquity of the sample, *i.e.* how long ago the exposure took place. The antiquity of a sample can be measured by trapped $^{40}Ar/^{36}Ar$, or the content of spallogenic ^{21}Ne (section

1.5.4.3). Becker and Pepin (1989) demonstrated that ilmenite grains separated from ancient regolith breccias, contained lower $^{15}N/^{14}N$ ratios than ilmenites from a recent soil. The study of lunar soils of different antiquities led Kerridge (1989) to propose that the $^{15}N/^{14}N$ ratio in the lunar regolith had increased by 50% from 3 to 1.5 Gyr ago.

Advocators of the secular variation model have attributed the low temperature isotopically heavy component (N_{LT}) to recently implanted solar wind nitrogen, located on the grain surfaces of lunar minerals. The isotopically light component (N_{MT}) is attributed to the ancient solar wind, originally surficially implanted on grain surfaces, but since incorporated into agglutinates and complex particles, by regolith gardening processes. The deeper siting of this nitrogen results in a higher release temperature during stepped heating extraction (Becker and Clayton, 1975, 1977).

Studies of lunar regolith breccias have added weight to the argument that solar wind nitrogen was isotopically lighter in the past. Most breccias formed up to ~3 Gyr ago, *e.g.* A79035 (Clayton and Thiemens, 1980), therefore since their formation they have remained "closed" to any subsequent bombardment or implantation processes (section 1.5.4.4). The absence of a low temperature, isotopically heavy component in regolith breccias, implies that the breccias have not been exposed to the recent solar wind and hence the isotopically light nitrogen signifies the solar wind composition up until the time of consolidation (Clayton and Thiemens, 1980).

However, there are several problems with advocating the secular variation model to account for the nitrogen isotopic variation in the lunar regolith. These are discussed below.

1). The secular variation model argues that the isotopic variation observed in lunar soils and breccias is caused by processes occurring within the convective zone. This derives from the observations (von Steiger and Geiss, 1989) that the composition of solar radiation for most elements (except those with a low first-ionisation potential) corresponds well with solar photospheric abundances. Although several possible mechanisms have been proposed, each is in contradiction with our current understanding of solar physics. These include an increased production of ^{15}N by ^{16}O spallation in the Sun, accretion by the Sun of ^{15}N-rich material from outside the solar system, a change in the solar wind source dynamics, contamination of the solar surface by ^{14}N-rich matter, and a change in the solar wind flux at

the lunar surface. The mechanisms are discussed by previous workers (Kerridge, 1975, 1980; Kerridge *et al.*, 1977; Ray and Heymann, 1980; Geiss and Bochsler, 1982) and the major problems surrounding each mechanism is given in Kerridge (1989). It should be noted that the magnitude of variation which is required for each of these mechanisms is insufficient to account for the observed results.

2). Recent workers (Norris *et al.*, 1983; Kerridge *et al.*, 1992b) has disputed the theory that the isotopically light nitrogen is attributed to the release of that element from complex particles such as agglutinates. Their independent work on agglutinate separates from lunar soil A12023 (Norris *et al.*, 1983), and lunar breccia A79035 (Kerridge *et al.*, 1992b) have shown that the nitrogen liberated from these fractions is not isotopically lighter than the respective sample from which the agglutinates were separated. Becker and Pepin (1989) and Kerridge *et al.* (1992b) also showed that a similar isotopic release pattern was also obtained from pure mineral separates, *i.e.* ilmenite and pyroxene, which were devoid of agglutinates. In addition, a study of A67601 plagioclase, with a recent exposure history of 49 Myr, has revealed a $\delta^{15}N$ variation from +49‰ to ~-56‰ (Kim *et al.*, 1995b). This implies that the light nitrogen cannot be due to ancient solar wind, as it would not be expected to be present (even in moderate amounts) in a young soil. The above studies have suggested that the isotopically light nitrogen is present in all types of regolith soil and not restricted to complex particles, such as agglutinates.

3). The secular variation model is based on the assumption that nitrogen located on the surface of lunar soil grains is implanted from the recent solar wind. However, the surface location of the nitrogen is not necessarily evidence for a solar origin, as during stepped heating extractions ^{40}Ar is released conjointly with solar wind ^{36}Ar, and, with the exception of the first few steps, reveal constant $^{40}Ar/^{36}Ar$ ratios (Frick *et al.*, 1988). The origin of parentless ^{40}Ar in the regolith, from the re-implantation of lunar atmospheric species, has been discussed in section 1.5.4.3.

4). The secular increase in $^{15}N/^{14}N$ of 50%, proposed by Kerridge (1989), is not consistent with the magnitude of variation exhibited by the solar noble gases. Noble gas data have revealed a 50% decrease in the ratios $^{4}He/^{36}Ar$ and $^{132}Xe/^{36}Ar$, a 20% decrease in the $^{4}He/^{3}He$ ratio and a 3% increase in the $^{20}Ne/^{22}Ne$ during the same period as the $^{15}N/^{14}N$ variation (Eberhardt *et al.*, 1972; Geiss, 1973; Kerridge, 1980; Pepin, 1980; Becker and

Pepin, 1989). However, it should be noted that Kerridge *et al.* (1991b) has stated that these variations do not necessarily reflect a compositional change in the solar convective zone, and for many workers, *e.g.* Wieler and Baur (1995), the proposed variations, including $^{15}N/^{14}N$, are controversial.

1.7.4.2. Isotopic mixing with non-solar nitrogen

The observation of "excess" nitrogen in the lunar regolith (section 1.7.2.2), and the problems associated with explaining the magnitude of the $\delta^{15}N$ variation when compared to noble gas data or current solar models, have led to the suggestion that the observed variation is due to mixing of solar wind nitrogen with one or several non-solar sources (Becker and Clayton, 1975; Geiss and Bochsler, 1982, 1991; Ray and Heymann, 1982; Norris *et al.*, 1983; Frick *et al.*, 1988). The potential sources which have been proposed for the "excess" nitrogen are indigenous lunar nitrogen (Becker and Clayton, 1975), a fractionated lunar atmosphere (Ray and Heymann, 1982), primitive meteoritic nitrogen (Norris *et al.*, 1983) and terrestrial atmospheric nitrogen (Geiss and Bochsler, 1991). However, it should be noted that if the "excess" nitrogen is of a non-solar origin, the magnitude of the excess implies that the lunar regolith is dominated by that component, *i.e.* assuming ^{36}Ar is retained with ~100% efficiency (Geiss and Bochsler, 1982, 1991; Bochsler, 1993), >90% of regolith nitrogen must be non-solar. This has led Kerridge (1993) to suggest that the trend in $^{15}N/^{14}N$ must reflect a variation in the isotopic composition, not just the proportion, of the non-solar component, and that a hypothetical non-solar nitrogen component would need to have a flux which resembles the solar wind and an isotopic composition which varies by ~40% over the lifetime of the regolith.

An additional problem when attempting to constrain the origin of lunar nitrogen is to determine a mechanism which can produce the required isotopic variation without affecting the nitrogen elemental abundance more than is observed (Kerridge, 1980, 1989; Kerridge *et al.*, 1992a). This has been the major problem when advocating isotopic mixing between a ^{15}N-enriched solar wind and a ^{14}N-enriched non-solar component (Becker and Clayton, 1975; Geiss and Bochsler, 1982, 1991; Norris *et al.*, 1983). However, isotopic mixing between ^{14}N-enriched solar radiation and a ^{15}N-enriched non-solar component (Ray and

Heymann, 1982) is even more problematic, due to the difficulty of locating a suitably enriched ^{15}N source in the solar system (Kerridge, 1980; Prombo and Clayton, 1985). It is not clear how many non-solar components have combined to obtain the observed trends but initial modelling studies by Kerridge *et al.* (1992a) have indicated that two component mixing may be too simplistic.

1.7.4.3. Recent theories to account for the nitrogen isotopic variation

In addition to the theories discussed above regarding the origin for the nitrogen in the lunar regolith, Kerridge *et al.* (1992a) have suggested that the isotopically heavy and light components may represent different energies of solar implantation, as opposed to different generations of solar wind particles. These workers have attributed the isotopically heavy nitrogen to solar wind implanted particles at relatively low energies, hence located at the outer layers of the sample, whereas the light nitrogen is attributed to solar energetic particles, located at depth within the sample due to their higher implantation energy. This theory may be analogous to that proposed for the solar noble gases (Wieler *et al.*, 1986), *i.e.* $^{20}Ne/^{22}Ne$, which are discussed in section 1.7.5.2.

In addition, the study of a plagioclase separate from A67601 (exposure age = 49 Myr) and lunar rock A68815 (exposure age = 2 Myr) have led to an estimate of the isotopic composition of the recent solar wind with $\delta^{15}N = +38 \pm 6‰$ (Kim *et al.*, 1995a, b). These workers postulate that the solar wind variation does not display a linear trend and has undergone two isotopic extremes to a minimum of <-280‰ and a maximum of >+160‰ in the last 3.5 Gyr. A recent study (Kerridge, 1993) has also shown that a correlation of $\Sigma\delta^{15}N$ with antiquity, *i.e.* $^{40}Ar/^{36}Ar$ (section 1.5.4.3), is more complex than previously thought as the earlier study (Kerridge, 1989) was based on a sample population that was too restrictive and had antiquities of <2 Gyr. Kerridge (1993) has shown that the $\delta^{15}N$ of lunar samples initially experienced a long term decrease which reached a minimum around 2 Gyr ago, followed by a more recent increase to beyond its original value.

1.7.5. Noble gas abundances and isotopic compositions in the lunar regolith

As previously discussed in section 1.6. the majority of the noble gases in lunar soils and breccias are solar in origin. Noble gas concentrations are highest in lunar soils and lowest in lunar rocks and follow an inverse correlation with grain size, consistent with the surface location of implanted solar wind gases (Eberhardt *et al.*, 1970). The noble gas concentrations for lunar breccias are intermediate to those for lunar soils and rocks.

The retention efficiency of noble gases in the lunar regolith was shown to increase with atomic weight of the implanted species, *i.e.* H and He are poorly retained whereas Kr and Xe are efficiently retained, with the best retention efficiencies observed for carbon and nitrogen (DesMarais *et al.*, 1974a). However, the study of He, Ne and Ar in mineral separates from regolith soils (Signer *et al.*, 1977; Wieler *et al.*, 1980, 1983) have shown that pristine mineral grains, most notably ilmenite and pyroxenes, have the highest retentivities for solar noble gases and reveal isotopic ratios consistent with the Solar Wind Composition Experiment (Geiss *et al.*, 1972b). Hence, recent studies of noble gases in lunar soils and breccias have concentrated on the analysis of single or multi-grains of lunar minerals, primarily ilmenite and pyroxene, using either stepped pyrolysis or CSSE extraction techniques (section 1.7.1.1 and 1.7.1.2 respectively). Some recent studies have also extracted noble gases from lunar minerals using a laser vapourisation technique (Nichols *et al.*, 1994; Humbert *et al.*, 1997; Wieler *et al.*, 1999).

1.7.5.1. Noble gas studies of lunar soils and breccias by stepped heating extraction

Stepped heating extractions of ilmenites, separated from lunar soils and breccias of differing antiquities (Frick *et al.*, 1988; Becker and Pepin, 1989; Pepin, 1989) have revealed the presence of two distinct noble gas components. The first component, liberated at a temperature of ~700°C, displays elemental abundances which compare well to solar values (Cameron, 1982; Anders and Grevesse, 1989), and $^{4}He/^{3}He$ and $^{20}Ne/^{22}Ne$ ratios, similar to that obtained by the Solar Wind Composition Experiment (Table 1.2). The second component is liberated at a higher temperature, and hence is believed to be more deeply sited. Elemental abundance data, reveal that this component is depleted in ^{4}He and ^{22}Ne,

but is enriched in ^{84}Kr and ^{132}Xe, when normalised to ^{36}Ar (Becker and Pepin, 1989). These workers have suggested that the high temperature component, is produced by the diffusion, and subsequent fractionation, of originally surface sited solar wind implanted gases, whereby the light gases are diffused outwards from the soil and the heavy gases are diffused into mineral grains. However, in order to account for the observed depletions and enrichments in noble gas abundances, Frick *et al.* (1988) estimated that between 70-95% of implanted solar wind Xe would have to be lost, with corresponding higher losses for the lighter solar noble gases.

1.7.5.2. Noble gas studies of lunar soils and breccias by CSSE

Noble gas studies of lunar soils and breccias by CSSE also reveals the presence of two distinct components (Wieler *et al.*, 1986; Benkert *et al.*, 1993; Wieler and Baur, 1994). The resolution of these components is most obvious for neon whereby the initial release displays $^{20}Ne/^{22}Ne = 13.8$ (Benkert *et al.*, 1993), close to the ratio in the solar wind (Table 1.2). Progressively more severe etching liberates $^{20}Ne/^{22}Ne$ ratios which tend towards a value of 11.2. As this component is more deeply sited than solar wind Ne, and hence implanted at a higher energy, it has been attributed to solar energetic particles (Wieler *et al.*, 1986) and termed SEP. Etique (1981) has shown that this component can reside in lunar soils to depths of up to 30 μm. It has also been identified, or inferred, in the majority of lunar samples and some gas-rich meteorites (Pedroni *et al.*, 1991; Benkert *et al.*, 1993). Recent space probe measurements (Selesnick *et al.*, 1993) have shown that the $^{20}Ne/^{22}Ne$ ratio of 11.2 in lunar soils may be close to that obtained from direct measurement of solar energetic particles. However, the SEP noble gas component in the regolith is an order of magnitude too abundant to be accounted for by solar energetic particles of typical energies ($\sim 10^7$ eV/amu). Wieler *et al.* (1986) have suggested that a proportion of the SEP component could represent a low energy, *i.e.* $<10^5$ eV/amu, SEP component, of higher flux than the spacecraft SEP measurements, and could constitute up to 50% of the total implanted solar Ne (Wieler *et al.*, 1986; Benkert *et al.*, 1993). Furthermore, the SEP-Ne $^{20}Ne/^{22}Ne$ of 11.2 is close to the ratio of 10.6 obtained for a solar flare Ne component in meteorites (Black, 1972).

Similar to the observations for Ne, etching of lunar soils also reveal a decrease in $^{36}Ar/^{38}Ar$ with increasing depth in regolith mineral grains, from a value of ~5.5 to 4.9 (Wieler *et al.*, 1986). The initial release has been identified by these workers as implanted solar wind argon, and its $^{36}Ar/^{38}Ar$ has been confirmed by many other workers (Warasila and Schaeffer, 1974; Frick *et al.*, 1975; 1988; Becker *et al.*, 1986), whereas the deeper sited component is attributed to solar energetic particles (Wieler *et al.*, 1986; Benkert *et al.*, 1993). The decrease in $^{36}Ar/^{38}Ar$ is also due to the contribution of spallogenic ^{38}Ar at depth within the sample (Frick *et al.*, 1975).

1.7.5.3. Recent noble gas observations

Recent noble gas data (Wieler *et al.*, 1996; Wieler and Baur, 1995) have shown that Ar:Kr:Xe ratios are constant in single grains from individual lunar soils, and hence have conserved the true relative abundances of these elements in the solar wind. This implies that the excess nitrogen cannot be accounted for by losses of ^{36}Ar by diffusion as discussed in point 3 in section 1.7.2.2. Furthermore, Wieler and Baur (1995) has suggested that the enrichment, above solar values, of $^{132}Xe/^{36}Ar$ in the lunar regolith (Cameron, 1982; Anders and Grevesse, 1989) indicate an enrichment of ^{132}Xe in the source region of the solar wind. It has been observed (Cook *et al.*, 1980; Meyer, 1985; Anders and Grevesse, 1989) that elements with first ionisation potential (FIP) ≤10 eV are 4-5 times more abundant in the solar wind and SEP's than in the solar photosphere. This is believed to be due to ion-neutral separation in the chromosphere (von Steiger and Geiss, 1989).

1.7.6. Carbon and hydrogen abundances in the lunar regolith

1.7.6.1. Hydrogen abundances and isotopic compositions in lunar soils and breccias

Hydrogen abundance measurements in lunar soils and breccias have suggested that the majority of hydrogen is located either on grain surfaces or within agglutinates (DesMarais *et al.*, 1974b; Epstein and Taylor, 1975). Typical hydrogen abundances in lunar soils and regolith breccias are 50-100 μg/g, compared to <1 μg/g in lunar rocks. In

addition, hydrogen isotopic composition measurements (Epstein and Taylor, 1970, 1971, 1972, 1973; Friedman *et al.*, 1970, 1971; Hintenberger *et al.*, 1970) have shown that the ratio of deuterium to hydrogen (D/H) in the lunar regolith is depleted by a factor of three, when compared to the terrestrial D/H ratio of 1.5×10^{-4}. Although contamination, *e.g.* terrestrial water, can mask the true isotopic composition of the hydrogen in the lunar regolith, it has proved possible to correct for this (Epstein and Taylor, 1973) to obtain δD for trapped hydrogen of -1000‰, *i.e.* no deuterium. The absence of deuterium on the solar surface is due to its destruction early in the Sun's history, and hence it is not mixed to the surface. The δD ratio is calculated by a comparable method to that for nitrogen (Equation 1.1), with Stardard Mean Ocean Water (SMOW) as the internationally recognised standard. Hydrogen also displays substantial diffusive loss from grain surfaces hence the soils do not display typical solar H/He ratios. Furthermore, although the surface location of the hydrogen is not conclusive proof of a solar origin (see discussion on ^{40}Ar, section 1.7.4.1), the aforementioned workers have advocated the solar wind as the origin of the hydrogen. However, because of the low D/H ratio in the lunar soils, it is believed that any deuterium observed at high temperatures may be associated with cosmic-ray spallation (Epstein and Taylor, 1972).

1.7.6.2. Carbon abundances and C/N ratios in lunar soils and breccias

Lunar soils and breccias contain 100-150 ppm of carbon, in contrast with lunar rocks which contain typically <10 ppm. Carbon analysis have been performed by many workers (Moore *et al.*, 1970, 1971, 1972, 1973; Kaplan *et al.*, 1970, 1976; Gibson and Moore, 1972, 1973; DesMarais *et al.*, 1973, 1975; Chang *et al.*, 1974b; Petrowski *et al.*, 1974; Basu *et al.*, 1975; Kerridge *et al.*, 1975b, 1978; Becker *et al.*, 1976; Filleux *et al.*, 1978). Studies of grain size fractions of lunar soils have shown (DesMarais *et al.*, 1975) that ~50% of the carbon is surface correlated, *i.e.* enriched in the finer grain sizes. Filleux *et al.* (1978) showed that 30-50% of the carbon was located in the outer 0.5 μm of grains; a result independently confirmed by Becker *et al.* (1976). The surficial location of the carbon has led the aforementioned workers to infer that the carbon in the lunar regolith is implanted from the solar wind, and retained in a similar manner to nitrogen. Kerridge *et al.* (1975b)

and DesMarais (1978) have suggested that ~90% of the total lunar carbon is believed to be from solar wind implantation and ~10% of indigenous carbon. In addition, there is a trace amount of carbon due to meteorite contamination of the lunar surface (section 1.6.4). Deuterated acid dissolution of lunar soils (Abell *et al.*, 1970) have shown that 15-25% of carbon is in some form of chemically combined state, *i.e.* CH_4 and deuterocarbons, termed C_{hyd} (Cadogan *et al.*, 1972; Pillinger *et al.*, 1972, 1973, 1974; Bibring *et al.*, 1974). These species follow the observed correlation between concentration and lunar surface exposure and have inferred a solar wind origin for the carbon (Abell *et al.*, 1971; Cadogan *et al.*, 1971, 1972; Holland *et al.*, 1972a; Chang *et al.*, 1974a, b).

Evidence for a secular increase in $^{13}C/^{12}C$ in lunar soils and breccias has been proposed (Becker, 1980b; Becker and Epstein, 1981), although the magnitude of the variation is ~25% that exhibited for nitrogen. The $\delta^{13}C$ values are calculated in a similar way to $\delta^{15}N$ (equation 1.1), using Pee Dee Belemnite (PDB) as the internationally accepted standard. On the basis of the minimal mass difference between carbon and nitrogen, a similar magnitude of variation would be expected if both elements originated from the same source. Carbon and nitrogen are produced by similar nucleosynthetic processes, during the evolution of a main sequence star to a red giant, where the dominant reaction is the conversion of 4 ^1H atoms to ^4He, as part of the initial stage of the CNO cycle. However, despite a strong correlation between carbon and nitrogen abundances in lunar soils, only a weak correlation is evident between $\delta^{13}C$ and $\delta^{15}N$ (Becker, 1980). This detracts from a mass-dependent fractionation process as a mechanism for causing an increase of ^{15}N in the solar wind.

The C/N ratios obtained for a variety of Apollo and Luna soils typically range from 1-2 (Moore *et al.*, 1971; Holland *et al.*, 1972b; Simoneit *et al.*, 1973a, b), with ratios between 1.25-1.65 for a suite of Apollo 16 soils (Kerridge *et al.*, 1975b). These ratios are also similar to the equivalent ratios of 1.06 and 1.1 in the solar photosphere and corona respectively (Anders and Grevesse, 1989). However, the C/N ratios obtained for lunar soils (Kerridge *et al.*, 1978) are approximately a factor of two lower than the solar system values of 3.2 (Anders and Grevesse, 1989). This implies that if ^{36}Ar was retained with ~100% efficiency, not only would >90% of the nitrogen need to be of non-solar origin (section 1.7.4.2), but also 70-80% of the carbon. This is deemed unlikely (Becker, *pers. comm.*).

Furthermore, Wieler and Baur (1995) have stated that as the C/N ratios in SEP's (Brenemann and Stone, 1985) are similar to solar values (Cameron, 1982; Anders and Grevesse, 1989), at least 50% of lunar nitrogen is non-solar, although this may be higher due to the contribution of meteoritic carbon to the lunar regolith.

1.8. Aims and objectives of this work

Low temperature resolution stepped heating nitrogen extractions of lunar soils and breccias have revealed an isotopically heavy-light-heavy or V-shaped profile which was later observed to be more correctly defined as a W-shaped profile (Carr *et al.*, 1985a) during high resolution pyrolysis extractions. Nitrogen isotopic variations of 20-50% have been observed both between individual soils and breccias and within a single sample, and the mechanism for the variation is currently unresolved. Several theories invoking either a solar origin or solar wind mixing with several non-solar sources have been proposed to explain the observed variations.

The aims of this work are to investigate the variations in $^{15}N/^{14}N$ observed during stepped heating extraction of a variety of lunar soils and breccias. In order to constrain the isotopic composition and origin of individual nitrogen components, a series of high-resolution, stepped combustion and pyrolysis extractions are undertaken, using temperature increments of 10°C, constituting the highest resolution performed to date. To determine the location of the isotopically heavy and light nitrogen within lunar soils, a study of grain size, magnetic and density separates of a typical lunar soil, A12023 (Chapter 3) is undertaken. Unfortunately, due to sample availability, no pure mineral separates, *i.e.* ilmenite, could be analysed. In addition, the occurrence of the W-shaped isotopic profile, observed in pyrolysis extractions of lunar breccias by Carr *et al.* (1985a, b), is investigated to determine whether it is also observed for lunar soils, and in stepped combustion extractions of soils and breccias. A study of the differences in abundance and isotopic profiles using the two extraction techniques has also been undertaken. Comparisons of the nitrogen release characteristics are made for a variety of Apollo samples, including A12023 (Chapter 3), lunar breccia, A79035 (Chapter 4) and some Apollo 16 highland soils (Chapter 5).

The instrument used for this study is Finesse, a gas source, static vacuum mass

spectrometer that is capable of analysing picomole quantities of nitrogen and measuring $\delta^{15}N$ with a precision of ±0.2‰, more sophisticated than the instrument employed by Carr *et al.* (1985a, b). In conjunction with the nitrogen abundance and isotopic measurements, the gas extraction system has been modified to allow carbon abundance measurements, and the mass spectrometer has been set up for semi-quantitative abundance measurements of ^{36}Ar, ^{38}Ar and ^{40}Ar. Before the instrument could be used for sample analysis, the operating parameters needed to be established and the performance assessed . A full description of the instrument , its calibration and the protocol for sample analysis is given in Chapter 2. The high sensitivity of the mass spectrometer enabled the use of higher temperature resolution (to a minimum of 10°C temperature steps) without a corresponding increase in required sample size. For the majority of the analyses in this study of lunar samples, temperature resolution of 25°C and 50°C were sufficient, but for some experiments where detailed resolution was necessary, temperature resolution of 10°C were employed.

The identification of lunar nitrogen components has been aided by conjoint carbon and argon abundance measurements. This has enabled measurement of the C/N ratio, argon isotopic ratios, *i.e.* $^{36}Ar/^{38}Ar$ and $^{40}Ar/^{36}Ar$, and an estimation of $N/^{36}Ar$ ratios, for all the sample analysed in this work. Although the argon data is semi-quantitative, this data determine any deviations of these ratios from typical solar wind values. Such data can further constrain the isotopic composition and origin of the nitrogen in the lunar regolith.

Chapter 2
Experimental Techniques

2.1. Introduction

The advent of stable isotope mass spectrometry can be traced back to the "accidental" discovery of the isotope ^{13}C, whilst using the first positive ion mass spectrograph to investigate the abundance of neon isotopes (Aston, 1919). The existence of ^{13}C, however, was not confirmed by optical spectroscopy for a further ten years (King and Birge, 1929). When compared to other light elements, *e.g.* C, H, S, Si and O, which are abundant in terrestrial samples, little literature data are available for the distribution of nitrogen stable isotopes, *i.e.* ^{15}N and ^{14}N. Kaplan (1975) has suggested that this is due to the difficulty in the measurement of an element of trace (ppm) abundance in geological specimens, but which constitutes almost 80% of the Earth's atmosphere.

To some extent this problem has been overcome by the analysis of extraterrestrial samples, *i.e.* lunar soils, using stepped pyrolysis (Chang *et al.*, 1974a; Becker and Clayton, 1975) and later stepped combustion techniques (Frick and Pepin, 1981; Lewis *et al.*, 1983), previously discussed in section 1.7.1.1. These techniques enable the various sources of nitrogen within a sample to be resolved, providing the components are liberated at different temperatures. It is generally accepted that nitrogen released at temperatures of <200°C is mainly attributable to atmospheric gases, 200-500°C as organic materials and at higher temperatures from nitrogen indigenous to the sample which is free from contamination.

2.1.1. Dynamic vacuum mass spectrometers

The early gas source mass spectrometers (Nier, 1947) operated in the dynamic vacuum mode and for many years were considered the definitive design. During analyses the mass spectrometer was left open to the pumping system, and rapid and repeated comparisons of sample and reference gas, were measured by means of a 4-way "changeover" valve. The sample and reference gas were bled through two capillaries, each

from their own reservoirs. The disadvantage with dynamic instruments was that large sample sizes were required, as the majority of sample gas would not contribute in any way to the analysis. For a typical measurement, a dynamic mass spectrometer would typically require 28 to 56 μg of N_2. Assuming an average geological sample contains 10 ppm of nitrogen, then the initial sample size would be in the order of 2.8 to 5.6 g. This technique, therefore, becomes impractical with samples that are in limited supply or of a valuable nature such as extraterrestrial material, *e.g.* lunar samples, meteorites and interstellar grains.

2.1.2. Static vacuum mass spectrometers

The necessity for analysing samples of smaller size, such as the Apollo or Luna soils, led to the development of static vacuum mass spectrometers. Initially developed for noble gas analysis (Reynolds, 1956), it was suggested as a technique for the measurement of nitrogen abundances (Irako *et al.*, 1975; Gardiner and Pillinger, 1979) and then for nitrogen isotopic analysis (Fallick *et al.*, 1980), before finally being developed independently by Brown and Pillinger (1981) and Frick and Pepin (1981).

The use of static vacuum mass spectrometers resulted in an increase in sensitivity of about three orders of magnitude compared to dynamic vacuum instruments. This improvement was due to the isolation of the mass spectrometer from the pumping system prior to the gas being admitted and hence it acted as its own sample reservoir. The order of magnitude loss of precision for the isotopic measurements, was overshadowed by the increase in sensitivity and hence a corresponding decrease in required sample size (Wright *et al.*, 1988b). An extensive discussion of static versus dynamic mass spectrometers has been detailed elsewhere with reference to carbon (Wright *et al.*, 1983; Wright, 1984; Carr *et al.*, 1986) and nitrogen (Boyd *et al.*, 1988; Wright *et al.*, 1988b) isotopic analysis.

2.1.3. A static vacuum mass spectrometer for the analysis of picogram quantities of nitrogen

The lunar samples studied in this work were analysed for nitrogen abundance and isotopic compositions using a semi-automated, static vacuum mass spectrometer, capable of analysing picogram quantities of nitrogen. A comprehensive description of the design and operation of this mass spectrometer, colloquially known as Finesse, is given in this chapter. Its design is modified from the instrument described by Wright *et al.* (1988b) and extends the principles of the extraction and purification techniques previously detailed by Boyd *et al.* (1988). Major modifications have been made to the operation of the mass spectrometer (section 2.2) and the inlet section and pumping systems (section 2.3), which have further improved the precision and accuracy of the instrument by a factor of 10, and hence resulted in a corresponding reduction in the sample size required for analysis. This system is now capable of performing stepped heating extractions (typically 20-30 temperature steps) to a $\delta^{15}N$ precision of $\leq\pm 0.5‰$.

2.2. The mass spectrometer

The mass spectrometer is constructed from a Dennis Leigh Technology analyser head with a 110 mm radius flight tube and a 90° magnetic sector (DLT, Winsford, Cheshire, UK). This company was subsequently taken over and closed to trade The total volume of the mass spectrometer, including source and collector housing (SH and CH in Figure 2.1) is estimated to be ~0.5 x 10^{-3} m^3. A schematic of the mass spectrometer and associated electronic hardware is given in Figure 2.1.

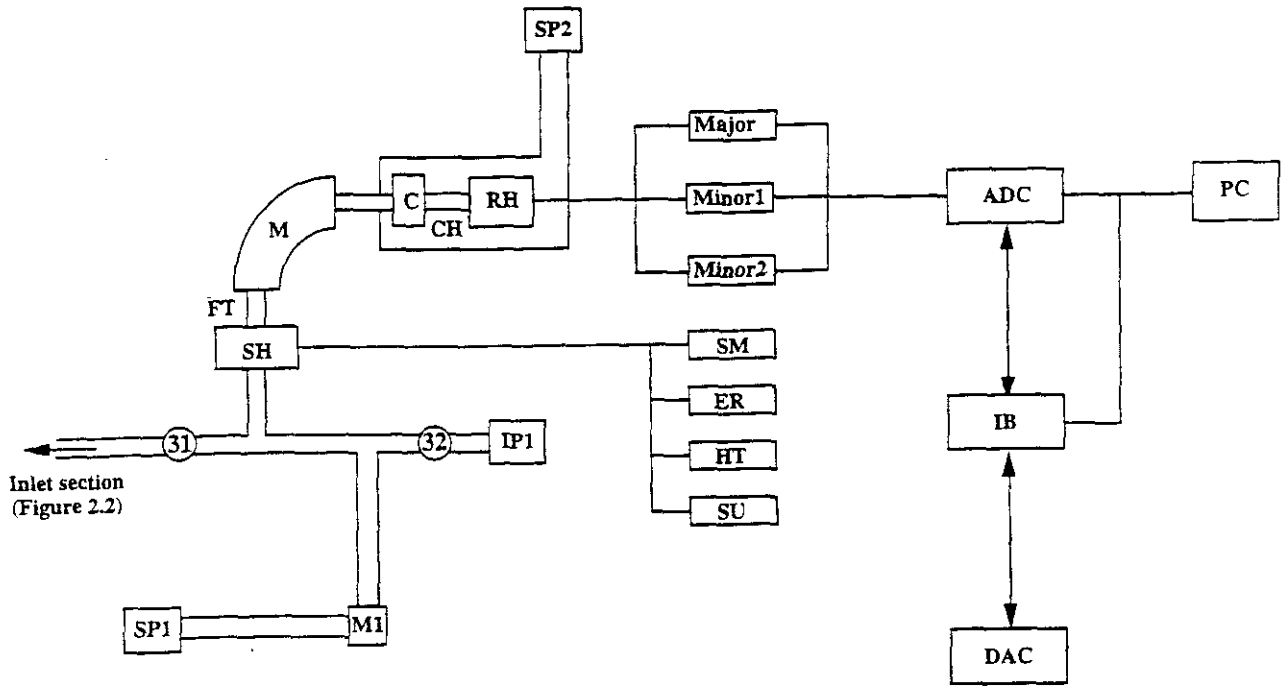

Figure 2.1. Schematic of the mass spectrometer.
The abbreviations are as follows: SP1 and SP2, molecular sieve sorption pump; M1, CR38 manual valve; 31, Nupro 4BK all-metal bellows valve; 32, CRP38 stainless steel valve; IP1, ion pump; SH, source housing; FT, flight tube; M, magnet (90° sector); C, collectors; CH, collector housing; RH, remote head amplifier; Major, minor1 and minor2, second stage amplifiers; SM, source monitor; ER, emission regulator; HT, high voltage supply; SU, scan unit; ADC, analogue/digital converter; DAC, digital/analogue converter; IB, interface bus; PC, Elonex 386 computer.

2.2.1. The ionisation source

The ionisation source is a traditional "nude" Nier type design as described by Wright *et al.* (1988b) and utilises a tungsten filament (DLT, Winsford, Cheshire, UK). A tungsten filament is preferred to others such as rhenium, because it has been observed to be more durable, although a rhenium filament is expected to degas quicker. Increased durability ensures that the mass spectrometer is operational for longer periods of time as the filament has a greater life expectancy. Ionisation source parameters are controlled by a source control box IOS 5001 (DLT, Winsford, Cheshire, UK) and the standard operating parameters are given in Table 2.1.

Source parameter	Value
Trap current	100 μA
Filament current	3.75 A
Source current	0.12 mA
Ionisation energy	76.1 eV
Repeller plate	-2.1 V
Focus plate	3.16 kV
Ion acceleration voltage	3.92 kV

Table 2.1. Mass spectrometer source parameters for Finesse.

2.2.2. Mass spectrometer pumping systems

The analyser is connected to a Triode (Starcell)^{TM} ion pump (VG Hastings, Sussex, UK), in conjunction with a VPS60 power supply (VG Hastings, Sussex, UK), by a CRP38 high vacuum, bakeable stainless steel valve (VG Hastings, Sussex, UK) and to the inlet section *via* a modified NUPRO 4BK all-metal bellows valve (NUPRO, Oxford Valve and Fitting Co, Oxon, UK). These valves are shown as 32 and 31 respectively in Figure 2.1 and the mass spectrometer ion pump is shown as IP1. If the mass spectrometer is at atmospheric pressure, *i.e.* after filament replacement or vacuum loss, it can be evacuated to a pressure of 10^{-3} mbar using a MS50 sorption pump (VG Hastings, Sussex, UK) packed with 0.5 nm molecular sieve (SP1 in Figure 2.1). Its operation is controlled *via* a manual CR38 valve (VG Hastings, Sussex, UK), shown as valve M1 in Figure 2.1. Once the target pressure has been attained, valve M1 is closed and the mass spectrometer is transferred for continued pumping on IP1. The advantages of using sorption and ion pumps are discussed in section 2.3.1. After vacuum loss the mass spectrometer is baked out at 200-250°C for 48-72 hours by means of a demountable oven.

2.2.3. The collector assembly

Ion beams are focussed into the bucket collectors (C in Figure 2.1) by means of a 90° sector magnet (M in Figure 2.1) generating a flux density of 0.4T. The collector assembly utilised on this instrument is a modification of that described by Carr *et al.* (1986) for carbon

isotopic analysis. The system uses three separate Faraday collectors, one each for m/z 28 ($^{14}N^{14}N^+$), 29 ($^{15}N^{14}N^+$) and 30 ($^{15}N^{15}N^+$). In previous instruments (Wright *et al.*, 1983), the incident ion beams were scanned over the collector in order to allow abundance and isotopic measurements to be made. However, in this instrument the collectors are fixed and the three ion beams are focussed directly into the appropriate collectors. The advantage of this method is that it minimises the length of time for each measurement and hence allows a greater number of measurements to be made over the same period. In this instrument, 100 measurements are made on each collector in 2 minutes, compared to 15 scans and a total analysis time of 7 minutes for the instrument detailed in Wright *et al.* (1988b). The collection of a greater number of measurements will ultimately improve the accuracy of the data obtained. This is essential when dealing with an element such as nitrogen with a short life in the mass spectrometer. Stability is further improved by maintaining the collector housing (CH in Figure 2.1) at a pressure of 10^{-3} mbar during the extraction by use of a second molecular sieve sorption pump (SP2 in Figure 2.1).

2.2.4. Electronic systems and computer technology

The m/z 28, 29 and 30 collectors are attached to a remote head amplifier (RH in Figure 2.1) and contain feedback resistors appropriate to each collector. The resistances for each collector are given in Table 2.2 and include the maximum current which can be measured by each amplifier. The remote head amplifier is connected to the inputs of three second stage amplifiers (major, minor1 and minor2 in Figure 2.1) which have variable gains between x1 and x1000. The outputs from the amplifiers are alternately multiplexed *via* relays into a 16-bit bipolar analogue to digital converter (ADC in Figure 2.1) and the digital output is fed into one of two Elonex 386 computers (PC in Figure 2.1) to enable monitoring of the three ion beams during gas analysis.

The system described herein, utilises two Elonex 386 computers: one used for valve control of the inlet section and gas handling, whilst the other is used for mass spectrometer control. The computer programs have both been written in Turbo Basic by Jim Ball with subsequent modifications by Jez Higgins at the Planetary Science Unit (now known as Planetary Science Research Institute and herein referred to as PSRI). Inlet valves are

computer controlled by means of operator written valve sequences using a series of open "O", close "C" and wait "W" commands. The mass spectrometer computer initially measures the baseline in the mass spectrometer in order to zero each amplifier prior to gas admittance. When the gas is admitted, *i.e.* valve 32 shut and valve 31 opened (Figure 2.1), a background scan is performed from m/z = 46 to 26, whereby the presence of primarily oxygen, argon and CO_2 is monitored. After the background scan, valve 31 is closed and the peaks are centred before data are acquired.

Collector	Amplifier Resistance (GΩ)	Maximum current (A)
Major (m/z = 28)	0.1	10^{-9}
Minor1 (m/z = 29)	1.0	10^{-10}
Minor2 (m/z = 30)	10.0	10^{-11}

Table 2.2. Collector amplifier resistances and maximum current for Finesse.

The ion beam intensity (m/z 28, 29 and 30) and the ratio between the ion beams (28/29 and 28/30) are measured from the top of the respective peaks to the baseline on either side and between the peaks. The measurements are corrected for amplifier off-set and for the tailing effect of the m/z 28 peak on the m/z 29 peak. The latter, also known as "abundance sensitivity" has been estimated as 15 ppm for a 3 ng aliquot of reference gas. These corrections have been incorporated into the mass spectrometer computer program by Jim Ball and Jez Higgins at PSRI. At the end of each analysis, the mean 28/29 ratio and standard error are determined. Furthermore, assuming exponential decay of the ion beams, and knowing the time that the ion beams were focussed into the appropriate collector, it is possible to determine the m/z 28 and 29 peak heights at the time the gas was admitted to the mass spectrometer, assuming no equilibration period. This is referred to herein as I28 (or I29) where "I" stands for intercept. The data are displayed on the computer VDU and are stored on the hard disk for future reference. The gas in the mass spectrometer is then pumped away by IP1 *via* valve 32 (Figure 2.1).

2.2.5. Argon measurement

At the end of each analysis, the ion beam intensity due to m/z 36, 38, and 40 is measured by the minor1 collector. This allows semi-quantitative peak height measurements of argon abundances and an estimation of the argon isotopic ratios, *e.g.* $^{36}Ar/^{38}Ar$. The argon peaks are initially measured at a gain of 10 on the minor1 amplifier, although if this gain is too high, the argon peak is re-scanned at a lower gain, and if necessary re-measured on the major collector until a suitable peak height measurement is obtained. Several problems are encountered when attempting to measure argon yields using a nitrogen mass spectrometer. Unlike noble gas instruments, no getter is used, hence the measurement of small amounts of argon are susceptible to hydrocarbon interferences. This is especially true with the measurement of ^{36}Ar from small amounts of air or reference gas, *i.e.* ≤1.4 ng of N_2, and hence such data are not included herein. A further problem is that the ion source is not set up at the maximum sensitivity required for argon, and hence measurement of ^{36}Ar, and especially ^{38}Ar, from air is difficult. Some attempt has been made to calibrate the instrument for argon using ^{40}Ar from AIR (the nitrogen calibration standard) with limited success by using the calculated yield of nitrogen from the aliquot of AIR and the true $N/^{40}Ar$ (~83). However, the data obtained from the study does not compare well with the accepted values and hence is omitted from this work.

It should be noted that the argon data in this work should be regarded as a preliminary attempt to measure argon ratios using a static vacuum mass spectrometer which has been specifically designed for the measurement of nitrogen abundances and isotopic compositions. For the purpose of comparison of the release profiles of nitrogen and ^{36}Ar in lunar soils and breccias, the ^{36}Ar yields have been converted to conventional noble gas units, *i.e.* cm^3 STP/g (herein referred to as ccSTP g^{-1}). The method used for the conversion is detailed in section 3.3.2. The argon measurements obtained in this work are semi-quantitative, used only as an aid for identifying individual components in lunar soils, *i.e.* $^{36}Ar/^{38}Ar$ and $^{40}Ar/^{36}Ar$, and are not directly comparable with noble gas data obtained by other workers (section 1.7.5).

2.3. The gas extraction system

In essence, the configuration for the inlet section and the protocol for gas extraction and purification is similar to that described by Boyd *et al.* (1988). However, several modifications have been made to the inlet and these are detailed in this section. The entire inlet system, with exception to parts of the gas extraction and purification sections, is constructed in 3/8 inch diameter stainless steel pipework as opposed to the pyrex glass-line technology previously employed. The advantages of this are that the inlet is more robust and less prone to breakages. A cleaner vacuum can be attained by the use of sorption and ion pumps as opposed to the oil diffusion pumps previously employed (section 2.3.1). The sample gas is manipulated around the inlet by the use of two types of BK series air-actuated valves (Nupro, Oxford Valve and Fitting Co, Oxon, UK). The configuration of the inlet is illustrated in Figure 2.2.

2.3.1. Pumping systems

There are two separate pumping systems for the inlet:

1). The "main line" which evacuates the gas extraction and purification sections and the sample volumes, *i.e.* the line routinely used during sample analysis.

2). The "back line" which pumps out the reference gas aliquotting section (section 2.3.2), the section used for loading calibration standards (section 2.3.3), the sample loading section (section 2.4.1) and the capacitance manometer for the measurement of carbon abundances (section 2.4.5).

Note that the pumping systems remain separate during routine analysis by the closure of the gate valve (GV) and valves 1, 6 and 13 (Figure 2.2).

Both of these sections are maintained at high vacuum by two Triode (Starcell)^{TM} ion pumps in conjunction with IPS60 power supplies (VG Hastings, Sussex, UK). These can monitor pressures in the range of 10^{-4} to 10^{-9} mbar. The main line and back line ion pumps are shown as IP2 and IP3 respectively in Figure 2.2. The main line will usually be maintained at a pressure of $\leq 10^{-8}$ mbar, whereas the back line will operate at ~10^{-7} mbar.

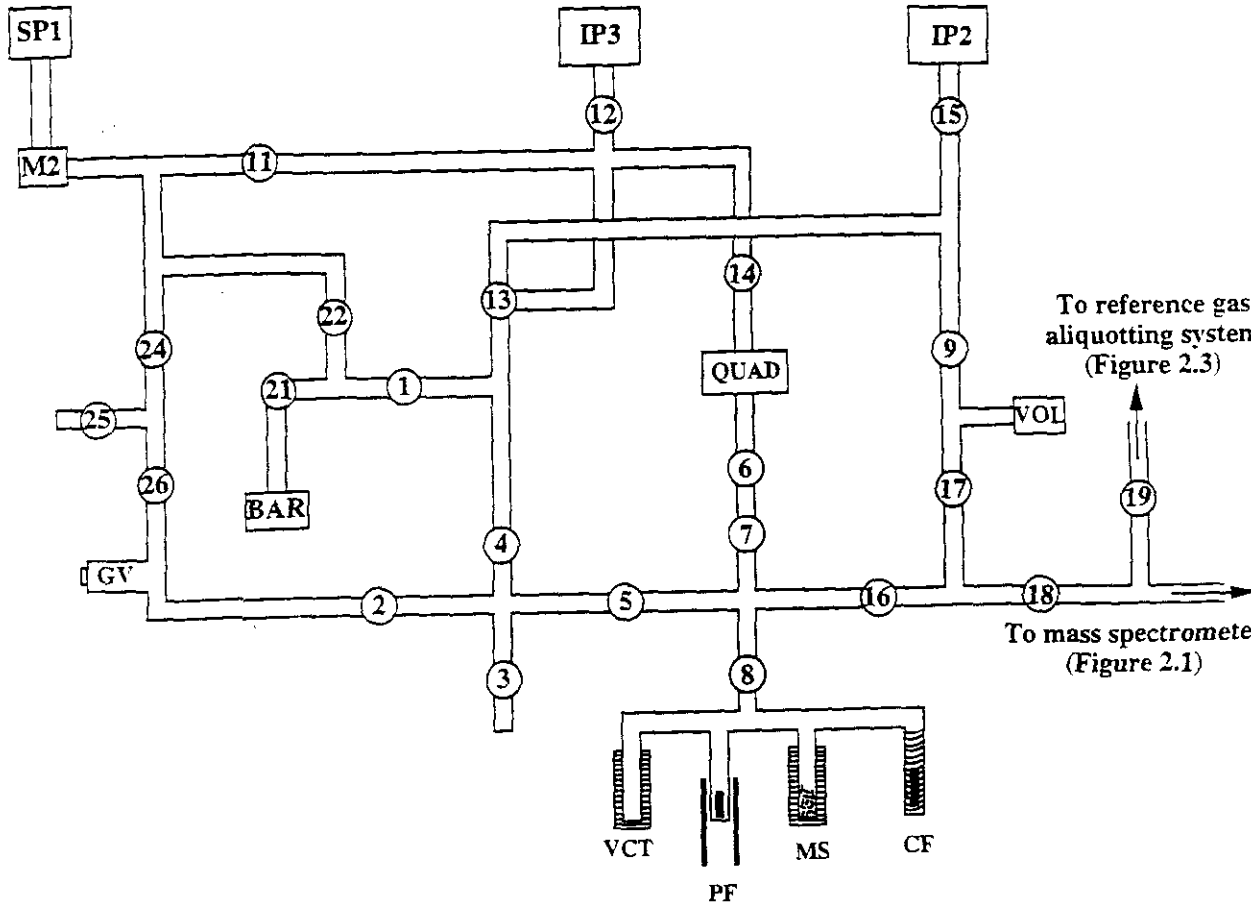

Figure 2.2. Schematic of the inlet section.

The abbreviations are as follows: GV, gate valve; 2, 3 and 4 etc, BK series air-actuated valves; VCT, variable temperature cryogenic trap; PF, platinum furnace; MS, molecular sieve; CF, copper oxide furnace; VOL, expansion volume; QUAD, quadrupole mass spectrometer; IP2, "main line" ion pump; IP3, "back line" ion pump; M2, manual valve; BAR, capacitance manometer.

Rough pumping for inlet pressures of $>10^{-3}$ mbar, *e.g.* after loading a sample, is achieved using sorption pump SP1 (Figure 2.2) *via* manual valve (M2 in Figure 2.2). Once the base pressure of 10^{-3} mbar is reached, valve M2 is closed and the inlet section is transferred to ion pump IP2 for continued pumping. The combination of sorption pump and ion pump provides a completely oil-free pumping system and hence a greatly reduced hydrocarbon background. Secondary benefits include the elimination of noise and vibration effects.

2.3.2. Reference gas aliquotter

The reference gas used for Finesse is *99.998% pure cylinder nitrogen (White Spot* Grade, British Oxygen Corporation, Ipswich, UK) which is stored in a metal cylinder (REF in Figure 2.3). In order to calculate accurately the correct isotopic composition of any sample gas analysed on this instrument, the reference gas has to be initially calibrated with respect to AIR or a known nitrogen standard (section 2.5.2). Subsequent checks were periodically made to ensure that the isotopic composition of the reference gas had not altered.

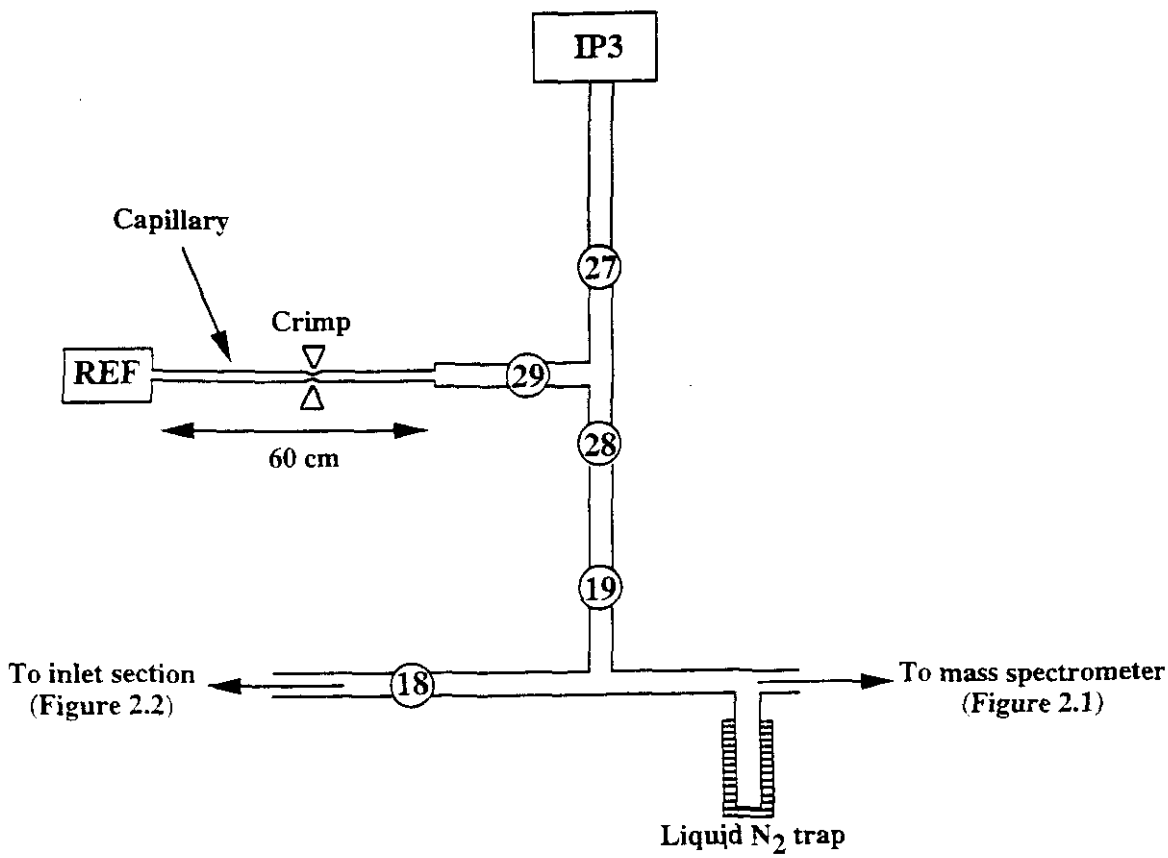

Figure 2.3. Schematic of the reference gas aliquotting system.
The abbreviations are as follows: 18, 19 etc, BK-series air-actuated valves; REF, reference gas volume; IP3, "back line" ion pump.

Previous mass spectrometers utilised two reference gases: a fixed volume and a variable volume aliquotting system (Wright *et al.*, 1983; Carr *et al.*, 1986; Wright *et al.*, 1988b). However this method of reference gas metering proved to be too cumbersome, time consuming and expensive for the automated mass spectrometers and hence a new system has been developed.

For Finesse, the major ion beam intensity (I28) for the sample gas is matched by an equal pressure of reference gas by the use of a capillary gas pipette of length 60 cm, illustrated in Figure 2.3. The capillary has been crimped in order to restrict the flow of reference gas into the inlet to a rate of 28 pg s^{-1}. Initial testing of the capillary aliquotting system was carried out by Russell (1992) using the carbon static vacuum mass spectrometer described by Carr *et al.* (1986). These tests concluded that restricting the flow of the reference gas, from a volume containing about 100 torr of CO_2, through the capillary, caused no isotopic fractionation. Previous observations (Halstead and Nier, 1950) had confirmed that a high pressure of reference gas ensured that no isotopic fractionation occurred during the capillary aliquotting process. The capillary aliquotting system was also tested on Finesse prior to the commencement of this study and the results obtained for the CO_2 study by Russell have been confirmed for N_2 reference gas (Franchi, *pers. comm.*).

Using the capillary aliquotting technique, the quantity of reference gas to be admitted into the mass spectrometer is determined, not by adjusting the volume of the aliquotter, but by altering the "bleed" time, *i.e.* the number of seconds that reference gas is bled into the constant volume contained by valves 27, 28 and 29 (Figure 2.3). The I28 is proportional to the bleed time for any given aliquot of reference gas and is plotted in Figure 2.4, for a range of bleed times from 1s (28 pg) to 120s (3.4 ng).

After the reference gas has been bled into the inlet volume for the desired length of time, valve 29 is closed, and the gas is expanded up to valve 31 (Figure 2.1). Before being admitted into the analyser, any trace contaminants, *e.g.* CO_2, are removed by a liquid N_2 cold trap, at a temperature of -185°C, placed between the inlet and the mass spectrometer.

There are several advantages to this method of reference gas aliquotting:

1). The speed of operation is greater when compared to the manual adjustment of volumes by motor driven bellows.

2). The elimination of operator errors associated with the selection of the variable volume size.

3). The elimination of systematic errors and inconsistencies associated with the analysis of aliquots of reference gas where valve control and equilibration times are controlled manually by the operator. The accuracy of computer controlled reference measurements will

also highlight any sudden decrease in sensitivity within the mass spectrometer or a gradual decrease of I28, resulting in the need to replenish the reference gas supply.

4). The instrument is fully automated for reference gas measurements at any bleed time within the range of times stated herein. Single aliquots of reference gas can be analysed automatically with variables such as the pumping time for the mass spectrometer between analyses specified by the operator. The automation of reference gas measurements greatly increases the data collection capability of the instrument and aids in the initial setting up and periodic monitoring of its performance.

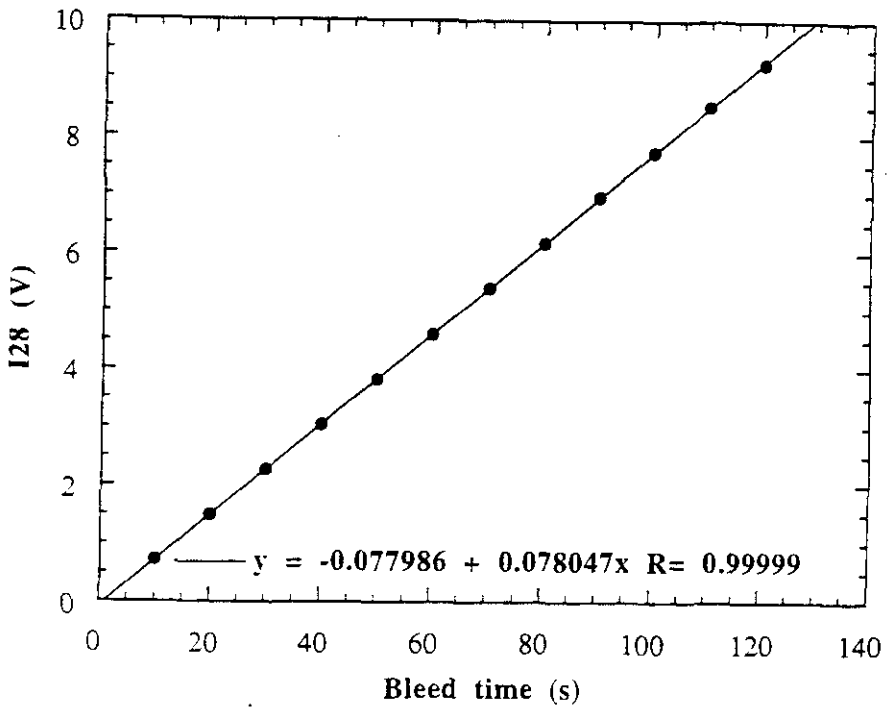

Figure 2.4. Plot of I28 (V) against reference gas bleed time (s).

2.3.3. Standard loading section

In order that calibration standards could be loaded and analysed quickly and efficiently, an extra port was attached to the back line inlet section (valve 25 in Figure 2.2). This was designed to enable loading of two nitrogen standards at once and utilised a 1/4 inch diameter flexi-section to crack a glass vessel containing the standard. The nitrogen standards used are rubidium-ammonium sulphate ($Rb_2(NH_4)SO_4$), prepared from NBS-N1 and NBS-N2 ammonium sulphates and the preparation protocol is given by Boyd and Pillinger

(1991). The solid standards were loaded into glass tubes on a separate extraction line, evacuated to a pressure of 10^{-6} mbar, sealed, and then combusted at 1000°C for 2 hours.

Also attachable to the aforementioned port is a 300 ml cylinder filled and replenished regularly with local air, at a pressure of 1.5 mbar. Air aliquots of size 0.5 ml are metered to enable calibration of the mass spectrometer and to determine the isotopic composition of the reference gas. This is discussed further in section 2.5.2.

2.3.4. Quadrupole mass spectrometer

Following the purification of the sample gas (section 2.4.3), a small aliquot (calculated as ~6% from inlet volume calibrations) is admitted into a Masstorr DX quadrupole (VG Quadrupoles, Cheshire, UK) situated between valve 6 and valve 14 in the inlet section (QUAD in Figure 2.2). The quadrupole is used to determine approximately the amount of nitrogen in the sample so that the operator can decide the proportion which is to be admitted into the mass spectrometer to obtain the optimum performance from the instrument. The quadrupole is used for the measurement of mass 14 (preferable to m/z 28 to minimise measurement of CO interferences). It is typically computer controlled in conjunction with the valve control sequences, but can also be manually operated if non-routine analyses are required.

2.4. Operation of the instrument

The protocol for sample gas extraction and purification is similar to that described by Boyd *et al.* (1988) and hence will only be detailed briefly here. However, the sample loading mechanism is a new design and hence is described in some detail.

2.4.1. Sample loading

A platinum bucket containing the sample for analysis (section 2.6.3 and 2.6.4 for preparation procedure) is loaded onto a rotatable dish attached to an arm which is connected to a mini rotary drive (VG Generators Ltd, East Sussex, UK). The connecting arm can be

locked to prevent the dish from accidentally rotating. A schematic of the loading system is given in Figure 2.5. The dish is situated inside a vertical section of 3/4 inch diameter stainless steel pipework, located between a M Series UHV C-Loc gate valve (Caburn MDC, East Sussex, UK) and valve 26. The gate valve (GV in Figure 2.5) is a manual valve with a Viton O-ring seal which separates the high vacuum extraction section from the backing line.

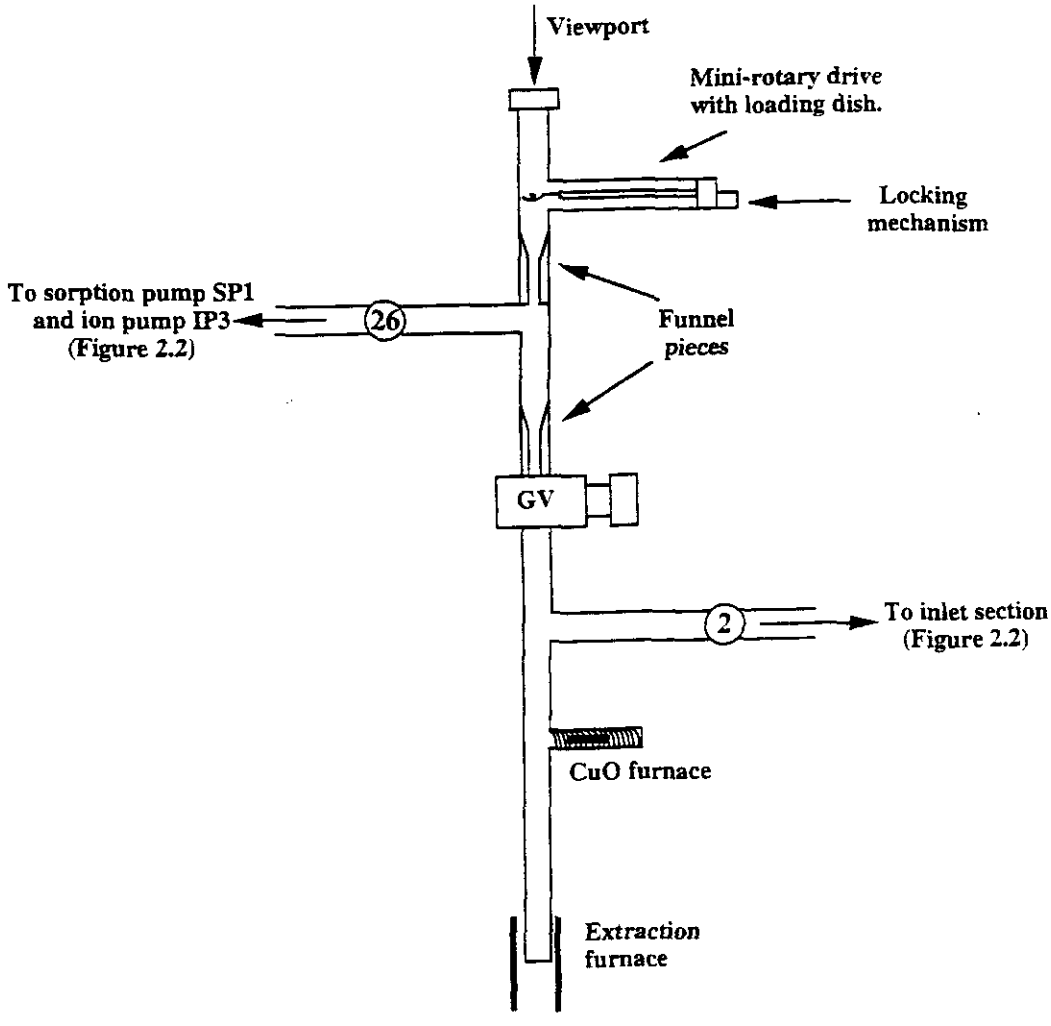

Figure 2.5. Schematic of the sample loading system.
The abbreviations are as follows: GV, gate valve; 2 and 26, BK-series air-actuated valves.

The sample is loaded onto the dish *via* the viewport with the gate valve and valve 26 closed (Figure 2.5). It is first evacuated to a pressure of 10^{-3} mbar using sorption pump SP1 (Figure 2.2) and then transferred to ion pump IP3 (Figure 2.2) for pumping overnight, in order to remove any adsorbed terrestrial gases.

Following the completion of the initial blank measurements (section 2.9.2), the gate valve is opened fully and the loading dish unlocked and rotated to allow the sample to drop vertically into the gas extraction section. To ensure the safe passage of the sample through

the gate valve, two funnel pieces have been placed inside the metal pipework between the loading dish and the gate valve: one above the T-shaped section leading to valve 26 and the other above the gate valve (Figure 2.5). These are constructed from stainless steel and are designed to ensure that the sample drops cleanly through the gate valve when opened. After the sample is loaded into the extraction section, the gate valve is closed and the extraction can commence (section 2.4.2).

2.4.2. Gas extraction

As some of the samples in this work are analysed by stepped combustion, the extraction section also includes a CuO finger, similar to that described by Boyd *et al.* (1988). The finger generates an oxygen pressure of a few torr by heating the CuO finger to a temperature of 850°C. In order to ensure that sufficient oxygen is generated, the oxygen pressure is monitored regularly, and is increased if necessary by the procedure detailed in Boyd *et al.* (1988). The sample is heated by a resistance wire furnace (designed and built on-site), up to a maximum of 1300°C and the temperature is varied by the use of variable transformers (Zenith Electrical Co, Milton Keynes, UK). The temperature is controlled by a chromel-alumel thermocouple and monitored by a model 6100 digital thermometer (Comark Electronics Ltd, West Sussex, UK). Further description of the design of the furnaces are given in Boyd *et al.* (1988).

A typical stepped extraction step takes 31 minutes, during which time the furnace is heated to the next designated temperature step and gas extracted during the previous step is purified and processed (section 2.4.3). For a combustion extraction, the temperature of the CuO furnace is increased to 850°C for 25 minutes (ramp time ~2 minutes), in order to liberate oxygen and to combust the sample. The CuO furnace temperature is then reduced to 600°C for 5 minutes, to reabsorb the majority of the oxygen and then reduced further to 450°C for 1 minute to reabsorb any remaining oxygen. For a pyrolysis extraction the temperature of the CuO furnace is decreased to ~200°C and remains at this temperature throughout the duration of the step.

2.4.3. Sample gas purification

The purification section consists of a molecular sieve trap (containing 0.5 nm molecular sieve), a CuO finger, a platinum finger and a variable cryogenic trap (Figure 2.2), similar to that described by Boyd *et al.* (1988). The purification procedure mentioned herein typically lasts 22 minutes and is designed to remove any species which could directly or indirectly interfere with the m/z 28 and 29, *i.e.* CO & CO_2, and to reduce any nitrogen oxide species to N_2 gas.

At the end of an extraction step, the purification section is isolated from ion pump IP2 (Figure 2.2) and the molecular sieve is cooled to -196°C with liquid N_2. The purification section is opened to the extraction section and the extracted sample gas is transferred onto the molecular sieve for 2 minutes. At the end of this period, the purification section is again isolated, the liquid N_2 removed, and the molecular sieve heated to 180°C to release the trapped gases. Simultaneously, the CuO finger is heated to 850°C for 6 minutes to ensure full oxidation of CO, CH_4 and volatile hydrocarbons to CO_2. The platinum furnace remains at a temperature of 1050°C to allow the breakdown of nitrogen oxides, *e.g.* NO_2, to N_2. The temperature of the CuO finger is then decreased to 600°C for 6 minutes and 450°C for a further 10 minutes to resorb all the excess oxygen, whilst the variable cryogenic trap is cooled to -170°C to condense CO_2, H_2O and SO_2 and hence separate these species from N_2 and the noble gases.

2.4.4. Sample gas measurement

Once the purification procedure is complete, the sample gas is expanded into the inlet and 6% is admitted into the quadrupole as described in section 2.3.4. The operator will choose the suitable computer valve sequence, in accordance with the required percentage of N_2 to be admitted into the mass spectrometer. The percentage of gas admitted for each valve sequence has been calculated from calibration of the relevant volumes in the inlet. Note that when sample gas is admitted to the mass spectrometer, the purification section is isolated, to ensure the safety of the mass spectrometer in the event of a glass line vacuum failure. Furthermore, as with the reference gas measurements, any residual CO_2 gas is removed

prior to analysis by the use of a liquid N_2 trap (Figure 2.3). Following the nitrogen and argon measurements in the mass spectrometer, any remaining sample gas in the inlet volumes is pumped away by ion pump IP2 (Figure 2.2).

2.4.5. Carbon abundance measurements

Carbon abundances are measured on a model 390HA capacitance manometer (MKS Baratron, Massachusetts, USA), connected to a metal liquid N_2 trap, located by valve 21 (Figure 2.2). The pressure of CO_2 in the baratron is displayed on a digital meter with a saturation pressure of 1 torr. The baratron is calibrated by the measurement of known quantities of CO_2 gas, to obtain a multiplication factor which enables the pressure of an aliquot of CO_2 to be converted into a quantitative yield (section 2.5.3). Once the mass spectrometer has been isolated from the inlet section for sample analysis, the variable cryogenic trap is heated to a temperature of -140°C and the CO_2 is expanded to the baratron. The CO_2 pressure is constantly monitored on the meter during this procedure, in order to determine when all the CO_2 has been released. The temperature chosen for this purpose is sufficiently high to release all the CO_2 but still low enough such that SO_2 and H_2O still remain trapped, and is dependent on the relative quantities of these species in the sample. The time needed to transfer all the CO_2 is also variable although is typically 3 minutes for the lunar samples in this work.

When all the CO_2 has been transferred from the cryotrap, it is condensed onto the cold finger of the baratron at liquid N_2 temperatures. Once the baseline pressure is reached, the baratron is transferred onto IP3 to allow any non-condensible gases to be pumped away. The baratron is then isolated and the liquid N_2 trap removed. The CO_2 pressure is then measured and the carbon yield calculated from the obtained conversion factor (section 2.5.3). The CO_2 in the baratron and the remaining gases in the purification section are pumped away by ion pumps IP3 and IP2 respectively (Figure 2.2).

2.5. Evaluation and calibration of the mass spectrometer

Nitrogen isotopic compositions are attained by comparison of the 28/29 ratios in the sample under analysis to an equal pressure of reference gas, with a known $\delta^{15}N$ relative to AIR, as given by Equation 1.1. As the static vacuum mass spectrometer allows only a single comparison of sample and reference gas, as opposed to the rapid and repeated comparisons using dynamic instruments, it is imperative to assess the internal precision, sensitivity and reproducibility of the mass spectrometer (section 2.5.1). The instrument also required calibration, in order that the yield and isotopic composition data obtained could be considered as quantitative and comparable both within, and between laboratories (section 2.5.2). Furthermore, the nitrogen background level, herein referred to as the "blank measurement", both during recovery of the instrument after maintenance and routinely thereafter, were assessed to ensure the instrument operated with an optimum blank level (section 2.9). These assessments were all carried out for the first time as part of the work associated with this study but thereafter were repeated as a matter of routine throughout the course of this investigation.

2.5.1. An assessment of precision and zero-enrichments

The internal precision of the instrument needed to be assessed before and during abundance and isotopic measurements. The internal precision is expressed in per mil (‰) as the fractional error on a single measurement of sample or reference gas and is calculated from the standard error (SE) on the mean 28/29 ratio for each analysis (Equation 2.1).

$$\text{internal precision (‰)} = \frac{SE}{mean} \times 1000 \qquad \textbf{Equation 2.1.}$$

The term $\frac{SE}{mean}$ is herein referred to $error_{sam}$ or $error_{ref}$ depending on whether it represents the error for the sample or reference gas measurement respectively, and can be used to calculate the error in the $\delta^{15}N$ value for any sample and reference gas comparison (Equation 2.2).

$$\text{error in } \delta^{15}N \text{ value } (‰) = \left[(\text{error}_{sam})^2 + (\text{error}_{ref})^2 \right]^{0.5} \qquad \textbf{Equation 2.2.}$$

The internal precision is affected by several factors: statistical fluctuations in ion beam intensities, instrumental noise from electrical components, and changes in the 28/29 ratio of the nitrogen during analysis. The first two problems are minimised by the collection of a large number of data points. Furthermore a smoothing program was added to the mass spectrometer computer program by Jez Higgins (PSRI), to remove any 28/29 measurements which deviate by more than 3σ from the mean 28/29 ratio for a single analysis.

The dominant cause of changes in the 28/29 ratio in the mass spectrometer is the presence of species, *e.g.* CO, which can interfere with the measurement of m/z 28 and 29. This is discussed in section 2.9.1, in conjunction with the measurement of the background gas in the mass spectrometer, in the absence of admitted sample or reference gas. The effect of CO interference in the mass spectrometer would result in a decrease of 28/29 ratio during the analysis, from the 28/29 ratio for atmospheric N_2 (136:1) towards the equivalent ratio for CO (89:1). This is especially a problem during recovery of the mass spectrometer after vacuum loss or filament replacement, but thereafter the CO interference should be minimal.

The precision of the $\delta^{15}N$ measurements were ascertained from the analysis of aliquots of reference gas in two separate experiments. The first required the analysis of reference gas aliquots at a variety pressures, such that the precision for different sized aliquots could be calculated. This also yielded information about the variation of 28/29 ratio with increasing aliquot size, and enabled determination of the minimum size, below which the internal precision was unacceptably poor. In the second experiment, repeated measurements of equal sized aliquots of reference gas were made, in order to ascertain the reproducibility of the mass spectrometer, and to ensure that no instrumental drift occurred during the pumping period between successive analyses. This experiment was termed a "zero enrichment" test as under ideal conditions, the comparison of two equal sized aliquots of reference gas would have a $\delta^{15}N$ value of 0‰.

Run	Size (ng)	28/29 (±SE)*	Mean 28/29 (±σ)	Error (‰)**
1	0.280	127.806 ± 0.047	128.125 ± 0.438	3.42
2		127.417 ± 0.055		
3		127.912 ± 0.033		
4		127.958 ± 0.048		
5		127.736 ± 0.039		
6		128.442 ± 0.010		
7		128.155 ± 0.022		
8		128.527 ± 0.045		
9		128.863 ± 0.002		
10		128.431 ± 0.078		
11	0.616	132.746 ± 0.036	132.841 ± 0.116	0.87
12		132.916 ± 0.033		
13		132.737 ± 0.029		
14		132.696 ± 0.039		
15		132.902 ± 0.010		
16		132.741 ± 0.006		
17		132.960 ± 0.022		
18		132.793 ± 0.040		
19		132.869 ± 0.042		
20		133.051 ± 0.020		
21	0.924	134.507 ± 0.026	134.631 ± 0.083	0.62
22		134.521 ± 0.027		
23		134.615 ± 0.020		
24		134.551 ± 0.042		
25		134.714 ± 0.019		
26		134.653 ± 0.020		
27		134.653 ± 0.034		
28		134.751 ± 0.021		
29		134.641 ± 0.030		
30		134.706 ± 0.025		
31	1.232	135.569 ± 0.020	135.620 ± 0.057	0.42
32		135.556 ± 0.035		
33		135.593 ± 0.037		
34		135.633 ± 0.029		
35		135.519 ± 0.024		
36		135.648 ± 0.033		
37		135.668 ± 0.021		
38		135.675 ± 0.032		
39		135.665 ± 0.039		
40		135.675 ± 0.058		
41	1.568	136.184 ± 0.025	136.186 ± 0.020	0.15
42		136.182 ± 0.022		
43		136.175 ± 0.030		
44		139.199 ± 0.034		
45		136.167 ± 0.026		
46		136.186 ± 0.023		
47		136.191 ± 0.018		
48		136.159 ± 0.031		
49		136.233 ± 0.029		
50		136.188 ± 0.025		
51	1.876	136.565 ± 0.030	136.601 ± 0.032	0.23
52		136.584 ± 0.041		
53		136.659 ± 0.034		
54		136.647 ± 0.037		
55		136.573 ± 0.020		
56		136.623 ± 0.026		
57		136.601 ± 0.027		
58		136.578 ± 0.025		
59		136.599 ± 0.024		
60		136.573 ± 0.018		
61	2.184	136.824 ± 0.030	136.832 ± 0.031	0.23
62		136.792 ± 0.033		
63		136.862 ± 0.034		
64		136.834 ± 0.024		
65		136.822 ± 0.030		
66		136.807 ± 0.033		
67		136.884 ± 0.032		
68		136.873 ± 0.027		
69		136.799 ± 0.037		
70		136.822 ± 0.027		

Table 2.3. continued.

Run	Size (ng)	28/29 (±SE)*	Mean 28/29 (±σ)	Error (‰)**
71		137.089 ± 0.031		
72		137.073 ± 0.038		
73		137.078 ± 0.029		
74		137.017 ± 0.029		
75	2.520	137.099 ± 0.030	137.084 ± 0.033	0.24
76		137.078 ± 0.030		
77		137.054 ± 0.032		
78		137.095 ± 0.030		
79		137.115 ± 0.037		
80		137.137 ± 0.028		
81		137.263 ± 0.027		
82		137.322 ± 0.031		
83		137.286 ± 0.030		
84		137.252 ± 0.037		
85	2.856	137.248 ± 0.033	137.260 ± 0.028	0.20
86		137.231 ± 0.031		
87		137.270 ± 0.033		
88		137.262 ± 0.027		
89		137.249 ± 0.030		
90		137.221 ± 0.038		
91		137.417 ± 0.031		
92		137.407 ± 0.033		
93		137.463 ± 0.030		
94	3.164	137.477 ± 0.029	137.446 ± 0.042§	0.31
95		137.486 ± 0.024		
96		137.489 ± 0.030		
97		137.455 ± 0.027		
98		137.459 ± 0.027		
99		137.614 ± 0.038		
100		137.642 ± 0.028		
101		137.652 ± 0.029		
102	3.472	137.629 ± 0.025	137.631 ± 0.014§§	0.10
103		137.619 ± 0.026		
104		137.631 ± 0.023		
105		137.701 ± 0.031		
106		137.684 ± 0.036		
107		137.709 ± 0.032		
108		137.713 ± 0.026		
109	3.780	137.703 ± 0.030	137.705 ± 0.022	0.16
110		137.733 ± 0.029		
111		137.702 ± 0.003		
112		137.725 ± 0.032		
113		137.716 ± 0.023		
114		137.656 ± 0.034		

Table 2.3. Table of 1σ errors (‰) for different sized aliquots (ng) of reference gas. * denotes the standard error (SE), ** denotes the standard deviation (σ) expressed in ‰, § denotes 8 analyses of the 3.164 ng aliquot, §§ denotes 6 analyses of the 3.472 ng aliquot.

For the first experiment, 10 analyses of reference gas were made for each 10s bleed time interval, from 10 to 120s inclusive, using a 10 minute pumping out time between measurements. The results are given in Table 2.3 and are shown graphically in Figure 2.6. The mean 28/29 ratio obtained for each aliquot size and the standard deviation (±σ) was calculated in order to determine the internal precision (shown as "Error" in Table 2.3), in per mil (‰), as given by Equation 2.2. Note that in this instance, the term "SE" in Equation 2.2 is replaced by σ as the error on the 28/29 measurement.

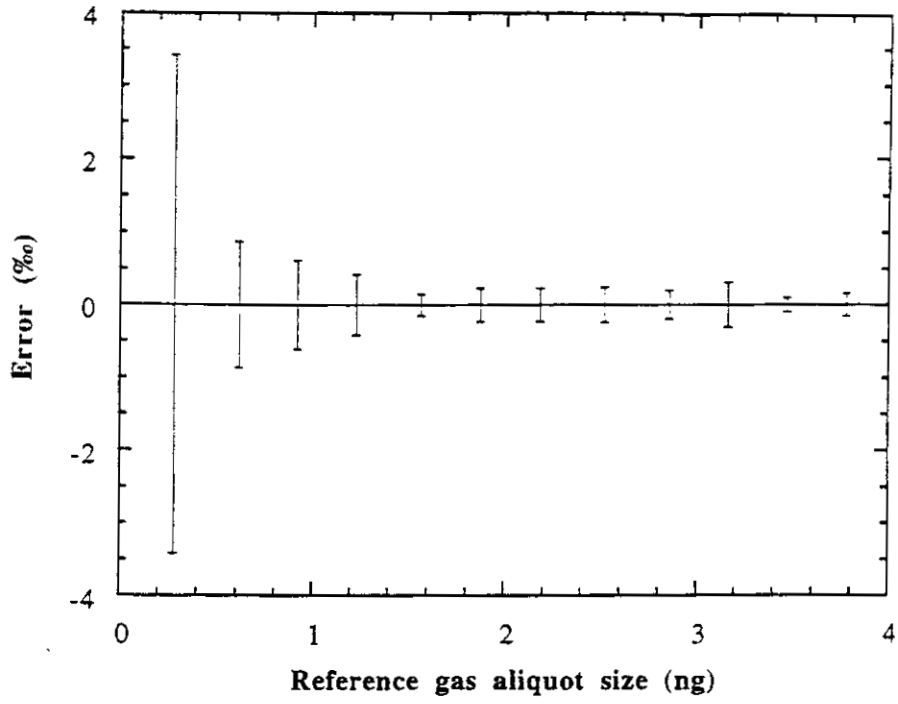

Figure 2.6. Plot of 1σ errors (‰) against reference gas aliquot size (ng).

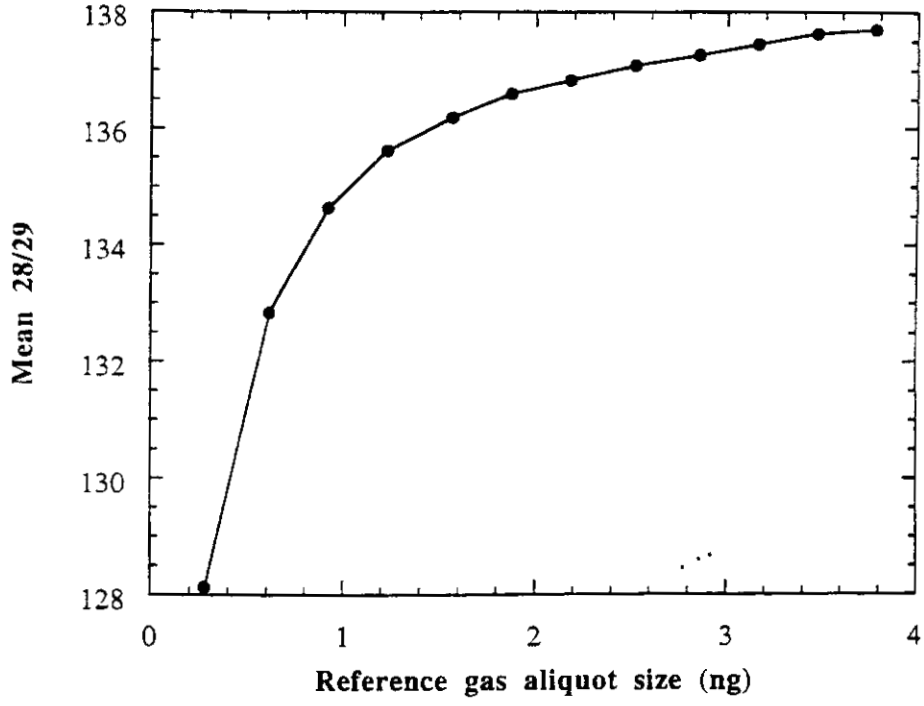

Figure 2.7. Plot of 28/29 ratio against reference gas aliquot size (ng).

The results displayed in Table 2.3 and Figure 2.6 show that the mass spectrometer suffers a loss of precision with decreasing sample size. In this work, $\delta^{15}N$ measurements with a precision of less than $\leq \pm 1$‰, *i.e.* aliquot size of ≥0.6 ng, is considered adequate (as the lunar samples display large variations in $\delta^{15}N$), although the experiment shows that the

mass spectrometer can routinely measure isotopic compositions with a precision of ±0.2‰. For small amounts of reference gas (<0.6 ng), the precision ranges from ±1.0-3.5 ‰. This is compared to a range of ±3‰ to ±0.5‰ for 0.6 ng and 1.4 ng of reference gas respectively in a similar experiment by Wright *et al.* (1988b).

Figure 2.7 displays the variation in 28/29 ratio with increasing reference gas aliquot size and illustrates that the variation is more pronounced for small amounts of gas, typically <0.6 ng. This is believed to be primarily due to the presence of interfering species (CO and hydrocarbons) in the mass spectrometer, which, assuming a constant level of interference, would be expected to contribute more to smaller sized aliquots. However, the possibility of isotopic fractionation occurring for such aliquots cannot be eliminated. A valid method for determining whether fractionation has occurred would be to measure the total abundance and isotopic composition of a number of small aliquots which have been allowed to accumulate in the mass spectrometer. Unfortunately, such an experiment was not performed during the course of this work, although it should be stressed that due to the high precision errors for aliquots <0.6 ng (Table 2.3 and Figure 2.6), analysis of gas aliquots of this size were avoided wherever possible. It is therefore believed that isotopic fractionation has not altered the majority of results obtained in this study and the contribution of CO interference is minimised by the accurate matching of source pressures of sample and reference gas.

For the zero enrichment experiment, 71 equal sized aliquots of reference gas were consecutively analysed by the mass spectrometer over a 16 hour period. The size of each gas aliquot was 3.164 ng, equivalent to 100s bleed time, and the mass spectrometer was pumped out for 10 minutes between successive runs. The $\delta^{15}N$ values were calculated by comparison of a single analysis with the mean of the two runs conducted either side, *i.e.* run 2 was compared with the mean of runs 1 and 3. Hence the data shown in Table 2.4, and illustrated graphically in Figure 2.8, represents 69 comparisons of reference gas aliquots. The standard errors for the $\delta^{15}N$ measurements are expressed in per mil, and are calculated using Equations 2.1 and 2.2.

Run	Mean 28/29 (±SE)*	$\delta^{15}N$ (‰)**	Run	Mean 28/29 (±SE)*	$\delta^{15}N$ (‰)**
1	137.931 ± 0.040	-0.29 ± 0.37	37	138.067 ± 0.033	-0.22 ± 0.31
2	137.995 ± 0.038	-0.78 ± 0.32	38	138.115 ± 0.032	0.05 ± 0.31
3	137.979 ± 0.028	1.20 ± 0.32	39	138.101 ± 0.022	-0.03 ± 0.35
4	137.747 ± 0.032	-0.21 ± 0.30	40	138.100 ± 0.041	0.13 ± 0.32
5	137.848 ± 0.030	0.00 ± 0.30	41	138.091 ± 0.029	-0.02 ± 0.29
6	137.889 ± 0.024	0.04 ± 0.31	42	138.118 ± 0.025	-0.11 ± 0.29
7	137.932 ± 0.020	-0.13 ± 0.28	43	138.138 ± 0.032	-0.07 ± 0.29
8	137.984 ± 0.019	0.20 ± 0.30	44	138.129 ± 0.025	0.15 ± 0.32
9	137.949 ± 0.030	-0.04 ± 0.35	45	138.100 ± 0.032	0.01 ± 0.34
10	137.981 ± 0.038	-0.11 ± 0.31	46	138.111 ± 0.035	-0.04 ± 0.31
11	137.980 ± 0.031	0.25 ± 0.25	47	138.124 ± 0.029	-0.03 ± 0.29
12	137.959 ± 0.020	-0.26 ± 0.27	48	138.125 ± 0.026	-0.10 ± 0.32
13	138.007 ± 0.026	0.10 ± 0.31	49	138.118 ± 0.032	0.16 ± 0.36
14	137.982 ± 0.033	0.05 ± 0.33	50	138.083 ± 0.036	-0.06 ± 0.37
15	137.985 ± 0.031	-0.04 ± 0.35	51	138.093 ± 0.037	0.06 ± 0.36
16	138.003 ± 0.032	0.06 ± 0.37	52	138.086 ± 0.037	-0.09 ± 0.40
17	138.009 ± 0.041	-0.13 ± 0.35	53	138.095 ± 0.031	0.04 ± 0.47
18	138.033 ± 0.031	0.02 ± 0.33	54	138.080 ± 0.055	-0.22 ± 0.43
19	138.020 ± 0.033	0.16 ± 0.31	55	138.075 ± 0.041	0.35 ± 0.34
20	138.013 ± 0.031	-0.19 ± 0.30	56	138.010 ± 0.031	-0.10 ± 0.32
21	138.050 ± 0.025	-0.30 ± 0.33	57	138.043 ± 0.030	0.10 ± 0.34
22	138.034 ± 0.035	nm	58	138.048 ± 0.035	-0.20 ± 0.34
23	137.935 ± 0.034	-0.13 ± 0.33	59	138.080 ± 0.030	0.14 ± 0.37
24	138.049 ± 0.035	-0.23 ± 0.33	60	138.057 ± 0.036	-0.08 ± 0.38
25	138.127 ± 0.025	-0.18 ± 0.36	61	138.074 ± 0.041	-0.02 ± 0.33
26	138.142 ± 0.041	0.26 ± 0.34	62	138.068 ± 0.028	0.07 ± 0.33
27	138.109 ± 0.032	-0.19 ± 0.32	63	138.056 ± 0.032	0.06 ± 0.36
28	138.146 ± 0.028	-0.06 ± 0.32	64	138.064 ± 0.036	-0.17 ± 0.38
29	138.131 ± 0.036	0.17 ± 0.32	65	138.088 ± 0.036	0.09 ± 0.37
30	138.099 ± 0.024	-0.11 ± 0.35	66	138.065 ± 0.038	0.12 ± 0.35
31	138.114 ± 0.039	0.15 ± 0.34	67	138.067 ± 0.031	-0.21 ± 0.37
32	138.098 ± 0.032	-0.04 ± 0.27	68	138.104 ± 0.037	0.08 ± 0.37
33	138.122 ± 0.032	-0.20 ± 0.26	69	138.083 ± 0.039	0.09 ± 0.32
34	138.135 ± 0.010	0.19 ± 0.32	70	138.085 ± 0.030	
35	138.093 ± 0.038	-0.17 ± 0.36	71	138.110 ± 0.027	
36	138.103 ± 0.034	0.31 ± 0.34			

Table 2.4. Zero enrichment experiment for 71 reference gas measurements using an aliquot size of 3.164 ng (100s bleed time).

* denotes the standard error.

** $\delta^{15}N_n = \left(\frac{(28/29_{(n-1)} + 28/29_{(n+1)}) \times 0.5}{(28/29)_n} - 1 \right) \times 1000$ ‰

(where n is the run number).

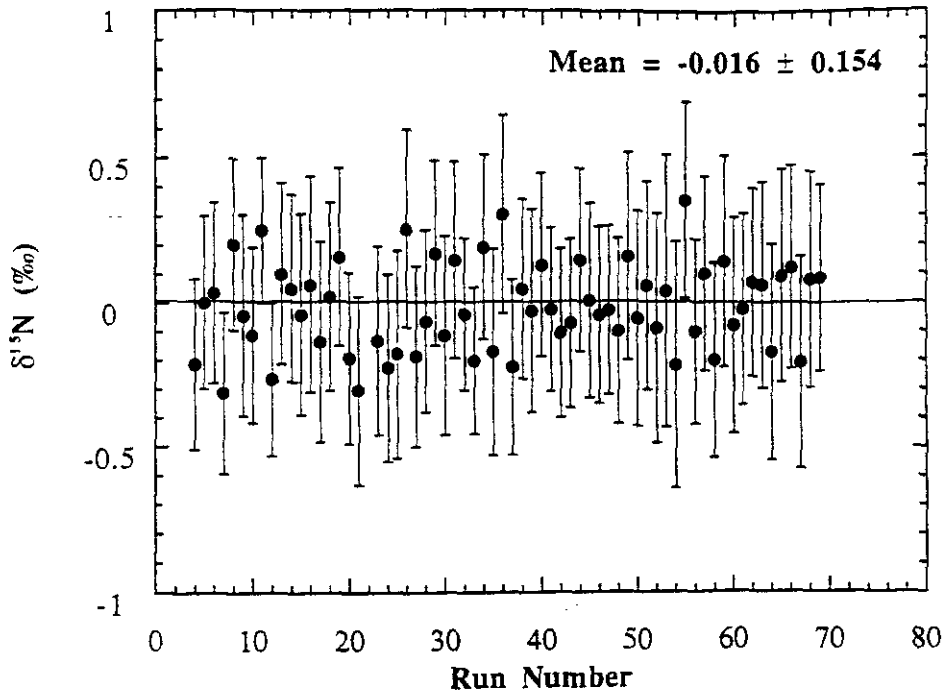

Figure 2.8. *Plot of zero enrichment experiment for 71 reference gas measurements using an aliquot size of 3.164 ng (100s bleed time).*

During the course of the zero enrichment experiment, the 28/29 ratio drifted by 2.9‰ between extreme values (Table 2.4). The zero *enrichment* study yielded an average $\delta^{15}N$ value of -0.0016‰ with a 1σ error of ±0.154‰. This is in full agreement with the 1σ-errors calculated in Table 2.3 and confirms that the mass spectrometer can repeatedly analyse aliquots of nitrogen with a precision of ±0.2‰.

2.5.2. Calibration of the instrument

In order to obtain the "true" isotopic composition, *i.e.* relative to AIR, of any aliquot of nitrogen, the isotopic composition of the reference gas also needs to be determined relative to AIR. In addition, it is essential to be able to determine the quantitative yield of nitrogen in any aliquot of sample or reference gas. These calibration measurements are crucial to ensure that the yield and isotopic data obtained from Finesse are accurate and reliable.

Calibration of the instrument is carried out after loss of vacuum or after any routine maintenance, and thereafter is repeated regularly to ensure that the sensitivity of the mass spectrometer, or the isotopic composition of the reference gas has not changed. The two types of nitrogen standards that are used for calibration are rubidium-ammonium sulphates ($Rb_2(NH_4)SO_4$) and local air. The rubidium-ammonium sulphate standards are prepared from NBS-N1 and NBS-N2 ammonium sulphates which have been dissolved in rubidium sulphate to produce milligram sized samples of a known concentration and isotopic composition. Further details of standard preparation and analysis is given by Boyd and Pillinger (1991).

Two batches of $Rb_2(NH_4)SO_4$ were analysed, a selection of results are given in Table 2.5. The expected nitrogen yields (ng) are calculated assuming that the nitrogen concentration of batch N2 1d was 335 ppm from a previous study (Russell *pers. comm.*), and 1660 ppm for batch N2 2e (Boyd and Pillinger, 1991). The multiplication factor required to convert I28 measurements to quantitative amounts of nitrogen is termed the "conversion factor", and is calculated from the ratio of the expected yield (assuming the abundances quoted above) to the I28 value. The latter has been corrected assuming that 100% of the nitrogen was admitted into the mass spectrometer.

Batch No.	Weight (mg)	Expected N yield (ng)	$I28_{tot}$* (V)	Conversion factor**
N2 1d	1.324	443.5	220.5	2.1
N2 1d	1.326	444.2	163.2	2.7
N2 1d	1.177	394.4	136.0	2.9
N2 2e	0.328	543.9	286.3	1.9

Table 2.5. Calibration of nitrogen yields by Finesse using $Rb_2(NH_4)SO_4$ standards.
* denotes the I28 (V) measurement assuming that 100% of the nitrogen was admitted into the mass spectrometer.
** conversion factor (defined in text) $= \left(\frac{\text{Expected N yield}}{I28_{tot}}\right)$.

The isotopic composition of the reference gas with respect to AIR is calculated from the difference between the standard relative to the reference gas and the standard relative to

AIR. The $Rb_2(NH_4)SO_4$ standards analysed were the same as in Table 2.5 and the data obtained are given in Table 2.6. The $\delta^{15}N$ values for the standards with respect to AIR have been calculated as +27.5‰ (Russell *pers. comm.*) for the N2 1d batch and +20.4‰ (Boyd and Pillinger, 1991) for the N2 2e batch.

Batch No.	True $\delta^{15}N$ (‰) (rel. to AIR)	Std $\delta^{15}N$ (‰) (rel. to ref)	Ref $\delta^{15}N$ (‰) (rel. to AIR)
N2 1d	+27.5	+28.45	-0.95
N2 1d	+27.5	+26.14	+1.36
N2 1d	+27.5	+22.72	+4.78
N2 2e	+20.4	+19.01	-1.39

Table 2.6. Determination of the nitrogen isotopic composition of the reference gas using $Rb_2(NH_4)SO_4$ standards.

Table 2.5 and 2.6 shows that there are many problems associated with the use of $Rb_2(NH_4)SO_4$ standards as a means of calibration. The inconsistency of both the calculated conversion factor, and reference gas isotopic composition relative to AIR can be explained as having been introduced during the complicated preparation of the standards, or as errors introduced during subsequent sample handling. It was therefore decided that AIR would be a better standard for nitrogen calibration, as it would retain a constant isotopic composition and could be replenished easily without risk of additional contamination. The AIR was stored in a metal cylinder of volume 300 ml with two modified manual valves acting as an aliquotting system to provide single aliquots of 0.5 ml (section 2.3.3). A single measurement was made, on different days, on one aliquot of AIR after a single purification step. The conversion factor was calculated by the same method as detailed for the $Rb_2(NH_4)SO_4$ standards, where the expected yield of nitrogen for a 0.5 ml aliquot was calculated as ~830 ng. The $\delta^{15}N$ value for the reference gas relative to AIR was calculated from the mean 28/29 ratios as given by Equation 1.1 and the associated errors for the $\delta^{15}N$ measurements are calculated using Equation 2.2. The data obtained from the AIR calibration experiment are given in Table 2.7.

Run	Mean 28/29 (±SE)*	Conversion factor	$\delta^{15}N$ (‰)**
ALI1	135.872 ± 0.056	1.78	-0.90 ± 0.55
REF	135.995 ± 0.050		
ALI2	136.056 ± 0.061	1.82	0.00 ± 0.64
REF	136.055 ± 0.058		
ALI3	135.951 ± 0.048	1.88	0.76 ± 0.54
REF	135.848 ± 0.055		
ALI4	136.174 ± 0.064	1.80	0.28 ± 0.62
REF	136.135 ± 0.055		
ALI5	136.179 ± 0.064	1.76	0.18 ± 0.62
REF	136.154 ± 0.055		
ALI6	136.224 ± 0.061	1.76	0.67 ± 0.58
REF	136.133 ± 0.051		
ALI7	136.292 ± 0.062	1.83	0.85 ± 0.61
REF	136.177 ± 0.055		
ALI8	137.848 ± 0.016	1.76	-1.36 ± 0.17
REF	138.035 ± 0.017		
Total		1.79 ± 0.04	0.06 ± 0.80

Table 2.7. Calibration of nitrogen yields and reference gas isotopic composition using local AIR.

* denotes the standard error (SE), ** denotes the standard error expressed in ‰.

Table 2.7 shows that, compared to $Rb_2(NH_4)SO_4$ standards, local AIR provides a more accurate and reproducible means of calibrating the instrument for both nitrogen yields and the isotopic composition of the reference gas relative to AIR. The conversion factor obtained from the above measurements was 1.79 ± 0.04, which allows accurate determination of the nitrogen yield from any aliquot of sample or reference gas. The isotopic composition of the reference gas relative to AIR was calculated as $\delta^{15}N_{AIR}$ = 0.06 ± 0.80‰, which enables the measured isotopic composition of any sample gas aliquot to be corrected for this offset. However, it should be noted that any change in sensitivity in the mass spectrometer necessitates re-calibration of the instrument to ensure that the data obtained remains accurate and reliable.

2.5.3. Baratron calibration

The baratron is calibrated using known quantities of CO_2 gas, measured on a separate instrument and transferred *via* evacuated glass take off vessels. The CO_2 is transferred to the baratron and trapped onto the cold finger using liquid N_2. The baratron is then isolated and the abundance of carbon was measured using an identical procedure to that used during sample analysis (section 2.4.5). The baratron meter reading (V) is shown in Table 2.8 for each known CO_2 yield (μg) and is plotted in Figure 2.9. The conversion factor is calculated from the gradient of the graph (in this case 1V = 0.88 μg carbon), and a precision of ±10% is assumed for all carbon abundance measurements obtained in this work.

Baratron meter reading (V)	Carbon yield (μg)
1.142	1.03
1.183	1.07
3.920	3.09
3.609	3.38
8.120	7.14

Table 2.8. Calibration of the baratron using known carbon yields (μg).

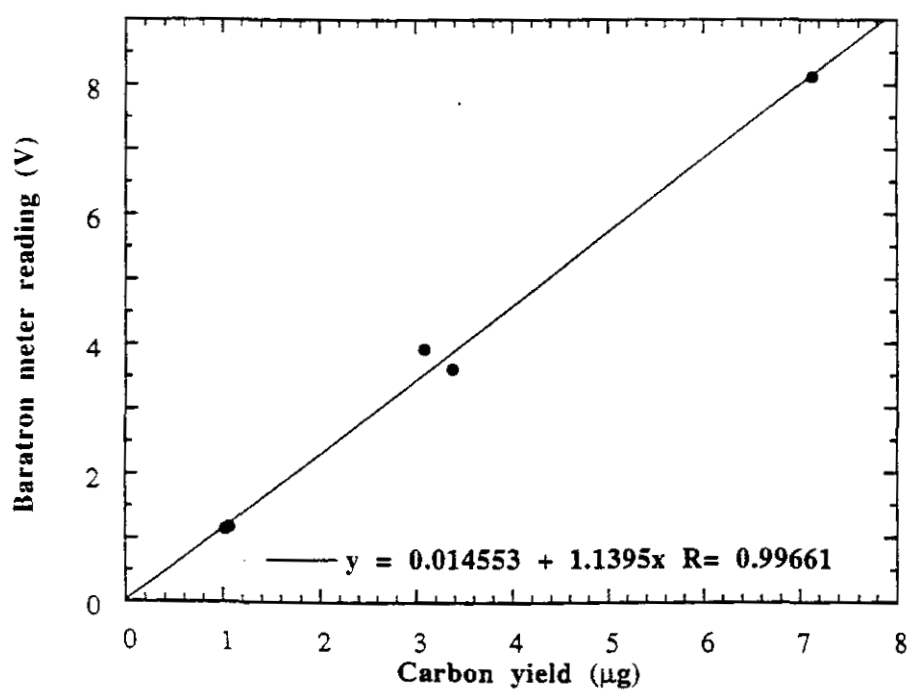

Figure 2.9. Plot of baratron meter reading (V) against known carbon yield (μg) for the calibration of the baratron.

2.6. Sample handling procedure

Nitrogen constitutes 78% of the Earth's atmosphere and hence it becomes exceedingly difficult to eliminate the effects that exposure of a sample to the atmosphere during sample preparation will have on its nitrogen isotopic composition. The stepped heating (combustion and pyrolysis) techniques go some way to identifying possible contamination components, but ideally atmospheric contamination during sample handling should be reduced as much as possible. This is especially true with lunar soils and breccias as they are of a valuable nature, are often in short supply, and are essentially "pristine" from the point of view of terrestrial exposure. The following sections are descriptions of the precautions and techniques which have been employed to reduce atmospheric contamination of lunar samples.

2.6.1. Storage of lunar samples

The bulk of the lunar sample collection is currently stored in the Lunar Sample Building at JSC, Houston, Texas, USA. The samples are stored under high security and extensive clean room conditions, in large cabinets filled with flowing, high-purity nitrogen gas that contains less than 5.7 ppm H_2O, 20 ppm O_2 and 2 ppm Ar. Extreme care was initially taken when determining which materials could be used to build these cabinets and possible interfering elements such as Rb and Pb were avoided. The sample vaults all have a high positive pressure to direct the passage of unfiltered air towards the exterior of the cabinets. Aluminium, teflon or stainless steel tools are used for any sample which requires sawing or chipping, to minimise contamination still further. Further details of sample storage and curation have been given by Vaniman *et al.* (1991).

The lunar samples available for use in this study were stored in glass vials or stainless steel tubes. Some had been delivered in nitrogen filled teflon bags as originally supplied by NASA. They were kept inside two locked combination safes which were inside a locked clean room at the PSRI. Any samples that have undergone chemical treatments (section 2.7.1) or size, density or magnetic separations (section 2.7.2) were stored in pre-cleaned glass bottles, the procedure for which is given in section 2.6.2. In order to prevent

any dust, clothing fibres or dirt contaminating the samples, access to the clean room could only be gained wearing a lint free overall, hat, disposable plastic gloves and overshoes.

2.6.2. Cleaning of equipment

Tweezers and sample spatulas (BDH, Lutterworth, Leicestershire, UK) were cleaned in a test tube using a 1:1 solution of AnalaR methanol and AnalaR toluene (BDH Chemicals Ltd, Poole, Dorset, UK) by sonicating them in a model FS100b ultrasonic bath (Decon Laboratories Ltd, Hove, East Sussex, UK) for 20-30 minutes. The waste chemicals were then poured into a suitable waste bottle and the tweezers and spatulas were placed into the test tube which was covered with aluminium foil and left overnight in a drying oven at ~100°C.

Glassware (including sample bottles, test tubes and beakers) were left to soak overnight in a bath of chromic acid. This was prepared by dissolving 150 g of GPR sodium dichromate ($Na_2Cr_2O_7$) in 150 ml water and slowly adding 1 winchester (2.5 litres) of GPR sulphuric acid (BDH Chemicals Ltd, Poole, Dorset, UK). The chromic acid was allowed to cool to around 40°C before use. The following day, the glassware was rinsed thoroughly and repeatedly with tap water and then distilled water, to ensure all the chromic acid had been removed, covered in aluminium foil and then placed in the drying oven. The lids for sample bottles were sonicated in methanol for ~20 minutes and allowed to dry in the same manner.

The thicker foil, used for sample weighing (section 2.6.4) was cut into squares, after removal of the edges and also sonicated in a 1:1 solution of AnalaR methanol and toluene for ~20 minutes and then wrapped in aluminium foil and dried. Once dried, it was stored in an aluminium foil-lined dish in the clean room.

2.6.3. Platinum bucket preparation

In order to ensure that all the sample was loaded into the extraction section, the sample was placed into a platinum envelope. A previous study (Norris, 1987 *unpublished data*) has indicated that platinum releases very little nitrogen over the required temperature

range. The platinum bucket was made from 25 μm thick platinum foil with a purity of 99.95% (Goodfellow, Cambridge, UK). The buckets usually measure 5 mm x 4 mm and weigh between 10-20 mg, depending on the amount of sample required. Platinum buckets for nitrogen extraction experiments were cleaned using the protocol established by Russell (1992). Two empty buckets were cleaned for at least 2 hours at 1000°C in an open 6 mm quartz tube to remove any contamination adsorbed during preparation. After cooling, a third bucket containing 2-3 CuO pellets of length 2-4 mm (BDH Chemicals Ltd, Poole, Dorset, UK) was added to the tube which was then evacuated to a pressure of 10^{-6} mbar and then sealed. The sealed tube was then combusted at 1000°C for at least 12 hours and allowed to cool to room temperature whilst remaining sealed.

This cleaning protocol was adapted from the procedure defined by Ash (1990) for preparing platinum buckets for carbon analysis, whereby the buckets were allowed to cool to 600°C under vacuum. However, the carbon procedure was shown to give high nitrogen blanks (Franchi, 1988), because the oxygen was reabsorbed onto the CuO during cooling and hence the nitrogen was absorbed onto the buckets once the tube was opened to the atmosphere. The adapted procedure (Russell, 1992) allowed the buckets to cool in an oxygen-rich environment and hence oxygen, as opposed to nitrogen, was absorbed onto the buckets.

2.6.4. Sample weighing procedure

Once the sealed tube had cooled to room temperature, it was taken into the clean room and broken so that the sample could be weighed into the platinum bucket. The balance used was a Sartorius Supermicro S3D (Sartorius Ltd, Belmont, Surrey, UK) with a precision of ±0.5 μg. To minimise contamination, the surface used was covered with a clean piece of aluminium foil and any tweezers or spatulas used to handle the bucket or the sample were pre-cleaned (section 2.6.2). Extra-thick aluminium foil of thickness 50 μm (Goodfellows, Cambridge, UK), which was also pre-cleaned (section 2.6.2) was used as a counterbalance for the platinum bucket and to aid sample manipulation. Once the sample had been weighed, the platinum bucket was closed and the sample was re-weighed several times

to check that no sample was lost out of the bucket. The sample could then be loaded onto the rotatable dish using the procedure described in section 2.4.1.

2.7. Sample preparation

2.7.1. Acid residue preparation

The preparation of acid resistant residues were carried out by Dr J.W.Arden from the Dept. of Earth Sciences, University of Oxford. The protocol used for these residues is the same as previously described by Ash (1990) and employed by previous workers (Russell, 1992; Newton, 1994) for investigations into presolar diamond and other resilient species in meteorites, and will only be described briefly here. For the lunar samples studied in this work, the purpose of acid treatment was to remove any surficial contamination, organics or silicates in order to attempt to constrain the isotopically light nitrogen component within lunar soils and breccias. The objective of this investigation is to determine whether the isotopically light nitrogen is due to the contribution of carbonaceous chondrite material in the lunar regolith and the results are discussed in section 4.4.

An Apollo 12 soil (A12023) and an Apollo 17 breccia (A79035) were treated with HF/HCl using the following procedure. The sample was etched in HF/HCl to remove surficial contamination, then treated with 9M HF - 1M HCl to remove silicates, and then with 1M HCl to remove any fluorides formed during the previous stage. Finally the residue was washed with distilled water, acetone and then dried. This process would typically take 3-4 weeks. At this stage in the proceedings, the HF/HCl residue would usually be treated with carbon disulphide (CS_2) in order to remove any sulphur remaining after the breakdown of sulphide minerals. As lunar samples typically contain low amounts of sulphur (200-500 ppm for a suite of Apollo 16 soils - Kerridge *et al.*, 1975b), this process was not deemed necessary. The HF/HCl stage removes typically 99 wt.% of the soil.

Only A79035 was treated with chromic (H_2CrO_4) and perchloric acid ($HClO_4$). The chromic acid was prepared by dissolving 0.39 g of potassium dichromate in 10 ml of 2N H_2SO_4 and heating a known amount of the HF/HCl residue for 1 day at 70°C. This time period was adjudged to be sufficient for any carbon in an organic form to be oxidised. The

residue was then fumed with $HClO_4$ at 70°C and left under an infra-red lamp to dry. Once completed, the remaining residue was washed with distilled water, acetone and then dried. The combination of the chromic and perchloric acid treatment should only leave diamond, silicon carbide, spinels and some nitrides in tact, and resulted in removal of a further 50% of the HF/HCl residue.

2.7.2. Grain size, density and magnetic separates

The analysis of size, density and magnetic separates from lunar soils has provided a useful technique for establishing possible location sites for nitrogen within the regolith. For this study, a selection of size, density and magnetic separates from Apollo 12 soil, A12023 (section 3.5), were analysed, as well as the finest grain size (<10 μm) of some Apollo 16 soils (section 5.3.1).

All the fractions used in this work had previously been prepared: the Apollo 12 sample by Mrs D. Fabian and the Apollo 16 samples by Prof. C.T. Pillinger. An extensive study of the A12023 grain size, density and magnetic separates had previously been undertaken for CH_4 and C_{hyd} (Pillinger *et al.*, 1978; Woodcock and Pillinger, 1978) and a small number had been analysed for nitrogen abundance and isotopic compositions (Norris, 1987 *unpublished data*).

2.7.2.1. Grain size separates

The Apollo 12 soil was separated into fourteen size fractions[1] ranging from >1 mm to "smoke" using 2 g of bulk material. The grain size fractions were obtained by wet sieving in spectroscopic grade methanol, using stainless steel sieves, as described by Pillinger *et al.* (1978). The smoke fraction was obtained from the sample that was suspended when the methanol was decanted off the <30 μm fraction. Decanting was used to minimise solvent evaporation and hence reduce carbon residue contamination. Microscopic and electron

[1] The grain size fractions for soil A12023 were as follows: >1 mm, 500 μm-1 mm, 250-500 μm, 152-250 μm, 106-152 μm, 75-106 μm, 53-75 μm, 40-53 μm, 30-40 μm, 20-30 μm, 15-20 μm, 10-15 μm, <10 μm and smoke.

microscopic analyses made at the time of separation, confirmed the grain size uniformity of each size fraction.

The Apollo 16 samples were separated using the same technique, although fewer fractions were obtained.

2.7.2.2. Density separates

Density separations were performed on all grain size fractions between 30 μm and 500 μm. using the technique described by Gardiner *et al.* (1977). Each size fraction was centrifuged in tetrabromoethane (BDH Reagent grade, ρ = 2.96 g cm^{-3}) and iodomethane (BDH Reagent grade, ρ = 3.3 g cm^{-3}) to provide three density ranges, *i.e.* ρ < 2.96 g cm^{-3} (low density), ρ = 2.96-3.3 g cm^{-3} (medium density) and ρ > 3.3 g cm^{-3} (high density). Heavy liquids were removed by repeated washing in carbon tetrachloride and AnalaR or SpectraR acetone or methanol.

2.7.2.3. Magnetic separates

The ρ < 2.96 g cm^{-3} and ρ = 2.96-3.3 g cm^{-3} density fractions were magnetically separated using the procedure described by Cadogan *et al.* (1973) and Pillinger *et al.* (1978). This involved the use of a magnetic separator, similar to that described by Housley *et al.* (1972), but modified by replacing the screw thread with a 0.01 mm micrometer.

The magnetic fractions were separated by decreasing the distance (in 0.5 mm intervals) between the sample, which was immersed in methanol (BDH AristaR), and a soft iron rod attached to the central pole of a small cylindrical magnet. The index for each magnetic fraction is characterised by the distance between the rod and magnet, *i.e.* M3.0 indicates the fraction collected at a distance of 3.5-3.0 mm. Non-magnetic material is referred to as NM and magnetic material collected by contact between the magnet and sample is termed MT. The entire process was repeated several times to ensure accurate and total separation. The magnetic fractions after separation were collected by washing the rod with methanol and then extracting the solvent.

2.8. Elimination of low temperature (<350°C) contamination

In order to obtain an accurate isotopic profile for lunar samples at low (<600°C) temperatures, it was necessary to ensure that isotopic extremes were not subdued by surface or atmospheric contamination effects. Two techniques were employed for this purpose: on-line pre-combustion and potassium permanganate pre-combustion.

2.8.1. On-line pre-combustion technique

This technique was only employed during stepped pyrolysis extractions in order to remove contamination which could mask any low temperature indigenous nitrogen components. This was deemed necessary as during pyrolysis extraction, diffusion is the sole release mechanism and hence contamination would not be removed so efficiently and could be retained in the sample to higher temperatures. In contrast this procedure was not undertaken for the combustion extraction as it was believed that any low temperature contamination would be rapidly removed in the initial few steps. A temperature of 350°C was chosen as a suitable pre-combustion temperature, as it occurred after the release of the contamination products (typically T≤300°C) but prior to the liberation of the indigenous nitrogen (typically T>400°C). The comparison of abundance and isotopic composition for two extractions: an "ordinary" stepped combustion extraction and a combustion extraction following pre-combustion, have suggested that there is little, if any, release of indigenous nitrogen at temperatures below 350°C.

The sample was loaded into the extraction tube, but before beginning the incremental heating procedure, the sample was repeatedly combusted at 350°C until all the gas had been extracted. The procedure adopted for the pre-combustion steps was identical to that used for stepped combustion experiments (section 2.4.2). The number of steps required to remove all the low temperature gas varied from 4 to 12, but was usually ~6 steps. If the sample was left in the extraction tube overnight after pre-combusting, the extraction furnace was left at room temperature and was isolated from the inlet. The CuO furnace was left overnight at 450°C. On the following day, a couple of combustion steps were measured at 350°C, as a final confirmation of the removal of all gases, before the stepped pyrolysis extraction

commenced. Throughout this thesis, this technique has been adopted for all stepped pyrolysis extractions unless otherwise stated.

2.8.2. Potassium permanganate ($KMnO_4$) pre-combustion

The on-line precombustion technique described in section 2.8.1 has gone some way to constraining the isotopic composition of low temperature, indigenous lunar nitrogen. However it would be advantageous to have removed the majority of the contamination before loading the sample into the extraction section. A suitable pre-combustion technique was investigated for the first time by Dr J.Newton and described in Newton (1994). It involves an off-line combustion with potassium permanganate ($KMnO_4$) being used to supply the oxygen. The sample and $KMnO_4$ are loaded into two separate platinum buckets and placed in a single glass tube, evacuated in an identical way to platinum bucket preparation (section 2.6.3) and combusted in a furnace at the required temperature. In order to ensure a sufficient supply of oxygen, the amount of $KMnO_4$ used was 50 times the anticipated carbon yield (Newton, *pers. comm.*). Two samples studied in this work used this technique: A63340 <10 μm (section 5.4) and A79035 HF/HCl (section 4.4.3) which were combusted at a temperature of 350°C for 12 and 17 days respectively. The aim of using this technique was to find a chemical treatment that was not as harsh as $HClO_4$ but which would remove more low temperature components than the HF/HCl treatment.

2.9. Assessment of the blank contributions

In order to obtain precise abundance and isotopic composition data, it is imperative that the magnitude and isotopic composition of the full system blank is accurately known. Such blanks are measured using an identical protocol to that for sample analysis, in order to correct the measured abundance and isotopic values for the sample. The blanks are measured from the mass spectrometer, purification section and extraction section at the start of each sample analysis. Typical values for the nitrogen blanks from the aforementioned sections are ~2 pg, 0.25 ng and ≤1 ng respectively.

2.9.1. Background rise rate

The background rise rate is a measure of the increase of m/z 28, 29 and 30 within the mass spectrometer during an analysis. After the mass spectrometer has been exposed to atmosphere, *e.g.* following filament replacement, the rise rate is initially high (~0.5-1.0 ng min^{-1}) but decreases each day as the vacuum improves and the filament degasses. Within two or three weeks of repair, the background rise rate is ~1 pg min^{-1}. Figure 2.10 is a graph of background rise rate of m/z 28 within the mass spectrometer (pg min^{-1}) against the number of days since repair and illustrates the recovery rate of the instrument.

During this recovery period, it is important to eliminate any species from the mass spectrometer that could ultimately interfere with the measurement of nitrogen, *e.g.* $^{12}C^{16}O^+$ (m/z 28) and $^{13}C^{16}O^+$, $^{12}C^{17}O^+$ (m/z 29). The contribution of $^{12}C^{17}O^+$ is small as the $^{16}O/^{17}O$ ratio of terrestrial oxygen is approximately 2600:1. Therefore the 28/29 ratio of CO is similar to the $^{12}C/^{13}C$ ratio of terrestrial carbon, *i.e.* 89:1. As the 28/29 ratio of atmospheric N_2 is 136:1, failure to remove interfering species from the mass spectrometer can have a significant effect on the $\delta^{15}N$ measurements (section 2.5.1).

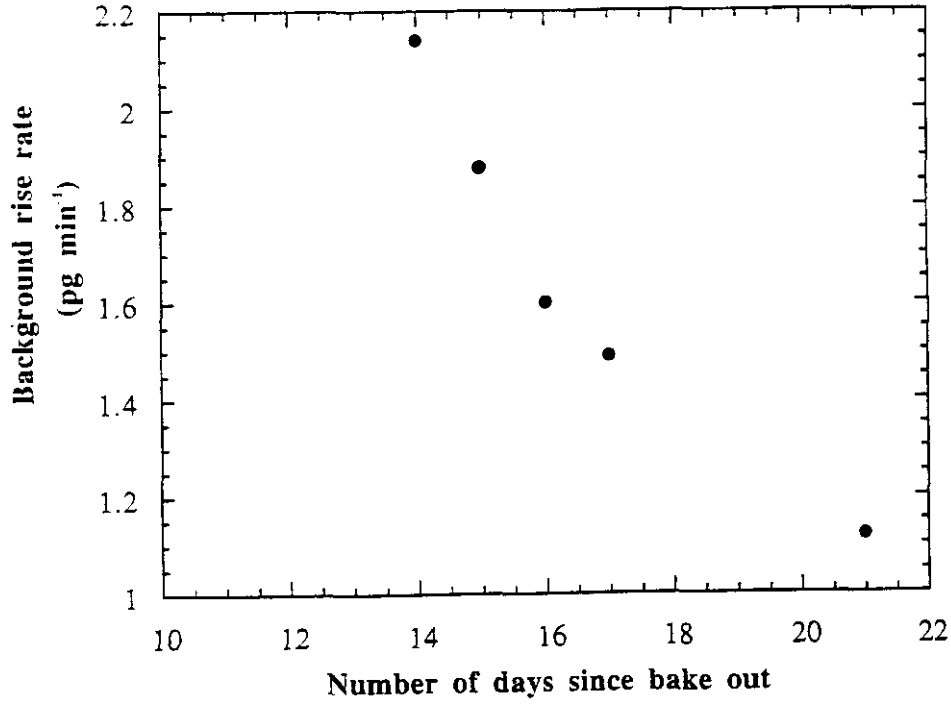

Figure 2.10. Plot of background rise rate of m/z 28 in the mass spectrometer (pg min^{-1}) against the number of days since bake out.

2.9.2. System blank evaluation

The full system blank needs to be evaluated prior to starting a stepped extraction analysis. The procedure is identical to that for each subsequent sample step, however the extraction section furnace remains at 1200°C throughout the measurement which enables a measurement of the abundance and isotopic composition of the system blank at the highest extraction temperature. Typical blank yields for both stepped combustion and pyrolysis extractions are between 0.5-1.0 ng with $\delta^{15}N$ values ranging from -5‰ to -15‰. This is consistent with the lower end range of $\delta^{15}N$ values from -11 to +20‰, obtained for mantle-derived rocks (Javoy *et al.*, 1984; Javoy and Pineau, 1986; Exley *et al.*, 1987), although Geiss and Bochsler (1982) have stated that the bulk terrestrial nitrogen is unlikely to differ from atmospheric nitrogen, *i.e.* 0‰, by more than 20‰. It should be noted that for low blank abundances (<0.6 ng) the $\delta^{15}N$ measurements are subject to precision errors which can be >1‰ and can be affected from CO interferences (section 2.5.1). Some of the analyses in this work utilised both stepped combustion and pyrolysis steps and in these cases a high temperature blank measurement was necessary using both extraction techniques, prior to commencement of the extraction.

2.9.3. Stepped combustion on an empty extraction section

The abundance of nitrogen contributing to the blank measurement is expected to decrease slightly during the course of an experiment and hence the measured blank at 1200°C at the start of the day can only be used as an estimation of the true blank. In order to obtain the true blank at any given temperature, a 100°C resolution stepped combustion experiment was performed on an empty extraction section. The data obtained are given in Appendix A1 and are illustrated in Figure 2.11. The axes have been previously described in section 1.7.3.2. Note that with the exception of the 1200°C step, the yield for each step was lower than the measured blank of 0.81 ng at the start of the extraction and hence the data are not corrected. The bulk $\delta^{15}N$ value of -6.9‰ compares well with the isotopic composition of the initial 1200°C blank with $\delta^{15}N$ = -6.3‰ and the range of $\delta^{15}N$ values for all blank measurements in this study. It should be noted that the errors associated with the $\delta^{15}N$

measurement for the empty sample extraction section highlight the difficulty in obtaining accurate isotopic compositions for low amounts of nitrogen (<0.6 ng).

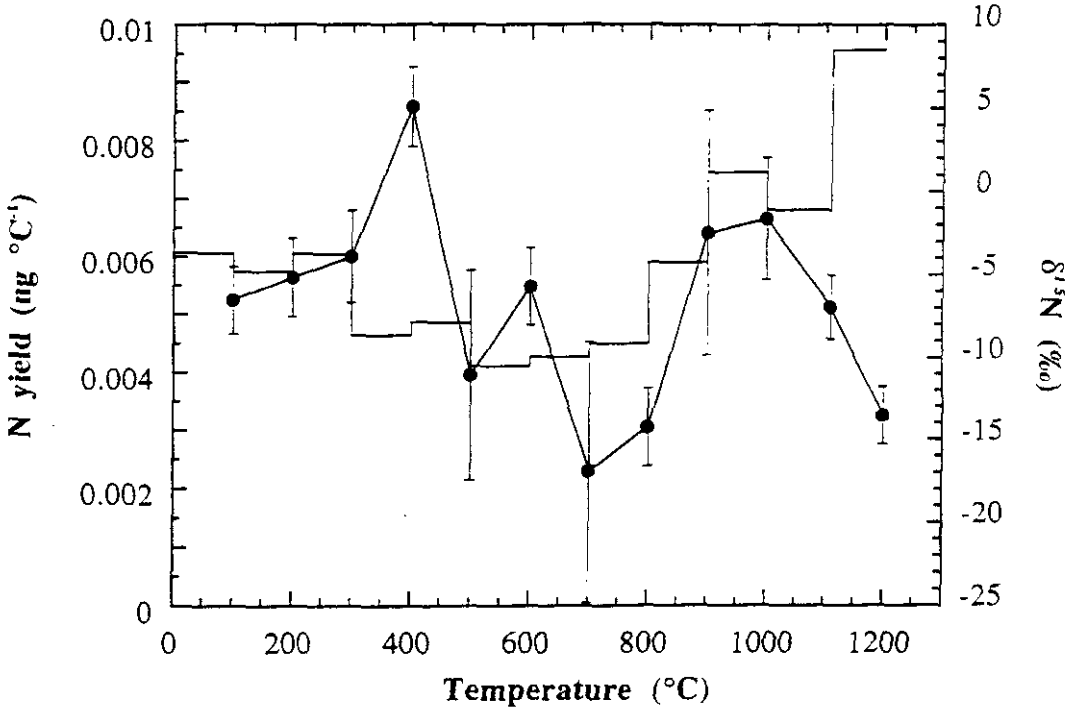

Figure 2.11. Blank extraction on an empty combustion section.

2.9.4. Platinum bucket blank

Blank measurements are also made on empty platinum buckets for both combustion and pyrolysis extractions. The platinum buckets are prepared and cleaned using an identical procedure to that described in section 2.6.3, and care is also taken to ensure that the buckets are of an equivalent size to those used during sample analysis. The platinum buckets are analysed for nitrogen and carbon abundances and nitrogen isotopic compositions (using temperature steps of 50°C), with the pyrolysis extraction utilising multiple combustion steps at 350°C (section 2.8.1). The nitrogen stepped extraction profiles are illustrated in Figures 2.12a and 2.12b the data are given in Appendix A2.

Stepped combustion of a 16.4 mg platinum bucket yields 15.8 ng of nitrogen with a bulk $\delta^{15}N$ = -13.0‰ (Figure 2.12a), comparable with 12.3 ng nitrogen and $\delta^{15}N$ = -10.2‰ respectively for the stepped pyrolysis of a 19.2 mg bucket (Figure 2.12b). The nitrogen yield in both extractions is higher than the initial blank measurement over two temperature ranges: 200-400°C due to the liberation of loosely bound nitrogen contamination, and

>1000°C as the bucket is only cleaned up to this temperature (section 2.6.3). This is done to avoid a tendency for the platinum envelope to become brittle and hence difficult to close once the sample has been loaded. The isotopic profiles are similar and tend towards lighter compositions at higher temperatures. The smoother profile for the pyrolysis extraction compared to the combustion is due to the removal of the low temperature gas prior to the pyrolysis.

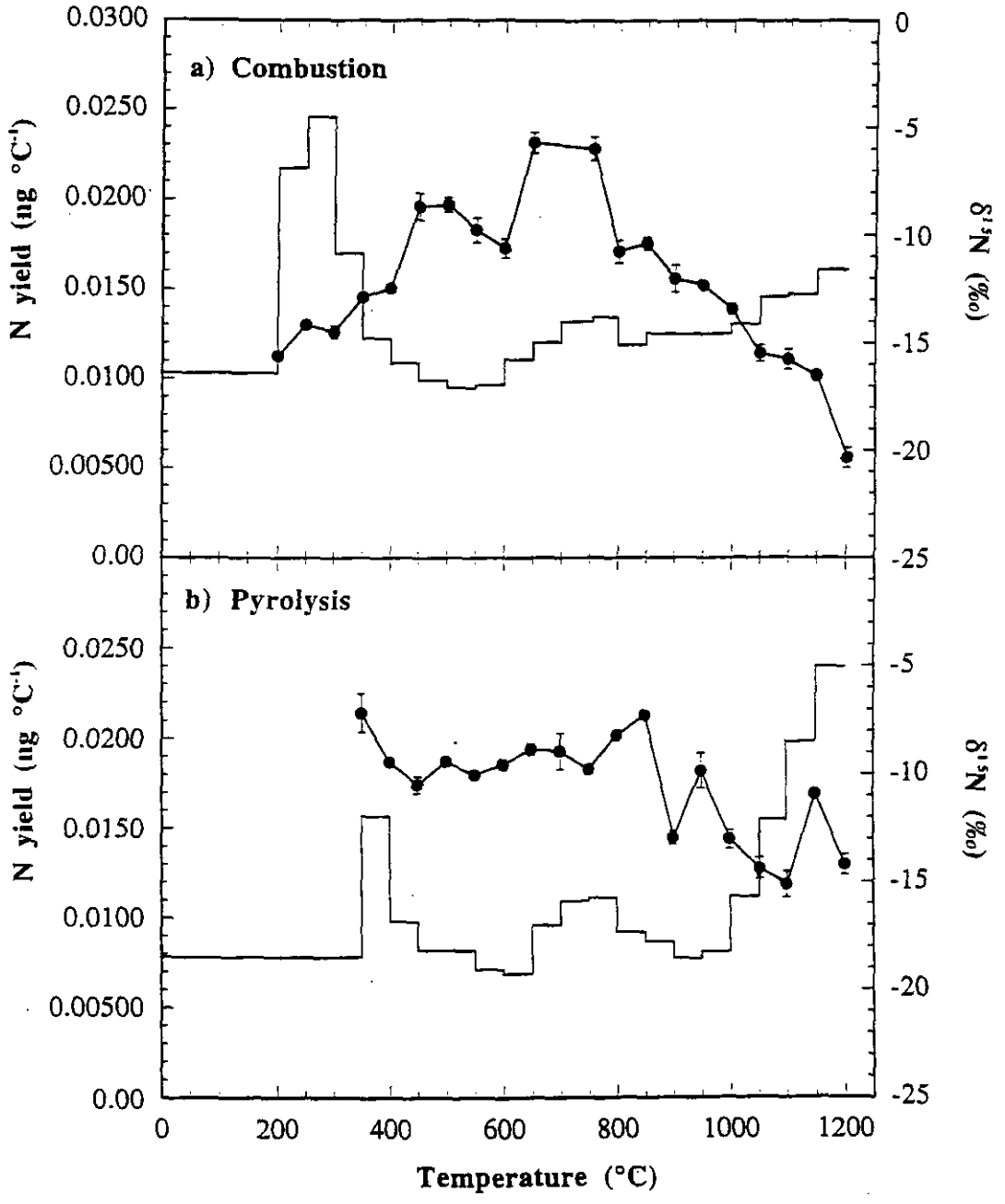

Figure 2.12. Nitrogen abundances (ng $°C^{-1}$) and isotopic compositions (‰) for an empty platinum bucket from 200-1200°C by stepped combustion (Figure 2.12a) and stepped pyrolysis (Figure 2.12b).

The platinum buckets yield 59.4 ng and 43.1 ng of carbon for the stepped combustion and pyrolysis respectively. As with the nitrogen, the majority of the carbon is liberated at temperatures of ≤400°C and is attributed to organic contamination. No significant data could be obtained from the ^{40}Ar measurements.

2.10. Blank correction and presentation of the data obtained in this study

The nitrogen abundance and isotopic compositions obtained from stepped pyrolysis and combustion of lunar soils and breccias are displayed graphically as a stepped release profile (Figures 1.5a and b). A description of the axes and the terminology used for individual nitrogen components in lunar soils and breccias are given in section 1.7.3.2.

Throughout this work the total nitrogen released from the lunar samples (ΣN) and the bulk isotopic composition ($\Sigma\delta^{15}N$) are corrected to eliminate the contribution of contamination. Unless otherwise stated, for the pyrolysis extractions, the samples are pre-combusted at a temperature of 350°C prior to the commencement of the stepped pyrolysis (section 2.8.1). The data obtained from the pre-combustion steps are excluded for the pyrolysis extractions, whereas for the combustion extractions a temperature of <400°C is deemed suitable.

The nitrogen abundance data are blank corrected using the combustion or pyrolysis blank measured at a temperature of 1200°C at the start of the day (section 2.9.2), unless otherwise stated. However, the $\delta^{15}N$ measurements are only corrected when the sample yield is a minimum of three times greater than the initial nitrogen blank. This is a precautionary measure which is taken to avoid situations where over compensation for the blank contribution may result in extreme $\delta^{15}N$ values. The temperature above which the $\delta^{15}N$ values are corrected for the nitrogen blank are given in the text, specific to each sample analysis.

Chapter 3

A detailed investigation of the yield and isotopic components in lunar soil A12023

3.1. Introduction

In order to investigate the origin, abundance and isotopic composition of nitrogen within lunar samples, it is deemed necessary to undertake a comprehensive study of a typical lunar soil. The sample chosen for this purpose is a basaltic soil from the Apollo 12 site, A12023, as it had been studied by many other workers (Moore *et al.*, 1971; Becker & Clayton, 1978; Kerridge *et al.*, 1978; Pillinger *et al.*, 1978; Norris, 1987 *unpublished data*) and hence could be used as a comparison with this work. A brief description of the geology of the Apollo 12 site and the chemistry and mineralogy of soil A12023, is given in section 3.2.

Lunar soil A12023 has been analysed using both stepped combustion and stepped pyrolysis extraction techniques, described in section 2.4.2. Replicate nitrogen analyses of the bulk soil have been performed throughout the duration of this work (section 3.3.1.1) although as continuous modifications were made to both the instrumentation and analytical procedures during this period, the latter analyses are deemed more reliable. In addition to the nitrogen abundance and isotopic data, conjoint argon yields and carbon abundances are also measured. Using diagnostic tracers such as $^{36}Ar/^{38}Ar$, $N/^{36}Ar$ and C/N ratios, it is hoped that the origin of the nitrogen in the lunar regolith could be identified.

To further investigate the siting and origin of the nitrogen within lunar soils, a variety of grain size, density and magnetic separates from A12023 are also analysed and the data obtained are given in sections 3.4 and 3.5. These include a dual combustion and pyrolysis extraction, performed on a <10 μm grain size fraction of A12023 in order to constrain the origin of the isotopically light nitrogen components. Finally, the conclusions regarding the nitrogen, argon and carbon inventory in A12023 are discussed (section 3.6).

3.2. The Apollo 12 site

3.2.1. Geology and mineralogy of the Apollo 12 site

The Apollo 12 landing site, illustrated in Figure 3.1, was chosen partly to determine the capability of the lunar module (LM) to land at a pre-designated location. This objective was achieved by landing within 200 m of the Surveyor 3 spacecraft (S in Figure 3.1) in the southeastern Oceanus Procellarum (3.2°S, 23.4°W). The site was also selected as it was a flat, lightly cratered mare region that was younger than the Apollo 11 site at Mare Tranquillitatis and hence contained basalts of more varied chemical and mineralogical compositions. Ejecta rays from the Copernicus Crater, 400 km to the north, cross the landing site and it was hoped that the formation age of the crater, previously estimated as 200 Myr (Hartmann, 1968), could be dated.

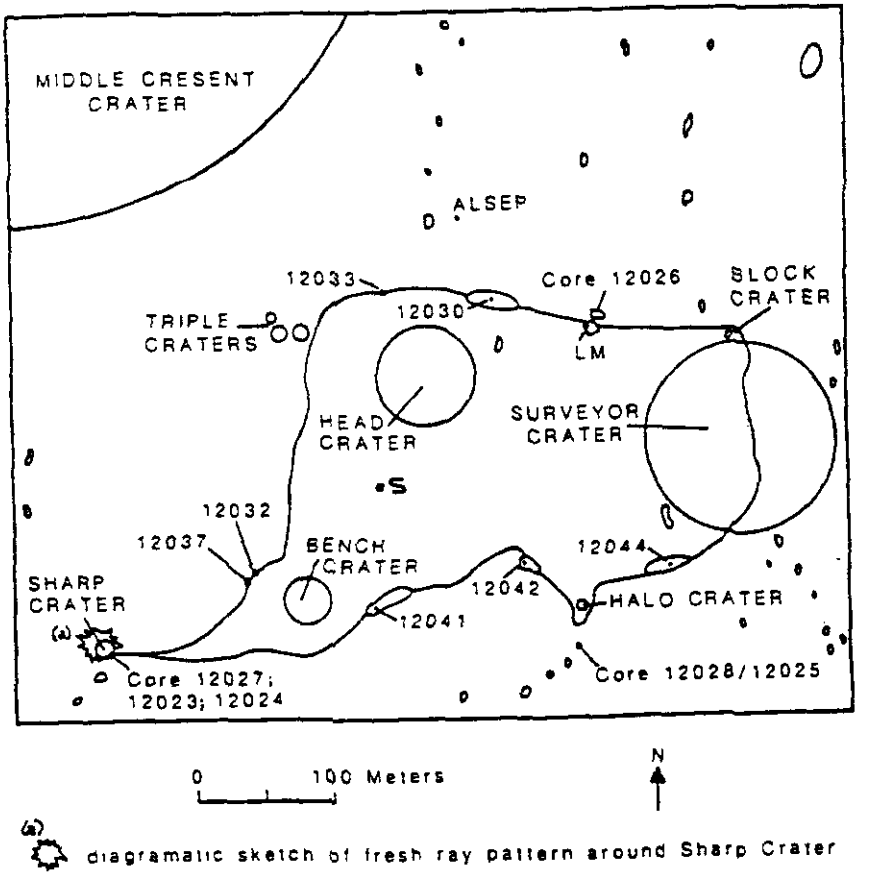

Figure 3.1. Geology of the Apollo 12 landing site.
LM = lunar module, S = Surveyor 3.
Five digit generic sample number previously defined in section 1.3.1.

The geology of the Apollo 12 site is detailed in Rhodes *et al.* (1977) and Wilhelms (1984). They suggest that the site consists of a layer of ejecta from the Imbrium basin formation event, which overlays the pre-Imbrium megaregolith. These layers are covered by at least three distinct types of low-Ti basaltic lavas, and mainly consist of olivine and pigeonite (low-Ca pyroxene) basalts, but with the presence of some ilmenite basalts. The crystalline rocks collected from the Apollo 12 site display a wide range of mineral compositions and reflect the varied geological units present at the site. Pyroxene, in the form of pigeonite and subcalcic augite, is the dominant mineral in all but two samples, with ilmenite abundances ranging from <1 to 25% and olivine present in most samples up to ~50%. In addition, plagioclase is present in every rock sample in amounts which vary from 5% to an upper limit of ~70% (LSPET, 1970).

The Apollo 12 fines and breccias are chemically distinct from the crystalline rocks and are generally lighter in colour due to differing proportions of the mineral phases. The major constituents of the fines are pyroxenes (40%), in the form of augite, subcalcic augite and pigeonite, plagioclase (20%), glass (~20%) and olivine (~5-10%). The glass occurs as irregular fragments or spherical beads in the regolith, or as amorphous coatings on some samples (section 1.6.1.2), and can vary from colourless to dark brown in colour. The minor constituents of lunar fines include ilmenite, tridymite, cristobalite and nickel-iron (LSPET, 1970).

3.2.2. Chemistry and mineralogy of Apollo 12023

Lunar soil A12023 was collected from a depth of 20 cm at the bottom of a trench on the east rim of Sharp Crater (Figure 3.1). The original weight of the sample was 407.9 g. It has been classified as a sub-mature soil, similar in mineralogy to other Apollo 12 soils, with $I_s/FeO = 55$ (Kerridge *et al.*, 1978), a complex exposure history and a ^{15}N-spallation age of 690 ± 80 Myr (Becker and Clayton, 1978). Studies of the major element chemistry of the bulk soil and grain size, density and magnetic separates from A12023 (Woodcock and Pillinger, 1978) and trace element studies (Warren *et al.*, 1978) have indicated that A12023 is a typical soil containing pyroxene, plagioclase, glass and olivine in decreasing order of abundance with the minor constituents, *e.g.* ilmenite, constituting only a few percent. The

major element chemistry for A12023 compared to other Apollo 12 soils is given in Table 3.1.

Sample	SiO_2	TiO_2	Al_2O_3	FeO	MgO	CaO	Reference
A12001	46.0	2.8	12.5	17.2	10.4	10.9	(1)
A12023	**~46**	**2.8**	**13.9**	**15.4**	**11.2**	**10.9**	**(2)**
A12032	46.5	2.9	15.2	14.1	9.4	10.7	(3)
A12033	48.2	2.3	15.1	12.9	8.4	10.6	(4)
A12037	44.8	3.5	15.1	14.9	10.2	10.5	(3)
A12042	45.7	2.7	13.0	16.2	10.4	10.6	(4)
A12070	45.7	2.8	13.0	16.4	10.5	10.4	(4)

Table 3.1. Major element chemistry of A12023 compared to other Apollo 12 soils. References: (1) Laul and Papike (1980), (2) Woodcock and Pillinger (1978), (3) Frondel *et al.* (1971), (4) Cuttitta *et al.* (1971).

3.3. Stepped heating extraction of bulk soil A12023

Replicate analyses of whole-soil, A12023, are performed by stepped combustion and stepped pyrolysis techniques, and the nitrogen data are given in Appendix B1. In addition to the nitrogen abundance and isotopic composition, argon isotopic ratios, *i.e.* $^{36}Ar/^{38}Ar$ and $^{40}Ar/^{36}Ar$, and $N/^{36}Ar$ are obtained for the high resolution extractions (FIN37 and FIN44), together with carbon abundance measurements and C/N ratios. The argon and carbon data for A12023 are discussed in sections 3.3.2 and 3.3.3 respectively and are also given in Appendix B1.

3.3.1. Nitrogen abundance and isotopic composition of A12023

The nitrogen data presented in this work are blank corrected, and the total nitrogen (ΣN) and bulk isotopic composition ($\Sigma\delta^{15}N$) are corrected to eliminate the contribution of low temperature contamination, in accordance with the procedures detailed in section 2.10 unless otherwise stated.

Table 3.2 displays the ΣN (ppm) and $\Sigma\delta^{15}N$ values (‰) for replicate analyses of A12023 in this study, and compares the data with that of previous workers. It should be noted that previous workers used much larger samples, typically >100 mg (Becker and Clayton, 1978; Kerridge *et al.*, 1978) compared to ~1 mg in this work.

Extraction No.	Weight (mg)	ΣN (ppm)	$\Sigma\delta^{15}N$ (‰)	Technique	Reference
FIN7	**1.158**	**46.8**	**+37.3**	**Stepped combustion**	**(1)**
FIN10	**1.539**	**92.3**	**+17.9**	**Stepped combustion**	**(1)**
FIN23	**0.863**	**92.2**	**+22.6**	**Stepped combustion**	**(1)**
FIN37	**3.315**	**116.0**	**+23.4**	**Stepped combustion**	**(1)**
FIN9*	**1.133**	**85.2**	**+31.9**	**Stepped pyrolysis**	**(1)**
FIN27*	**0.816**	**73.9**	**+20.2**	**Stepped pyrolysis**	**(1)**
FIN44	**2.791**	**122.8**	**+21.9**	**Stepped pyrolysis**	**(1)**
	131.1	73.6	+24.7	Bulk combustion	(2)
	130.5	70.6	+22.5	Bulk combustion	(2)
	2.985	72	+21	Stepped pyrolysis	(3)
	2.569	67	+29	Stepped pyrolysis	(3)
	973	75	+28.5	Stepped pyrolysis	(4)

Table 3.2. The ΣN (ppm) and $\Sigma\delta^{15}N$ (‰) for combustion and pyrolysis extractions of A12023 from this study compared to previous work.
References: (1) This work, (2) Kerridge *et al.* (1978), (3) Norris (1987 *unpublished data*), (4) Becker and Clayton (1978).
* no combustion steps at 350°C hence the nitrogen abundances and $\delta^{15}N$ values at a temperature of <400°C have been subtracted from the total.

The data obtained for replicate analyses of A12023 show reasonable consistency between stepped combustion and pyrolysis extraction techniques. The exceptions to this are FIN37 and FIN44 which are discussed below. Furthermore, there is general agreement between the data obtained in this study and the results of previous workers (Becker and Clayton, 1978; Kerridge *et al.*, 1978; Norris, 1987 *unpublished data*). The total nitrogen from A12023 in the current study ranges from 46.8 ppm (FIN7) to 122.8 ppm (FIN44) and

the $\Sigma\delta^{15}N$ varies from +17.9‰ (FIN10) to +37.3‰ (FIN7). These values are within the range of abundances and isotopic compositions obtained for a variety of lunar soils by previous workers (Petrowski *et al.*, 1974; Becker and Clayton, 1975, 1977, 1978; Kerridge *et al.*, 1975a, b; Kaplan *et al.*, 1976; Becker, 1980a; Clayton and Thiemens, 1980; Norris, 1987 *unpublished data*). Figure 3.2 displays a plot of ΣN (ppm) against $\Sigma\delta^{15}N$ (‰) for the A12023 data obtained in this study (filled circles), and available literature data from the aforementioned workers for lunar soils from a variety of sites (open circles).

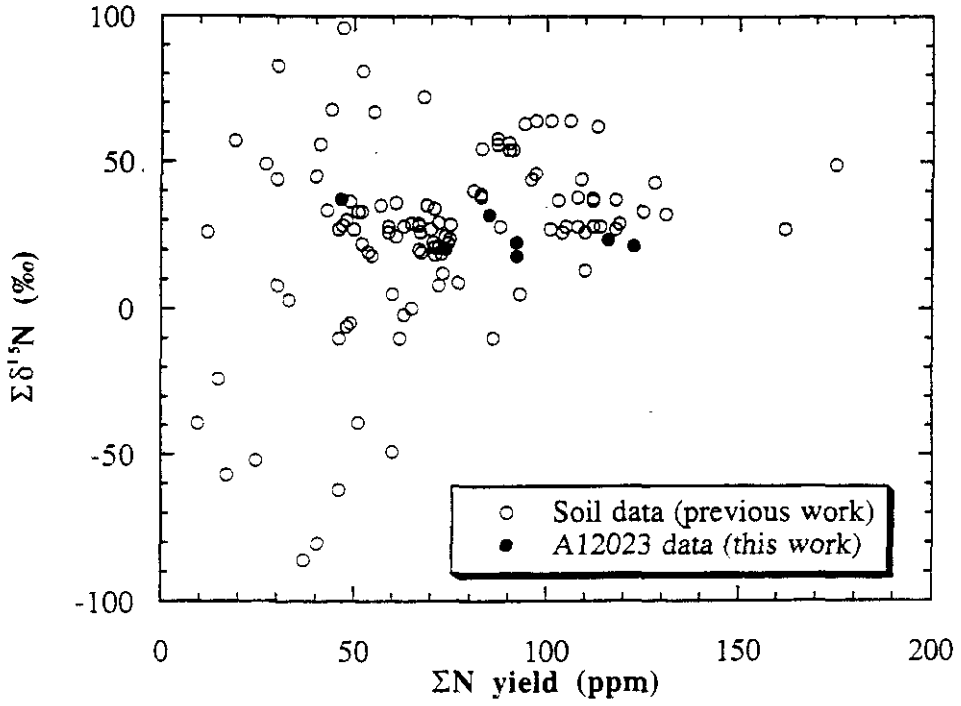

Figure 3.2. A plot of ΣN (ppm) and $\Sigma\delta^{15}N$ (‰) for A12023 in this study (filled circles) and for a variety of lunar soils by previous workers (open circles).
References for literature data are given in the text.

The major observation from Table 3.2 is that the nitrogen yields for extractions FIN37 and FIN44 are significantly higher than those obtained for the low resolution analyses, *e.g.* FIN23 and FIN27, although interestingly the $\Sigma\delta^{15}N$ values are similar. Both FIN37 and FIN44 utilised high resolution temperature steps (typically 10°C) across the release of LTN, compared to the earlier analyses which used 25°C or 50°C resolution. However, the nitrogen content of a sample will not increase due to the temperature resolution with which the nitrogen is extracted, unless the nitrogen is incompletely extracted from the sample in previous analyses. The consistency between the nitrogen data obtained by

previous workers, including bulk combustion extraction at 1220°C by Kerridge *et al.* (1978), and from the low resolution analyses in this work detract from such an explanation.

One possible explanation for the higher nitrogen yields for the high resolution extractions is that the blank measured at the start of the analysis is systematically underestimated. Previous stepped heating extractions for an empty extraction section and an empty platinum bucket (section 2.9.3 and 2.9.4 respectively) have shown that the nitrogen blank increases with temperature. If the total excess of nitrogen in the high resolution extractions, compared to the low resolution extractions, *i.e.* FIN37 compared to FIN23 for combustion and FIN44 compared to FIN27 for pyrolysis, is averaged over the total number of steps for each extraction, the blank would have to be underestimated by 1.7 ng and 3 ng per step for the combustion and pyrolysis respectively. This seems excessive as the initial blank measured at the start of the extraction is typically <1 ng. The lowest nitrogen yields for extractions FIN37 and FIN44 were obtained from the highest temperature steps, *i.e.* 1250°C for FIN37 and 1200°C for FIN44, following the release of HTN. This nitrogen is believed to be, at least in part, representative of the nitrogen blank at 1200°C and constitutes an increase in the nitrogen blank of up to 60% during the course of the extraction. The increase does not account for the required underestimation of the nitrogen blank in order to account for the increased yield for the high resolution extractions.

A more plausible explanation is that the higher yields are due to the use of a larger platinum bucket than used for the blank extractions (section 2.9.4). The high resolution extractions require a sample size which is approximately 3 times larger than that needed for a low resolution analysis, and hence a larger platinum bucket is required to hold the sample. The platinum bucket would contribute to the total blank in the system but this would not be reflected in the initial blank measurements as the sample had not yet been introduced to the extraction system. With the assumption that the ratio of nitrogen extracted from the platinum bucket for the high and low resolution extractions respectively is equivalent to the ratio of sample size for these extractions, the contribution of nitrogen blank from the platinum bucket can be estimated. The increased platinum bucket size accounts for approximately 77% of the excess nitrogen for the high resolution combustion but only 31% of the excess for the pyrolysis extraction. Note that this is an approximate calculation and assumes that the platinum buckets used for the blank experiments (section 2.9.4) are of equivalent size as the

buckets used for the low resolution extractions. Furthermore, the increased nitrogen yield liberated from a larger platinum bucket would not be expected to affect the $\delta^{15}N$ measurements significantly.

Other possible explanations, such as a sample weighing error, have been discarded as the phenomenon has been observed in two separate analyses. Furthermore the yield discrepancy is not believed to be due to incorrect calibration of the mass spectrometer as this is regularly checked. The possibility of preferential sorting in favour of the coarser grain sizes in the earlier extractions due to operator inexperience has also been eliminated as the lower yields obtained from the earlier analyses are more consistent with data by previous workers. The sample may have suffered increased contamination as a result of a longer residence time between the previous and current analyses, although this is not reflected in the amount of nitrogen liberated at low temperatures.

In conclusion, two explanations may be invoked to account for the increased nitrogen yields observed in the high resolution studies, when compared to earlier analyses in this work and by previous workers. It appears that the higher yields are a combination of increased nitrogen blank from the larger platinum bucket that was utilised in the high resolution extractions, and a underestimation of the blank as this is expected to increase during the extractions. The resultant effect of the latter is a slight increase in $\Sigma\delta^{15}N$ between the uncorrected and blank corrected data, *e.g.* an increase in $\Sigma\delta^{15}N$ from +14.7 to +15.7‰ for the pyrolysis extraction of A75080 (FIN150). The effect on N_{LT} for the same analysis is more extreme (+77.1 to +90.3‰).

3.3.1.2. High resolution stepped combustion and stepped pyrolysis extraction of A12023

In order to ascertain the isotopic composition of individual components in A12023, the soil was analysed by high resolution stepped combustion (FIN37) and stepped pyrolysis (FIN44) extraction. Replicate analyses had shown that the majority of the nitrogen was liberated between 600-900°C, hence temperature resolution of 10°C was employed across this region. To ensure that there was sufficient nitrogen available for analysis during each step, initial sample weights of 3.3 and 2.8 mg, for the combustion and pyrolysis respectively, were used, compared to 0.9 - 1.5 mg for the low resolution analyses. The

nitrogen abundance and isotopic profiles are shown in Figures 3.3a (FIN37) and 3.3b (FIN44) and the data are given in Appendix B1. The combustion extraction (FIN37) yielded 116.0 ppm of nitrogen with a $\Sigma\delta^{15}N$ of +23.4‰, comparable with 122.8 ppm and $\Sigma\delta^{15}N$ of +21.9‰ for the pyrolysis extraction (FIN44). Both extractions confirm that the nitrogen is released from the sample over two distinct temperature ranges: as a broad release between 600-900°C (LTN), which constitutes 75-80% of the total nitrogen, and as a narrow release between 1000-1200°C (HTN) as defined in section 1.7.3.2 (Figures 1.5a and 1.5b).

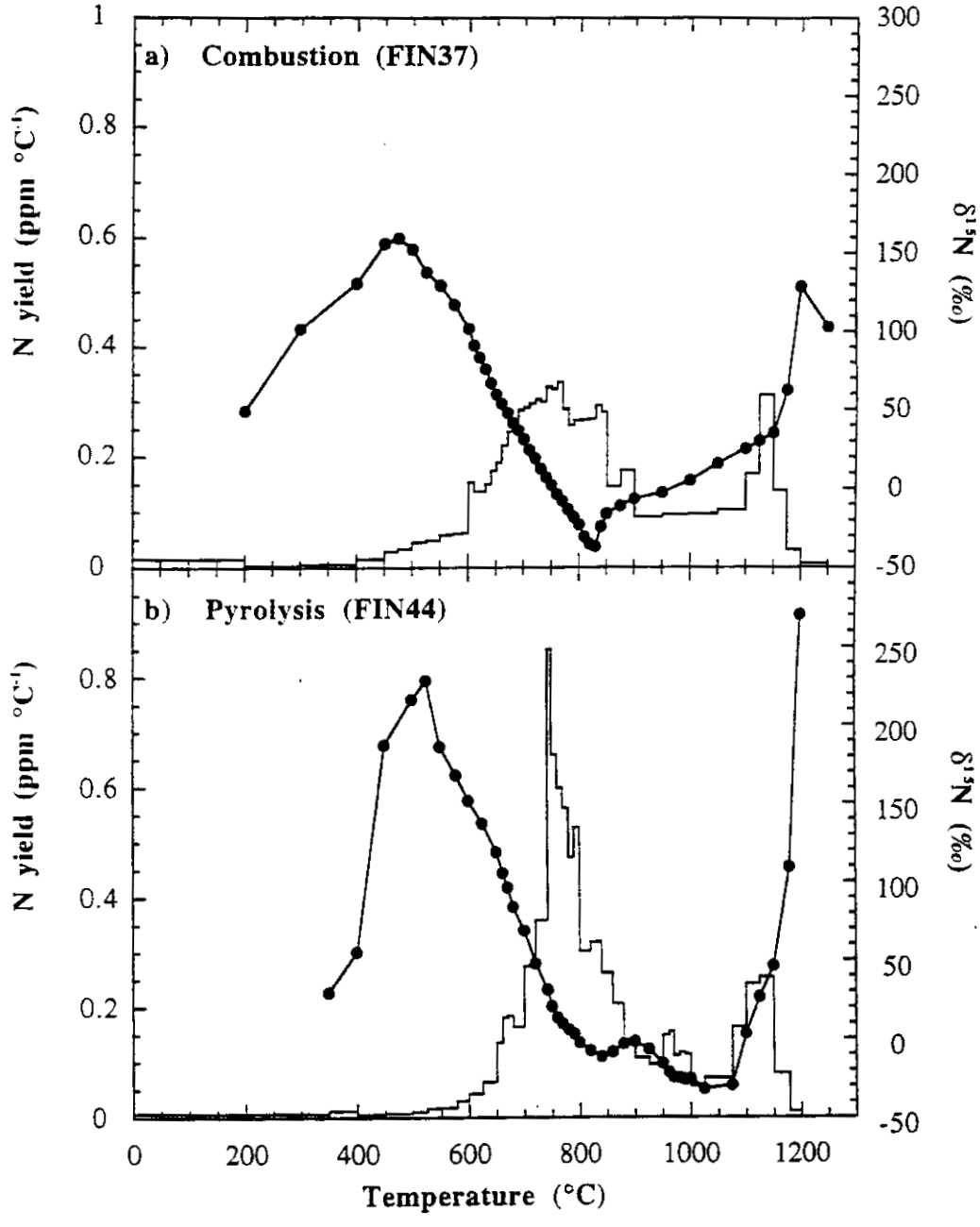

Figure 3.3. Nitrogen yields (ppm $°C^{-1}$) and isotopic compositions (‰) for the high resolution combustion (Figure 3.3a) and pyrolysis (Figure 3.3b) of lunar soil A12023.

Despite a similar temperature range for LTN by both extraction techniques, there are slight differences in the shape of the release profile. The release of LTN by stepped combustion is broadened to lower temperature with a lower maximum yield, compared to the release of LTN by pyrolysis. This strongly suggests that the release of a proportion of LTN is affected by the presence of oxygen in the extraction section during combustion, whilst the remainder of LTN is released by diffusion as observed during the pyrolysis extraction.

The existence of both the V-shaped and W-shaped isotopic profile for nitrogen in lunar breccias has been confirmed by replicate analyses (Carr *et al.*, 1985a, b). However, the current study has revealed that the W-shaped profile is also present in lunar soils but is restricted to the pyrolysis extractions, whereas the V-shaped profile is only observed in combustion extractions. Early observations of the V-shaped profile in pyrolysis extractions (Becker & Clayton, 1975, 1977; Becker *et al.*, 1976) were most likely due to the relatively large temperature increments (typically ~100°C) that were employed. Figure 3.3b illustrates that the isotopic variation defining the W-shape occurs across a temperature range of just over 200°C, and therefore the use of 100°C steps would readily smooth out this profile.

	A12023 Combustion (FIN37)		A12023 Pyrolysis (FIN44)	
	$\delta^{15}N$ (‰)	Temp (°C)	$\delta^{15}N$ (‰)	Temp (°C)
Heavy (N_{LT})	+159.8	475	+228.6*	525
Light (N_{MT})	-36.6	830	-11.3	840
Light (N_{HT})	ND***	ND**	-31.9	1025
Heavy	+128.8	1200	+270.1*	1200

Table 3.3. A comparison of the $\delta^{15}N$ values (‰) and release temperatures (°C) of individual nitrogen components from the high resolution combustion (FIN37) and pyrolysis (FIN44) extractions of A12023.

* = $\delta^{15}N$ value subject to significant blank correction.

*** = ND, *i.e.* component not detected.

N_{LT}, N_{MT} and N_{HT} defined in section 1.7.3.2 (Figures 1.5a and 1.5b).

Table 3.3 compares the maximum (and minimum) $\delta^{15}N$ values and corresponding release temperatures for the various nitrogen isotopic components from FIN37 and FIN44. It should be noted that the temperatures correspond to the extreme $\delta^{15}N$ value for each

component. Both extraction techniques reveal the presence of a low temperature, isotopically heavy component (N_{LT}), albeit at different temperatures, with $\delta^{15}N$ = +159.8‰ at 475°C for the combustion and +228.6‰ at 525°C for the pyrolysis. The $\delta^{15}N$ of N_{LT} for the pyrolysis extraction is subject to significant blank corrections as the nitrogen yield for the 525°C step is only twice the initial blank measurement (section 2.10). A more realistic isotopic composition for N_{LT} is $\delta^{15}N$ = +151.7‰ for the 600°C step, where the nitrogen yield is 3.1 times the initial blank. Both extractions also resolve an isotopically light component (N_{MT}) with $\delta^{15}N$ = -36.6‰ at 830°C for the combustion, and $\delta^{15}N$ = -11.3‰ at 840°C for the pyrolysis extraction. In addition, the pyrolysis extraction also reveals the presence of a second isotopically light component (N_{HT}) at a temperature of 1025°C with $\delta^{15}N$ = -31.9‰. This component is not detected (ND in Table 3.3) in the combustion extraction which would suggest that it is either absent or masked. If it is masked, a viable explanation may be that the release of N_{HT} is shifted to a lower release temperature during combustion, by the presence of oxygen in the extraction section. The temperature shift may result in the release of N_{HT} coinciding with the liberation of N_{MT}, and if this is the case, the temperature decrease may be as much as 200°C. The observation that the release temperature of N_{LT} is a minimum of ~50°C lower in the combustion extraction, compared to the pyrolysis, may suggest that a similar phenomenon is occurring at low temperature. This hypothesis is investigated further in section 3.4.2.2.

Both extractions also release isotopically heavy nitrogen at 1200°C with $\delta^{15}N$ = +128.8‰ for the combustion and +270.1‰ for the pyrolysis, although the nitrogen yield for the latter is only 1.7 times the initial blank. A more realistic $\delta^{15}N$ for the heavy nitrogen would be +109.2‰ for the blank corrected 1179°C step. Interestingly, the $\delta^{15}N$ values display a sudden increase from +35 to +63‰ for the combustion and from +46 to +109‰ for the pyrolysis extractions at a temperature of 1150°C, following the release of the majority of HTN. The significance of this observation will be discussed later in conjunction with data obtained from density and magnetic separates (section 3.5).

From Table 3.3 and Figures 3.3a and 3.3b several observations can be made:

1). The majority of the nitrogen (LTN) has a release temperature of 600-900°C that is relatively unaffected by the presence of oxygen during extraction and has a weighted average

$\delta^{15}N$ value of +8.7‰ for the combustion and +20.1‰ for the pyrolysis. The discrepancy is due to the lighter isotopic composition of N_{MT} in the combustion extraction when compared to the pyrolysis extraction.

2). The high temperature nitrogen (HTN) is released at a temperature of 1000-1200°C, independent of extraction technique, and has a weighted average $\delta^{15}N$ value of +36.3‰ for the combustion and +26.3‰ for the pyrolysis. Note that the isotopic compositions for LTN and HTN do not total that calculated for the whole-rock, as the temperature ranges for these components exclude the nitrogen liberated at temperatures of <600°C and between 900-1000°C. The isotopic compositions show the greatest deviation as the temperature range of 600-900°C excludes the release of N_{LT}.

3). The liberation of N_{LT} is shifted to a lower temperature by a minimum of 50°C by the presence of oxygen when heating the sample. Note that this may be as much as 125°C if an appropriate blank correction is applied to the yield and isotopic data.

4). A proportion of the isotopically light nitrogen (N_{HT}) is also released at a higher temperature during the pyrolysis extraction. This temperature shift appears to be ≈200°C. Note that the majority of the light nitrogen (N_{MT}) is released at a similar temperature regardless of the method of extraction used.

3.3.2. Argon analysis for the high resolution extractions of A12023

In order to determine whether the nitrogen in the lunar regolith is predominantly of a solar origin, it is extremely valuable to have a measure of how nitrogen correlates with the solar noble gases. Argon lends itself particularly well to conjoint analyses with nitrogen. The "excess" nitrogen in the lunar regolith, *i.e.* $N/^{36}Ar$ a factor of 10 higher than the solar value, has been the cause of much debate regarding the origin of nitrogen in lunar soils (section 1.7.2.2). In addition to nitrogen abundance and isotopic composition measurements, it would therefore prove valuable to be able to measure the $N/^{36}Ar$ ratio for soils in this work, together with $^{36}Ar/^{38}Ar$ and $^{40}Ar/^{36}Ar$. As previously discussed (section 2.2.5), the argon data obtained in this work is semi-quantitative and the instrument has not been calibrated for argon measurement. For the purpose of this work, the mean $N/^{36}Ar$ ratio (calculated from the comparison of peak heights) for all the samples analysed, has been

compared to the mean literature value for $N/^{36}Ar$ of 380 (Frick *et al.*, 1988; Becker and Pepin, 1989; Humbert *et al.*, 1997) and a multiplication factor has been calculated to enable the "true" $N/^{36}Ar$ ratio to be determined for each temperature step. Note that the argon data are internally consistent during a single extraction but cannot be readily compared between extractions. The argon yields have been calculated using the ppm nitrogen content of a sample, and the $N/^{36}Ar$ ratio, and have been converted to conventional noble gas units of ccSTP g^{-1}.

	Combustion (FIN37)	Pyrolysis (FIN44)
Mean $^{36}Ar/^{38}Ar$	6.05	6.49
Mean $^{40}Ar/^{36}Ar$	1.51	1.93
Mean $N/^{36}Ar^{*}$	301.3	400.0

Table 3.4. Comparison of mean $^{36}Ar/^{38}Ar$, $^{40}Ar/^{36}Ar$, and $N/^{36}Ar$ for the stepped combustion and pyrolysis of A12023.
* denotes the $N/^{36}Ar$ normalised to the mean literature value (see text).

Table 3.4 displays the mean $^{36}Ar/^{38}Ar$, $^{40}Ar/^{36}Ar$ and $N/^{36}Ar$ ratios obtained from the high resolution stepped combustion and pyrolysis of A12023. The $^{36}Ar/^{38}Ar$ and $^{40}Ar/^{36}Ar$ ratios are not precise and can only be used for interrun comparisons. Although they cannot be directly compared to the data obtained by other workers they can be used as diagnostic tracers for identifying solar wind contributions to the lunar regolith. Figure 3.4a and 3.4b illustrates the $N/^{36}Ar$ (plot (i)), $^{40}Ar/^{36}Ar$ and $^{36}Ar/^{38}Ar$ (plot (ii)), and the nitrogen and ^{36}Ar yields (plot (iii)) for the stepped combustion (Figure 3.4a) and pyrolysis (Figure 3.4b) respectively of A12023. The $N/^{36}Ar$, $^{40}Ar/^{36}Ar$ and $^{36}Ar/^{38}Ar$ data are given in Appendix B1.

The $^{36}Ar/^{38}Ar$ ratio for the combustion extraction (Figure 3.4a (ii)) displays a similar trend to that observed in conventional noble gas analyses (section 1.7.5.2). Note that an equivalent trend has been observed for all the lunar soils and breccias analysed in this study. The $^{36}Ar/^{38}Ar$ ratio decreases slightly across the release of LTN and HTN from a value of ~6.3 to ~5.8. The sudden decrease of $^{36}Ar/^{38}Ar$ in the last four steps of the extraction are

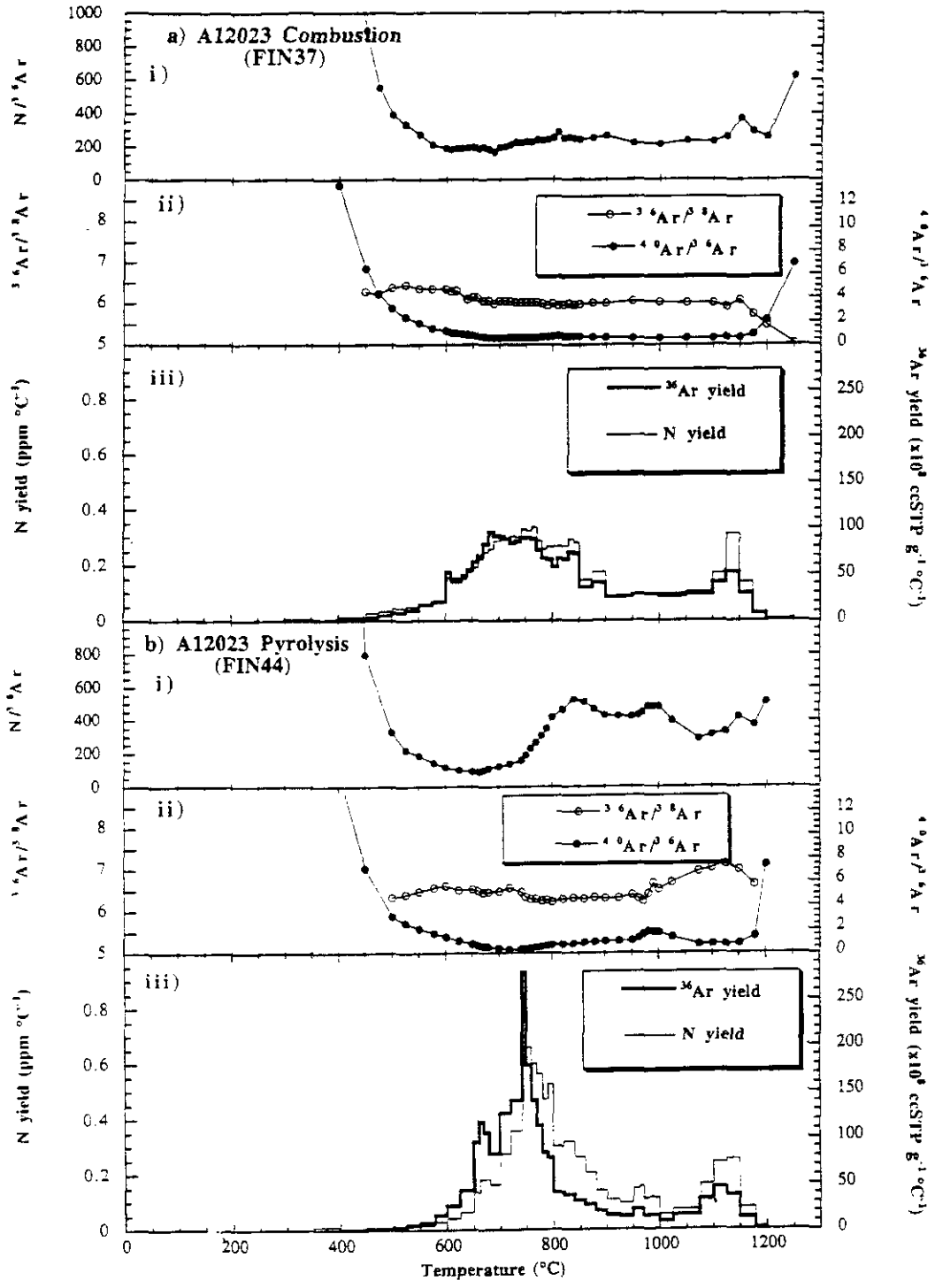

Figure 3.4. Conjoint nitrogen and ^{36}Ar data, and argon isotopic ratios against temperature for the stepped combustion (Figures 3.4a) and stepped pyrolysis (Figures 3.4b) of A12023. The plots are as follows: (i) $N/^{36}Ar$, (ii) $^{36}Ar/^{38}Ar$ (left ordinate) and $^{40}Ar/^{36}Ar$ (right ordinate), (iii) N yield in units of ppm $°C^{-1}$ (left ordinate) and ^{36}Ar in units of ccSTPg^{-1} $°C^{-1}$ (right ordinate).

due to the liberation of cosmogenic ^{38}Ar at temperatures in excess of 1150°C. Although the $^{36}Ar/^{38}Ar$ ratio obtained in this work are higher than those of previous workers, *e.g.* Wieler

et al. (1986), it is believed that the trends are consistent with the interpretation of $^{36}Ar/^{38}Ar$ from noble gas studies (section 1.7.5.2). The trend can be interpreted as the initial release of surface-sited solar wind argon, followed by the higher temperature release of SEP-Ar, which would be implanted deeper into the soil. Other workers, *e.g.* Becker and Pepin (1989) have attributed the high temperature release to fractionated heavy solar noble gases (section 1.7.5.1), although recent work, *e.g.* Wieler and Baur (1995) have shown that no fractionation of heavy noble gases occurs (section 1.7.5.3). The $^{36}Ar/^{38}Ar$ ratio for the pyrolysis extraction (Figure 3.4b (ii)) also displays a decreasing trend up to a temperature of 1000°C, from a value of ~6.5 to ~6.3. However, above 1000°C, the $^{36}Ar/^{38}Ar$ ratio increases to a value of 7.1 before decreasing due to the release of cosmogenic ^{38}Ar. The increase in the $^{36}Ar/^{38}Ar$ ratio is not evident for any other sample analysed in this study and hence is believed to be due to the semi-quantitative nature of the argon measurements.

The $^{40}Ar/^{36}Ar$ ratios obtained for both the stepped combustion and pyrolysis extractions (Figures 3.4a (ii) and 3.4b (ii) respectively) are essentially constant with mean values of 1.5 and 1.9 respectively, and compares well with previous work (Frick *et al.*, 1988). The deviations of the $^{40}Ar/^{36}Ar$ ratios are noted in the initial and final steps of each extraction, during which the ratios are higher than the mean values. The higher $^{40}Ar/^{36}Ar$ ratios at the start of the extraction is believed to be due to the liberation of re-implanted atmospheric gases, *i.e.* ^{40}Ar, which reside on the outer surfaces of lunar soils (section 1.6.1.3). The increase in $^{40}Ar/^{36}Ar$ in the final steps of the extraction is due to the liberation of radiogenic ^{40}Ar. Note that the surface siting of re-implanted ^{40}Ar causes a major problem when advocating a solar origin for regolith nitrogen, as it contradicts the hypothesis that surface correlated gases are implanted from the modern-day solar wind (section 1.7.4.1, point 3).

An interesting observation from the conjoint nitrogen and argon studies is that the $N/^{36}Ar$ ratios obtained by stepped combustion (Figure 3.4a (i)) are constant with a mean value of 301. The discrepancy between this value and the $N/^{36}Ar$ obtained by previous workers of ~380 (Frick *et al.*, 1988; Becker and Pepin, 1989; Humbert *et al.*, 1997) is due to the semi-quantitative nature of the measurements. Although the constant $N/^{36}Ar$ ratios may suggest an equivalent origin, *i.e.* solar wind, for both species, it has been shown from $^{40}Ar/^{36}Ar$ ratios that the surface siting of an element is not necessarily proof of a solar

origin. The observation of constant N/^{36}Ar ratios may also imply that both species reside in the same layer, *i.e.* radiation damaged layer, hence are liberated conjointly during stepped combustion (Figure 3.4a (iii)), although they may not have been incorporated by the same mechanism. The N/^{36}Ar ratios obtained during the pyrolysis (Figure 3.4b (i)) are not constant and range from a minimum of ~89 at 660°C to a maximum of ~523 at 840°C: a variation from 2.4 to 14.3 times the solar value of Anders and Grevesse (1989). This appears to be due to the delayed release of nitrogen during pyrolysis by ~50°C, when compared to ^{36}Ar (Figure 3.4b (iii)). Note that ^{36}Ar is liberated at a similar temperature regardless of the extraction method employed, whereas the liberation of nitrogen appears to be shifted to lower temperature in the presence of oxygen during extraction. During stepped pyrolysis, diffusion is the sole heating mechanism, and as nitrogen has been shown to have a higher retention efficiency than the noble gases (DesMarais *et al.*, 1974a), it is released at a slightly higher temperature.

The conjoint nitrogen and argon measurements in this study have provided some new and interesting observations. The nitrogen liberated from lunar soil A12023 may be solar in origin as the N/^{36}Ar ratios during stepped combustion are constant. However, the observation of the conjoint liberation of ^{40}Ar and ^{36}Ar may detract from a solar origin for the nitrogen, as ^{40}Ar does not originate from the solar wind. This is investigated further using a joint combustion and pyrolysis extraction technique to isolate the isotopically lightest nitrogen on a <10 μm fraction of A12023 (section 3.4.2.2).

3.3.3. Carbon abundances and C/N ratios in A12023

In addition to conjoint nitrogen and argon abundances, carbon yields are also measured for lunar soil A12023, and other samples in this work. This has enabled measurement of the C/N ratios for individual nitrogen components within lunar soils and breccias to aid identification of the origin of lunar nitrogen. The carbon inventory in the lunar regolith has previously been discussed in section 1.7.6.2, and the protocol for the measurement of carbon abundances has been detailed in section 2.4.5. The carbon abundances (ppm) and C/N ratios for the combustion (FIN37) and pyrolysis (FIN44) extraction of A12023 are given in Appendix B1 and are plotted for FIN37 in Figure 3.5.

The combustion data are used in preference to the pyrolysis data, as during pyrolysis extraction the carbon is liberated mostly as CO_2 and CH_4 up to 800°C and as CO from ~600°C (Chang *et al.*, 1974a, b; Kerridge *et al.*, 1974), whereas during combustion all the carbon is liberated as CO_2.

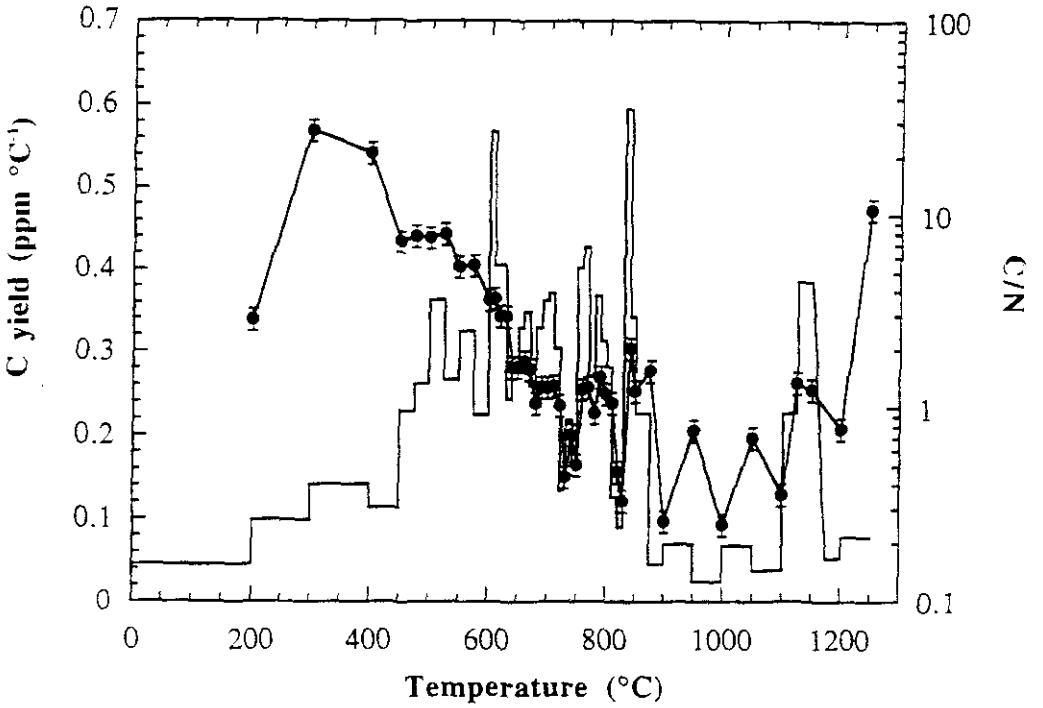

Figure 3.5. C/N ratios and carbon yield (ppm $°C^{-1}$) against extraction temperature (°C) for the high resolution combustion (FIN37) of A12023.

The combustion extraction yields a total of 179.7 ppm carbon, with a C/N ratio which varies from 0.4 to 21. The highest ratios are obtained at temperatures <400°C, due to terrestrial contamination, as no on-line pre-combustion (section 2.8.1) is employed for the combustion extractions. The C/N ratio decreases from a value of 7.2 at 400°C to 3.6 at 600°C, and then varies only between 0.4 to 3.6 for the remainder of the extraction (except the 1250°C step), with a mean value of 1.3 (600-1200°C). In addition, comparison of the total yields of carbon and nitrogen for the combustion of A12023 reveals a C/N ratio of ~1.5. Both of these results compare well to the C/N ratios obtained from lunar soils, *e.g.* Holland *et al.* (1972b), although the variation in C/N observed during the extraction may indicate the presence of carbon from elsewhere in the solar system (section 1.7.6.2). Furthermore, these values compare well to the C/N ratios of 1.06 and 1.1 in the solar photosphere and corona respectively (Anders and Grevesse, 1989). Despite the difficulty o

accurate measurement of low carbon abundances using the baratron, the errors for the carbon yields are estimated as ±10%. The errors for the nitrogen yields has been estimated as ±5%, and hence the errors for the C/N ratios are also shown as ±15% in Figure 3.5.

3.4. Stepped heating extraction of grain size separates from soil A12023

The data obtained from the whole-soil analyses of A12023 (section 3.3) indicate that the soil contains several nitrogen components with distinct isotopic compositions. To understand more about the nature and location of these components, a variety of grain size fractions from A12023 are analysed. The sieving techniques used to obtain these fractions are described in section 2.7.2.1. Section 3.4.1 discusses the nitrogen abundances and isotopic compositions obtained for 4 grain size fractions (<10 μm, 40-53 μm, 106-152 μm and >1 mm), and the data are compared to the whole-rock analyses presented in section 3.3.1.2. In addition, section 3.4.2 details a joint combustion and pyrolysis extraction of the <10 μm size fraction in order to further investigate the differences between the isotopic profiles obtained using the two techniques.

3.4.1. Nitrogen abundances and isotopic composition of four grain size separates from A12023

In this study, the <10 μm, 40-53 μm, 106-152 μm and >1 mm grain size fractions are analysed using stepped pyrolysis extraction. Ideally, comparisons of the abundance and isotopic profiles from each grain size separate, should be made using extractions of equivalent temperature resolution to minimise the effect of varying diffusion rates as a function of temperature, step size and total extraction time. The 40-53 μm (FIN189) and 106-152 μm (FIN188) fractions were analysed using 50°C resolution, whereas the >1 mm size separate (FIN151) employed higher resolution temperature steps (25-50°C). As with the whole-soil study (FIN44), a high resolution pyrolysis extraction (10°C and 25°C temperature steps) of the <10 μm fraction was used (FIN73) as no low resolution pyrolysis extraction was available. Table 3.5 displays the nitrogen extracted from each grain size

fraction both as a total yield (ΣN) and as a percentage of the total released as LTN (T≤1000°C) and HTN (T>1000°C). For comparison, the data obtained for FIN44 are also included. In addition to $\Sigma\delta^{15}N$ and the $\delta^{15}N$ of individual components, the variation in $\delta^{15}N$ between N_{LT} and N_{HT} has also been calculated ($\Delta\delta^{15}N$). The data for each extraction are given in Appendices B2.1-B2.4 inclusive.

The nitrogen release and isotopic profiles for each size fraction are given in Figures 3.6a to 3.6d and are compared with the whole-soil (Figure 3.6e). The nitrogen yield data are displayed on a logarithmic axis to aid comparison between the grain sizes. Note that the grain sizes all display the aforementioned W-profile, despite the lower resolution used for the 40-53 μm and 106-152 μm fractions. Furthermore, note that the sharp increase of $\delta^{15}N$ to higher values at a temperature of 1150-1200°C, observed for the whole-soil (section 3.3.1.2) are also present in the 40-53 μm and 106-152 μm fractions (Figures 3.6b and 3.6c respectively). The relevance of this observation is discussed in conjunction with data obtained from density and magnetic separates (section 3.5).

	<10 μm (FIN73)	40-53 μm (FIN189)	106-152 μm (FIN188)	>1 mm (FIN151)	Whole-soil (FIN44)
Total N (ppm)	217.2	67.6	45.3	37.9	122.8
$\Sigma\delta^{15}N$ (‰)	+11.9	+23.0	+24.4	+2.6	+21.9
LTN (% of total)	92	75	72	74	89
HTN (% of total)	8	25	28	26	11
N_{LT} (‰)	+135.7	+69.1	+52.7	+69.5	+151.7*
N_{MT} (‰)	-28.4	+1.2	-5.2	-21.0	-11.3
N_{HT} (‰)	-92.7	-14.4	-15.0	-57.3	-31.9
$\Delta\delta^{15}N$ (‰)**	227.8	83.5	67.7	126.8	183.6

Table 3.5. Nitrogen abundances (ppm) and isotopic compositions (‰) for <10 μm, 40-53 μm, 106-152 μm and >1 mm grain size fractions of A12023 by stepped pyrolysis.
* = realistic $\delta^{15}N$ value that is not subject to significant blank correction (section 3.3.1.2).
** = $\Delta\delta^{15}N$ defined as the variation in $\delta^{15}N$ between N_{LT} and N_{HT}.
N_{LT}, N_{MT} and N_{HT} defined in section 1.7.3.2 (Figure 1.5a and 1.5b).

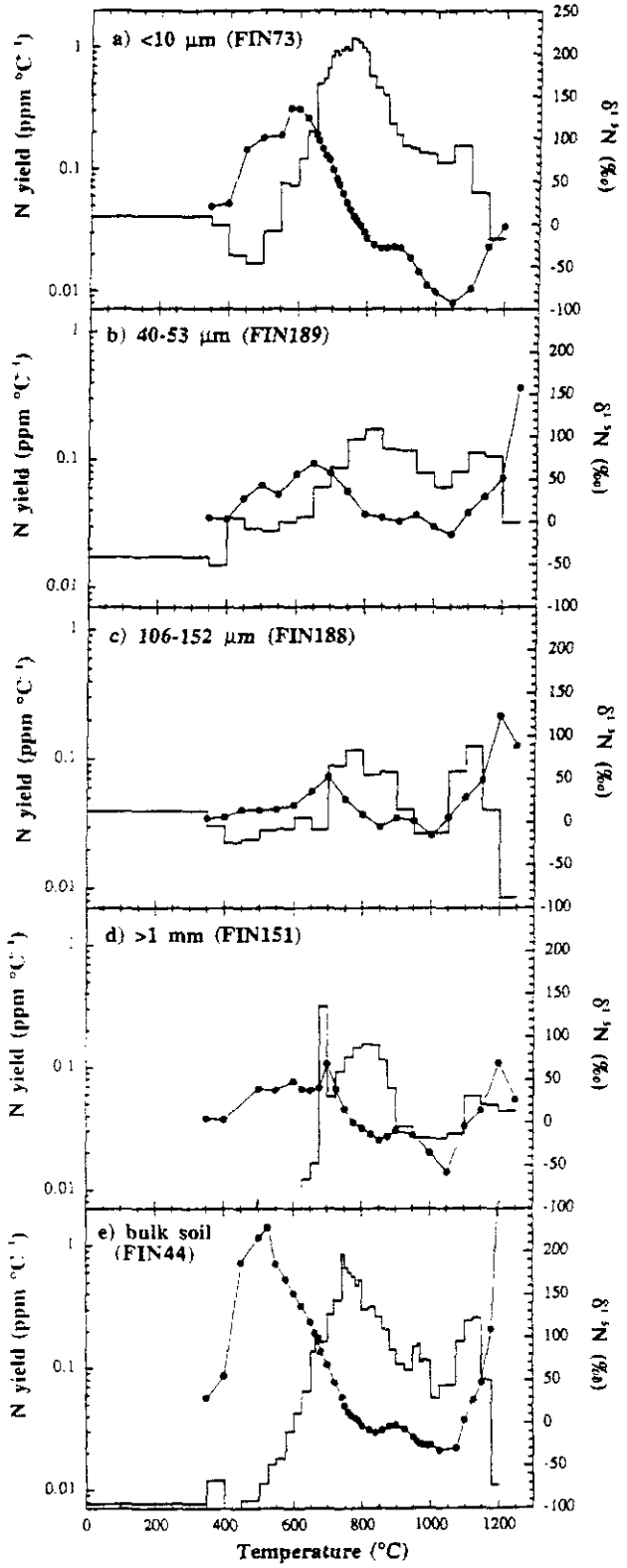

Figure 3.6. Nitrogen yields (ppm $°C^{-1}$) and isotopic compositions (‰) for the stepped pyrolyses of grain size separates from A12023. The grain size fractions are: a) <10 µm, b) 40-53 µm, c) 106-152 µm, d) >1 mm. The pyrolysis for the whole-soil (FIN44) is given for comparison in plot e).

From Table 3.5, it can be seen that there is a clear trend of increasing nitrogen concentration with decreasing grain size, ranging from 37.9 ppm (>1 mm fraction) to 217.2

ppm (<10 μm fraction). These observations compare well with the trends observed by previous workers (Goel and Kothari, 1972; Holland *et al.*, 1972a; Müller, 1974). There is also considerable variation in $\Sigma\delta^{15}N$ from +2.6‰ (>1 mm fraction) to +24.4‰ (106-152 μm fraction), although in this case the variation is not systematic. Figure 3.7a illustrates a plot of $\Sigma\delta^{15}N$ against ΣN for each grain size fraction and the whole-soil. The $\Delta\delta^{15}N$ ranges from 228‰ (<10 μm fraction) to 68‰ (106-152 μm fraction) and is plotted against $\Sigma\delta^{15}N$ in Figure 3.7b. Furthermore, Figure 3.7c displays a plot of $\Delta\delta^{15}N$ for each extraction against the percentage of the total nitrogen released as LTN. The latter has been shown (Table 3.5) to vary significantly from 72% (106-152 μm fraction) to 92% (<10 μm fraction).

From Figures 3.7a, b and c, it becomes clear that the pyrolysis extraction of the >1 mm (FIN151) fraction does not correlate with the trends exhibited by the other grain sizes. A possible explanation for the discrepancy is that the >1 mm size fraction was the remnant of the soil after sieving of the individual grain sizes, and hence would contain agglutinates and glasses which had not been separated. Despite the crushing of this size fraction, the extraction may have comprised of an unrepresentative fraction of the sample. Interestingly, a combustion extraction of the >1 mm grain size fraction (FIN63) liberated 75.7 ppm nitrogen; a factor of two higher than obtained for the FIN151 (37.9 ppm), and a $\Sigma\delta^{15}N$ increased by ~10‰ (+13.2‰ compared to +2.6‰). The nitrogen data for FIN63 are given in Appendix B2.4. Although no combustion extractions were undertaken for the 40-53 μm and 106-152 μm size fractions, the ΣN and $\Sigma\delta^{15}N$ values obtained for the whole-soil (section 3.3.1.2 and Table 3.2) display similar values for both the stepped combustion and pyrolysis extraction. This is also observed for the <10 μm fraction (section 3.4.2.1) . Unfortunately, constraints on the sieving procedure did not allow for grain size distribution data to be obtained at the time of sieving (Pillinger *et al.*, 1978) and hence it is not known whether the >1 mm fraction constitutes a significant proportion of the whole-soil. In view of the discrepancy with the >1 mm pyrolysis extraction, the pyrolysis extraction data are omitted from any further discussion of grain size trends.

It should be noted that although the ΣN and $\Sigma\delta^{15}N$ data obtained for the >1 mm combustion extraction do not correlate with the grain size pyrolysis extractions in this study (Figure 3.7a and 3.7b), the percentage of nitrogen released as LTN (60%) correlates with

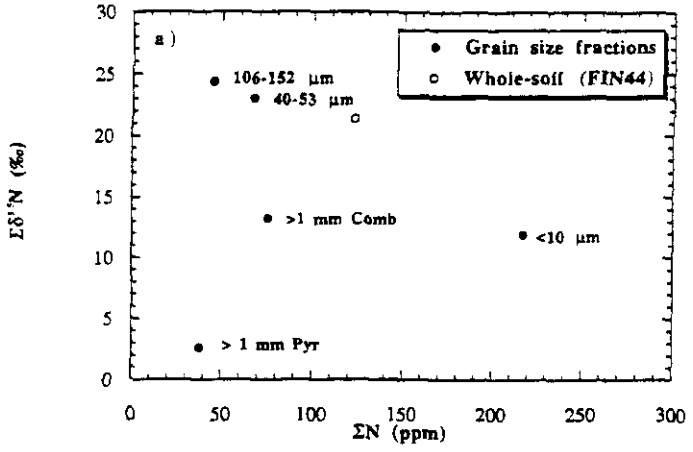

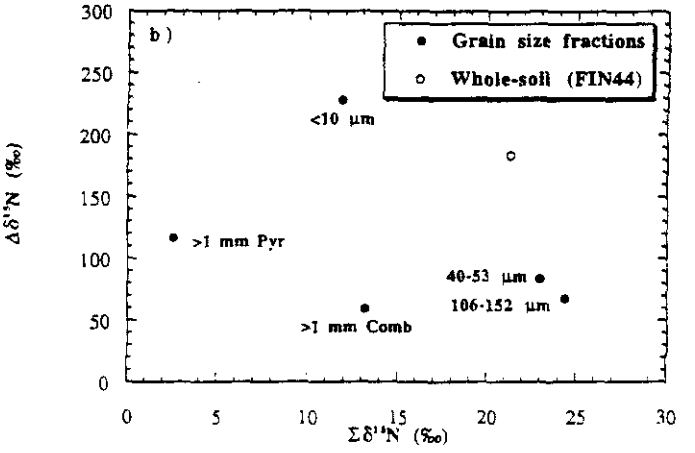

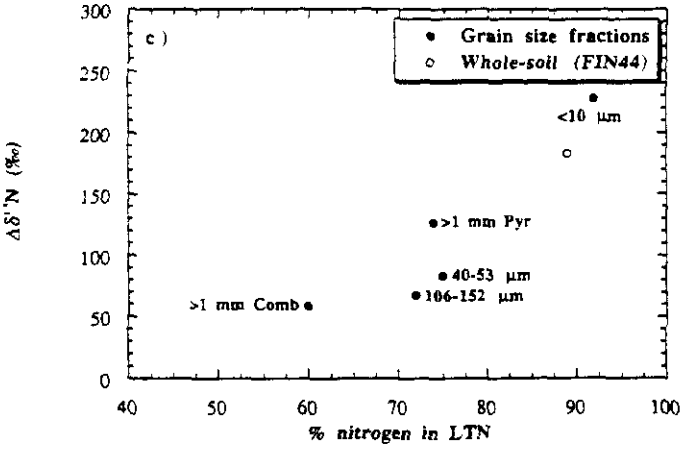

Figure 3.7. Grain size trends for size fractions from A12023. The trends are as follows: a) $\Sigma\delta^{15}N$ (‰) against ΣN (ppm), b) $\Delta\delta^{15}N$ (‰) against $\Sigma\delta^{15}N$ (‰), c) $\Delta\delta^{15}N$ (‰) against % nitrogen in LTN.

the observed trends (Figure 3.7c). The $\Delta\delta^{15}N$ for the combustion extraction (59‰) is calculated from the isotopic variation between N_{LT} and N_{MT}, as the N_{HT} component was not detected in any combustion analysis in this investigation, *e.g.* section 3.3.1.2. The difference in the shape of the isotopic profile for the stepped combustion may account for the higher $\Sigma\delta^{15}N$ (~10‰) than observed in the pyrolysis extraction.

The similarity of the shape of the isotopic profile for the whole-soil (Figure 3.6e) with the <10 μm fraction (Figure 3.6a) suggests that the whole-soil is dominated by <10 μm particles. The coarser grain sizes reveal a flatter isotopic profile (Figures 3.6b tto 3.6d inclusive). Unfortunately, without size distribution data (Pillinger *et al.*, 1978), this cannot be fully substantiated. If the whole-soil pyrolysis (FIN44) data are added onto Figures 3.7a to c (shown as open circles), it appears that the whole-soil has an apparent mean grain size between 10 and 40 μm. Note that in Figures 3.7b and 3.7c, $\Delta\delta^{15}N$ is calculated using the more realistic $\delta^{15}N$ for N_{LT} (+151.7‰) as discussed in section 3.3.1.2.

Several points can be made from Table 3.5 and Figures 3.7 regarding the nitrogen trends for the grain size fractions from A12023:

1). The nitrogen yield increases with decreasing grain size, with the highest yield (217 ppm) obtained for the <10 μm fraction. Figure 3.8 illustrates a plot of log ΣN (ppm) against log r^{-1} (μm), where r = grain size. This plot should display a straight line with a gradient of -1 if all the nitrogen is surface-correlated (Eberhardt *et al.*, 1970). However, the grain size fractions in this work (using an estimated grain size of 25 μm for the whole-soil) displays a gradient of -0.6. This indicates that a proportion of the nitrogen is located in complex particles, *i.e.* reworked agglutinates, located within grain interiors.

2). There is an increase in $\Sigma\delta^{15}N$ with increasing grain size, *i.e.* <10 μm fraction displays the lowest $\Sigma\delta^{15}N$ (+11.9‰).

3). The variation in $\Delta\delta^{15}N$, *i.e.* N_{LT}-N_{HT}, decreases with increasing grain size, hence is greatest (228‰) for the <10 μm fraction and lowest (68‰) for the 106-152 μm fraction.

4). The proportion of total nitrogen released as HTN increases with increasing grain size, *i.e.* the coarser size fractions liberate a higher percentage of the total nitrogen at temperatures above 1000°C.

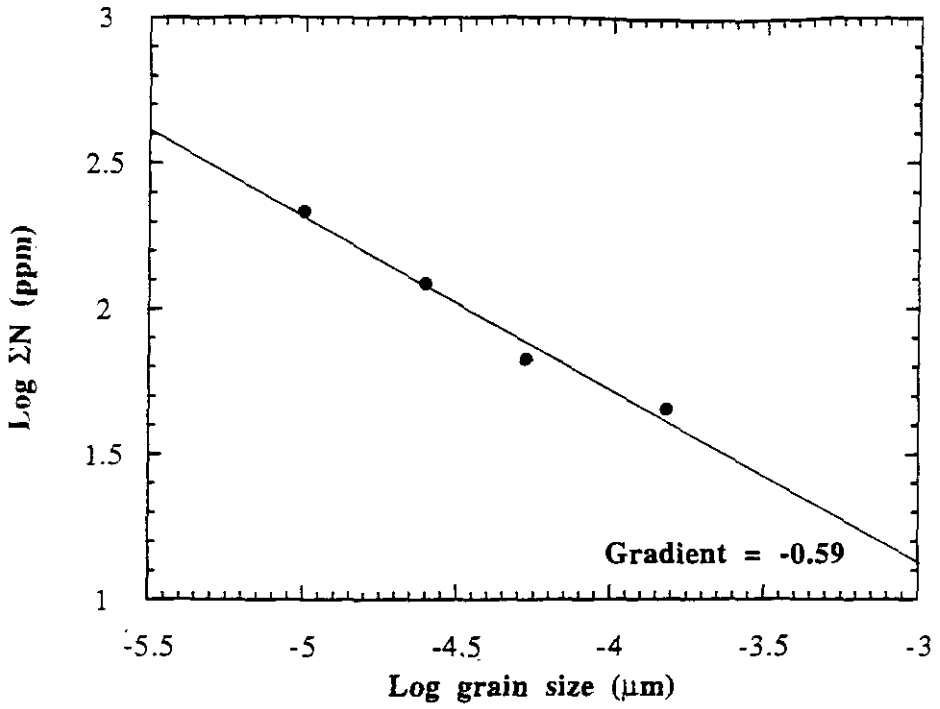

Figure 3.8. Plot of log ΣN concentration (ppm) against r^{-1}, where r = grain size (μm) for the grain size fractions from A12023. An estimated grain size of 25 μm is used for the whole-soil..

The results obtained from the study of grain size separates confirm that the nitrogen liberated from lunar soils displays similar trends to those observed by previous workers (Goel and Kothari, 1972; Holland *et al.*, 1972a; Müller, 1974). Similar trends have also been reported for carbon (section 1.7.6.2) and noble gases (Eberhardt *et al.*, 1970). The proportion of nitrogen released as LTN is dependent on grain size, with the highest percentage (>90%) liberated from the finest size fraction. The converse has been observed for HTN. This observation indicates that a significant proportion of nitrogen is located on grain surfaces, although the absence of an adequate correlation between log N and log r^{-1} (Figure 3.8) suggests that a proportion of the nitrogen has been reworked by gardening processes into grain interiors. The progressively higher contents of nitrogen liberated as HTN with increasing grain size, suggests that the coarser fractions contain higher amounts of complex secondary particles, *i.e.* agglutinates. The $\Delta\delta^{15}N$ obtained in this work for the >1 mm combustion (59‰) can be compared to a variation of 34‰ for an agglutinate separate from the 75-106 μm fraction of A12023 (Norris *et al.*, 1983). However, the relative abundance of the various fractions indicate an increasing portion of more complex agglutinates in finer size fractions (Pillinger *et al.*, 1978), although this could be present as

fine-grained fragments of agglutinates, located on grain surfaces. One explanation for this may be the complexity, and unknown time, of agglutinate formation compared to the constant exposure to solar wind and comparative simplicity of the surface mineral grains.

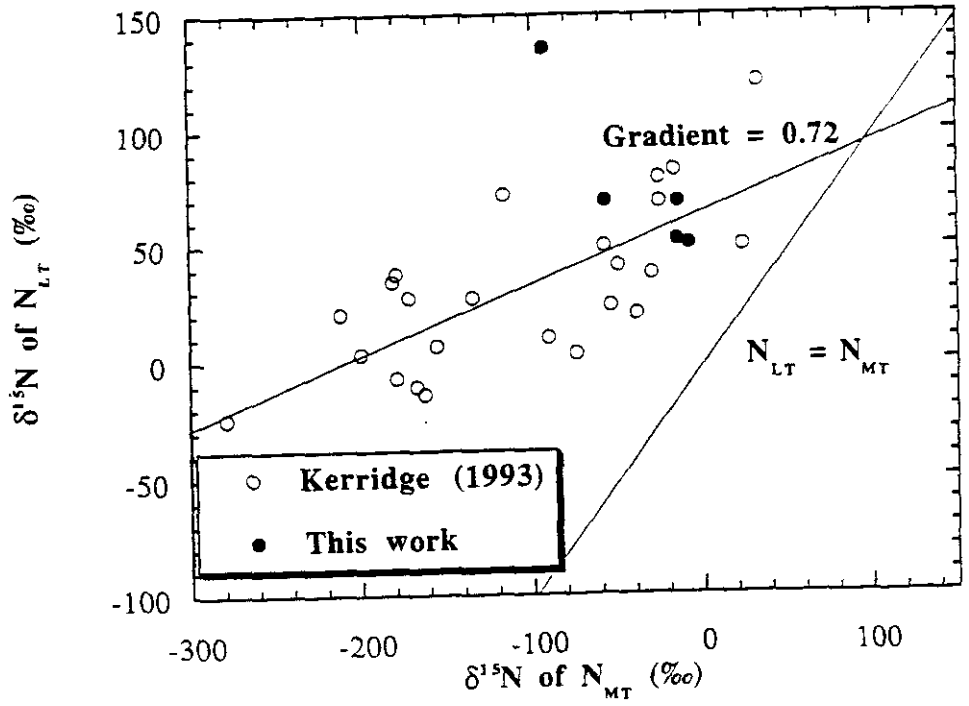

Figure 3.9. Plot of $\delta^{15}N$ (‰) of N_{LT} against N_{MT} (after Kerridge, 1993). The data from Kerridge (1993) is shown as empty circles. The data obtained from the current study is shown as filled circles.

The variation between the isotopic components observed in lunar soils has been investigated previously (Kerridge, 1993). Figure 3.9 displays a plot of $\delta^{15}N$ for N_{LT} and N_{MT} for a variety of mostly bulk regolith samples (open circles), each employing six or more steps during extraction (adapted from Figure 4 in Kerridge, 1993). Note that the data obtained by Kerridge (1993) only revealed the presence of a single isotopically light component. The data display a gradient of 0.72 and are compared to a 1:1 reference line, with the isotopic composition of N_{MT} coexisting with N_{LT}. The filled circles, in Figure 3.9, are the data obtained in this study for the pyrolysis extractions of the <10 μm, 40-53 μm, 106-152 μm and >1 mm fractions and include the >1 mm combustion data. The whole-soil is not included in the figure as the isotopic composition of N_{LT} (+151.7‰) is higher than any composition obtained by Kerridge (1993). This is most likely due to the low temperature resolution used in the earlier study. With the exception of the extraction of the

<10 μm grain size fraction, there is good correlation between the data obtained in the this work and Kerridge (1993).

3.4.2. Investigation of the isotopically heavy and light nitrogen in the <10 μm grain size fraction

Prior to undertaking an investigation into the occurrence and nature of the V-shaped and W-shaped isotopic profile displayed for nitrogen, it was necessary to choose an appropriate sample. The sample selected for this series of experiments is the <10 μm size grain fraction of A12023, as a low resolution combustion analysis (FIN29) had indicated that the majority of the nitrogen (>90%) was released at a temperature of <1000°C. The nitrogen data obtained for FIN29 are given in Appendix B2.1. Furthermore, the isotopic profile for the <10 μm fraction shows no evidence of high temperature, isotopically heavy nitrogen and displays the largest $\delta^{15}N$ variation of all the grain size fractions studied. It was hoped that by eliminating HTN and the associated isotopically heavy nitrogen, the isotopic compositions of N_{LT} and N_{MT} (and N_{HT} for the pyrolysis extractions) could be better constrained. The nitrogen data discussed in this section have also been reported previously (Brilliant *et al.*, 1994) for a comparison study of the whole-soil, <10 μm and >1 mm fraction of A12023, and lunar breccia A79035. The latter is discussed in (section 4.3).

3.4.2.1. High resolution stepped combustion and pyrolysis extraction of the <10 μm grain size fraction from A12023

The high resolution analyses are performed by stepped combustion and stepped pyrolysis using a mixture of 10°C, 20°C and 25°C temperature steps across the release of LTN, and the yield and isotopic profiles are shown in Figures 3.10a and 3.10b respectively. The data obtained are displayed in Appendix B2.1. The combustion extraction (FIN62) yields 221.2 ppm of nitrogen with $\Sigma\delta^{15}N$ of +14.1‰, comparable with 217.2 ppm and $\Sigma\delta^{15}N$ of +11.9‰ for the pyrolysis extraction (FIN73).

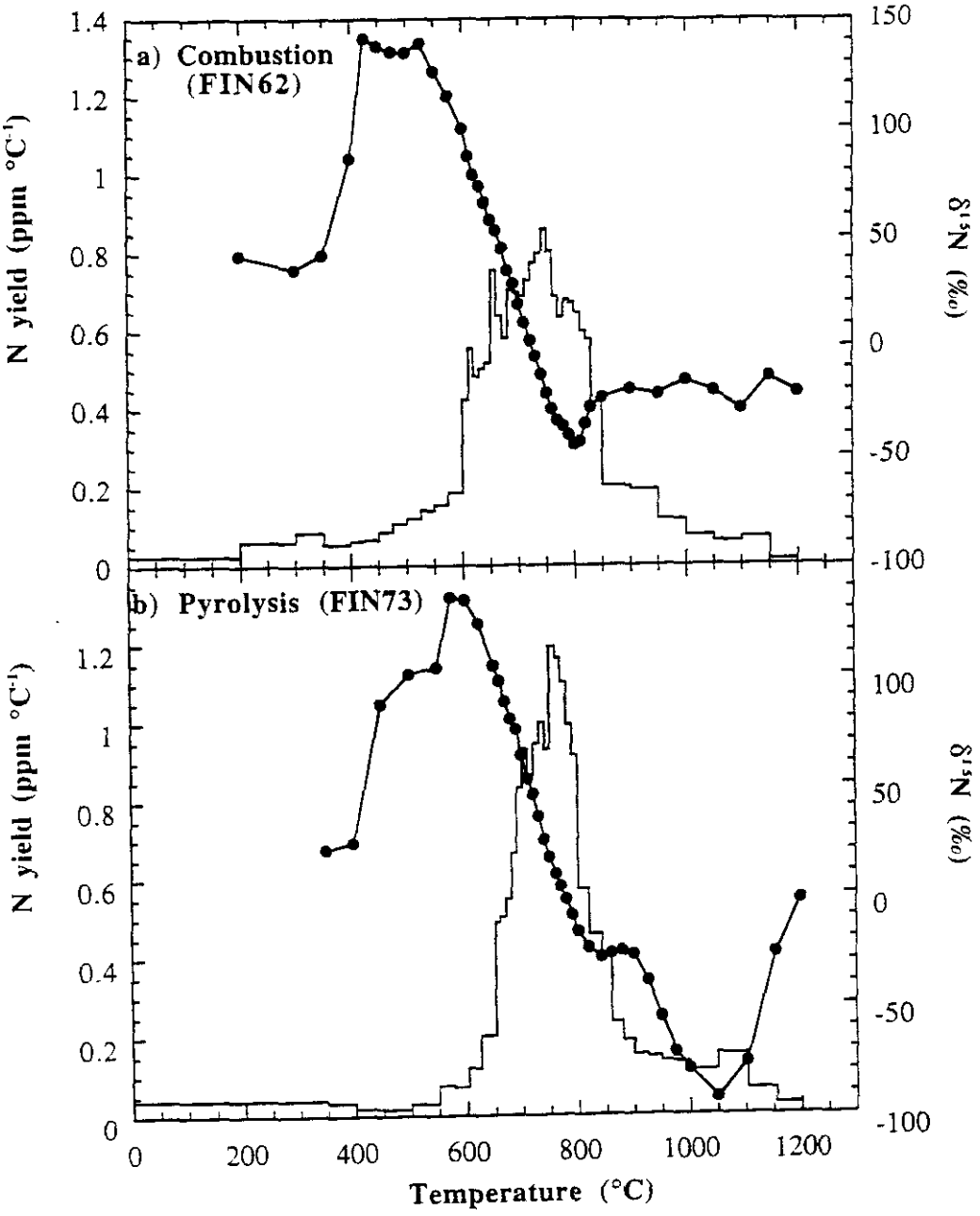

Figure 3.10. Nitrogen yield (ppm $°C^{-1}$) and isotopic composition (‰) for the high resolution combustion (Figure 3.10a) and pyrolysis (Figure 3.10b) of the <10 μm fraction of A12023.

Figure 3.10a and 3.10b confirms that HTN is virtually absent in the finest grain size, with the majority of the total nitrogen (92% for the pyrolysis and 97% for the combustion) released at temperatures of <1000°C. The $\delta^{15}N$ values and release temperatures of N_{LT}, N_{MT} and N_{HT} for both the combustion and pyrolysis extractions are given in Table 3.6. Both extractions liberate N_{LT} with $\delta^{15}N$ = +141.2‰ at 425°C for the combustion and $\delta^{15}N$ = +135.7‰ at 575°C for the pyrolysis, and also release N_{MT} with $\delta^{15}N$ = -44.7‰ at 800°C for the combustion and $\delta^{15}N$ = -28.4‰ at 840°C for the pyrolysis. The pyrolysis extraction

also reveals the presence of N_{HT} with $\delta^{15}N$ = -92.7‰ at a temperature of 1050°C, which was not detected during the combustion extraction. Note that the observation of the W-shaped profile during stepped pyrolysis extraction is consistent with the data obtained from the whole-soil (section 3.3.1.2) and other grain size fractions, *e.g.* 40-53 μm, 106-152 μm and >1 mm.

	<10 μm Combustion (FIN62)		<10 μm Pyrolysis (FIN73)	
	$\delta^{15}N$ (‰)	Temp (°C)	$\delta^{15}N$ (‰)	Temp (°C)
N_{LT}	+141.2	425	+135.7	575
N_{MT}	-44.7	800	-28.4	842
N_{HT}	ND*	ND*	-92.7	1050

Table 3.6. Comparison of the $\delta^{15}N$ (‰) values and release temperature (°C) for combustion and pyrolysis extractions of the <10 μm fraction from A12023.
*ND = component not detected.
N_{LT}, N_{MT} and N_{HT} defined in section 1.7.3.2 (Figure 1.5a and 1.5b).

Whilst discussing the difference in the isotopic profiles obtained by stepped combustion and pyrolysis, it is worthwhile to consider the effect that isotopic fractionation is likely to have on the isotopic composition of lunar soils and breccias. The process of isotopic fractionation results in the preferential release of the lighter isotope of an element, as observed for noble gas elemental abundances (Pepin *et al.*, 1970; Baur *et al.*, 1972). The prospect of obtaining isotopic ratios which had been subjected to negligible fractionation led Wieler *et al.* (1986) to develop the CSSE technique for the analysis of noble gases in lunar soils and breccias (section 1.7.1.2). In the case of nitrogen, isotopic fractionation would result in the preferential release of ^{14}N, compared to ^{15}N. Furthermore, isotopic fractionation should be greater during stepped pyrolysis, when compared to stepped combustion, as the nitrogen is liberated solely by diffusion in the former. During stepped pyrolysis, isotopic fractionation would result in the initial release of ^{14}N, followed by a progression at high temperatures to compositions which are isotopically heavier than observed in the combustion extractions. In contrast, the isotopic profiles obtained by the two techniques display trends to lighter compositions at higher temperatures, with the lightest isotopic compositions observed for the pyrolysis extractions. This suggests that the

difference in isotopic profiles obtained from stepped combustion and pyrolysis extractions is not due to isotopic fractionation during the extraction techniques.

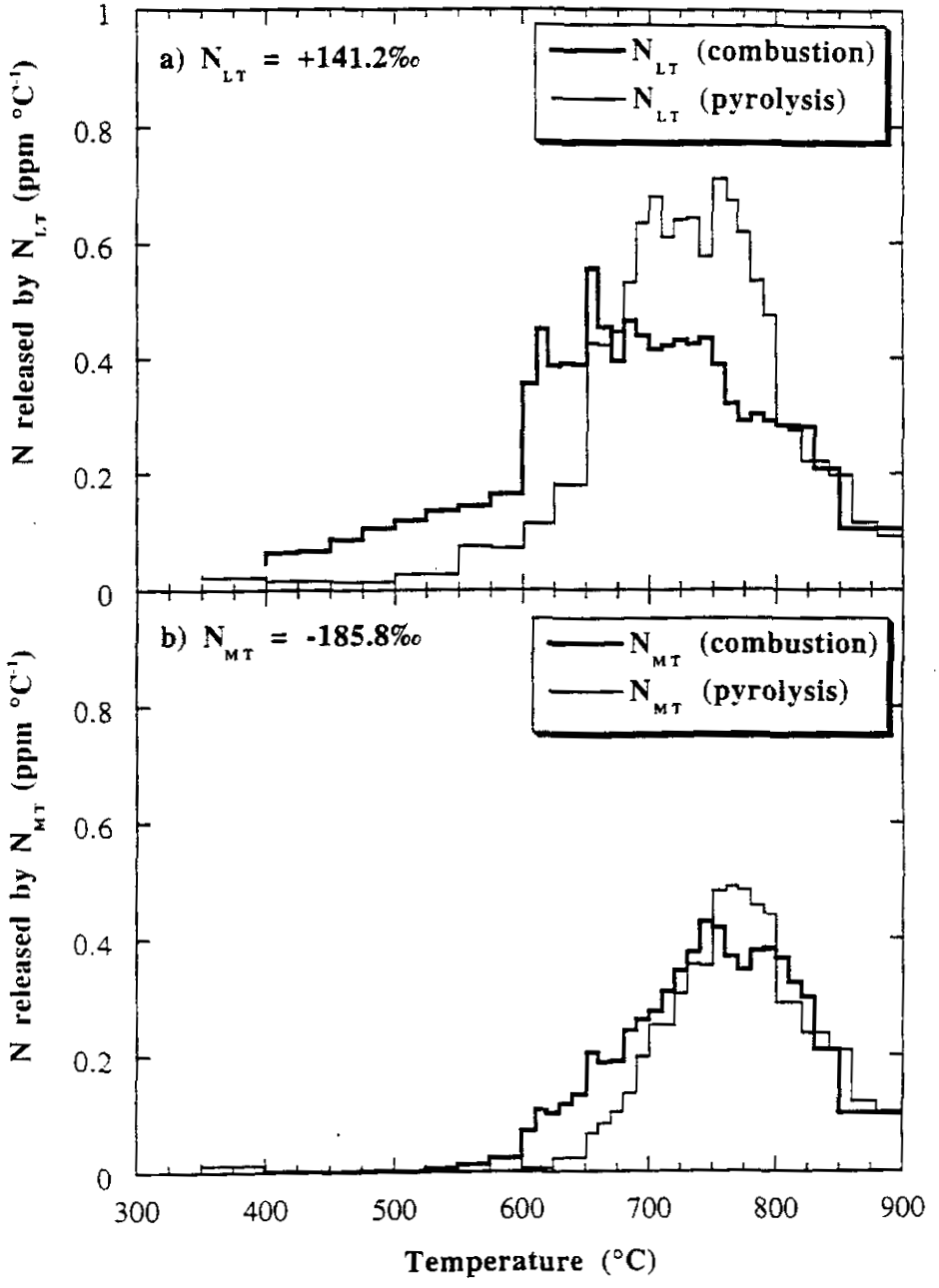

Figure 3.11. Comparison of the release profile for N_{LT} (Figure 3.11a) and N_{MT} (Figure 3.11b) for the combustion and pyrolysis of the <10 μm fraction of A12023. The end members chosen are $\delta^{15}N$ = +141.2‰ and -185.8‰.

Table 3.6 suggests that N_{LT} and a proportion of the light nitrogen (N_{HT}) is shifted to lower temperatures by the presence of oxygen during extraction, and that a minor temperature shift, may also be present for the majority of the light nitrogen (N_{MT}). Note that the temperature shift for N_{HT} is discussed *in section* 3.4.2.2. In order to confirm the

magnitude of the temperature shift for the liberation of N_{LT} and N_{MT}, the two components from FIN62 and FIN73 are deconvoluted by mathematical modelling. The end members chosen for these calculations are +141.2‰ and -185.8‰. The former value is chosen as the $\delta^{15}N$ of N_{LT} from FIN62 and the latter value is obtained by isolation of N_{HT} using joint combustion and pyrolysis extraction (section 3.4.2.2). These isotopic compositions represent the highest and lowest values obtained for the <10 μm fraction of A12023 in this investigation. Figure 3.11 displays the release profiles for N_{LT} (Figure 3.11a) and N_{MT} (Figure 3.11b) for the combustion and pyrolysis extractions. There is a small shift in the calculated release profile of N_{MT} between the pyrolysis and combustion extractions (~25-50°C) but this may be due in part to the wrong choice of end member compositions. However, the shift to lower temperatures (~100°C) of N_{LT} in the combustion is quite pronounced.

In order to accurately determine the magnitude of the temperature shift, best fit lines for the isotopic profiles obtained by the two techniques are compared (Figure 3.12a), with N_{LT} and N_{MT} as the end members. Note that the equations for the best fit lines are given in the figure caption. Using the equations, the release temperature for any $\delta^{15}N$ value can be calculated for both the stepped combustion (T_{comb}) and pyrolysis (T_{pyr}), and hence the temperature shift, ΔT (defined as $T_{pyr} - T_{comb}$) is determined. The temperature shift for a variety of $\delta^{15}N$ values are given in Table 3.7, and a plot of ΔT against pyrolysis extraction temperature is given in Figure 3.12b. The comparison of this offset for the heavy-light trend indicates that there is a clear temperature shift with a mean value of 56 ± 4°C in the presence of oxygen. Extrapolating Figure 3.11b reveals that if no other components were present in the soil, the mixing trends for combustion and pyrolysis would converge at ~1850°C, beyond the extraction limits of the analyses. The similarity in the gradients between the mixing trends for the combustion and pyrolysis confirm that the release of both N_{LT} and N_{MT} are shifted to lower temperatures by the presence of oxygen, although the shift for N_{MT} is less than for N_{LT}.

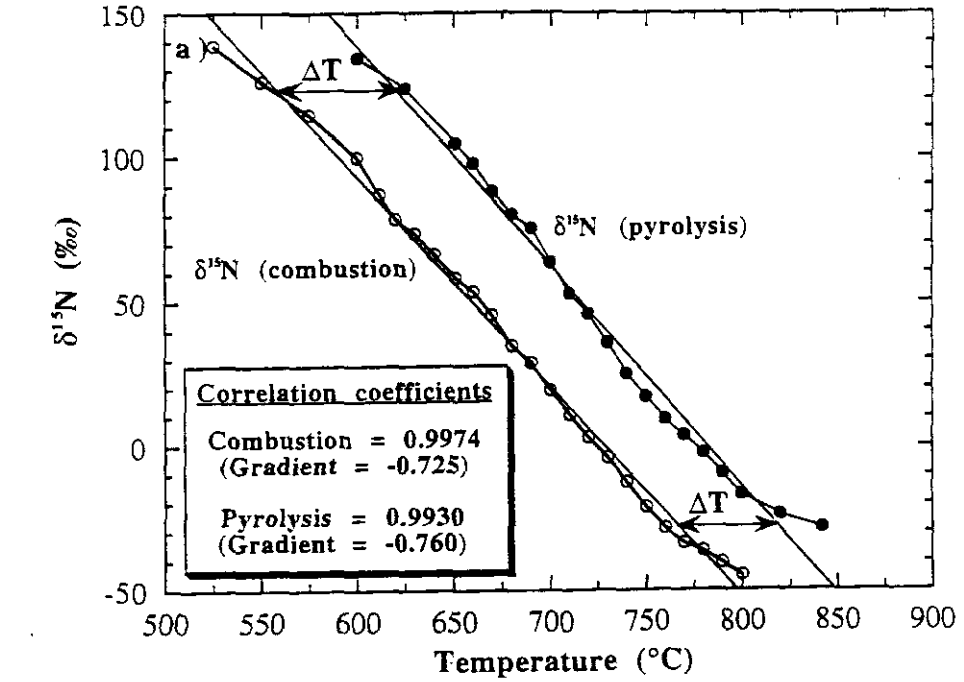

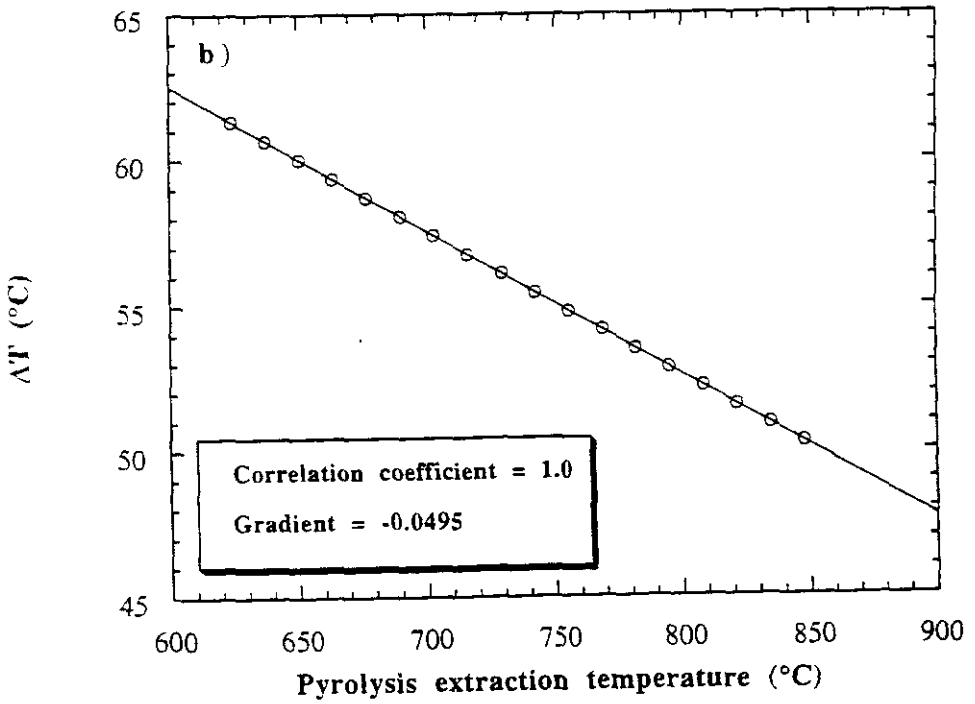

Figure 3.12. Isotopic mixing between N_{LT} and N_{MT} for the combustion and pyrolysis of the <10 μm fraction of A12023. The plots are as follows: a) comparison of the $\delta^{15}N$ values against temperature for the combustion and pyrolysis extractions. The equations for the best fit lines for each isotopic trend are as follows: $\delta^{15}N_{comb} = 527.81 - 0.724T$ and $\delta^{15}N_{pyr} = 594.62 - 0.760T$, where T is extraction temperature (°C), b) plot of ΔT, *i.e.* $T_{pyr} - T_{comb}$, against pyrolysis extraction temperature (°C).

$\delta^{15}N$ (‰)	T_{pyr} (°C)	T_{comb} (°C)	ΔT (°C)
+120	624.19	562.85	61.33
+110	637.34	576.66	60.68
+100	650.49	590.46	60.03
+90	663.64	604.26	59.38
+80	676.79	618.06	58.73
+70	689.94	631.86	58.08
+60	703.10	645.66	57.43
+50	716.25	659.47	56.78
+40	729.40	673.27	56.13
+30	742.55	687.07	55.48
+20	755.70	700.87	54.83
+10	768.85	714.67	54.18
0	782.00	728.48	53.53
-10	795.16	742.28	52.88
-20	808.31	756.08	52.23
-30	821.46	769.88	51.58
-40	834.61	783.68	50.93
-50	847.76	797.49	50.28
Mean	735.97	680.17	55.80

Table 3.7. Calculation of ΔT for $\delta^{15}N$ values (from +120‰ to -50‰) for the stepped combustion and pyrolysis of the <10 μm fraction from A12023.
ΔT defined in the figure caption for Figure 3.12b.

The differences observed in the isotopic profiles for the heavy-light trend by stepped combustion and pyrolysis extraction is further investigated by determining the variation in $\delta^{15}N$, *i.e.* $\delta^{15}N_{pyr} - \delta^{15}N_{comb}$, for equivalent extraction temperatures across the release of LTN. As the combustion and pyrolysis extractions utilise different temperature resolution, the $\delta^{15}N$ variation can only be calculated where an identical extraction temperature is used for both experiments. The $\delta^{15}N$ variation for each temperature step, between 650-800°C, is given in Table 3.8 and illustrated in Figure 3.13.

Figure 3.13 illustrates that the difference in the measured isotopic compositions between the two extraction techniques decreases with increasing temperature across the release of LTN. This can be compared to the decrease in temperature shift at higher temperatures and may be indicative of the less pronounced effects of the presence of oxygen at these temperatures. This will be discussed further from a companion study of a <10 μm size fraction of Apollo 16 soil, A60501 (section 5.3.1).

Temperature (°C)	$\delta^{15}N_{pyr}$ (‰)	$\delta^{15}N_{comb}$ (‰)	Variation $\delta^{15}N$ (‰)
650	+104.5	+58.4	46.1
660	+97.5	+53.6	43.9
670	+88.0	+45.4	42.6
680	+80.1	+35.0	45.1
700	+63.5	+19.4	44.1
720	+45.8	+3.1	42.7
740	+25.0	-12.4	37.4
760	+9.3	-28.4	37.7
770	+3.7	-33.6	37.3
780	-2.2	-36.2	34.0
790	-9.3	-40.4	31.1
800	-16.7	-44.7	28.0

Table 3.8. Variation in $\delta^{15}N$ (‰) for common extraction temperatures (°C) between 650-800°C for the combustion and pyrolysis of the <10 μm fraction from A12023.
Variation in $\delta^{15}N$ defined as $\delta^{15}N_{pyr} - \delta^{15}N_{comb}$.

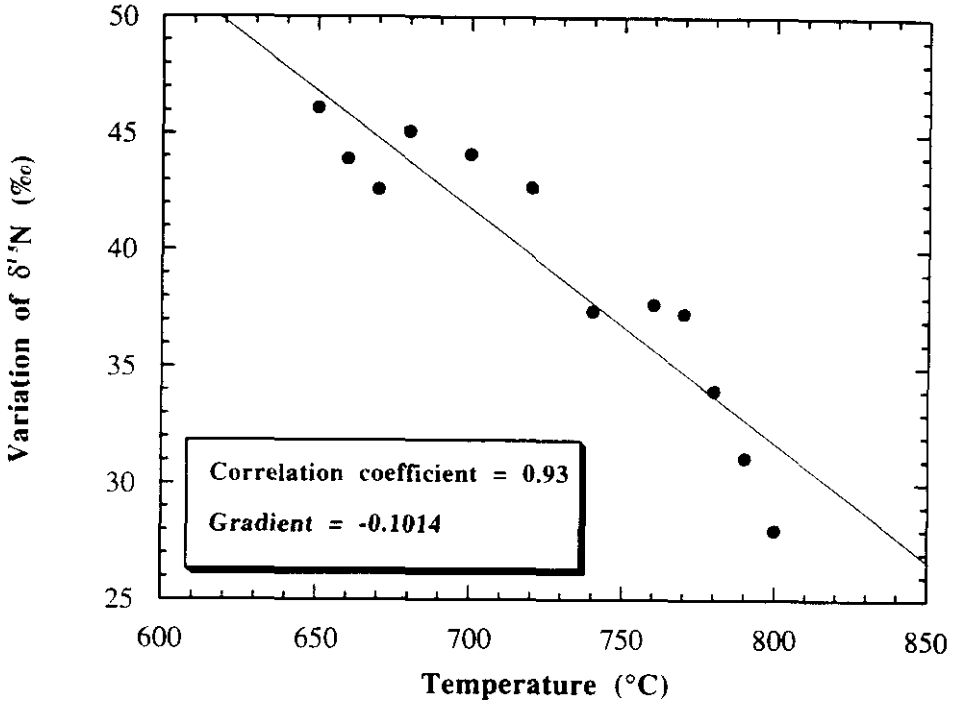

Figure 3.13. Variation in $\delta^{15}N$ (‰) against extraction temperature (°C) for the combustion and pyrolysis of the <10 μm fraction from A12023.
Variation in $\delta^{15}N$ defined in caption for Table 3.8 and in text.

3.4.2.2. Investigation of the temperature shift and isotopic composition of N_{HT} using a joint stepped combustion and pyrolysis extraction technique

In addition to the temperature shifts observed for N_{LT} and N_{MT} (section 3.4.2.1), N_{HT} also reveals clear evidence of a shift to lower temperatures during stepped combustion

extraction. This component appears to be released conjointly with N_{MT} in the presence of oxygen, and is responsible for the lighter values of N_{MT}, by approximately 16‰, observed during the combustion extraction compared to the pyrolysis extraction (Table 3.6). However, it should be noted that the release profiles for both techniques are similar at temperatures of >900°C (Figures 3.10a and 3.10b) and that the nitrogen associated with the liberation of N_{HT} constitutes a small proportion of the total. An estimation of the proportion of isotopically light nitrogen is given later in this section. Hence, it is possible that the true isotopic composition of N_{HT} may be significantly lighter than $\delta^{15}N$ = -93‰ observed in the pyrolysis extraction (FIN73).

In order to isolate the N_{HT} component, a high resolution, part pyrolysis, part combustion extraction was conducted using the <10 μm fraction of A12023 (FIN115). Using a combination of pyrolysis and combustion steps it was hoped that the light nitrogen component (N_{HT}), could be clearly resolved from that which was non-combustible. The sample was pyrolysed from 350°C to 890°C, until after the liberation of N_{MT}, but prior to the release of N_{HT}. To ensure that the correct point was reached on the isotopic profile, high resolution 10°C temperature steps were employed from 800°C. The sample was then combusted from 350-1250°C using 25°C temperature resolution from 700-900°C. The data obtained for FIN115 are given in Appendix B2.1 and the nitrogen abundance and isotopic profile obtained for the stepped combustion portion of the extraction is shown in Figure 3.14.

The pyrolysis part of the extraction yielded a total of 210.7 ppm nitrogen with $\Sigma\delta^{15}N$ = +25.8‰. The sample also liberated N_{LT} at 600°C with $\delta^{15}N$ = +144.1‰ and N_{MT} at 840°C with $\delta^{15}N$ = -28.0‰. Note that the isotopic compositions for the pyrolysis extraction are similar to those obtained for the "ordinary" pyrolysis, *i.e.* FIN73 (Table 3.6). The combustion extraction from 350-1250°C yielded a total of 25.3 ppm with $\Sigma\delta^{15}N$ = -85.3‰. The data are blank corrected using the nitrogen yield obtained from the 500°C step in the combustion, *i.e.* 0.71 ng. This was considered a more realistic blank measurement as the initial blanks had been performed at the start of the extraction two days earlier and would have decreased considerably in the intervening time. Below 875°C, the combustion extraction yielded 8.5 ppm of nitrogen with evidence for a release peak at 725°C and an associated light nitrogen component at 775°C with $\delta^{15}N$ = -185.8‰. This component is

believed to be a proportion of the light nitrogen, N_{HT}, which is liberated at a temperature of 1050°C during pyrolysis, and whose release is facilitated by the presence of oxygen. The combustion from 875-1250°C liberated 16.8 ppm of nitrogen with a hint of a second isotopic minimum at 1050°C with $\delta^{15}N = -91.9‰$. This component resembles N_{HT} observed in the "ordinary" pyrolysis (FIN73), and may have previously been shielded. Although the use of dual combustion and pyrolysis extraction clearly resolves the combustible nitrogen, it is still believed that not all of the light nitrogen has been resolved, and there is evidence to suggest that N_{HT} may have a true $\delta^{15}N < -186‰$. Note that this isotopic composition is similar to that obtained in this work for lunar breccias A79035 (section 4.3.1) and for other lunar breccias by previous workers (section 1.7.3.1).

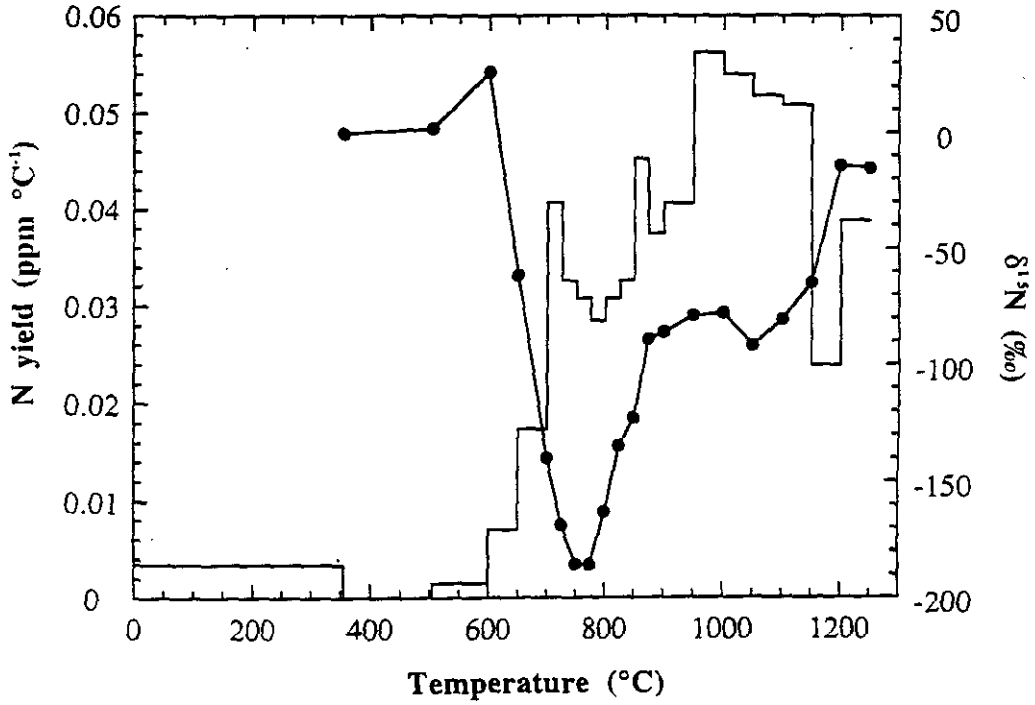

Figure 3.14. Nitrogen yield (ppm $°C^{-1}$) and isotopic composition (‰) for the combustion from 350-1200°C of the <10 μm fraction from A12023, after pyrolysis to 890°C.

The above extractions have shown that lunar soils contain two light components: N_{MT} and N_{HT}, although the detection of N_{HT} is restricted to pyrolyses or joint combustion and pyrolysis extractions. The release of N_{MT} is shifted to lower temperatures, although to a lesser degree than N_{LT}, by the presence of oxygen during extraction. However, the most significant temperature shift has been displayed for N_{HT}, which can have a release temperature as low as 725-750°C. The temperature shift that has been observed (~300°C)

and the associated light nitrogen ($\delta^{15}N$ = -186‰) indicates that the carrier of this component is combustible; then it is a possibility that it is carbonaceous in origin. An alternative explanation may be that the light nitrogen derives from Fe-metal grains within the minerals of the soils, which may be linked to the contribution of impacting meteorites on the lunar regolith (section 1.6.4). An investigation into this hypothesis has been undertaken by examining the argon and carbon profiles for the combustion of the <10 μm grain size fraction of A12023 for FIN115. Figure 3.15 is a plot of the C/N ratio and carbon release profile (Figure 3.15a), the $^{36}Ar/^{38}Ar$ (Figure 3.15b) and $N/^{36}Ar$ ratio (Figure 3.15c), and the data are given in Appendix B2.1.

The combustion part of the extraction liberates 130 ppm of carbon across two temperature ranges: 700-1000°C and 1050-1200°C, similar to the profile observed for nitrogen. Note that the carbon yields are blank corrected in a similar manner to the nitrogen data, using a blank of 7.32 ng (from the 700°C temperature step). Figure 3.15a shows that from 650-1200°C, the C/N ratio varies from 0 to 8 but is always less than 10. The mean C/N ratio over this region is 4.0. This is significantly higher than the C/N ratios of 1-2, observed in other lunar soils and breccias (section 1.7.6.2), but is only slightly higher than solar system value of 3.2 (Anders and Grevesse, 1989). The C/N ratio is also lower than the ratio, ranging from 16 to 94 (Lewis *et al.*, 1983), obtained from chemically resistant phases from carbonaceous chondrites, such as Allende and Murchison, which may detract from a carbonaceous origin for N_{HT}. However, the fluctuations in the ratio is a reflection of the difficulty of obtaining accurate carbon measurements using the capacitance manometer when the carbon yield is close to blank levels (in this case the carbon yield was less than twice the blank), and hence limited significance can be attached to the C/N variation. Note that the errors for the C/N ratios (~15%) are shown in Figure 3.15a. The $^{36}Ar/^{38}Ar$ ratio (Figure 3.15b) decreases throughout the extraction from 6 to 5.5. This is consistent with a solar wind origin for the argon (section 1.7.5.2), although it should be noted that the decrease in the $^{36}Ar/^{38}Ar$ ratios at high temperatures due to cosmogenic ^{38}Ar, is less than observed for the whole-soil (section 3.3.2).

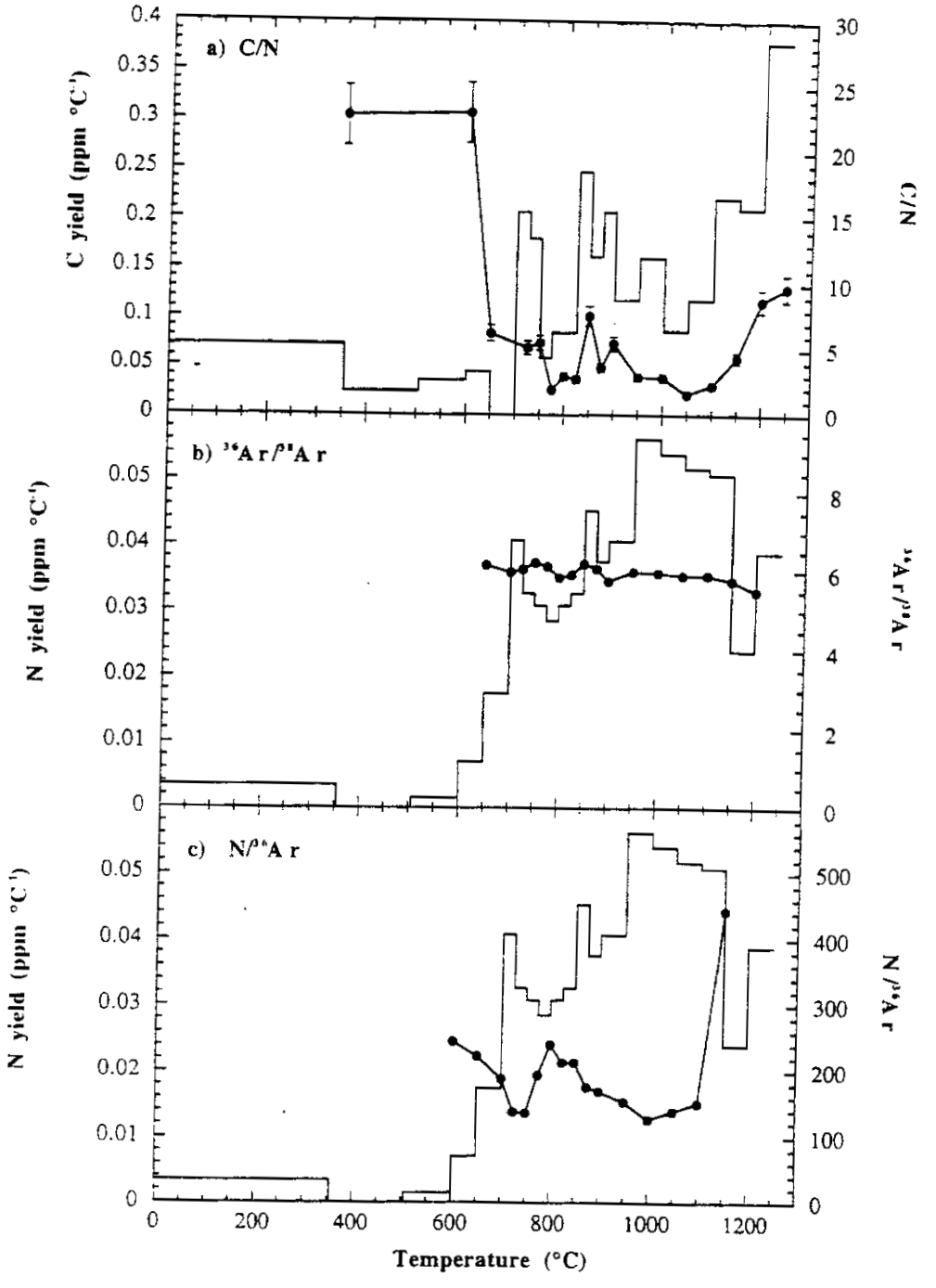

Figure 3.15. Plot of C/N ratios and carbon abundance profile (Figure 3.15a), $^{36}Ar/^{38}Ar$ ratio (Figure 3.15b) and $N/^{36}Ar$ (Figure 3.15c) for the combustion from 350-1200°C of the <10 μm fraction from A12023, after pyrolysis to 890°C.

The $N/^{36}Ar$ ratio varies considerably throughout the extraction (Figure 3.15c) with a mean value of 197 from 600-1200°C. The variation in the $N/^{36}Ar$ ratio suggests that the nitrogen may not be of solar origin, although there is no disputing the solar origin of the ^{36}Ar. Throughout the extraction the $N/^{36}Ar$ ratios are lower than the values of ~380 reported for other lunar soils and breccias, *e.g.* Humbert *et al.* (1997). However, the semi-

quantitative nature of the argon measurements may account for the discrepancy. Interestingly, the variation in the $N/^{36}Ar$ ratio is similar to the profile observed in pyrolysis extractions of lunar soil A12023 (Figure 3.4b (plot i)), which has been explained by the retention of nitrogen during pyrolysis, when compared to ^{36}Ar. An explanation for the observed variation during stepped combustion extraction has yet to be established.

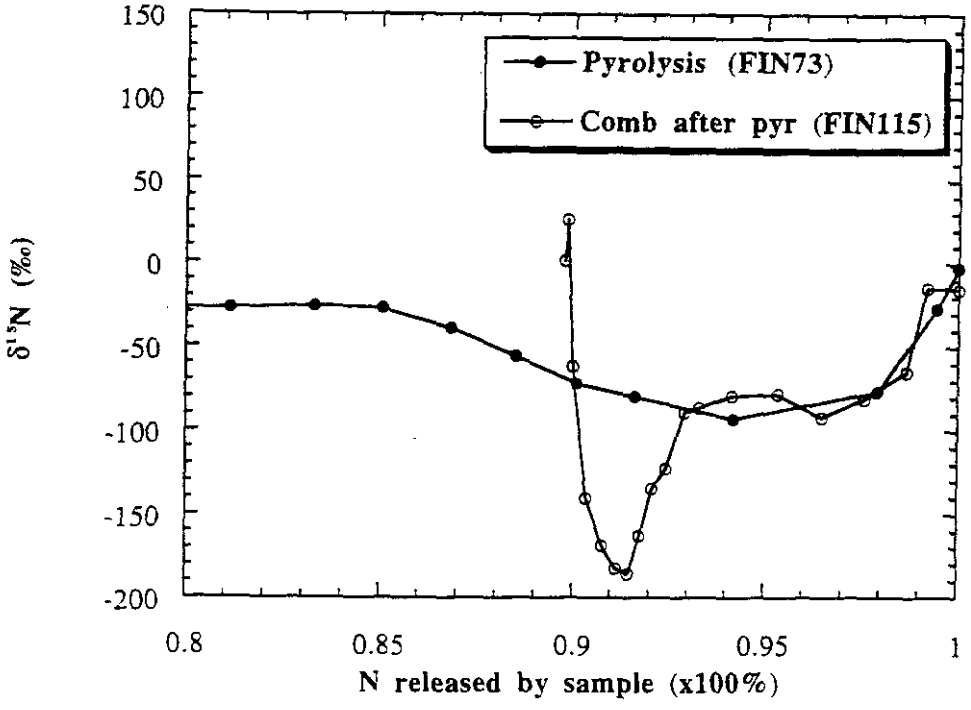

Figure 3.16. Cumulative release plot for the pyrolysis (FIN73) and combustion, after pyrolysis (FIN115), of the <10 μm fraction from A12023.

In conclusion, the release temperature of both the low temperature, isotopically heavy (N_{LT}) component and a proportion of the light nitrogen (N_{HT}) is enhanced by the presence of oxygen during extraction. The explanation for the temperature shift for N_{LT} is not clear and is investigated in section 4.6. Figure 3.16 displays a cumulative release plot for the high resolution pyrolysis (FIN73) and dual combustion and pyrolysis (FIN115) extractions of N_{HT} for the <10 μm fraction. The proportion of N_{HT}, whose release is enhanced to lower temperature during combustion extraction, constitutes approximately 3%. This component appears to contain isotopically light nitrogen with a $\delta^{15}N$ similar to that observed in lunar breccias. However, the C/N ratios are unable to confirm whether this component is implanted solar wind or carbonaceous in origin, although studies of lunar breccia A79035 (section 4.4) suggests that N_{HT} may be related to incorporation of

amorphous carbon due to frequent meteorite bombardments. Furthermore, the observation of a second isotopically light nitrogen component for FIN115 at 1050°C ($\delta^{15}N$ = -92‰) indicates that not all of the light nitrogen was resolved and hence the "true" isotopic composition of N_{HT} may be <-200‰. The variation in the $N/^{36}Ar$ ratio indicates that the light nitrogen component may not originate from the same source as ^{36}Ar, *i.e.* solar wind, and may not reside in the same location within the soil. Despite the semi-quantitative nature of the argon measurements, the $N/^{36}Ar$ ratios are similar to those for other lunar soils and breccias, and are between 3.4 and 12.1 times the solar value of Anders and Grevesse (1989).

3.5. Nitrogen abundances and isotopic composition from density and magnetic separates from the 106-152 μm fraction of A12023

The density and magnetic separates are analysed to determine the location of nitrogen and solar wind gases within lunar soil grains. The analysis of these separates enables the study of individual components from the soil, *i.e.* mineral grains or agglutinates, and their preparation from the 106-152 μm fraction of A12023 have been discussed in sections 2.7.2.2 and 2.7.2.3.

The density and magnetic separates are analysed by stepped pyrolysis using 50°C resolution. The four samples analysed for this work are the low density ($\rho<2.96$) NM (non magnetic) and M3.5 (the most magnetic fraction), and medium density ($2.96<\rho<3.3$) NM and M2.0 (the most magnetic material available) fractions. The data for each extraction are given in Appendix B3.1 ($\rho<2.96$) and B3.2 ($2.96<\rho<3.3$). Note that due to insufficient quantities of sample, no analyses were performed on the $\rho>3.3$, *i.e.* ilmenite, fractions. The mineralogical description of the density and magnetic separates are given in Table 3.9, and a description of the terminology used to define the magnetic properties of the separates are described previously (section 2.7.2.3).

The low density ($\rho<2.96$) NM fraction contains plagioclase while the magnetic fractions (from M3.0) contain agglutinates. The $2.96<\rho<3.3$ NM fractions consist mainly of plagioclase grains mixed with minerals such as pyroxene, whereas the magnetic fractions (from M1.5) contain mainly dark cindery grains with some contribution from microbreccias.

Density (ρ)	Mineralogy of non-magnetic fractions (NM)	Mineralogy of magnetic fractions*
<2.96	Crystalline plagioclase	Glass spheres and shards from M1.5 and in MT fractions. Dark cindery grains from M2.0.
2.96-3.3	Plagioclase intergrown with pyroxene	Glass covered grains in MT fractions. Dark cindery grains abundant in M1.5, M2.0 and M2.5.
>3.3	Olivine, ilmenite, and pyroxene	No highly magnetic fractions.

Table 3.9. Optical properties of density and magnetic separates from the 106-152 μm grain size fraction from A12023 (after Pillinger *et al.*, 1978).
* = magnetic properties defined in section 2.7.2.3.

	ρ<2.96		2.96<ρ<3.3		106-152 μm
	NM (FIN239)	M3.5 (FIN248)	NM* (FIN259)	M2.0 (FIN227)	Whole-soil (FIN188)
ΣN (ppm)	15.4	76.7	7.2	94.0	45.3
$\Sigma\delta^{15}N$ (‰)	+3.7	+27.6	+45.8	+21.7	+24.4
N_{LT} (‰)	+36.9	+91.0	+46.4	+58.1	+52.7
N_{MT} (‰)	-75.9	+9.4	-27.0	+8.1	-5.2
N_{HT} (‰)	-35.2	+1.8	+15.8	-16.9	-15.0

Table 3.10. Nitrogen yield (ppm) and isotopic compositions (‰) for density and mineral separates from the 106-152 μm fraction from A12023.
* = yield and isotopic composition for 2.96<ρ<3.3 not blank corrected as yields were close to blank levels.
N_{LT}, N_{MT} and N_{HT} defined in section 1.7.3.2 (*Figure 1.5a and 1.5b*).

Table 3.10 displays the ΣN (ppm), $\Sigma\delta^{15}N$ (‰) and $\delta^{15}N$ (‰) of N_{LT}, N_{MT} and N_{HT} for the density and magnetic separates from the 106-152 μm fraction of A12023. The nitrogen release and isotopic composition profiles are given in Figure 3.17 (a to d). Note that the nitrogen yields are plotted on a logarithmic axis to aid comparison between extractions. The data obtained from the pyrolysis extraction of the 106-152 μm size fraction (section 3.4.1) are given in Figure 3.17e for comparison purposes. Note that the

2.96<ρ<3.3 NM fraction has not been blank corrected as the nitrogen yields were typically 1-2 times the initial blank. The errors for the $\delta^{15}N$ measurements are plotted on Figure 3.17a to 3.17e, but are within the size of the data points.

The yield of nitrogen liberated from the separates vary from 7.2 ppm to 94.0 ppm for the 2.96<ρ<3.3 NM and M2.0 fractions respectively, with intermediate values for the ρ<2.96 fractions. The $\Sigma\delta^{15}N$ values vary from +3.7‰ for ρ<2.96 NM fraction to +45.8‰ for 2.96<ρ<3.3 NM. The high $\Sigma\delta^{15}N$ value for the latter is due to a spallogenic component, with $\delta^{15}N$ = +277‰, which constitutes ~25% of the total nitrogen content of the sample.

All the analyses in this work display the characteristic W-shaped profile observed for pyrolysis extractions, although with varying degrees of clarity. An interesting observation from Table 3.10 and Figures 3.17 is that for the non-magnetic, ρ<2.96 and 2.96<ρ<3.3 fractions (Figure 3.17a and 3.17c), N_{MT} is isotopically lighter than N_{HT}, whereas for the magnetic M2.0 and M3.5 fractions (Figure 3.17b and 3.17d) the converse is true. The ρ<2.96 and 2.96<ρ<3.3 NM fractions, contain primarily plagioclase grains and an abundance of intergrown plagioclase/pyroxene grains respectively, whereas the highly magnetic fractions contain agglutinates and microbreccia (Pillinger *et al.*, 1978). In order to invoke a secular increase in $^{15}N/^{14}N$ in the solar convective zone to account for the variation in $\delta^{15}N$ in lunar soils (section 1.7.4.1), it would be expected that the pure mineral grains would contain isotopically heavy nitrogen, whereas the agglutinates and microbreccia fraction would contain isotopically light nitrogen. As can be seen in Table 3.10 and Figures 3.17, the converse is true, with the isotopically heaviest nitrogen, N_{LT} ($\delta^{15}N$ = +91‰ and +58‰), located in the agglutinate and microbreccia fraction respectively, and the lightest nitrogen, N_{MT} ($\delta^{15}N$ = -76‰ and -27‰) in the plagioclase and plagioclase/pyroxene fractions. It should be noted that due to the low sample:blank ratios for the 2.96<ρ<3.3 NM fraction, a detailed discussion of isotopic variations is difficult and hence this observation is tentative. However, analyses of ilmenite fractions from lunar breccia A79035 (Becker and Pepin, 1989) and lunar soil A71501 (Frick *et al.*, 1988; Becker and Pepin, 1989) have revealed a similar isotopic trend to that displayed by the respective bulk samples. This implies that the pure mineral fractions also contain an isotopically light nitrogen component

which contradicts the theory that the agglutinates are the host of this component, as invoked by the secular variation model.

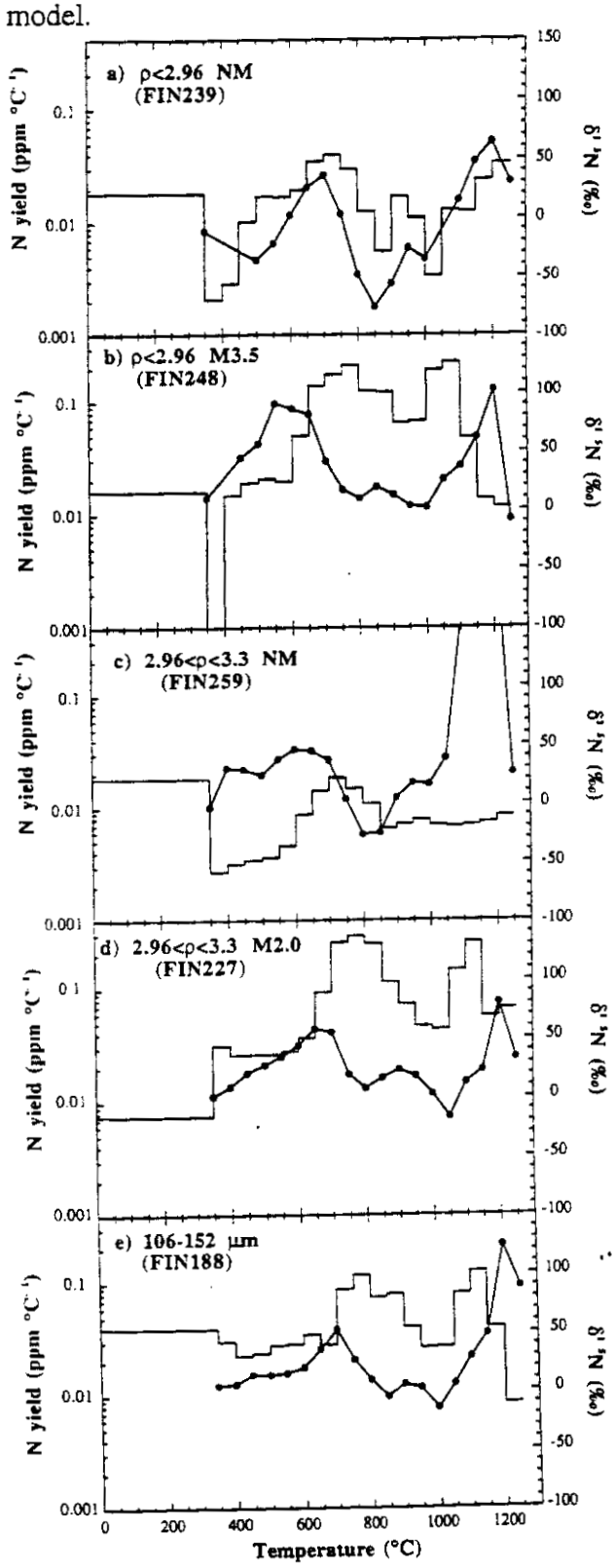

Figure 3.17. Nitrogen yield (ppm °C^{-1}) and isotopic compositions (‰) for the stepped pyrolysis of density and magnetic separates from the 106-152 µm fraction from A12023. The fractions are: a) ρ<2.96 NM. b) ρ<2.96 M3.5. c) 2.96<ρ<3.3 NM. d) 2.96<ρ<3.3 M2.0. The pyrolysis of the 106-152 µm fraction (FIN188) is given in plot e).

The $\rho<2.96$ and $2.96<\rho<3.3$ magnetic fractions yielded between 5 and 13 times more nitrogen than the NM fractions. As the magnetic fractions contain agglutinates ($\rho<2.96$) and microbreccia ($2.96<\rho<3.3$), the increased nitrogen content in these separates may be due to the smaller mean effective grain size of the agglutinates, when compared to the pure mineral fragments. Furthermore, the higher maturity of the agglutinates and microbreccias, compared to pure mineral fragments, would result in a greater period of accumulation and hence higher contents of nitrogen. In addition, it is known that plagioclase is relatively poor at retaining solar wind, whereas ilmenite and glass are extremely efficient (section 1.7.5), and this is confirmed by the higher nitrogen yields for the magnetic fractions (Table 3.10). The bulk soil profile (Figure 3.17e) can be obtained by adding the constituent yield and isotopic profiles together, although this can only be done quantitatively as not all of the density and magnetic fractions separated from the 106-152 μm grain size have been analysed.

The $2.96<\rho<3.3$ M2.0 fraction displays similar isotopic characteristics to the low density M3.5 fraction, although the former displays heavier N_{LT} and N_{HT} values (Table 3.10). This may be due to the microbreccia content of the fraction, or simply the lower degree of magnetism. Norris *et al.* (1983) and an independent study by Kerridge *et al.* (1992b) have shown that the agglutinates within the lunar soils are not host of the isotopically light nitrogen (section 1.7.4.1, point 2). This theory is substantiated further by examining the abundance release profiles for the magnetic and non-magnetic separates. For the non-magnetic fractions, HTN is essentially absent, whereas the magnetic fractions reveal a significant liberation of nitrogen (~30-35% of the total nitrogen) at temperatures of >1050°C. The observation implies that agglutinates and other complex particles contain nitrogen which has been retained in their interior, possibly since agglutinate formation, and is liberated at temperatures >1050°C. This temperature approximately coincides with the melting characteristics of a glass of a composition akin to lunar basalts indigenous to the Apollo 12 site. Furthermore, as has previously been discussed (section 3.4.1 and Brilliant *et al.*, 1994), the absence of HTN in the finest grain size fractions have suggested that this component is linked to the release from complex secondary particles such as agglutinates. This would be absent in the finest grain sizes as the <10 μm fraction consists of fewer nitrogen containing components, than the coarser grain size fractions.

Further evidence that the HTN component is attributed predominantly to nitrogen liberated from agglutinates can be seen from a comparison of the $\delta^{15}N$ values across the release of HTN. It has previously been noted (sections 3.3.1.2 and 3.4.1) that $\delta^{15}N$ values display a sudden increase at a temperature of ~1200°C, following the release of the majority of HTN. Comparisons of the weighted average $\delta^{15}N$ values, across a temperature range of 1050-1200°C for the analyses where this effect is most pronounced, *i.e.* high resolution combustion and pyrolysis of the whole-soil (FIN37 and FIN44 respectively) and grain size fractions 40-53 μm and 106-152 μm (FIN189 and FIN188 respectively), is given in Table 3.11. Note that the table also includes the percentage of HTN which is liberated across this temperature range. For comparison purposes, the data obtained are compared to the analysis of the ρ<2.96 M3.5 separate (FIN248) from this work, and the pyrolysis of the ρ<2.96 M3.5 separate from the 75-106 μm fraction by previous workers (Norris, 1987 *unpublished data*).

Extraction No.	Temperature Range (°C)*	Weighted average $\delta^{15}N$ (‰)	% of HTN
FIN37[1]	1050-1150	+27.6	83
FIN44[1]	1075-1150	+18.1	89
FIN189[1]	1050-1200	+24.7	91
FIN188[1]	1050-1150	+36.8	83
FIN248[1]		+27.6	
N057[2]		+32.3	

Table 3.11. Weighted average $\delta^{15}N$ (‰) and the percentage of HTN, for the release of nitrogen across the temperature range 1050-1200°C.

* The temperature range is defined by the release of HTN corresponding to a slight increase in $\delta^{15}N$ to heavier values.

References: (1) This work, (2) Norris (1987, *unpublished data*).

The $\Sigma\delta^{15}N$ of the agglutinate fraction (ρ<2.96 M3.5) of +27.6‰ is not dissimilar to the weighted average $\delta^{15}N$ from 1050-1150°C (+36.8‰) of the 106-152 μm grain size fraction from which the agglutinate fraction was separated. This compares to the observation by Norris *et al.* (1983) that the isotopic composition of the agglutinates in

A12023 is similar to the bulk $\delta^{15}N$ for the originating grain size fraction (75-106 μm). Table 3.11 shows that, with the exception of FIN44, there is good agreement between the weighted average $\delta^{15}N$ across the specified temperature range, and the analyses of agglutinate fractions from two independent studies. This suggests that the release of HTN is predominantly (80-90%) due to the liberation of nitrogen from agglutinates. The HTN release is admixed with a minor contribution of spallogenic nitrogen which is responsible for the sharp increase of $\delta^{15}N$ values at ~1200°C.

The study of magnetic and density separates from A12023, whilst useful in constraining possible origins for the isotopic components in the lunar regolith are not as informative as the "ordinary" size fractions, *e.g.* <10 μm. Although, this study did not enable precise isotopic measurements for the non-magnetic fractions, due to low nitrogen abundances, it has provided important observations regarding the origin of the nitrogen and has challenged the traditional solar wind model, invoked to account for the variation in $\delta^{15}N$, because both N_{LT} and N_{MT} appear to be surface-correlated. Further studies are required on a suite of pure mineral separates both from A12023 and other lunar samples to constrain these observations further. However, this study can be used in conjunction with the other A12023 analyses in this work and with the data obtained from a variety of other lunar samples (Chapters 4 and 5) in order to obtain a complete picture of nitrogen and argon in the lunar regolith.

3.6. Conclusions

In conclusion, the study of a typical lunar soil, A12023, has added some new and interesting observations to the current knowledge regarding the origin and isotopic composition of nitrogen in the lunar regolith. The use of stepped combustion and stepped pyrolysis extraction techniques has revealed nitrogen abundance and isotopic profiles of greater resolution than previously attained. In addition the conjoint measurement of argon and carbon (despite the semi-quantitative nature of the former) has proved invaluable in aiding identification of possible solar and non-solar components.

For all the samples analysed (with the exception of the <10 μm size separate), nitrogen is released over two temperature ranges: 600-1000°C (LTN) and 1000°C-1200°C

(HTN) regardless of the extraction method used. The $^{36}Ar/^{38}Ar$ ratios (although semi-quantitative) are consistent with those obtained by noble gas analysis and reveal a slight decrease with temperature, similar to the trend with increasing depth for noble gas studies. It is believed that all the ^{36}Ar, and most of the ^{38}Ar, originates from the solar wind, with increasing contribution at higher temperatures from SEP-Ar and cosmogenic ^{38}Ar. The $N/^{36}Ar$ ratio is constant during combustion extraction but varies considerably during pyrolysis extraction. The release of ^{36}Ar precedes that of nitrogen by 50°C approximately during pyrolysis extraction but is almost identical in release temperature during combustion. This suggests that the nitrogen is bound in some chemically dependent way within the grains or retained with higher efficiency than ^{36}Ar, when diffusion is the sole release mechanism. The variation in $N/^{36}Ar$ during the pyrolysis extractions is therefore due to the preferential retention of nitrogen compared to ^{36}Ar in the absence of oxygen. The surface location of nitrogen, compared to noble gases, and the constant $N/^{36}Ar$ ratios in the combustion extraction of the whole-soil and <10 μm grain size fraction, have been two of the major arguments in favour of a solar wind origin for lunar nitrogen. However, the conjoint liberation of ^{40}Ar with ^{36}Ar argues against the surface-sited location of recent solar wind, as invoked by the proponents of a secular variation of $^{15}N/^{14}N$ in the solar convective zone, as ^{40}Ar is re-implanted onto soil grains from the lunar atmosphere. A further problem when invoking a solar origin for the nitrogen is that the $N/^{36}Ar$ are an order of magnitude higher than the solar value of ~37 (Cameron, 1982; Anders and Grevesse, 1989).

The results presented in this chapter have confirmed that the isotopic profile for lunar soils is more complicated than previously thought. The combustion extraction displays a V-shaped profile, whereas the pyrolysis extraction always displays a W-shaped profile, independent of the grain size, density or magnetic index of the sample. The A12023 extractions all release a low temperature, isotopically heavy component (N_{LT}) between 450-650°C and a mid-temperature light component (N_{MT}) at 800-850°C. The $\delta^{15}N$ value of N_{LT} is difficult to constrain accurately due to the liberation of low amounts of nitrogen relative to the blank, and is likely to be higher than the highest value obtained from the <10 μm fraction, *i.e.* $\delta^{15}N = +141.2‰$. The use of on-line pre-combustion steps for the pyrolysis extractions was believed to resolve the problem of accurate $\delta^{15}N$ measurement due to the

contribution of terrestrial contamination, as this component would be removed prior to the start of the extraction.

The stepped pyrolysis extractions also reveal a second light component (N_{HT}) at a temperature of 1050°C which is not detected in the combustion extractions, suggesting that it is either absent or masked in the latter. If the component is masked, it seems likely that the release of N_{HT} is shifted to lower temperature in the presence of oxygen, causing it to be liberated, coincidentally, with N_{MT}. With the exception of the <10 μm grain size fraction, all the samples display an isotopically heavy component observed at high temperatures (>1100°C) which is generally believed to be spallogenic nitrogen.

The analysis of grain size fractions from A12023 in this study have confirmed the nitrogen trends reported previously (Goel and Kothari, 1972; Holland *et al.*, 1972a; Müller, 1974). The finest grain sizes reveal higher nitrogen abundances, but lower $\Sigma\delta^{15}N$, than coarser grain sizes, and a higher variation in $\delta^{15}N$ during the extraction. These trends indicate that the mean grain size of the whole-soil A12023 lies in the range 10-40 μm. In addition, the proportion of nitrogen released as LTN decreases with increasing grain size with a corresponding increase in the proportion of the nitrogen released as HTN. Hence, the finest grain size fraction, <10 μm, releases the majority (>90%) of the nitrogen as LTN and a negligible amount of nitrogen above 1000°C. This can be explained if we consider the soil as a mixture of a surface-correlated component, *i.e.* pure mineral grains, with a volume-correlated component, *i.e.* complex secondary particles such as agglutinates or microbreccia, whereby the finest grain sizes would have a higher ratio of exterior surface to interior volume than the coarsest grain sizes. The observation that HTN and high temperature heavy nitrogen is absent in the <10 μm fraction implies that the release of HTN is associated with the liberation of complex particles. The release temperature of HTN, *i.e.* 1000-1200°C, is consistent with the melting temperature of a glass with a similar composition to Apollo 12 basalts, and hence this suggests that glass-welded agglutinates are the dominant host of HTN.

The gradual increase in $\delta^{15}N$ across the temperature region 1050-1200°C coincides with the release of 80-90 % of HTN. The weighted average $\delta^{15}N$ across this region for the whole-soil (FIN37) and grain size fractions (FIN188 and FIN189) compares well with the $\Sigma\delta^{15}N$ obtained from agglutinate separates, both in this work, and previous work (Norris

1987, *unpublished data*), and confirms that the majority of HTN is due to the liberation of nitrogen from agglutinates. The increase of $\delta^{15}N$ to higher values, typically >100‰, above 1150-1200°C, and the decrease in the $^{36}Ar/^{38}Ar$ ratio, suggests that the remaining 10-20 % of HTN is due to the release of spallogenic ^{15}N.

The above observations contradict the theory which invokes a secular variation of $^{15}N/^{14}N$ in the solar convective zone, to account for the observed isotopic variation in lunar soils and breccias. The secular variation model postulates that the isotopically light nitrogen is attributed to ancient solar wind located within complex particles, such as agglutinates. However, in all analyses in this study (with the exception of the <10 μm fraction), N_{HT} is liberated just prior to the release of HTN. Furthermore, isotopically light nitrogen has been observed by previous workers (Frick *et al.*, 1988; Becker and Pepin, 1989) in pure mineral separates of lunar breccia, A79035, and immature soil A71501. This suggests that isotopically light nitrogen is present in all types of lunar sample, and not restricted to complex secondary particles. If the nitrogen retained in agglutinates and complex secondary particles is a measure of the solar wind composition at the time of agglutinate formation, it constrains the $\delta^{15}N$ of this component significantly (~+20 to +30‰).

The release of N_{LT} and the isotopically light component, N_{HT}, are shifted to lower temperatures by up to 200°C by the presence of oxygen in the extraction section. The release of the mid-temperature light component (N_{MT}) is only shifted by up to 40°C by the presence of oxygen in the extraction section. This has been confirmed by dual combustion and pyrolysis extractions of the <10 μm fraction and by deconvolution of N_{LT} and N_{MT}. These observations suggest that a proportion of the light nitrogen may be chemically bound within the sample and hence liberated at a higher temperature during pyrolysis, where diffusion is the sole heating mechanism. The dual combustion and pyrolysis extraction has isolated some of the isotopically light nitrogen and calculated that it has a $\delta^{15}N$ value of -186‰, slightly higher that that observed in lunar breccias. However, this component constitutes only 3% of the total light nitrogen, although as it has not been fully resolved, the isotopic composition may be <-186‰. The $^{36}Ar/^{38}Ar$ ratios for this component suggest that it may be solar in origin, as it displays a similar trend to that observed by noble gas analyses. Furthermore, the low C/N ratios (typically <10) detracts from a carbonaceous origin for the light nitrogen component, although the mean C/N ratio of 4.0, is not able to confirm a solar

wind origin (with typical C/N ratios of 1-2) for the component either. A carbonaceous component, such as pre-solar diamond is likely to have a C/N ratio of typically 16 to 94 (Lewis *et al.*, 1983), hence if the component is carbonaceous it has a much lower C/N than expected.

The density and magnetic separates (separated from the 106-152 μm grain size fraction) have yielded some useful information regarding the location of the light nitrogen in lunar soils. However, these separates are not as informative as fine grain size fractions for identifying components, since the latter do not contain complex secondary particles which complicate the lunar nitrogen inventory. The $\rho<2.96$ and $2.96<\rho<3.3$ magnetic fractions (agglutinates and breccia fragments respectively) liberated 5-13 times the amount of nitrogen than the non-magnetic (plagioclase) fractions. This confirms the noble gas data of previous workers (Signer *et al.*, 1977; Wieler *et al.*, 1980, 1983) that the nitrogen is relatively poorly retained in minerals such as plagioclase or plagioclase/pyroxene, compared to minerals such as ilmenite. The magnetic fractions also released ~30% of the total nitrogen as HTN at temperatures above 1000°C, whereas this component was essentially absent in the pure mineral fractions. This substantiated our conclusions from analyses of the whole-soil and grain size fractions, that HTN is liberated from agglutinates and complex particles at high temperatures (>1050°C). The isotopic data from the non-magnetic fractions are less reliable, due to the low amounts of nitrogen released from these samples. Nevertheless individual minerals such as plagioclase shows the best evidence for the light nitrogen (N_{MT}) component. The $\Sigma\delta^{15}N$ for the agglutinate fraction ($\rho<2.96$ M3.5) is +27.6‰, similar to the weighted average $\delta^{15}N$ of HTN for the106-152 μm grain size fraction (+36.8‰). This confirms previous work that the nitrogen in agglutinates is not isotopically lighter than the soils from which they were separated (Norris *et al.*, 1983; Kerridge *et al.*, 1992b).

The observations from lunar soil A12023 from this study have proved invaluable in establishing the origin of lunar nitrogen components within the lunar regolith and have formed the basis for the remaining chapters. Chapter 4 considers another aspect of the investigation into the isotopically heaviest and lightest nitrogen components in lunar soils and breccias. The former is investigated from two soils and an agglutinate breccia from the Apollo 17 site, and the latter is studied using an Apollo 17 regolith breccia, A79035.

Chapter 4

A study of the isotopically heaviest and lightest nitrogen components in lunar soils and breccias.

4.1. Introduction

The stepped combustion and pyrolysis of a typical lunar soil, A12023 (Chapter 3), reveals the presence of multiple nitrogen components. The soil displays a similar nitrogen isotopic variation to that observed for many lunar soils (section 1.7.3.1), with the release of a low temperature, isotopically heavy component (N_{LT}) with $\delta^{15}N \approx +150‰$, followed by isotopically light nitrogen (N_{MT} or N_{MT} and N_{HT} during pyrolysis) with typical $\delta^{15}N \approx -35‰$. Note that the isotopic compositions of N_{MT} or N_{MT} and N_{HT} varies depending on extraction technique used and the type of soil fraction, *i.e.* grain size or density and magnetic separates. In contrast, lunar breccias display no isotopically heavy component but reveal isotopically light nitrogen with $\delta^{15}N$ values ~-210‰ (section 1.7.3.1). Those workers, *e.g.* Becker and Clayton (1975), who advocate a solar origin for the nitrogen in the regolith have attributed the isotopically heavy and light nitrogen to implantation of the recent and ancient solar wind respectively (section 1.7.4.1). They have invoked a secular increase of $^{15}N/^{14}N$ of 20-50% in the solar convective zone over the lifetime of the regolith.

In order to investigate fully the $\delta^{15}N$ variation in the regolith, it is necessary to ascertain the isotopic compositions of the end-member components. This study investigates two groups of samples which contain some of the isotopically lightest and heaviest nitrogen observed to date. The isotopically lightest nitrogen has been observed in lunar breccia, A10046, with two isotopic minima of $\delta^{15}N$ = -267 and -278‰ (Carr *et al.*, 1985b). However, due to sample availability, it was decided to analyse A79035 which has also been well characterised and is known to contain isotopically light nitrogen with $\delta^{15}N$ values between -200 and -250‰ (Clayton and Thiemens, 1980; Carr *et al.*, 1985a; Frick *et al.*, 1988). The isotopic composition of the heavy nitrogen (N_{LT}) in lunar soils is investigated in a study of the Apollo 17 agglutinate breccia, A70019 and the soil samples A73321 and

A75080. The observation of the isotopically heavy component (N_{LT}) in lunar soils, and absence of this component in breccias (Clayton and Thiemens, 1980) may be consistent with recently implanted solar wind nitrogen, as postulated by a increase in $^{15}N/^{14}N$ of 20-50‰ in the solar convective zone over the lifetime of the regolith (section 1.7.4.1). However, the constant $^{40}Ar/^{36}Ar$ ratios obtained in stepped heating extractions (section 3.3.2 and Frick *et al.*, 1988) detracts from this suggestion, as ^{40}Ar, although surface sited is not of a solar origin. These have been analysed by previous workers (Chang *et al.*, 1974b; Petrowski *et al.*, 1974; Becker and Clayton, 1975; Becker, 1980a; Norris, 1987 *unpublished data*) and have displayed some of the highest $\delta^{15}N$ values (+145‰ to +170‰) for the isotopically heavy component (Norris, 1987 *unpublished data*).

Recent work (Norris *et al.*, 1983; Kerridge *et al.*, 1992b) has revealed that the nitrogen in agglutinates separated from lunar soils and breccias are not isotopically lighter than the sample from which they were separated. This has also been confirmed in the current study (section 3.5) which has shown that the agglutinates are not the host of the isotopically light nitrogen, as the agglutinates contain nitrogen with $\delta^{15}N$ values of +20 to +30‰. Therefore, the objective of this study is to determine an alternative origin for the isotopically light nitrogen.

The remainder of this section discusses the isotopically light nitrogen in breccia A79035 (section 4.1.1), and details the nucleosynthetic processes which can result in the production of ^{14}N (section 4.1.2). Section 4.2 details the geology of the Apollo 17 site (section 4.2.1) and describes the major element chemistry and mineralogy of the soils and breccias analysed (sections 4.2.2 and 4.2.3). The nitrogen, argon and carbon data for A79035 are given in section 4.3. An approximate mass balance calculation, described in section 4.4 using the mineral separate data of Kerridge *et al.* (1992b, 1993), has suggested that the isotopically light nitrogen in A79035 may have a $\delta^{15}N$ value of ~-323‰, similar to that observed for presolar diamond in acid residues from carbonaceous chondrites (Lewis *et al.*, 1983, 1987; Ash *et al.*, 1989a; Russell, 1992). I investigate in this study (section 4.4) the possibility of a minor presolar component in the lunar regolith due to the 1-2 wt.% contribution of carbonaceous chondrite debris (section 1.6.4) by analysing an HF/HCl (section 4.4.1) and $HClO_4$ (section 4.4.2) residue of A79035. The preparation protocol for these residues are similar to those employed for presolar diamond (section 2.7.1). Although

regolith gardening, due to frequent meteorite impacts and solar and cosmic ray bombardment, would be expected to modify all phases, it is possible that the most resilient phases, *i.e.* presolar grains, could remain in lunar soils and breccias. Using the current best estimate of 0.043 Å yr^{-1} (McDonnell and Flavil, 1974) for erosion on the lunar surface, diamond with a diameter of 2 nm would be expected to survive on the lunar surface for only ~465 years. However, the intense meteorite bombardment early in lunar history (>3.9 Gyr ago) could have buried the presolar diamond within the regolith, until it was brought to the surface by subsequent gardening processes, and hence it may still survive in some lunar soils and breccias. The conclusions regarding the possible presence of presolar diamond in lunar breccia A79035 is discussed in section 4.5. Section 4.6 displays the data obtained from the Apollo 17 soils and agglutinate breccia and section 4.7 discusses the possible origins for N_{LT} in the light of the data obtained. The conclusions from this investigation into the origin of the isotopically heavy and light nitrogen components in lunar soils and breccias, are discussed in section 4.8, together with the implications for the secular variation and excess nitrogen models for the isotopic variation in the regolith.

4.1.1. Light nitrogen in lunar breccia A79035

The Apollo 17 regolith breccia, A79035, has been studied by many workers for nitrogen abundances and isotopic compositions (Clayton and Thiemens, 1980; Carr *et al.*, 1985a; Frick *et al.*, 1988; Becker & Pepin, 1989; Brilliant *et al.*, 1992, 1994; Kerridge *et al.*, 1992b, 1993). The sample is known to contain significant amounts of light nitrogen with isotopic minima of $\delta^{15}N$ = -224‰ and -243‰ obtained by Carr *et al.* (1985a), and revealed the lightest bulk isotopic composition for any lunar sample with $\Sigma\delta^{15}N$ = -171‰ (Clayton and Thiemens, 1980). The light nitrogen was believed to represent the composition of the ancient solar wind at the time of consolidation of the breccia (Clayton and Thiemens, 1980). However, studies of mineral separates from A79035 (Becker and Pepin, 1989; Kerridge *et al.*, 1992b, 1993) have shown that ilmenite, pyroxene and agglutinates do not contain sufficiently light nitrogen to account for the lightest nitrogen observed in the bulk sample, and may infer one (or more) additional component(s).

4.1.2. Light nitrogen in the Solar System

4.1.2.1. Evolution of low (>0.5 $M_\odot$) and high (> 8 $M_\odot$) mass stars

The Solar System was formed (4.6 Gyr ago) from gas and dust produced in numerous nucleosynthetic events, which caused extensive reprocessing and homogenisation (Reeves, 1978). Despite the early suggestion that the solar nebula was well-mixed (Cameron, 1962), it has since been shown from oxygen isotope studies on chondrites (Clayton *et al.*, 1973) that it was not completely homogenised before condensation. Hence, it is now generally accepted that resilient presolar grains, formed around red giants and in the outburst of supernovae, are present in some primitive meteorites (Lewis *et al.*, 1987).

A typical star (>0.5 $M_\odot$), similar to the Sun, will become a red giant following the depletion of ^1H in its core, from the proton-proton reaction (section 1.4.1) and CNO cycling (the process by which ^1H is converted to ^4He, *via* ^{13}N, ^{13}C, ^{14}N, ^{15}N and ^{15}O intermediaries). The hydrostatic pressure will no longer support the mass of the core, and the star collapses under gravity. As a result, the core temperature increases sufficiently to allow ^4He burning to begin. The ^4He is ultimately converted to isotopes such as ^{12}C by interactions with ^8Be by a string of reactions known as the "triple alpha" process, and causes the star to expand, allowing the outer layers to cool to ~3000 K.

High mass stars (>8 $M_\odot$) evolve faster than low mass stars and can undergo sudden explosions. These supernovae, *e.g.* SN1987A in the Large Magellanic Cloud, are typified by a higher proportion of heavier elements and an Fe/Ni core. The core is produced by the second stage of the triple-alpha process, whereby further reactions between ^4He and ^{12}C will produce heavier elements such as ^{16}O, ^{20}Ne and ^{24}Mg and ^{56}Fe. Without an additional input of energy, no fusion after the Fe-forming stage can occur, and the core begins to collapse. The resulting temperature increase causes degeneration of the Fe elements into ^4He and neutrons, and ultimately leads to collapse of the core into a dense mass. In Type II supernovae, *e.g.* SN1987A, this triggers a highly energetic explosion. Type I supernovae occur in binary systems where a more evolved star will accrete mass from its companion, and synthesize He, C and O in several novae explosions. If the mass of the star exceeds a

critical mass, termed as the Chandrasekhar limit, core collapse will occur and trigger a supernova explosion.

4.1.2.2. Identification of presolar grains in some primitive meteorites

For several decades, many workers have studied primitive meteorites in order to detect traces of nucleosynthetic products from stellar sources, such as supernovae, to understand the origin and early evolution of the Solar System (see review by Kerridge and Matthews, 1988). The first observation of such an isotopic signature in meteorite samples was an exotic xenon component, in the CR chondrite Renazzo (Reynolds and Turner, 1964), which was later found to be of a nucleosynthetic origin and termed Xe-HL (Lewis and Anders, 1983), due to the enrichments of the two lightest (^{124}Xe and ^{126}Xe) and heaviest (^{134}Xe and ^{136}Xe) isotopes (Lewis *et al.*, 1975). The carrier of Xe-HL was termed Cδ by Swart *et al.* (1983). The first nitrogen isotopic measurement of Cδ for an $HClO_4$ residue from Allende (a type CV3 carbonaceous chondrite) was by Lewis *et al.* (1983), and revealed a minimum $\delta^{15}N$ value of -326‰. A study of Cδ in residues enriched in Xe-HL led to the first identification of diamond (Lewis *et al.*, 1987). Since this time, isotopic measurements of Cδ have revealed $\delta^{13}C$ values ranging from -32‰ to -38‰ (Swart *et al.*, 1983; Ash, 1990; Russell, 1992) and $\delta^{15}N$ values of approximately -350‰ (Lewis *et al.*, 1983, 1987; Ash *et al.*, 1989a; Russell, 1992). Diamond has been detected (Lewis *et al.*, 1989) in acid residues, using such techniques as transmission electron microscopy (TEM). The concentration of diamond within carbonaceous chondrites vary from 37 to 467 ppm and the concentration of the nitrogen within the diamond ranges from 3185 to 8994 ppm (Russell, 1992) with C/N ratios significantly in excess of 100. Similar diamond concentrations have also been obtained by Huss *et al.* (1996). The isotopic composition of the diamond from carbonaceous chondrites has a mean $\delta^{15}N$ of -348.4‰ (Russell, 1992). Recently, the abundance values of Russell (1992) have been superceded (Newton *et al.*, 1995; Newton, 1994) by a diamond abundance of 732 ± 188 ppm from an acid residue of Acfer 094 (an ambiguous CO3 or CM2 carbonaceous chondrite), which has been found to contain 2% nitrogen. The vast majority of the nitrogen is released across a narrow temperature range of 500-600°C.

In addition to discussing presolar grains for their characteristic isotopic signatures, it is useful to discuss another type of presolar material, *i.e.* silicon carbide (SiC), in terms of nucleosynthetic production. Silicon carbide was first characterised by an anomalous neon signature, consisting of almost pure ^{22}Ne, that was released at a temperature of 1050°C during stepped heating (Black and Pepin, 1969), and which was termed Ne-E (Black, 1972). It was later discovered (Eberhardt *et al.*, 1981) that Ne-E contained two components: low temperature/density Ne-E(L), found to be presolar graphite (Amari *et al.*, 1990) and the high temperature/density Ne-E(H). In an independent study, Srinivasan and Anders (1978), discovered a xenon component, Xe-S, which was enriched in ^{128}Xe, ^{130}Xe and ^{132}Xe, and believed to be produced in the helium shell of a red giant (Clayton and Ward, 1978). The carrier of Ne-E(H) and Xe-S were later identified as silicon carbide (Zinner *et al.*, 1987; Tang & Anders, 1988). Stepped combustion extractions have shown that SiC contains isotopically heavy carbon with $\delta^{13}C$ values ranging from +1000‰ to +1400‰ (Wright *et al.*, 1988a; Ash *et al.*, 1989b; Alexander *et al.*, 1990; Ash, 1990), and also isotopically light nitrogen with $\delta^{15}N$ values as low as -626‰ for Cold Bokkeveld (Russell, 1992). In a recent study of Acfer 094, Newton *et al.* (1995) have measured isotopically heavy nitrogen with $\delta^{15}N = +1151‰$ at 950°C. Furthermore, the $^{36}Ar/^{38}Ar$ ratios are constant in diamond separates from a variety of primitive chondrites with a range of values from 4.7 to 5.2 (Huss and Lewis, 1994).

4.2. The Apollo 17 site

4.2.1. Geology of the Apollo 17 site

The Apollo 17 mission was the final and most extensive of all the lunar landing missions. During the mission, the Lunar Roving Vehicle travelled a distance of 35 km and collected 110.5 kg of lunar material (741 individual samples). The Apollo 17 mission also incorporated a comprehensive package of scientific experiments, performed on the lunar surface, *e.g.* seismic profiling, gravity measurements, atmospheric studies, measurement of the electrical properties of the Moon and detection of cosmic rays. In addition, there were a considerable number of orbital experiments and photographic tasks (Baldwin, 1973).

The landing site was selected for its geological diversity based upon orbital data obtained during the Apollo 15 mission. The region selected was the highland-mare boundary at Taurus-Littrow (20.2°N, 30.8°E), near the southeastern rim of the Serenitatis basin, in the Taurus Mountains to the south of Littrow crater. A map of the Apollo 17 landing site is given in Figure 4.1. The site was chosen to enable examination of the North and South highland massif, which formed approximately 4.0 Gyr ago (Hinners, 1973). In addition, the valley between the massifs, the Lee Lincoln Scarp and the landslip at the base of the South massif (possibly formed from secondary ejecta from the Tycho crater to the southwest) were believed to be valuable sampling sites (Hinners, 1973).

It was hoped that the landing site would contain basalts that were younger (<3.2-3.7 Gyr) and highland rocks that were older (>3.7-4.0 Gyr) then had been found on previous missions. Preliminary studies of the landing site (Hinners, 1973) indicated that the valley between the massifs was young with relatively few craters dating from an era of volcanic activity (3.6-3.8 Gyr). However, the depth of the regolith (11-14 m) was more consistent with the highland regolith at the Apollo 16 site than the mare sites (<5 m) which indicated that the area was older than had been anticipated, and that many of the smaller craters may have been obliterated. The Apollo 17 samples proved to be significantly more diverse than those from any other Apollo site, with the collection of mare basalts, a variety of breccia types, previously unidentified igneous rocks, dark and light mantle soils and orange and black glasses of a pyroclastic origin; the proportions of which varied considerably at individual collection sites. Further description of the geology of the Apollo 17 landing site is given by Schmitt and Cernan (1973).

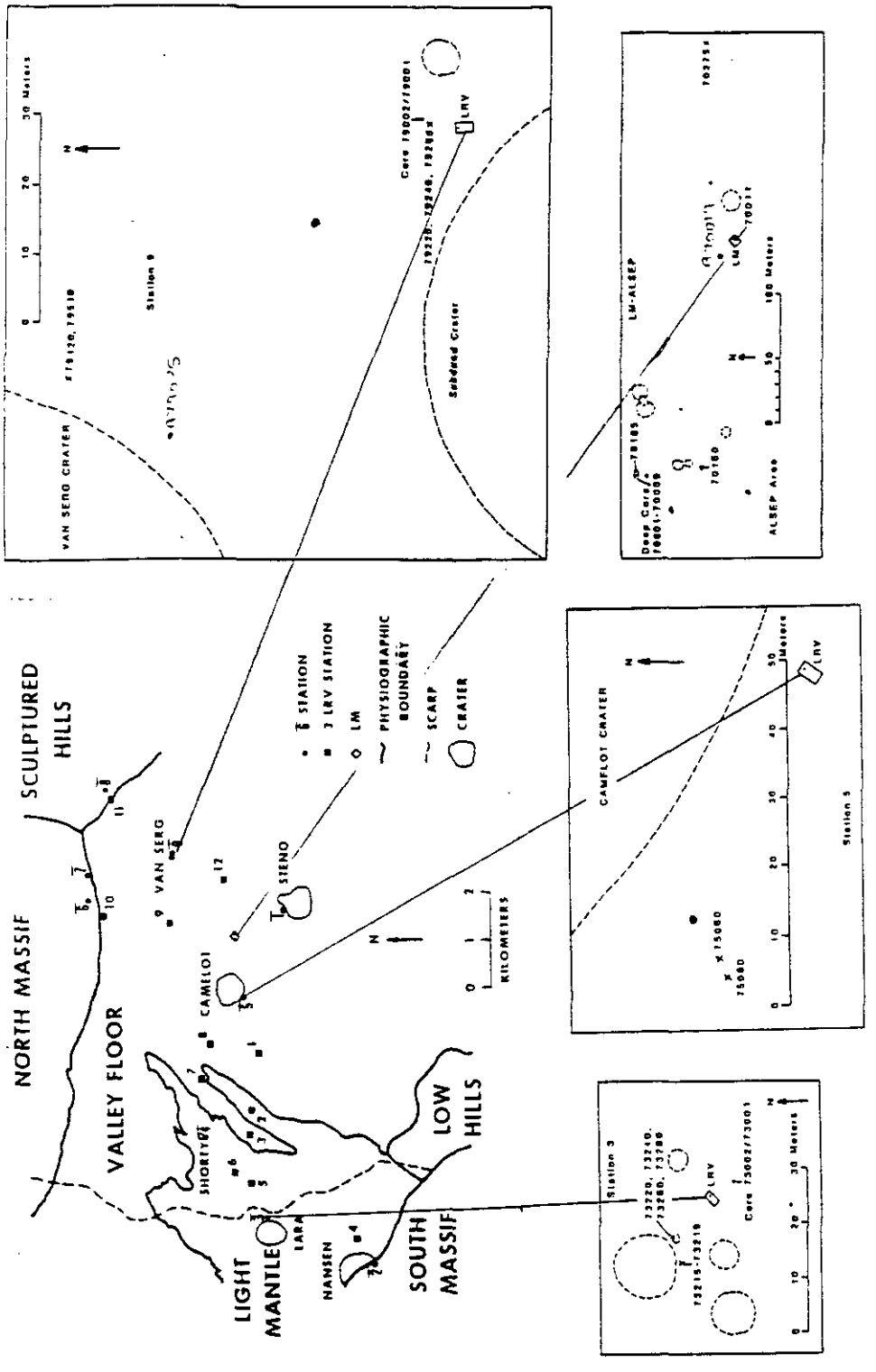

Figure 4.1. Geology of the Apollo 17 site (after Graf, 1993).
Five digit generic sample number defined in section 1.3.1.

4.2.2. Chemistry and mineralogy of regolith breccia A79035

Regolith breccia, A79035, was collected from the ejecta blanket around the 90 m wide Van Serg crater at station 9 of the Taurus-Littrow region (Figure 4.1) with a regolith thickness estimated to be 11-14 m. The crater is believed to have formed 1.5-3.7 Myr ago (Yokoyama *et al.*, 1976). Thin section analysis indicates that A79035 is a moderately friable dark matrix breccia consisting of glass and shocked mineral and glass debris constituting ~95% of the total (LSPET, 1973). The remainder of the rock consists of a variety of basalt, mineral, lithic and glass clasts. The petrology of the sample is given in LSPET (1973) and the mineralogy is given in Table 4.1. Breccia A79035 is believed to have formed approximately 2.5 ± 1 Gyr ago (Clayton and Thiemens, 1980), although recent antiquity estimates (Kerridge *et al.*, 1992b), based on the low $^{40}Ar/^{36}Ar$ ratio (~2), suggest an age of 955 ± 80 Myr. The breccia has a ^{21}Ne-exposure age of 600 ± 50 Myr (Hintenberger *et al.*, 1974). Since its formation, A79035 has been buried and has not been exposed to the solar wind.

	% in A79035	% in A70019
Matrix	95 Glass Shocked mineral debris Glass debris	90 Dark glass (60) Brown pyroxene (15) Plagioclase (15)
Basalt	1-2	8
Glass	1-2	1
Minerals	~1	1

Table 4.1. Mineralogy of regolith breccia A79035, and agglutinate breccia A70019. References: LSPET (1973).

4.2.3. Chemistry and mineralogy of A70019, A73221 and A75080

Lunar sample, A70019 is an impact produced agglutinitic breccia collected from the lunar module (LM) site at Taurus-Littrow (Figure 4.1). However, previous nitrogen

analyses of this sample (Petrowski *et al.*, 1974; Becker & Clayton, 1975; Norris, 1987 *unpublished data*) had revealed a similar yield and isotopic profile to a typical lunar soil, despite its identification as a breccia. The breccia appeared to form during an impact which excavated a shallow crater, and hence up until the time of formation, the sample was exposed to the solar wind. No age constraints could be found in the literature for the impact. The sample contains mostly (90%) matrix material consisting of a mixture of dark glass, pyroxenes, plagioclase and silicates in differing proportions depending on the location within the sample. The majority of the rock consists of dark basalt including plagioclase and brown pyroxene, with a particle size of <100 μm (LSPET, 1973). A further description of the sample is given in LSPET (1973) although no major element chemistry could be found, due to the heterogeneous nature of the sample. The mineralogy of A70019 is given in Table 4.1.

Major elements	% in A73221[1]	% in A75080[2]
SiO_2	45.20	40.27
TiO_2	1.86	9.41
Al_2O_3	21.03	11.31
FeO	8.85	17.20
MgO	8.97	9.59
CaO	12.86	10.97
Petrography	**% in A73221[3]**	**% in A75080[3]**
Agglutinates	26.3	35.3
Basalt	3.0	19.7
Microbreccia	46.6	3.4
Plagioclase	11.3	9.0
Clinopyroxene	8.0	20.3
Ilmenite	0.3	5.7
Glasses	3.5	5.6

Table 4.2. Major element chemistry and mineralogy of A73221 and A75080.
References: (1) Rose *et al.* (1974), (2) Apollo 17 Preliminary Examination Team (1974), (3) Heiken and McKay (1974).

Lunar soil, A73221, is the <1 mm fraction of a skim sample from a 0.5 cm layer of medium-grey soil collected from the rim of Ballet crater at Station 3 (Figure 4.1). Ballet

crater has a diameter of 10 m and has a formation age of 2 Myr (Yokoyama *et al.*, 1976) or 4 Myr (Crozaz *et al.*, 1974). The soil has been classified as sub-mature with I_s/FeO of 43.0 and an agglutinate content of 26.3%, although no exposure age, based on the trapped $^{40}Ar/^{36}Ar$ ratios could be found in the literature. The major element chemistry (Rose *et al.*, 1974) and mineralogy (Heiken and McKay, 1974) are given in Table 4.2.

Lunar soil, A75080, was collected from the upper 5 cm of the regolith on the south-west rim of Camelot crater at Station 5 (Figure 4.1), close to a basalt boulder. These boulders cover ~30% of the station site and are believed to have been excavated by a large impact from a depth of approximately 11 m. Age determinations of the sample (Schaeffer *et al.*, 1976) have indicated that fragments range from <56 to 146 Myr. Apollo 75080 has been classified as a sub-mature soil with I_s/FeO of 40 and an agglutinate content of 35%. Noble gas studies of A75081, the <1 mm fraction of A75080, have revealed $^{40}Ar/^{36}Ar$ ratio of 0.82 and ^{21}Ne-exposure age of 230 Myr (Hintenberger *et al.*, 1974). Major element chemistry (Apollo 17 Preliminary Examination Team, 1974) and mineralogy (Heiken and McKay, 1974) of A75080 are given in Table 4.2.

4.3. Stepped combustion and pyrolysis of breccia A79035

4.3.1. Nitrogen abundance and isotopic composition of A79035

Lunar breccia A79035, is analysed by high resolution stepped combustion (FIN100) and pyrolysis (FIN125) techniques using 10°C temperature steps across the release of LTN. The nitrogen abundance and isotopic profiles for the combustion and pyrolysis extractions are displayed in Figures 4.2a and 4.3a respectively, and the data are given in Appendix C4.1. For the initial steps of each extraction, the nitrogen yields were less than 3 times the initial blank, and hence the isotopic compositions have not been blank corrected (section 2.10). The uncorrected $\delta^{15}N$ measurements, *i.e.* at temperatures of <500°C for FIN100 and <625°C for FIN125, are displayed in Figures 4.2a and 4.3a by hollow circles. The release profiles for A79035 are directly compared with the high resolution combustion (FIN37) and pyrolysis (FIN44) extractions of A12023, which are displayed in Figures 4.2b and 4.3b respectively.

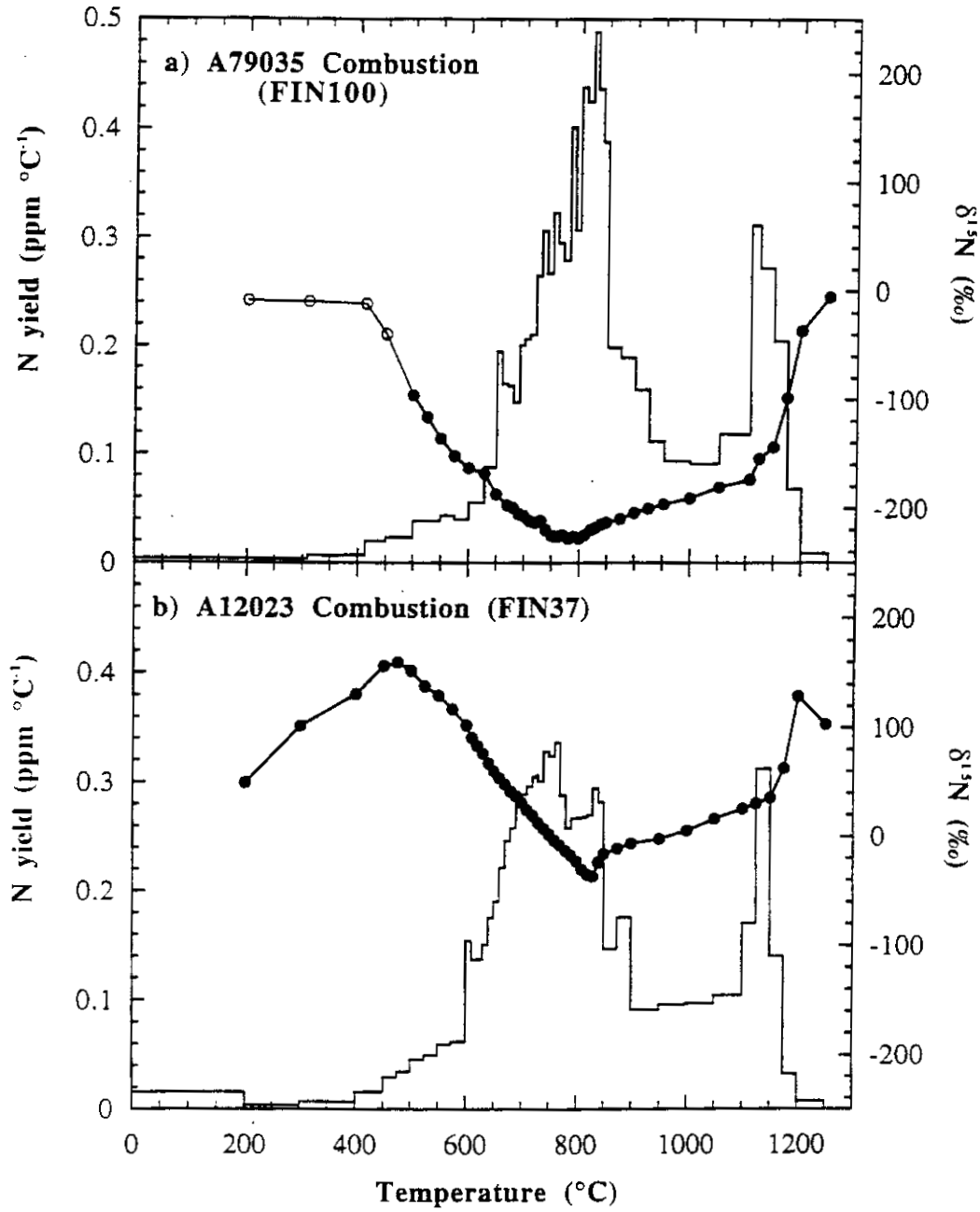

Figure 4.2. Nitrogen yields (ppm $°C^{-1}$) and isotopic compositions (‰) for the high resolution combustion of breccia A79035 (Figure 4.2a) and soil A12023 (Figure 4.2b). The hollow circles for A79035 represent uncorrected $\delta^{15}N$ values due to the low yields of nitrogen liberated at a temperature of <500°C.

The A79035 extractions liberate nitrogen across two distinct temperature ranges: 600-1000°C and 1000-1200°C, which is consistent with the release of LTN and HTN as observed for A12023. The minor variations in the release profiles are attributed to the nitrogen liberated from constituent minerals. However, the release of LTN for FIN125

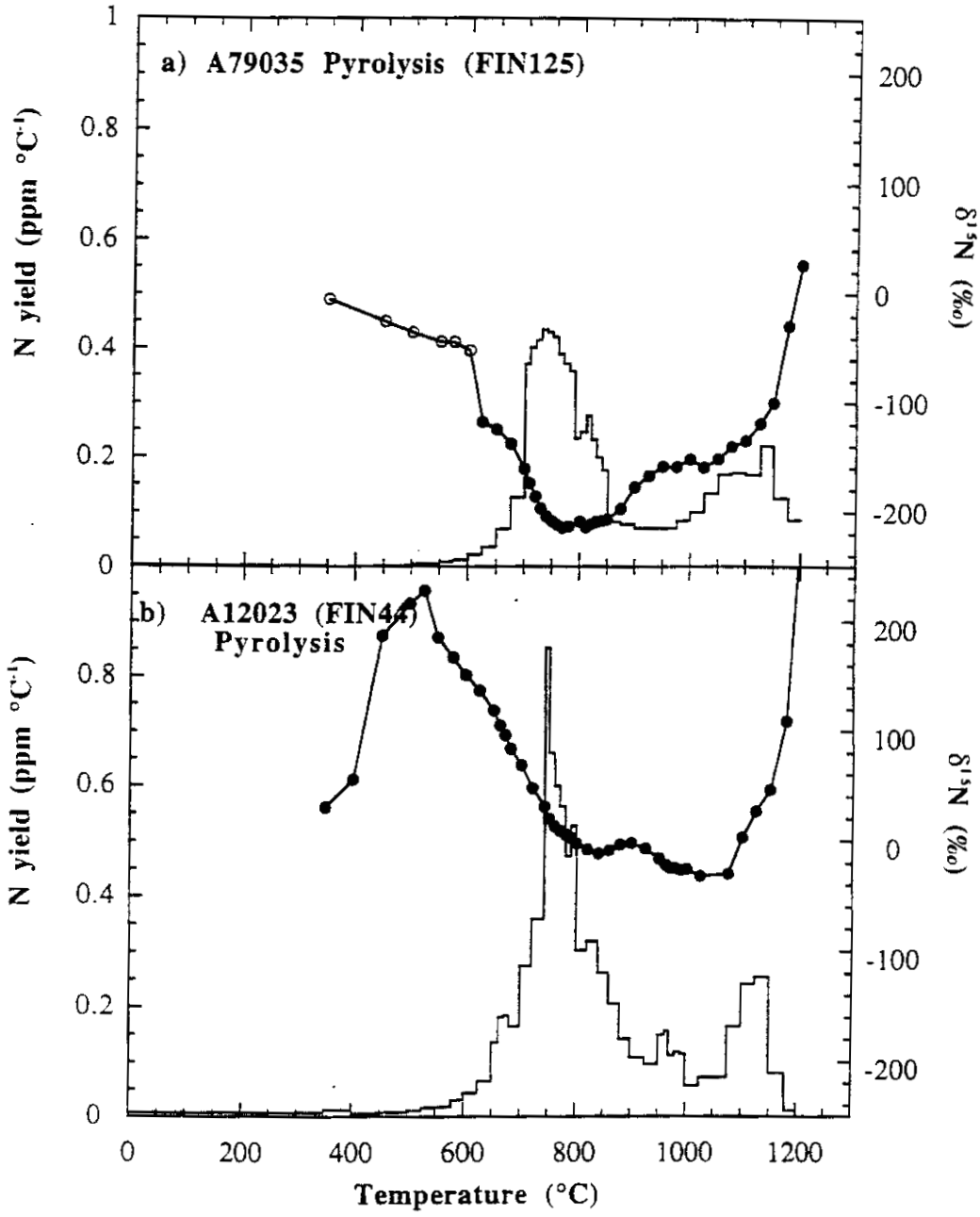

Figure 4.3. Nitrogen yields (ppm $°C^{-1}$) and isotopic compositions (‰) for the high resolution pyrolysis of breccia A79035 (Figure 4.3a) and soil A12023 (Figure 4.3b). The hollow circles for A79035 represent uncorrected $\delta^{15}N$ values due to the low yields of nitrogen liberated at a temperature of <625°C.

(Figure 4.3a) displays a minor tail, which is due to a problem during purification of the nitrogen from the 790°C temperature step. This resulted in an estimated loss of 74% of the total gas from that step, and estimated nitrogen, carbon and argon abundances. Hence the $\delta^{15}N$ value for the 790°C step has been omitted in Figure 4.3a.

Grain size	ΣN (ppm)	$\Sigma\delta^{15}N$ (‰)	Min. $\delta^{15}N$ (‰)	Technique	Reference
Whole rock	**120.4**	**-185.2**	**-227.8 (N_{MT})**	**Stepped comb**	**(1)**
	97.1	**-159.3**	**-214.5 (N_{MT})**	**Stepped pyr**	**(1)**
			-159.6 (N_{HT})		
	113.8	-109.1	-200.4	Stepped comb	(2)
	60.3[a]	-166.4	-224 (N_{MT})	Stepped pyr	(3)
			-243 (N_{HT})		
	93.0[b]	-171.0	-210	Stepped pyr	(4)
Agglutinates					
125-175 µm (Irregular)	20.0[c]		-180 (approx.)	Stepped pyr	(5)
125-175 µm (Spheroidal)	26.0[c]		-180 (approx.)	Stepped pyr	(5)
Ilmenite					
90-125 µm	6.1[d]	-149	-166	Stepped pyr	(6)
125-175 µm	5.2[d]	-125	-140	Stepped pyr	(6)
175-250 µm	2.9[d]	-174	-183	Stepped pyr	(6)
25-150 µm	32.4[e]	-6.6	-176	Stepped comb/pyr	(7)
Pyroxene					
90-125 µm	4.3[d]	-76	-91	Stepped pyr	(6)
125-175 µm	2.3[d]	-125	-140	Stepped pyr	(6)
175-250 µm	2.0[d]	-199	-212	Stepped pyr	(6)

Table 4.3. A comparison of ΣN (ppm) and $\Sigma\delta^{15}N$ values (‰) for A79035 for this work with published results.
(a) extraction from 500°C to 1200°C, (b) extraction from 600-1300°C, (c) extraction from 550-1040°C, (d) extraction from 600-1040°C, (e) extraction from 300-1500°C.
References: (1) This work, (2) Frick *et al.* (1988), (3) Carr *et al.* (1985a), (4) Clayton and Thiemens (1980), (5) Kerridge *et al.* (1993), (6) Kerridge *et al.* (1992b), (7) Becker and Pepin (1989).

As with soil A12023, the LTN release peak for the combustion of A79035 is broader than for the pyrolysis, although the latter precedes that for the combustion with a maximum yield per 10°C step for the pyrolysis at 730-740°C, compared to 810-820°C for the combustion. This has not been observed for any other lunar sample in this work, where

both extraction techniques were used, and hence is attributed to inaccurate temperature measurement for the combustion of A79035, due to a possible problem with the thermocouple shifting position during the extraction.

Table 4.3 shows the ΣN (ppm), $\Sigma\delta^{15}N$ (‰) and the minimum $\delta^{15}N$, obtained in this work and by previous workers (references given in the table caption) for the whole-rock and mineral separate analyses of A79035. The combustion extraction (FIN100) yields a total of 120.4 ppm nitrogen with $\Sigma\delta^{15}N$ = -185.2‰, compared to the pyrolysis extraction (FIN125) which liberates a total of 97.1 ppm nitrogen with $\Sigma\delta^{15}N$ = -159.3‰. The variation in ΣN between this study and previous work may be due to the accidental removal of indigenous nitrogen in earlier studies (Clayton and Thiemens, 1980; Carr *et al.*, 1985a). This may have occurred as a result of the relatively high temperatures, *i.e.* 500-600°C, from which the stepped heating extraction commenced. However, as a similar discrepancy is observed for the two extractions in this study, it seems more likely that it is due to the heterogeneous nature of lunar breccias and is not entirely unexpected. It should be noted that there is good agreement for the isotopic composition of the light nitrogen component in the whole-rock analyses, with $\delta^{15}N$ values ranging from -200 to -243‰.

The isotopic profile for the combustion extraction display the typical V-shaped profile, whereas the profile obtained for the pyrolysis extraction is W-shaped. This is consistent with the observations in this study for A12023 (section 3.3.1.2) and for previous studies of lunar breccias (Carr *et al.*, 1985a, b). The low temperature, isotopically heavy component (N_{LT}) is not present in A79035, which confirms the observations of previous workers (Clayton and Thiemens, 1980; Carr *et al.*, 1985a; Frick *et al.*, 1988; Brilliant *et al.*, 1992, 1994). The maximum $\delta^{15}N$ value for this component is ~-12‰ and ~-4‰ for the combustion and pyrolysis respectively, which may be indicative of terrestrial contamination (~0‰), or indigenous to the breccia. The highest isotopic composition of this component obtained by previous workers is $\delta^{15}N \approx +17$‰ (Clayton and Thiemens, 1980).

Both extractions liberate the isotopically light nitrogen component, N_{MT}, with a weighted average $\delta^{15}N$ = -225.8‰ (750-810°C) for the combustion, and a weighted average $\delta^{15}N$ value of -212.3‰ (760-820°C) for the pyrolysis. In addition the pyrolysis extraction also reveals N_{HT} (although less well defined compared to A12023) at 1025°C with $\delta^{15}N$ of -159.6‰. The differences in the isotopic composition of N_{HT} for the pyrolysis extraction in

this study compared to that obtained by Carr *et al.* (1985a) are problematic to explain. Sample heterogeneity may be important as Carr *et al.* only recovered 60 ppm from the sample (compared to 95 ppm for this work).

The isotopic profiles obtained for the stepped combustion of breccia A79035 and soil A12023 (Figures 4.2a and 4.2b) are similar in shape, although the $\delta^{15}N$ values are markedly different. The isotopic profiles between N_{LT} and N_{MT} define a mixing trend from $\delta^{15}N$ = +159.8‰ to -36.6‰ for A12023, and $\delta^{15}N$ = -10‰ to -227.8‰ for A79035. The similarity in the isotopic profiles between N_{LT} and N_{MT} are not as well defined for the pyrolysis extractions (Figures 4.3a and 4.3b) as for the combustion extractions, although this may be linked to the uncorrected $\delta^{15}N$ values for A79035 at a temperature of <625°C. The similarities in the isotopic profile and the contrasting isotopic compositions of lunar soils and breccias has been the cause of much debate, *e.g.* Frick *et al.* (1988). The isotopically light nitrogen in lunar breccias has been attributed to implantation of the ancient solar wind (section 1.7.4.1). However, several observations have detracted from this hypothesis, *e.g.* isotopically light nitrogen in pure mineral separates of soils and breccias (Becker and Pepin, 1989; Kerridge *et al.*, 1992b), and in a plagioclase separate of immature soil A67601 (Kim *et al.*, 1995). Furthermore, agglutinates separated from grain size fractions of lunar breccia A79035 (Kerridge *et al.*, 1992b) and A12023 (Norris *et al.*, 1983) do not contain nitrogen that is isotopically lighter than the respective parent sample, hence agglutinates are not the host of the light nitrogen (section 3.5). A further hypothesis (Müller, 1974), suggested that the isotopically light nitrogen was nitrogen chemically bound within the sample, *i.e.* in the form of NH_3 or NH_4^+, whereas the heavy nitrogen was due to the presence of molecular nitrogen. However, Kerridge *et al.* (1992b) refutes this theory as no known fractionation processes can account for a variation in $\delta^{15}N$ of ~200‰. Instead, Kerridge *et al.* (1992b) proposes that N_{LT} and N_{MT} represent the energy, and hence implantation depth of solar particles into the regolith, similar to SW and SEP in noble gas studies (section 1.7.5.2). By this definition N_{LT} would be attributed to solar wind implantation and N_{MT} to the implantation of solar energetic particles (SEP). However, this contradicts the study of Ne isotopes in regolith minerals (Wieler *et al.*, 1986; Frick *et al.*, 1988; Becker and Pepin, 1989), which indicates that SEP-Ne is isotopically heavier than SW-Ne.

The major problem encountered when discussing isotopic mixing trends between N_{LT} and N_{MT} (or N_{HT}) in lunar soils and breccias is the determination of the end-member compositions. The "true" isotopic composition of the low temperature, isotopically "normal" component in A79035 has not yet been determined, although the experiment would entail thorough removal of terrestrial contamination at low temperatures, and the use of an appropriately sized sample to obtain accurate isotopic compositions. The observation of isotopically light nitrogen in lunar breccias with $\delta^{15}N$ = ~-220‰ is well documented, *e.g.* Clayton and Thiemens (1980). The observation that a proportion of N_{HT}, from a <10 μm grain size fraction of A12023 (section 3.4.2.2), has a $\delta^{15}N$ value of -186‰, has revealed some similarity between the isotopic compositions for the soils and breccias. Although this component constitutes only ~3% of N_{HT} (although it may not have been fully resolved and may have a $\delta^{15}N < -186$‰), it has been mixed with N_{MT}, and the majority of N_{HT} in lunar soils to mask the "true" composition of the light nitrogen. This may explain the observation of a more pronounced N_{HT} component (compared to N_{MT}) for A12023, whereas for A79035 N_{MT} exhibits a lighter $\delta^{15}N$ value. The C/N and $N/^{36}Ar$ ratios obtained for the isotopically light nitrogen with $\delta^{15}N$ = -186‰, are not conclusive proof of a solar or non-solar origin for this component and hence a further investigation is undertaken in this study (section 4.4).

4.3.2. Argon analysis of A79035

Noble gas studies of the whole-rock (Wieler *et al.*, 1983; Frick *et al.*, 1988) and mineral separates (Becker and Pepin, 1989; Benkert *et al.*, 1993; Nichols *et al.*, 1994) of breccia A79035 by stepped pyrolysis or CSSE, have revealed $^{36}Ar/^{38}Ar$ and $^{20}Ne/^{22}Ne$ ratios which exhibit a similar trend to those observed in other lunar soils and breccias. Their results indicate that regolith soils and breccias contain two distinct reservoirs of noble gases. The interpretation of the reservoirs is given in sections 1.7.5.1 to 1.7.5.3 inclusive.

Conjoint nitrogen and argon zbundances (although the latter is semi-quantitative) are measured for A79035 to determine whether the nitrogen is solar in origin. Figure 4.4a and 4.4b displays the $N/^{36}Ar$ (plot (I)), $^{40}Ar/^{36}Ar$ and $^{36}Ar/^{38}Ar$ (plot (ii)), and the nitrogen and ^{36}Ar yields (plot (iii)) for the stepped combustion (Figure 4.4a) and pyrolysis (Figure 4.4b)

respectively of A79035. The $N/^{36}Ar$, $^{40}Ar/^{36}Ar$ and $^{36}Ar/^{38}Ar$ data are given in Appendix C4.1. and the calculation of the $N/^{36}Ar$ ratios and ^{36}Ar yields are given in section 3.3.2.

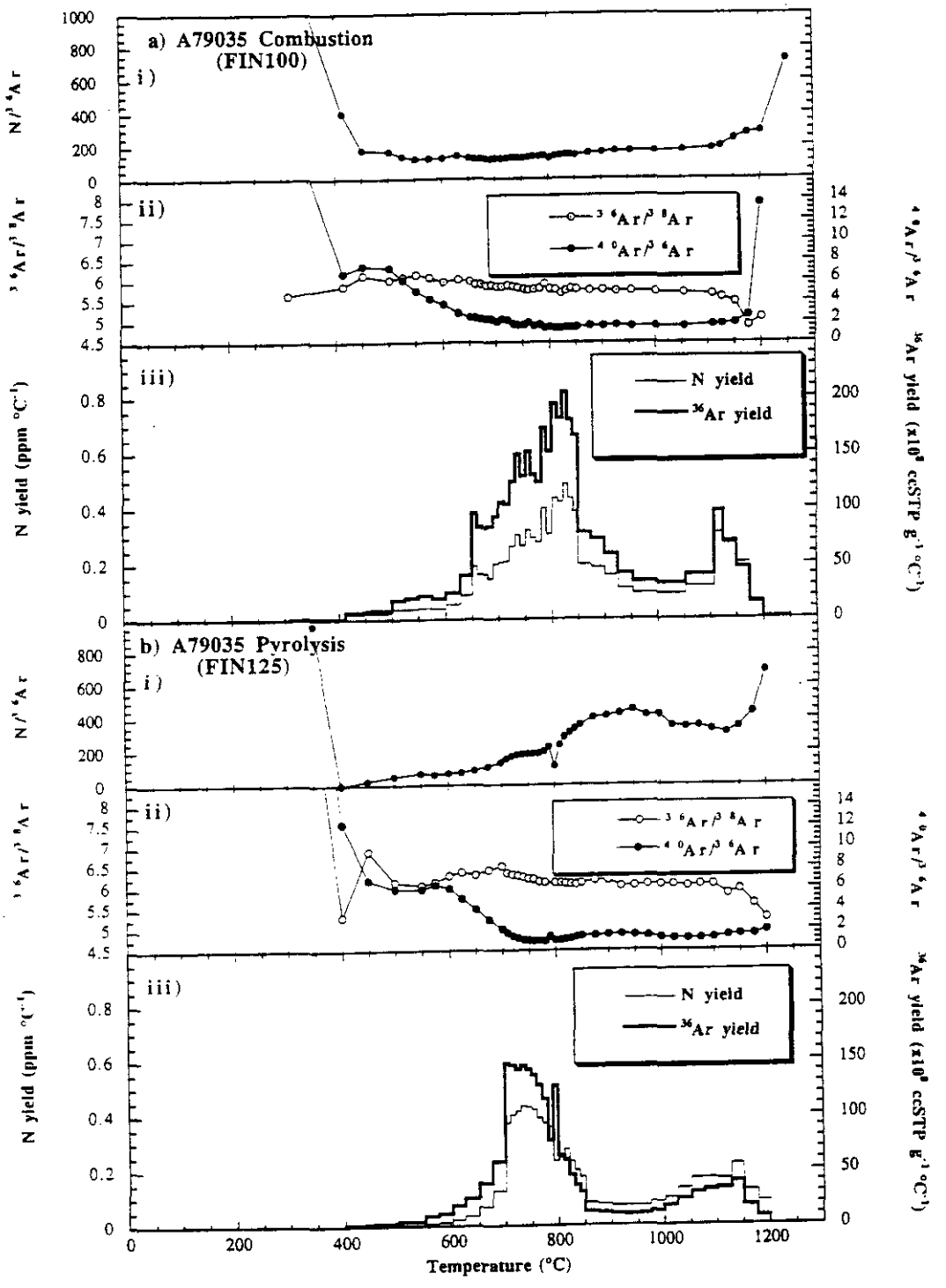

Figure 4.4. Conjoint nitrogen and ^{36}Ar data, and argon isotopic ratios against temperature for the stepped combustion (Figures 4.4a) and stepped pyrolysis (Figures 4.4b) of A79035. The plots are as follows: (i) $N/^{36}Ar$, (ii) $^{36}Ar/^{38}Ar$ (left ordinate) and $^{40}Ar/^{36}Ar$ (right ordinate), (iii) N yield in units of ppm $°C^{-1}$ (left ordinate) and ^{36}Ar in units of ccSTPg^{-1} $°C^{-1}$ (right ordinate).

The $^{36}Ar/^{38}Ar$ ratios obtained for A79035 in this study (Figure 4.4a (ii) and Figure 4.4b (ii)) decrease slightly throughout the extractions from values of 6.2 to 5.5 for the combustion, and 6.3 to 5.9 for the pyrolysis. The sharp decrease at temperatures of ≥1150°C, to values of 5.1 and 5.3 for the combustion and pyrolysis respectively, is attributed to the liberation of cosmogenic ^{38}Ar. These ratios can be taken as comparable to the solar $^{36}Ar/^{38}Ar$ ratios of previous workers (section 1.7.5.1 and 1.7.5.2).

The $^{40}Ar/^{36}Ar$ ratios obtained for both the stepped combustion and pyrolysis extractions (Figures 4.4a (ii) and 4.4b (ii) respectively) are essentially constant with mean values of 3.3 and 2.4 respectively, and compares well with previous work (Frick *et al.*, 1988). The $^{40}Ar/^{36}Ar$ ratios are higher than the mean value in the initial and final steps of each extraction, consistent with the liberation of re-implanted atmospheric ^{40}Ar (section 1.6.1.3) at low temperatures, and of radiogenic ^{40}Ar at high temperatures. The $^{40}Ar/^{36}Ar$ ratios are consistent with the data obtained by previous workers (Frick *et al.*, 1988) for breccia A79035, and for soil A12023 in this work (section 3.3.2). The constant $^{40}Ar/^{36}Ar$ ratio contradicts the secular variation model for the solar wind as this postulates that the initial release of nitrogen from lunar soils and breccias is implanted from the modern-day solar wind (section 1.7.4.1). However, ^{40}Ar is clearly not of a solar wind origin (section 1.6.1.3).

During the stepped combustion extraction of A79035, nitrogen and ^{36}Ar are liberated conjointly (Figure 4.4a (iii)) and hence the $N/^{36}Ar$ ratio (Figure 4.4a (i)) remains constant with a mean value of 173. Note that as discussed in section 3.3.2, the $N/^{36}Ar$ ratio cannot be directly compared with the equivalent ratios obtained by other workers. The constant $N/^{36}Ar$ ratios may imply a solar wind origin for the nitrogen although, as has been discussed for ^{40}Ar, a surface location for the nitrogen is not necessarily proof of a solar origin, although a similar location for the nitrogen and ^{36}Ar, *e.g.* radiation damaged layer, cannot be ruled out. Furthermore the $N/^{36}Ar$ ratio in this work and previous studies is ~4.7 times higher than the solar value of ~37 (Cameron, 1982; Anders and Grevesse, 1989). For the pyrolysis extraction, the $N/^{36}Ar$ ratio (Figure 4.4b (i)) displays greater variation across the release of LTN with a gradual increase from a value of 29 at 450°C to 453 at 950°C. The sudden decrease in the $N/^{36}Ar$ ratio at 800°C is due to the estimated nitrogen and ^{36}Ar yield

for the 790-800°C step, which has been previously discussed (section 4.3.1). The $N/^{36}Ar$ ratio across the release of HTN decreases from 453 to a minimum of 311 at 1125°C. The $N/^{36}Ar$ profile obtained during pyrolysis extraction of A79035 is equivalent to the profile obtained for A12023 (section 3.3.2), and can be explained by the retention of nitrogen to slightly higher temperatures (~50°C) during pyrolysis, where diffusion is the sole release mechanism (Figure 4.4b (iii)). The observation of this phenomena in two distinct types of lunar sample, *i.e.* soil and breccia, implies that it is not a feature of exposure age, chemical composition or mineralogy of the respective samples. During stepped combustion, the presence of oxygen will liberate nitrogen and ^{36}Ar at the same temperature, whereas during pyrolysis molecular nitrogen will be liberated at a slightly lower temperature than nitrogen chemically bound within the sample. A possible carrier of the chemically bound nitrogen is discussed in section 5.3.2, by investigating the correlation between isotopic composition and Fe-metal content of some Apollo 16 soils.

4.3.3. Carbon abundances and C/N ratios from A79035

The carbon abundances for A79035 are measured using the procedure detailed in section 2.4.5, and the yields and C/N data are given in Appendix C4.1. The carbon stepped combustion release profile and C/N ratios are plotted in Figure 4.5, with errors of 15% for the C/N measurements (section 3.3.3). The combustion data are used in preference to the pyrolysis data as previosly discussed (section 3.3.3).

The stepped combustion extraction liberates 307.3 ppm carbon across two temperature ranges: 650-850°C and 1100-1200°C, equivalent to the release of LTN and HTN. The C/N ratio decreases from a value of 24 at 450°C to a minimum of 0.8 at 810°C, but remains relatively constant across the release of carbon (650-1200°C) with ratios of <5. The mean C/N ratio over this temperature range is 2.2, which is consistent with previous analyses of lunar soils and breccias (section 1.7.6.2). However, the C/N ratio is intermediate to solar photospheric values of 1.1 (Anders and Grevesse, 1989) and the solar system ratio of 3.2 (Anders and Grevesse, 1989). The high C/N ratios in the initial steps of the extraction are due to terrestrial contamination, as no attempt was made to remove this component during combustion extraction. Thus some contamination may have remained in

the sample to higher temperatures and is likely to explain the decrease in the C/N ratios at the start of the extraction. If this is the case the mean ratio from 650-1200°C may be less than the calculated value of 2.2. However, the constant C/N ratios during the liberation of the carbon (and nitrogen) suggests a similar siting for both elements, and hence if a solar origin is invoked for the majority of the carbon, an equivalent origin is likely for the nitrogen.

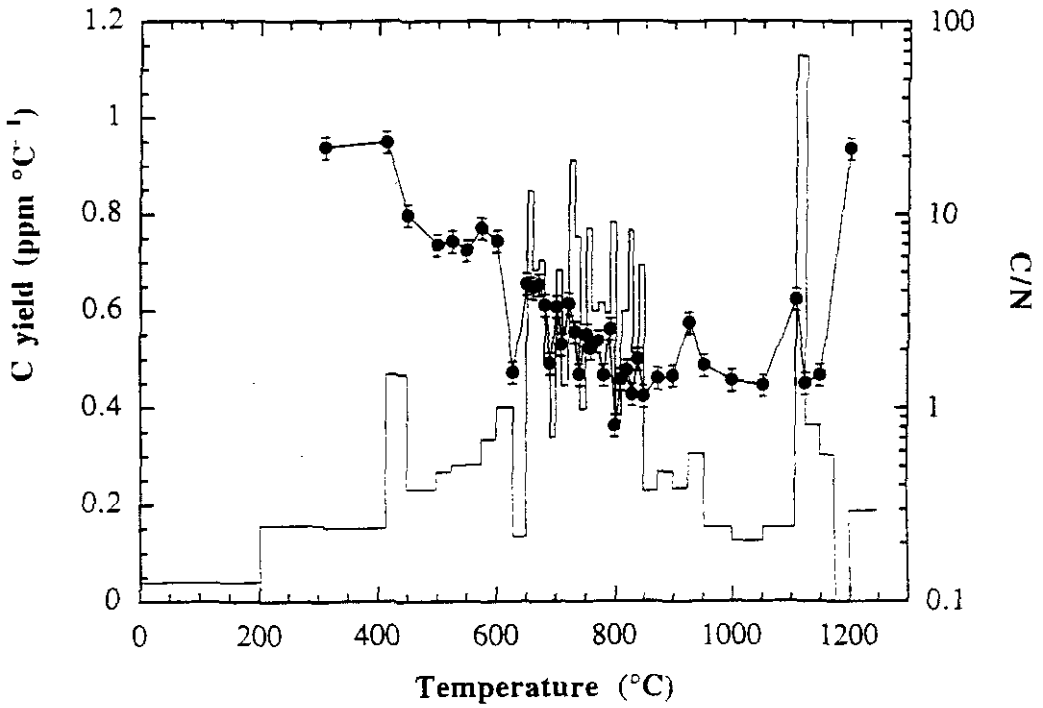

Figure 4.5. C/N ratios and carbon yield (ppm $°C^{-1}$) against extraction temperature (°C) for the stepped combustion extraction (FIN100) of A79035.

4.4. The search for presolar diamond in lunar breccia A79035

The nitrogen data obtained from the stepped combustion and pyrolysis extractions of A79035 in this work, confirms the presence of isotopically light nitrogen with $\delta^{15}N$ values of ≈-220‰. Furthermore, a proportion of the light nitrogen (N_{HT}), constituting ~3% of the total light nitrogen in A12023 has a $\delta^{15}N$ value of ≤-186‰ (section 3.4.2.2). Such isotopically light nitrogen has not previously been observed in lunar soils, although light nitrogen with $\delta^{15}N$ values as low as -348‰ are commonly observed in resilient interstellar grains from some carbonaceous chondrites (section 4.1.2.2).

The observation of isotopically light nitrogen in a variety of grain size fractions, density and magnetic separates of lunar soils in this work (sections 3.4 and 3.5) and by

previous workers (Norris *et al.*, 1983; Kerridge *et al.*, 1992b) have shown that complex particles, such as coarse grained agglutinates, are not the host of the isotopically light nitrogen. The question then remains as to the nature of the carrier of the proportion of N_{HT}, which is observed in A12023 with $\delta^{15}N \leq -186‰$. With the assumption that A79035 contains four components: agglutinates, ilmenite, pyroxene and a single unknown component, a mass balance calculation is undertaken to determine the isotopic composition of the additional component. The data used for this model (Kerridge *et al.*, 1992b; Kerridge, 1993) were taken from pyrolysis extractions of ilmenite, pyroxene and agglutinates separates from a range of grain size fractions (from 90-250 μm) from A79035 (references 5 and 6 in Table 4.3) and were all obtained under similar laboratory conditions. The yield of the unknown component is determined from the addition of the nitrogen abundances from the individual mineral extractions (68.8 ppm), and subtraction of this yield from the total nitrogen abundance of 97.1 ppm obtained from the whole-rock in the current study (FIN125). Hence the unknown component constitutes 28.3 ppm of the total nitrogen. The isotopic composition of the component is determined by the addition of the product of yield and $\delta^{15}N$ of the lightest nitrogen for each mineral fraction, and comparison with the equivalent product for FIN125 (Equation 4.1). Re-arranging Equation 4.1, and substitution of the calculated yield (28.3 ppm) for the unknown component results in an isotopic composition of this component with $\delta^{15}N = -323‰$. This is similar to the $\delta^{15}N$ of presolar diamond as observed in carbonaceous chondrites (section 4.1.2.2), and hence, using the identical protocol to that established for presolar grains (section 2.7.1) the possibility of presolar grains in breccia A79035 is investigated.

$$(N \times \delta^{15}N)_{wr} = (N \times \delta^{15}N)_{ilm} + (N \times \delta^{15}N)_{agg} + (N \times \delta^{15}N)_{pyr} + (N \times \delta^{15}N)_{x}$$

Equation 4.1.

where wr = whole-rock (FIN125), ilm = ilmenite, agg = agglutinate, pyr = pyroxene, x = unknown component.

4.4.1. Nitrogen abundances and isotopic composition of an HF/HCl residue of A79035

The protocol for the preparation of the HF/HCl residue is described in section 2.7.1. The HF/HCl treatment for A79035 removed 99.995% of the sample. The HF/HCl acid residue is analysed by both stepped combustion (FIN196) and stepped pyrolysis (FIN231) using 10 and 25°C temperature resolution across the major release of nitrogen (400-650°C for the combustion and 650-1000°C for the pyrolysis). The ΣN (in ppm and ppm of the whole-rock), $\Sigma\delta^{15}N$ and minimum $\delta^{15}N$ values for the extractions are displayed in Table 4.4. The nitrogen and carbon data are given in Appendix C4.2, and the nitrogen release and isotopic profiles for FIN196 and FIN231 are shown in Figures 4.6a and 4.6b respectively.

	ΣN (ppm of WR)	$\Sigma\delta^{15}N$ (‰)	Minimum $\delta^{15}N$ (‰)
Combustion FIN196	0.230	-60.8	-92.5
Pyrolysis FIN231	0.234	-95.6	-109.7

Table 4.4. A comparison of ΣN, $\Sigma\delta^{15}N$ and minimum $\delta^{15}N$ (‰) between the high resolution combustion (FIN196) and pyrolysis (FIN231) extraction of the HF/HCl residue from A79035.

The combustion and pyrolysis extractions of the HF/HCl residue from A79035 liberate 509.5 and 520.9 ppm of nitrogen respectively, both of which constitute 0.23 ppm of the whole-rock. The nitrogen is liberated in a single peak from 350-600°C during stepped combustion (Figure 4.6a), comparable with a release temperature of 460-520°C for presolar diamond from $HClO_4$ residues of carbonaceous chondrites in previous work (Lewis *et al.*, 1983, 1987; Russell *et al.*, 1991; Russell, 1992). The pyrolysis extraction (Figure 4.6b) liberated two releases of nitrogen over the temperature ranges 700-1000°C and 1000-1250°C, the former of which is consistent with a release temperature of ~800°C from previous pyrolysis extractions of presolar diamond (Verchovsky and Pillinger, 1994). The

higher release temperature for this component in the pyrolysis extraction may be the effect of diffusion out of the sample, in the absence of oxygen during extraction. Furthermore, carbonaceous material is known to decompose at temperatures of ~1000°C and hence this will account for the high temperature (1000-1250°C) release during stepped pyrolysis.

The $\Sigma\delta^{15}N$ (Table 4.4) differ significantly with values of -60.8‰ and -95.6‰ for the combustion (FIN196) and pyrolysis (FIN231) respectively. Both extractions reveal the presence of a single, isotopically light, nitrogen component with $\delta^{15}N$ = -92.5‰ at 600°C for FIN196, and $\delta^{15}N$ = -109.7‰ at 925°C for FIN231. Note that these isotopic compositions are significantly higher than the $\delta^{15}N$ values of -227.8‰ and -214.5‰ obtained for the combustion and pyrolysis extractions of the whole-rock (Table 4.3) respectively. In contrast to the pyrolysis extractions of A12023 (sections 3.3.1.2, section 3.4.1 and section 3.5) and whole-rock breccias (section 4.3.1), no light nitrogen N_{HT} component at 1050°C was observed during the pyrolysis of the HF/HCl residue. This indicates that N_{HT} was removed during the acid treatment and hence suggests that N_{HT} is located within the silicate matrix of the sample.

An HF/HCl residue of lunar soil A12023 was also prepared which resulted in a loss of 99.853% of the whole-rock. The residue is analysed by stepped combustion (FIN26) and liberates a total of 12.7 ppm nitrogen (equivalent to 0.019 ppm of the whole-soil), with a minimum $\delta^{15}N$ = -9.6‰ at 900°C. The isotopic composition of the nitrogen at a temperature of 600°C (a similar temperature which liberated $\delta^{15}N$ = -93‰ for FIN196) was only +7.8‰, and hence the soil was not deemed a suitable specimen to conduct further chemical treatments. The data for FIN26 are given in Appendix C4.2, but are not displayed in this work.

The argon yields for the combustion and pyrolysis of A79035 HF/HCl residues are close to blank levels and only reveal limited structure, hence are not included in this work. The combustion of the HF/HCl residue liberates 22696 ppm of carbon (10.2 ppm of the whole-rock), and the pyrolysis liberated 10578 ppm (4.8 ppm of the whole-rock). The carbon release profile for the stepped combustion extraction, and the C/N ratios are displayed in Figure 4.7, and the data are given in Appendix C4.2. The combustion data are preferred (section 3.3.3) and the errors for the C/N measurements are ±15%. The carbon is liberated as a single peak between 300-600°C during combustion, whereas the pyrolysis

(data given in Appendix 4.2) extraction displays two distinct releases at temperatures of 900-1000°C and 1050-1250°C, similar to the release peaks for nitrogen.

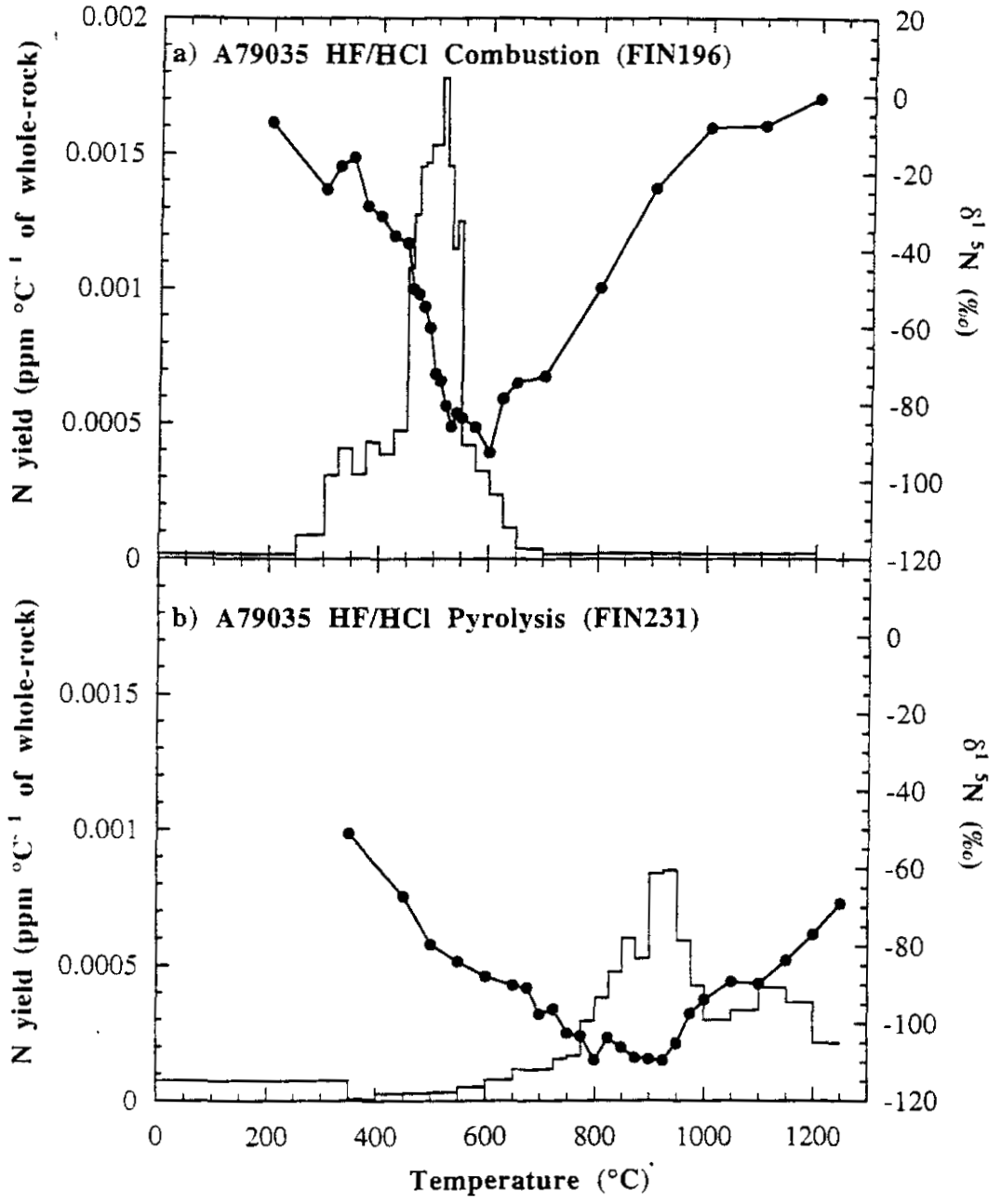

Figure 4.6. Nitrogen yield (ppm °C^{-1} of whole-rock) and isotopic compositions (‰) for the combustion (Figure 4.6a) and pyrolysis (Figure 4.6b) of the HF/HCl residue from A79035.

The C/N ratios for both extractions are higher than usually observed in lunar samples with mean values of 43 for the combustion and 33 for the pyrolysis. These values are significantly lower than the C/N ratios of >100 obtained by Russell (1992), but lie within the range of 16 to 94 (Lewis *et al.*, 1983), for chemically resistant phases from carbonaceous chondrites, such as Allende and Murchison. However, the variation in the C/N ratios

implies that the data cannot be used to conclusively confirm or eliminate the possibility of presolar diamond in the lunar regolith.

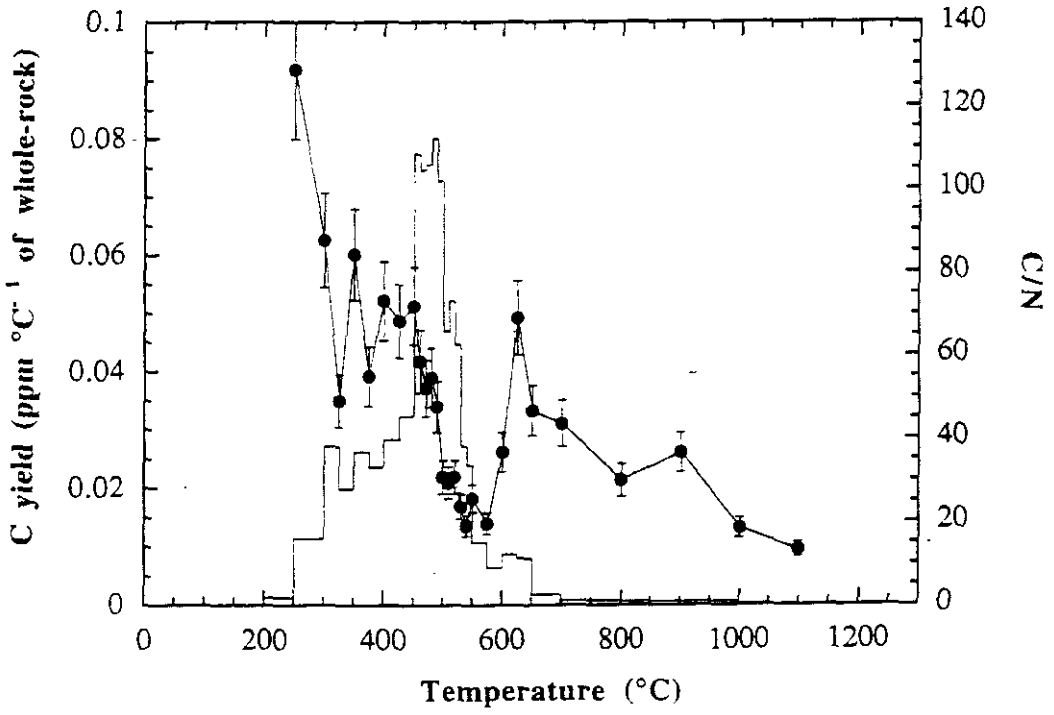

Figure 4.7. *C/N* ratios and carbon yields (ppm $°C^{-1}$ of whole-rock) for the combustion extraction (FIN196) of the HF/HCl residue from A79035.

4.4.2. Chemical treatment with H_2CrO_4 and $HClO_4$

In an identical procedure to the meteorite samples analysed by Russell (1992) and Newton (1994), the HF/HCl residue of lunar breccia A79035 was then treated with chromic (H_2CrO_4) and perchloric ($HClO_4$) acid to remove organics and non-crystalline forms of carbon, *e.g.* amorphous carbon and graphite (section 2.7.1). This was deemed necessary in order to determine whether the isotopically light nitrogen, N_{HT}, in A79035 could be attributed to presolar diamond, similar to that observed in $HClO_4$ residues of carbonaceous chondrites (section 4.1.2.2). As there was not sufficient HF/HCl residue remaining following FIN196 and FIN231, a second HF/HCl residue (99.90% weight loss), which had been prepared for an earlier study was then treated with $HClO_4$, which resulted in a further mass loss of 50%.

The $HClO_4$ residue is analysed by stepped combustion extraction (FIN6) using 10 and 25°C temperature resolution between 350-550°C. Unfortunately no argon or carbon

measurements are obtained and hence the origin of the nitrogen can not be determined using C/N ratios. The nitrogen release and isotopic profile for the analysis of the $HClO_4$ residue is displayed in Figure 4.8 and the data are given in Appendix C4.3. Note the difference in axes scale between this plot and the nitrogen extraction of the HF/HCl residue (Figure 4.6a).

The combustion extraction liberates 79.7 ppm of nitrogen (equivalent to 0.040 ppm of the whole-rock), with a $\Sigma\delta^{15}N$ = +5.7‰. The majority of the nitrogen and the isotopically light nitrogen component, observed in the HF/HCl residue, is not present in the $HClO_4$ residue. A minor release peak is present at a temperature of ~450°C, which coincides with the release temperature observed for presolar diamond by previous workers (Lewis *et al.*, 1983, 1987; Russell *et al.*, 1991, Russell, 1992). However, unlike the carbonaceous chondrite residues, there is clearly no indication of a major nitrogen component, isotopically light or otherwise. The isotopic composition varies throughout the extraction from $\delta^{15}N$ = -3.2‰ to +12.6‰ which is suggestive of the measurement of predominantly system blank, and possibly even some terrestrial organic nitrogen.

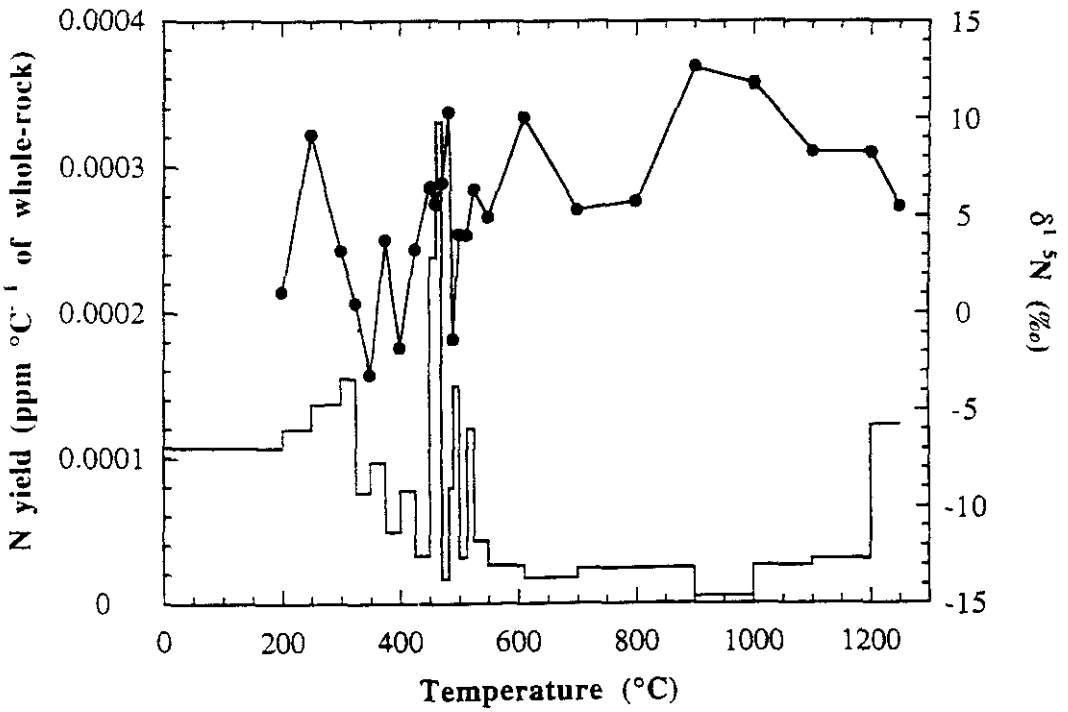

Figure 4.8. Nitrogen yield (ppm $°C^{-1}$ of whole-rock) and isotopic compositions (‰) for the combustion (FIN6) of the $HClO_4$ residue from A79035.

The nitrogen abundance and isotopic compositions obtained from the $HClO_4$ residue indicate that no presolar grains, similar to those found in carbonaceous chondrites, are

present in breccia A79035. In addition, a TEM analysis of the $HClO_4$ and HF/HCl residue, performed by Dr M.M.Lee (University of Essex), did not reveal the presence of a diamond component. However, it remains intriguing that some isotopically light nitrogen remained in the HF/HCl residue after treatment. Two possible conclusions can be drawn from these results. Either there is no presolar component in this particular sample (but maybe in other soils and breccias as it seems unlikely that there is no contribution of meteoritic diamond in the lunar regolith) or the diamond may be present in a modified form such as amorphous carbon. Presolar diamond residing in the lunar regolith, like all other components on the lunar surface is subject to interaction with the solar wind and solar and galactic particle irradiation. Such irradiation of very small diamond, the crystal size of which is less than the range of solar wind atoms, could weaken, or even alter, the crystal structure and hence increase its susceptibility to removal by harsh chemical treatments. An extreme possibility is the formation of amorphous carbon or graphite which combusts at a temperature of ~700-800°C (Grady, 1983). Amorphous carbon would easily be removed by the harsh $HClO_4$ acid treatment, which would possibly explain the removal of the potentially diamond-like component observed in the HF/HCl residue.

4.4.3. Preparative pre-combustion using $KMnO_4$

The above discussion suggests that if amorphous carbon is present in lunar breccia A79035, the $HClO_4$ acid treatment may have been too harsh and hence destroyed the component. An attempt was therefore made to treat the sample using a chemical treatment that was less severe than the $HClO_4$ treatment. The method that was chosen was off-line pre-combustion, using potassium permanganate ($KMnO_4$) as the oxygen provider. This procedure has been described in section 2.8.2. In addition, the technique has been successfully tested on a highland soil, A63340, which is known to contain excessively large amounts of carbon at low temperature (section 5.4).

The HF/HCl residue (weight = 0.44 mg) was pre-combusted off-line using 0.45 mg of $KMnO_4$, at a temperature of 350°C, using the procedure detailed in section 2.8.2. After 17 days of pre-combustion, the sample was transferred to the extraction system and analysed by high resolution stepped combustion (FIN261) using 10°C temperature resolution from

500-600°C and temperature steps of 25°C from 350-500°C and 600-650°C. The data from this extraction are given in Appendix C4.4. Figure 4.9a is a plot of the nitrogen release and isotopic profile and for the extraction and Figure 4.9b displays the carbon release and the C/N ratios. Note that the axes are on a different scale and that none of the abundances or $\delta^{15}N$ values are blank corrected.

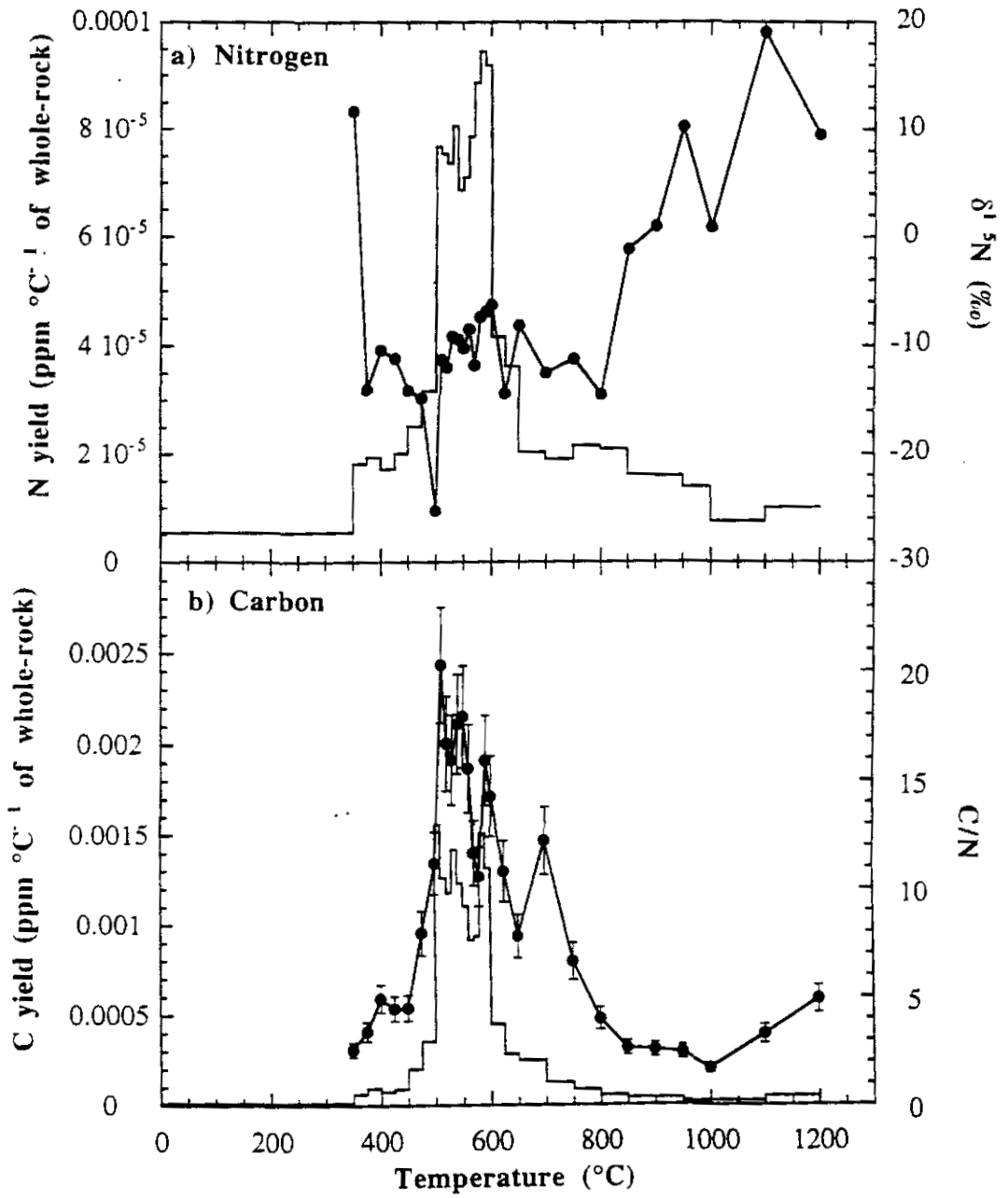

Figure 4.9. Nitrogen yields (ppm $°C^{-1}$ of whole-rock) and isotopic compositions (Figure 4.9a) and carbon yields (ppm $°C^{-1}$ of whole-rock) and C/N ratios (Figure 4.9b) for the $KMnO_4$ pre-combustion of the HF/HCl residue from A79035.

The nitrogen stepped combustion extraction after $KMnO_4$ treatment (Figure 4.9a) liberates a total of 51.8 ppm of nitrogen (0.023 ppm of the whole-rock) with $\Sigma\delta^{15}N$ = -5.7‰. This compares to the total abundance for the untreated HF/HCl residue (FIN196) of 510 ppm (0.23 ppm of the parent), *i.e.* a further 90% of nitrogen has been removed. The measured isotopic compositions reveal no evidence for isotopically light nitrogen across the release with $\delta^{15}N$ values varying from -5‰ and -15‰. Table 4.5 shows the nitrogen and carbon yields at temperatures of ≤350°C and >350°C for the $KMnO_4$ pre-combustion of the HF/HCl residue (FIN261) compared to the "ordinary" HF/HCl residue (FIN196).

The $KMnO_4$ extraction reveals a minor release of carbon between 500-600°C, although the C/N ratio is <20 across this region. This is lower than the minimum ratio of 50 (Newton, 1994), and at the lower end of the range (16 to 94) observed by Lewis *et al.* (1983) for presolar diamond in $HClO_4$ residues from a number of carbonaceous chondrites.

	HF/HCl $KMnO_4$ Comb (FIN261)	HF/HCl Comb (FIN196)
Nitrogen		
≤350°C	4.21	59.43
>350°C	47.63	486.87
Carbon		
≤350°C	10.89	4025.40
>350°C	451.14	21616.60

Table 4.5. Nitrogen and carbon yields (ppm) at temperatures of ≤350°C and >350°C for the $KMnO_4$ pre-combustion (FIN261) and "ordinary" combustion (FIN196) for the HF/HCl residue from A79035.

The data obtained from the $KMnO_4$ pre-combustion of the HF/HCl residue shows that this technique is effective at removing not only the low temperature contamination from the sample, but also the light nitrogen component with $\delta^{15}N \approx -100$‰ which is liberated at temperatures of 500-600°C in the "ordinary" HF/HCl combustion. One explanation is that the $KMnO_4$ treatment, like the $HClO_4$ treatment, is too harsh for the sample and hence also removes the isotopically light nitrogen. However, a more likely explanation is that the light

nitrogen is relatively loosely bound within the breccia and hence easy to remove during harsh chemical treatment, although it does survive the HF/HCl treatment. Alternatively, the light nitrogen may be residing on the surface of the breccia and hence is removed during the pre-combustion procedure.

4.5. Discussion of the isotopically light nitrogen components in lunar breccia A79035.

Lunar breccia, A79035, liberates isotopically light nitrogen with $\delta^{15}N \approx -220‰$, suggestive of a contribution of presolar diamond from early impacts on the lunar surface. In addition, the regolith is also known to contain 1-2% of carbonaceous chondrite debris from the impact and incorporation of meteorites on the Moon (section 1.6.4). When treated with HF/HCl and $HClO_4$, using an identical technique to that employed for the study of presolar grains in carbonaceous chondrites, the light nitrogen component is not observed. However, the release temperature of the nitrogen and carbon for the combustion (500-600°C) and pyrolysis (700-1000°C) for the HF/HCl residue, and the higher C/N ratios than for the whole-rock indicates a carbonaceous carrier for the light nitrogen. Furthermore, TEM analyses of the $HClO_4$ residue reveals no presence of presolar diamond in the sample and the C/N ratios obtained in this work are significantly lower than expected if pristine presolar diamond were to be present. The absence of light nitrogen in the $HClO_4$ residue indicates that there is no pristine presolar grains present, although amorphous carbon may exist (due to radiation damage). This would have been destroyed by the severe chromic and perchloric acid treatment. A potentially less harsh treatment (potassium permanganate) also destroyed the isotopically light nitrogen present in the HF/HCl residue ($\delta^{15}N \approx -100‰$). From the data obtained in this study it may be possible that there is some form of amorphous carbon from carbonaceous chondrite debris in lunar soils and breccias, although this study has been unable to properly constrain the properties of this component.

4.6. Stepped combustion and pyrolysis of A70019, A73221 and A75080

4.6.1. Nitrogen abundances and isotopic composition for A70019, A73221 and A75080

The agglutinate breccia A70019, and soil samples A73221 and A75080 are analysed for nitrogen abundance and isotopic compositions using both stepped combustion and stepped pyrolysis extraction techniques. The samples are heated to 1250°C using primarily 50°C resolution with 25°C steps employed across LTN (600-900°C).

The ΣN (ppm) and $\Sigma\delta^{15}N$ (‰) obtained for the stepped combustion and pyrolysis extractions of A70019, A73221 and A75080 from 350-1250°C are given in Table 4.6 and the data are given in Appendices C1 to C3. Also included in the table is a comparison with the bulk data obtained by previous workers (Chang *et al.*, 1974b; Petrowski *et al.*, 1974; Becker & Clayton, 1975; Becker, 1980a; Norris, 1987 *unpublished data*).

Sample	This work		Published work		
	ΣN (ppm)	$\Sigma\delta^{15}N$ (‰)	ΣN (ppm)	$\Sigma\delta^{15}N$ (‰)	Reference
A70019	73.4	+22.1 (C)	70	+49.0 (P)	(1)
	63.7	+24.1 (P)	70	-8.5 (P/C)	(2)
			62	+21.7 (P)	(3)
			57	+22.1 (P)	(3)
A73221	29.8	+27.0 (C)	41	+56.0 (P)	(1)
	44.9	+25.7 (P)	44	(P/C)	(5)
A75080	35.6	+25.8 (C)	40	+45.0 (P)	(1)
	53.8	+15.7 (P)	47	+28.4 (P)	(4)

Table 4.6. Comparison of ΣN (ppm) and $\Sigma\delta^{15}N$ values (‰) for A70019, A73221 and A75080 in this work with published results.
C = combustion extraction, P = pyrolysis extraction, P/C = pyrolysis to 1200°C followed by combustion at that temperature.
References: (1) Norris (1987, *unpublished data*), (2) Petrowski *et al.* (1974), (3) Becker & Clayton (1975), (4) Becker (1980a), (5) Chang *et al.* (1974b).

Table 4.7 displays the $\delta^{15}N$ value and the corresponding release temperature for the liberation of N_{LT} from each of the extractions in the current study. The nitrogen release and isotopic profile for the pyrolysis extractions of A70019, A73221 and A75080 across the release of N_{LT} are shown in *Figure 4.10 (a to c) respectively. The pyrolysis extractions are* used in preference to the combustion, as they enable comparison with previous studies, *e.g.* Norris (1987, *unpublished data*), and any low temperature contamination had been removed by on-line pre-combustion (section 2.8.1).

Sample	Extraction No.	$\delta^{15}N$ of N_{LT} (‰)	Temperature (°C)
A70019 Comb	(FIN35)	+125.7	500
A70019 Pyr	(FIN143)	+158.5	550
A73221 Comb	(FIN107)	+131.2	550
A73221 Pyr	(FIN146)	+136.3	650
A75080 Comb	(FIN104)	+121.5	500
A75080 Pyr	(FIN150)	+90.3	600

Table 4.7. A comparison of the $\delta^{15}N$ value (‰) and release temperature (°C) of N_{LT} for the stepped combustion and pyrolysis extractions of A70019, A73221 and A75080.

The abundance and isotopic profiles obtained for the agglutinate breccia and two soils show some similarities with lunar soil A12023. Figures 4.10 (a to c) illustrate that nitrogen is liberated across two temperature ranges (600-1000°C and 1000-1200°C), equivalent to LTN and HTN for other lunar soils and breccias in this work. In addition, the soils (including the agglutinitic breccia, A70019) liberate isotopically heavy nitrogen at a temperature of 600-700°C with $\delta^{15}N$ values ranging from +90.3 to +158.5‰, corresponding to N_{LT} observed for the pyrolysis of A12023 with $\delta^{15}N$ = +151.7‰ (section 3.3.1.2). A comparison of the major element chemistry of A12023 (Table 3.1) and A73221 and A75080 (Table 4.2) shows that, in general, A12023 lies between the measured values for the Apollo 17 samples. Soil A12023 is a mature soil with $I_s/FeO = 60$, compared to sub-mature soils A73221 and A75080 with maturity indices of 43 and 40 respectively. This difference would account for the higher yields observed for A12023 in this work (~120 ppm) and by other workers (Table 3.2), compared to the Apollo 17 soils (Table 4.6).

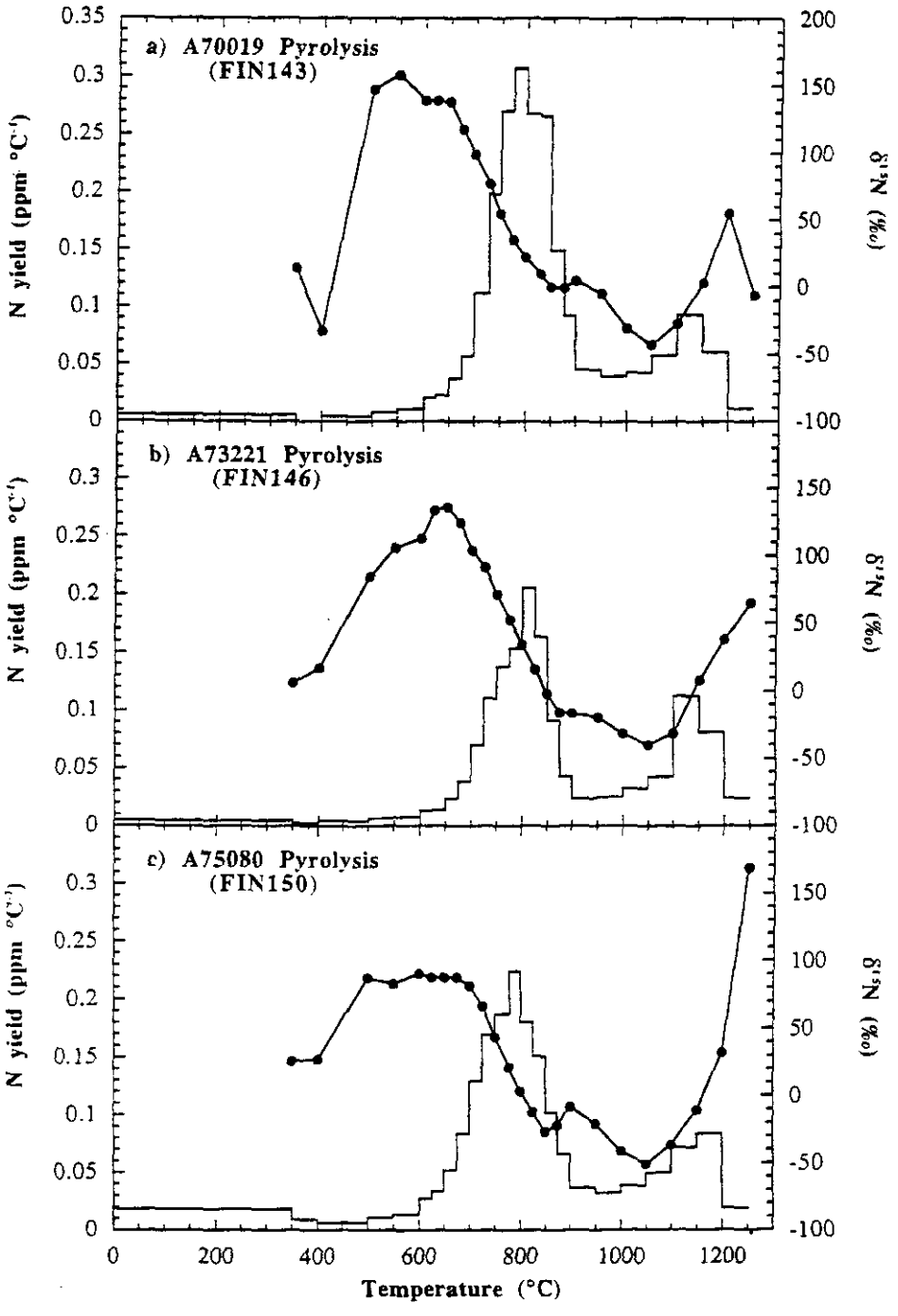

Figure 4.10. Nitrogen yields (ppm $°C^{-1}$) and isotopic compositions (‰) for the stepped pyrolysis extraction of A70019 (Figure 4.10a), A73221 (Figure 4.10b) and A75080 (Figure 4.10c).

The agglutinate breccia, A70019, also displays the isotopic characteristics of a lunar soil, as opposed to the light nitrogen signatures typically associated with lunar breccias, *i.e.* A79035 (section 4.3.1). The breccia is described as a glass-welded soil and hence it has been suggested that it may have undergone loss or fractionation of a significant amount of its

nitrogen during breccia formation (Norris, 1987 *unpublished data*). However, no known process can cause a fractionation of the required magnitude (~350‰). Furthermore, it has been proposed (Becker and Clayton, 1975) that due to the heterogeneity of the sample, it may be possible for two different laboratories to analyse fractions which contain significantly different nitrogen isotopic compositions.

Agglutinate breccia A70019 (Figure 4.10a) yields 73.4 ppm of nitrogen with a $\Sigma\delta^{15}N$ = +22.1‰ for the combustion (FIN35) and 63.7 ppm with $\Sigma\delta^{15}N$ = +24.1‰ for the pyrolysis (FIN143). Both extractions liberate N_{LT} with $\delta^{15}N$ = +125.7‰ at 500°C for FIN35 and $\delta^{15}N$ = +158.5‰ at 550°C for FIN143 (Table 4.7), although the latter is subject to significant blank corrections as the nitrogen liberated from the sample is only 1.7 times the initial blank. A more realistic $\delta^{15}N$ value for this component is +139‰ for the 600-625°C step where the yield is greater than twice the blank. Note that the isotopic composition of N_{LT} for A70019 is similar to that obtained for A12023 with $\delta^{15}N \approx +150‰$ (section 3.3.1.2). The ΣN for A70019 in this study compares well with the values obtained by previous workers (Table 4.6). The $\Sigma\delta^{15}N$ values are markedly different from those obtained by Petrowski *et al.* (1974) and Norris (1987, *unpublished data*), although they compare favourably with data obtained by Becker & Clayton (1975). The $\Sigma\delta^{15}N$ of +49.0‰ of Norris (1987, *unpublished data*) can be accounted for by the difference in the isotopic minimum ($\delta^{15}N$ = +2‰ at 1100°C in the earlier study, compared to -42.4‰ at 1050°C for FIN143). The light $\Sigma\delta^{15}N$ value of -8.5‰ obtained by Petrowski *et al.* (1974) has suggested that their sample fraction contains less heavy nitrogen than other workers. Assuming the reliability of the various sets of data in Table 4.6, it appears that isotopically heavy nitrogen is more abundant in some fractions of the sample than in others; an hypothesis which reinforces the argument for sample heterogeneity (Becker & Clayton, 1975).

Soil A73221 (Figure 4.10b) yields 29.8 ppm of nitrogen for the combustion (FIN107) and 44.9 ppm for the pyrolysis (FIN146) with $\Sigma\delta^{15}N$ values of +27.0‰ and +25.7‰ respectively (Table 4.6). The isotopic heavy component, N_{LT}, was liberated at a temperature of 550°C with $\delta^{15}N$ = +131.2‰ for the combustion and at 650°C with $\delta^{15}N$ = +136.3‰ for the pyrolysis (Table 4.7). The yields obtained in this study compare well with

previous work (Table 4.6), although the $\Sigma\delta^{15}N$ of +56.0‰ from Norris is higher than in this work, due to the liberation of heavy nitrogen in the earlier study with $\delta^{15}N$ = +170.0‰.

Lunar sample, A75080 (Figure 4.10c) liberates 35.6 ppm of nitrogen by stepped combustion (FIN104) and 53.8 ppm by stepped pyrolysis (FIN150) with $\Sigma\delta^{15}N$ values of +25.8‰ and +15.7‰ respectively. The N_{LT} component is liberated at a temperature of 500°C with $\delta^{15}N$ = +121.5‰ for the combustion and at a temperature of 600°C with $\delta^{15}N$ = +90.3‰ for the pyrolysis. This was believed to be lighter than for the other samples due to the *incomplete* removal of terrestrial contamination. The yield data compares reasonably well with that obtained by other workers (Table 3.6) but, as with A70019 and A73221, the $\Sigma\delta^{15}N$ value of +45.0‰ obtained by Norris (1987 *unpublished data*) is higher than that obtained in this work. This was due to the observation of an extremely heavy N_{LT} component in the earlier work with $\delta^{15}N$ = +156.0‰.

The stepped pyrolysis extractions of A70019, A73321 and A75080 in this study liberate $\Sigma\delta^{15}N$ with systematically lower values than data previously obtained (Table 4.6). In the case of the agglutinate breccia, A70019, this can be attributed to sample heterogeneity, although a similar explanation cannot be invoked for A73321 and A75080. The difference is due to the observation of higher $\delta^{15}N$ values N_{LT} in the earlier work (Norris, *1987 unpublished data*), which may be a feature of inaccurate blank measurement. The earlier work measured the system blank at room temperature, compared to 1200°C in the current study, and hence the nitrogen yield and isotopic compositions may be systematically in error. The $\delta^{15}N$ values obtained for N_{LT} in this study (Table 4.7) are blank corrected using an equivalent method to that used for all the samples presented in this thesis, and it is not believed that the blank measurement has been underestimated.

4.6.2. Argon analyses of A70019, A73221 and A75080

No noble gas data could be located in the literature for agglutinate breccia A70019 and soil A73221. However, noble gas data are available for the <1 mm fraction (A75081) of soil A75080. Previous work (Hintenberger *et al.*, 1974) has revealed a $^{40}Ar/^{36}Ar$ ratio of 0.82 and $^{36}Ar/^{38}Ar$ ratio of 5.30, with a ^{21}Ne-exposure age of 230 Myr. Similar data ($^{40}Ar/^{36}Ar$ = 0.79 and $^{36}Ar/^{38}Ar$ = 5.38) have been obtained by Bogard *et al.* (1974) for the

same soil. Therefore, the argon data from A75080 is displayed in this study, although it should be noted that equivalent trends are also observed for A70019 and A73221. Figure 4.11a and 4.11b illustrates the $N/^{36}Ar$ (plot (i)), $^{40}Ar/^{36}Ar$ and $^{36}Ar/^{38}Ar$ (plot (ii)), and the nitrogen and ^{36}Ar yields (plot (iii)) for the stepped combustion (Figure 4.11a) and pyrolysis (Figure 4.11b) respectively of A75080. Note that to enable comparison of the argon trends with other lunar soils and breccias in this work, the data from 350-1250°C is displayed. The $N/^{36}Ar$, $^{40}Ar/^{36}Ar$ and $^{36}Ar/^{38}Ar$ data for A75080 are given in Appendix C3 (the equivalent data for A70019 and A73221 are given in Appendices C1 and C2 respectively).

The $^{36}Ar/^{38}Ar$ ratio decreases throughout the extractions from 6.2 to 5.6 for the combustion (Figure 4.11a (ii)) and 6.6 to 6.3 for the pyrolysis (Figure 4.11b (ii)), consistent with previous argon data obtained in this study (section 3.3.2 and section 4.3.2). This trend has been interpreted by previous workers, *e.g.* Wieler *et al.* (1986), as due to the implantation of solar wind and solar energetic particles, with $^{36}Ar/^{38}Ar$ ratios decreasing from ~5.5 to 4.9 (section 1.7.5.2).

The $^{40}Ar/^{36}Ar$ ratios for the stepped combustion and pyrolysis of A75080 (Figure 4.11a (ii)) and 4.11b (ii) respectively) are essentially constant across the release of LTN and HTN, although there is slightly more variation during the pyrolysis extraction. The high $^{40}Ar/^{36}Ar$ in the initial few steps are due to the liberation of re-implanted atmospheric ^{40}Ar (section 1.6.1.3). The mean $^{40}Ar/^{36}Ar$ ratios for the combustion and pyrolysis extractions are 1.14 and 1.80 respectively. The constant nature of the $^{40}Ar/^{36}Ar$ ratios detract from a recent solar wind origin for N_{LT}, as this depends upon the grain surface location of the nitrogen. Clearly, the siting of ^{40}Ar implies that not all of the surface-correlated gases in the lunar regolith can be attributed to solar wind implantation. However, it may be that the ^{40}Ar and ^{36}Ar both reside in an equivalent layer, *i.e.* radiation damaged layer, but are of a different origin.

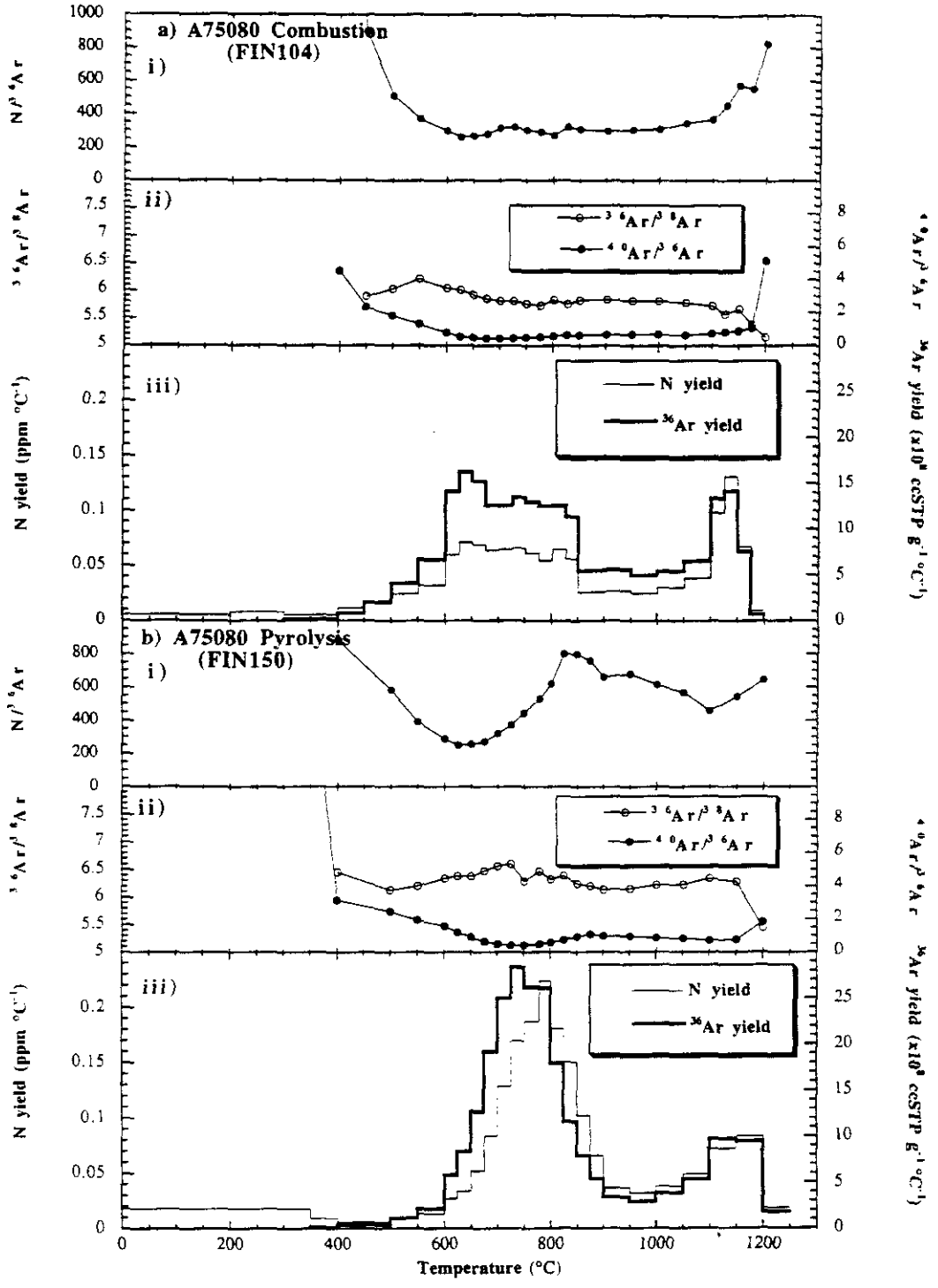

Figure 4.11. Conjoint nitrogen and ^{36}Ar data, and argon isotopic ratios against temperature for the stepped combustion (Figures 4.11a) and stepped pyrolysis (Figures 4.11b) of A75080. The plots are as follows: (i) $N/^{36}Ar$, (ii) $^{36}Ar/^{38}Ar$ (left ordinate) and $^{40}Ar/^{36}Ar$ (right ordinate), (iii) N yield in units of ppm $°C^{-1}$ (left ordinate) and ^{36}Ar in units of ccSTP g^{-1} $°C^{-1}$ (right ordinate).

During the combustion extraction, the nitrogen and ^{36}Ar are liberated conjointly (Figure 4.11a (iii)), hence the $N/^{36}Ar$ ratio (Figure 4.11a (i)) remains constant with a mean value of 339 from 600-1200°C. The constant $N/^{36}Ar$ values suggest that the nitrogen, like

the ^{36}Ar, is of solar wind origin, although the surface location of non-solar ^{40}Ar (and constant $^{40}Ar/^{36}Ar$ ratios) argues against a solar origin for nitrogen solely on the basis of its surficial location. Furthermore, the $N/^{36}Ar$ ratios are a factor of ~10 higher than the solar values of ~37 (Cameron, 1982; Anders and Grevesse, 1989). In contrast, during pyrolysis the $N/^{36}Ar$ ratio (Figure 4.11b (i)) displays greater variation with ratios decreasing to a minimum value of 248 at 625°C, before increasing to 803 at 825°C. Similar results have been obtained for other lunar soils and breccias in this work, *e.g.* A12023 and A79035 (section 3.3.2 and 4.3.2 respectively). The variation in the $N/^{36}Ar$ ratios during pyrolysis are attributed to the differences in the release temperatures (~50°C) of the nitrogen and ^{36}Ar (Figure 4.11b (iii)). During stepped pyrolysis, the nitrogen and argon are released solely by diffusion and hence the nitrogen is preferentially retained in comparison with the argon. This suggests that a proportion of the nitrogen is chemically bound within the sample; a hypothesis which is investigated in section 5.3.2.

4.6.3. Carbon abundances and C/N ratios in lunar soil A75080

Figure 4.12 displays the carbon release profile and C/N ratios for the stepped combustion (FIN104) of soil A75080. The combustion data are used in preference to the pyrolysis data (section 3.3.3). The carbon yields and C/N ratios for both the combustion and pyrolysis extractions of A70019, A73221 and A75080 are given in Appendices C1 to C3 inclusive.

The stepped combustion extraction of A75080 yields 68.4 ppm of carbon as three release peaks: 200-625°C, 650-850°C and >1000°C. The former is attributed to low temperature contamination which is present in the soil as no pre-combustion steps are performed for combustion extractions. The mid-temperature and high temperature releases are equivalent to LTN and HTN as observed during nitrogen extraction. Note that A73221 (FIN107) liberates a similar abundance of carbon (65.1 ppm), although the carbon yield for A70019 is higher (251.6 ppm) due to a higher content of low temperature contamination. The C/N ratio for A75080 displays a mean value of 3.3, although across the release of LTN and HTN (625-1175°C) the ratio remains constant with a mean value of 1.04. This is

consistent with previous analyses of lunar soils and breccias (section 1.7.6.2) and solar photospheric ratios of 1.1 (Anders and Grevesse, 1989).

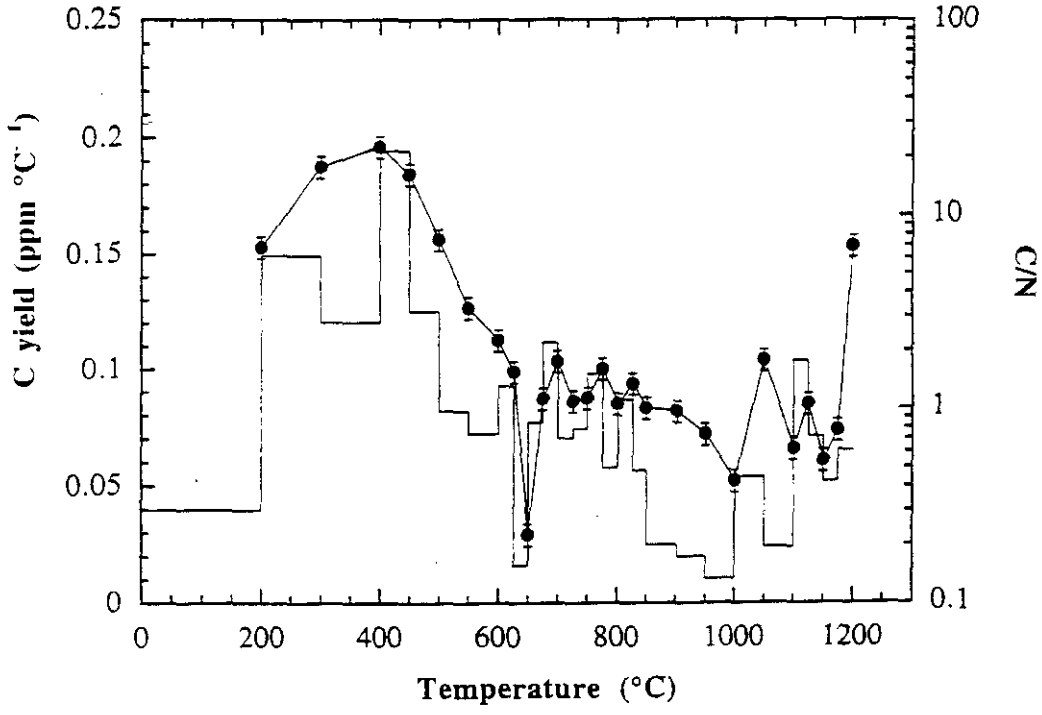

Figure 4.12. C/N ratios and carbon yields (ppm $°C^{-1}$) against extraction temperature (°C) for the stepped combustion extraction (FIN104) of A75080.

4.6.4. Nitrogen abundances and isotopic composition for the high resolution combustion of N_{LT} in A70019

The nitrogen, argon and carbon extractions of A70019, A73221 and A75080 (sections 4.6.1 to 4.6.3 inclusive) reveal similar abundance and isotopic profiles to those obtained by previous workers (Chang *et al.*, 1974b; Hintenberger *et al.*, 1974; Petrowski *et al.*, 1974; Becker & Clayton, 1975; Norris, 1987 *unpublished data*). The isotopic composition of N_{LT} for the three samples in this work (section 4.6.1) are lighter than the equivalent component in the analyses of Norris (1987, *unpublished data*), if the more realistic $\delta^{15}N$ value of +139‰ for A70019 is used (section 4.6.1). In order to ascertain accurately the isotopic composition of N_{LT} observed in lunar soils, it was decided to analyse one of the above samples using high resolution stepped combustion extraction. The sample chosen for this experiment was A70019, due to the similarity of the isotopic composition of N_{LT} from this and previous work. Furthermore, there was sufficient sample remaining to

warrant a high resolution study and was imperative that the nitrogen yields at low temperatures had to be several times in excess of the blank to obtain accurate isotopic compositions. Hence for this experiment 9.3 mg of sample was required compared to typical sample weights of 0.5-1.0 mg. In order to ensure the safe passage of all the sample into the combustion tube, two platinum buckets were used, both of which were prepared using the standard procedure (section 2.6.3).

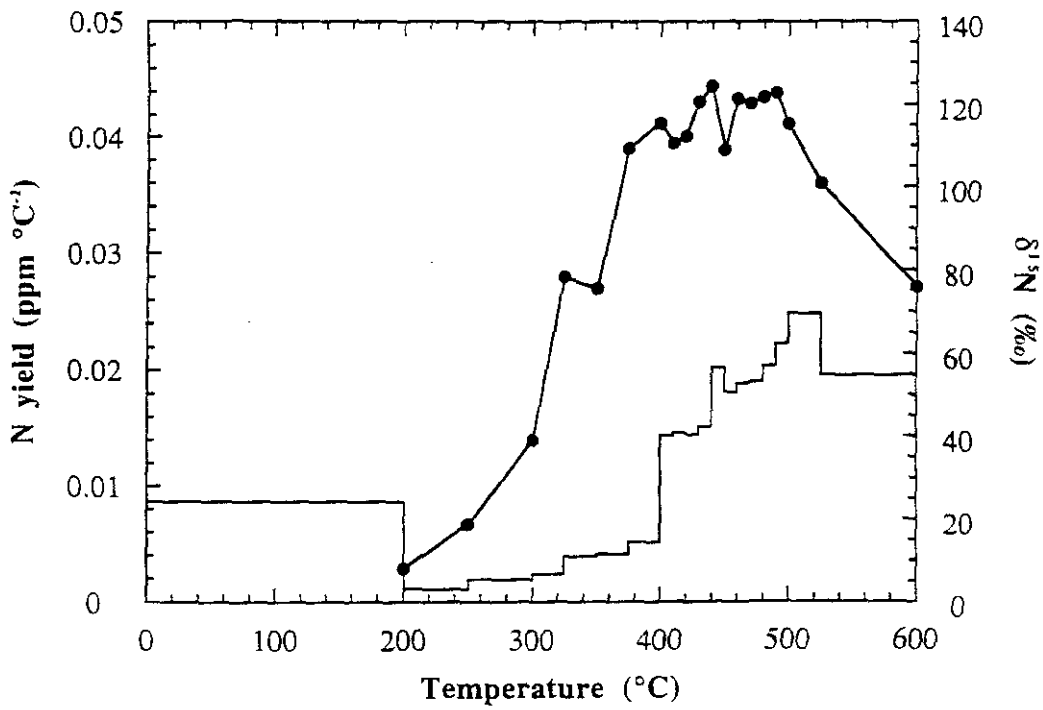

Figure 4.13. Nitrogen yields (ppm $°C^{-1}$) and isotopic compositions (‰) for the high resolution stepped combustion extraction of A70019 (FIN247) to a temperature of 600°C.

The sample is analysed by stepped combustion extraction (FIN247) to a temperature of 600°C, using 25°C temperature resolution from 300-525°C with 10°C steps from 400-500°C. The nitrogen release and isotopic profile for FIN247 up to 600°C is illustrated in Figure 4.13 and the nitrogen, carbon and argon data are given in Appendix C1. Note that the $^{36}Ar/^{38}Ar$, $^{40}Ar/^{36}Ar$, $N/^{36}Ar$ and C/N ratios are equivalent to the low-resolution combustion (FIN35) and are not discussed here.

The agglutinate breccia yields 6.14 ppm of nitrogen which is comparable with the 9.12 ppm obtained for the same temperature range from the earlier combustion (FIN35). The slightly lower nitrogen yields for FIN247, compared to FIN35, is believed to be due to sample heterogeneity. The nitrogen liberated from the breccia (up to a temperature of 600°C)

displayed a $\Sigma\delta^{15}N$ = +71.7‰, which compares well with +76.9‰ for the equivalent temperature range for FIN35.

Figure 4.12 illustrates that N_{LT} displays a uniform $\delta^{15}N$ value from 375-500°C with a weighted average value of +117.8‰. Some isotopically heavy nitrogen continues to be released above 500°C but it is believed that this is masked by the start of the release of N_{MT}. The isotopically heaviest nitrogen is released at a temperature of 440°C with $\delta^{15}N$ = +124.4‰, similar to +125.7‰ obtained from FIN35 at a temperature of 500°C. The temperature discrepancy (~60°C) is due to the possibility that the two buckets were at slightly different heights in the combustion tube, although efforts were made to avoid this problem.

4.7. Discussion of the isotopically heavy nitrogen component in agglutinate breccia A70019 and soils A73221 and A75080

The study of A70019, A73321 and A75080 in this work has indicated that the isotopic compositions of N_{LT}, are consistently lighter than those obtained by previous work (Norris, 1987 *unpublished data*) and this appears to be due to inappropriate blank corrections in the earlier study. The $\delta^{15}N$ of N_{LT} in this work (section 4.6.1) lie in the range +90.3‰ to +158.5‰, although the former is due to the contribution of terrestrial contamination and the latter due to the low nitrogen yields relative to the initial blank measurement. The mean $\delta^{15}N$ of N_{LT} in this study has a $\delta^{15}N$ value of +127.3‰ and is consistent with the data from other soils in this work, *i.e.* A12023 (section 3.3.1.2). The data obtained for A70019 is not consistent with its identification as an agglutinate breccia, but is more reflective of a lunar soil, probably held together by an atypically large splash of glass from some adjacent impact. The discrepancy in $\Sigma\delta^{15}N$ between this work and previous studies, *e.g.* Norris (1987, *unpublished data*) and Petrowski *et al.* (1974) may be a feature of sample heterogeneity.

The constant $N/^{36}Ar$ ratios obtained during stepped combustion of these samples suggest that N_{LT} is of a solar wind origin, which is consistent with the suggestions by previous workers of recent solar wind implantation with $\delta^{15}N$ values of ~110‰ (section 1.7.4.1). However, recent studies (Kim *et al.*, 1995) have indicated that the present day solar wind has a $\delta^{15}N$ value of +38 ± 6‰ (section 1.7.4.3). These workers suggest that the

whereby species implanted at different depths are diffused inwards (or outwards) to the same site. The "absence" of N_{LT} in breccia A79035 appears to be due to the loss of surface-correlated nitrogen during the impact which sealed the breccia, although whether the nitrogen originated solely from the solar wind is not conclusive. The preferential retention of nitrogen (LTN), when compared to ^{36}Ar during pyrolysis extraction of both lunar soils and breccias, suggests that LTN (or a proportion of LTN) may be in chemically bound form. This may also account for the shift to lower temperatures of the release of N_{LT}, and to a lesser extent N_{MT} in lunar soil A12023 (section 3.3.1.2).

The study of the isotopically light nitrogen in A79035 with $\delta^{15}N$ = -220‰ is consistent with the results obtained by other workers. This study (section 3.4.1 and 3.5) had indicated that the light nitrogen is not attributed to the ancient solar wind located within complex secondary particles, such as coarse-grained agglutinates, as this would be expected to be liberated at temperatures of >1050°C. The analyses by previous workers of mineral separates from A79035 (Table 4.3) also suggested that ilmenite, agglutinates and pyroxene were not the carriers of the isotopically light nitrogen and hence a presolar origin was considered. This study revealed no presence of isotopically light nitrogen in A79035, with $\delta^{15}N$ = -348‰ (Russell, 1992) or C/N > 50 (Newton, 1994) characteristic of presolar diamond in carbonaceous chondrites. In addition, a TEM analysis could not identify any such component. The acid residue analyses have indicated that the chemical treatment of the breccia removes all traces of the isotopically light nitrogen, together with terrestrial contamination. This has suggested that any presolar component is not resilient, but is loosely bound to enable removal by the treatment, and hence may be present in the form of amorphous carbon. The $^{36}Ar/^{38}Ar$ ratios for A79035 have suggested that the isotopically light nitrogen may be of a solar wind origin. It may be possible that this component represents solar wind or SEP radiation admixed with a minor component of presolar diamond, which was destroyed during the breccia formation event. Alternatively, the observation of excessively light nitrogen with $\delta^{15}N$ = -186‰ for the joint combustion/pyrolysis extractions of the <10 μm fraction of A12023 (section 3.4.2.2), has suggested that this component may be common to both breccias and soils and hence the amorphous carbon may be simply due to regolith gardening processes.

The data obtained from the study of lunar soils and breccias in this work has detracted from a secular variation of $^{15}N/^{14}N$ in the solar corona over the lifetime of the regolith. If the current estimates of the $\delta^{15}N$ values for the present day solar wind are correct (Kim *et al.*, 1995), the significantly higher isotopic compositions for N_{LT} in this study (section 3.3.1.2 and 4.6.1) may suggest either the fractionation of the component or the presence of a proportion of isotopically heavy, non-solar nitrogen. In addition, the observation of isotopically light nitrogen in A12023 with $\delta^{15}N$ values similar to that observed in lunar breccias, suggest that a proportion (possibly ~3%) of the light nitrogen may be attributed to amorphous carbon. Hence, if the remainder of the nitrogen is of solar origin, the difference in isotopic composition for the solar components may not be as large as previously estimated, and may be similar to that exhibited for some noble gases, *i.e.* $^{20}Ne/^{22}Ne$. The higher release temperature for the isotopically light nitrogen may be due to the greater energy with which this component was implanted. Hence, it is likely that the isotopically heavy nitrogen is attributed to solar wind implantation, whereas the isotopically light nitrogen is due to the implantation of higher energy particles, possibly with energies intermediate to solar wind and solar energetic particles. This is consistent with a recent study by Kerridge *et al.* (1992b).

Chapter 5

Nitrogen isotope studies of the <10 μm grain size fraction of Apollo 16 soils

5.1. Introduction

In this chapter, I investigate the nitrogen abundance and isotopic compositions of five highland soils from the Apollo 16 site, using stepped combustion and stepped pyrolysis extraction techniques. The objective of this study is to determine whether the release characteristics of the highland soils are significantly different from those of mare origin, *e.g.* A12023 (Chapter 3) or A70019, A73221 and A75080 (Chapter 4), and to investigate any correlation between the nitrogen inventory of the soils and their exposure history. These differences may result from the contrast in chemistry, mineralogy and geological history between the three sites.

The lunar highlands are heavily cratered and enriched in Ca and Al with plagioclase feldspar as the dominant mineral (LSPET, 1972). They are believed to have formed during the period of differential melting 4.45 Gyr ago and have been modified by intense meteorite bombardment prior to 3.9 Gyr ago (section 1.5.2). In contrast, the lunar maria have formed from basaltic lavas during the period of volcanic activity up to 1 Gyr after the cessation of intense bombardment. This has resulted in the covering of many of the early craters (section 1.5.3). The maria are lightly cratered and are enriched in Fe and Ti, with pyroxene as the dominant mineral (Table 1.3).

For this study, the <10 μm grain size fractions of five Apollo 16 soils (A60501, A63340, A64421, A67701 and A68501) are analysed. These grain size separates had been prepared for a previous study (Cadogan *et al.*, 1973) using the procedure detailed in section 2.7.2.1. For comparison throughout this investigation, the data obtained are compared to the combustion (FIN62) and pyrolysis (FIN73) extraction of the <10 μm fraction of A12023 (section 3.4.2.1) which is illustrated in Figure 3.10a and 3.10b respectively. A further objective of this study is to determine whether the two extraction methods reveal a similar

difference in isotopic profiles to that observed for A12023 and the Apollo 17 soils, or whether the observed contrast is site dependent.

The analyses of a suite of grain size fractions from A12023 (section 3.4.1), have shown that the proportion of the total nitrogen released as HTN increases with grain size, and constitutes <10% of the total for the <10 μm fraction. The study concluded that HTN is attributed to the release from complex particles at temperatures >1050°C, admixed with a minor contribution of spallogenic nitrogen (Brilliant *et al.*, 1994). The former would be essentially missing in the finest size fraction as the trapped interior surfaces can only exist in larger grains. Hence, analysis of the <10 μm grain size fraction provides the best opportunity to study the surface-correlated component of a lunar soil, with minimum contribution from gases trapped in its interior.

The Apollo 16 soil samples have been studied by many workers for light element compositions (Cadogan *et al.*, 1973; DesMarais *et al.*, 1973; Epstein and Taylor, 1973, 1975; Kothari and Goel, 1973; Moore *et al.*, 1973; Müller, 1973; Wszolek *et al.*, 1973; Becker and Clayton, 1975, 1977; Kerridge *et al.*, 1975b, 1977; Becker, 1980a; Brown and Pillinger, 1981; Frick *et al.*, 1988; Kim *et al.*, 1995a, b), noble gas contents (Bogard and Nyquist, 1973; Signer *et al.*, 1977; Frick *et al.*, 1988; Becker and Pepin, 1994; Wieler and Baur, 1995) and maturity parameters, *e.g.* agglutinate content and I_s/FeO (Bogard and Nyquist, 1973; Hintenberger and Weber, 1973; Kirsten *et al.*, 1973; Walton *et al.*, 1973; Charette and Adams, 1975; Kerridge *et al.*, 1975b; Eberhardt *et al.*, 1976; Morris, 1976). The origin of the nitrogen in the lunar regolith is an issue which is currently unresolved by the aforementioned workers and the various models (and associated problems) which have been invoked are discussed in sections 1.7.4.1 to 1.7.4.3 inclusive. The major problem encountered by these workers is to account for the "excess" of nitrogen, *i.e.* $N/^{36}Ar$ a factor of 10 higher than solar values (section 1.7.2.2), which implies either the loss of solar noble gases from the regolith, or a non-solar origin for the nitrogen.

In addition, a small but significant component of finely divided metallic iron (0.5-0.9 wt.%) has been identified in the lunar regolith (Runcorn *et al.*, 1970; Greenwood and Howe, 1970). This originates from the reduction of indigenous ferrous iron (Fe^{2+}) to superparamagnetic metal particles (Fe^0) by reactions with solar wind implanted hydrogen in the lunar regolith, and provides a reliable measure of surface exposure history (section

1.5.4.2). This parameter, together with other maturity indices, *e.g.* agglutinate content and ^{36}Ar, measures of antiquity, *e.g.* ^{21}Ne-exposure age, have provided the basis for current interpretations.

The geology of the Apollo 16 landing site, together with a description of the chemistry, mineralogy and exposure histories of the samples analysed for this investigation are given in section 5.2. The nitrogen yield and isotopic data obtained from the stepped combustion and pyrolysis extractions of these soils are discussed in section 5.3.1. Section 5.3.2 details an investigation into the relationship between nitrogen abundances and isotopic composition with the exposure histories of the soils. The argon and carbon data from the Apollo 16 soils are given in sections 5.3.3 and 5.3.4 respectively. Section 5.4 details a $KMnO_4$ pre-combustion extraction on highland soil A63340, which was performed to remove the low temperature (<350°C) contamination from the sample. This procedure has been detailed in section 2.8.2 and employed for breccia A79035 (section 4.4.3). A discussion of the results from the study of Apollo 16 soils are given in section 5.5 and the conclusions are given in section 5.6.

5.2. The Apollo 16 site

5.2.1. Geology of the Apollo 16 site

The Apollo 16 landing site is located near the Descartes Mountains in the Cayley Plains region of the central lunar highlands (9°S, 15.5°E). The primary objective of the mission was to sample material from these locations, which were believed to be volcanic in origin, and also from the surrounding areas, *e.g.* North and South Ray craters. The latter are recent impact craters with formation ages of 50 Myr and 2 Myr respectively (Behrmann *et al.*, 1973; Marti *et al.*, 1973). In addition, the location of the landing site also enabled sampling at distance from the nearest mare site. During the mission, three EVA's were made using the Lunar Roving Vehicle which resulted in the collection of a total of ~96 kg of lunar soils, rocks and core samples.

The samples returned by the Apollo 16 mission suggested that neither the Cayley Plains or the Descartes region of the lunar highlands are volcanic in origin. The returned

samples consist of polymict breccias, impact melts and some pristine anorthositic rocks which indicated that the samples are impact processed (LSPET, 1972). The majority of samples are highly shattered bedrock, *i.e.* cataclastic anorthosite. Age dating of some of the lunar samples (Schaeffer and Husain, 1973; Tera *et al.*, 1974; Schaeffer *et al.*, 1976; James, 1981) has suggested that this region may consist of impact ejecta deposits from the Early Imbrium, Orientale and Nectaris Basins which formed between 3.8 to 3.9 Gyr (James, 1981; Wetherill, 1981; Spudis, 1984), although the precise formation age of the Imbrium basin is not known. The Apollo 16 site is quite uniform with only minor differences in chemistry between the soils collected from Smoky Mountain in the north and Stone Mountain in the south. The chemical compositions of soils collected from the Cayley Plains lie between the two extremes (McKay *et al.*, 1991). A detailed review of the geology of the Apollo 16 landing site and the current theories surrounding its origin is given by Spudis (1984).

5.2.2. The Apollo 16 soil samples

The five soil samples analysed in this study are A60501, A63340, A64421, A67701 and A68501. These samples are chosen for a comparison of different stations at the landing site as they are known to exhibit a range of light element compositions (Kerridge *et al.*, 1975b). Note that the soils, with the exception of A63340, are separated from the <1 mm fraction of the bulk sample at the Lunar Curatorial Facility, Houston, Texas, USA. Soil A63340 was separated from a reserve sample with a grain size of <1 cm. The major element chemistry and petrology of the samples are given in Table 5.1 and include maturity parameters such as I_s/FeO and ^{21}Ne-exposure age. The chemistry for A12023 is also included to aid comparison between the soils from each site. The location of the collection sites for the samples is shown in Figure 5.1.

Major elements	% in A60501[1]	% in A63340[3]	% in A64421[5]	% in A67701[7]	% in A68501[8]	% in A12023[9]
SiO_2	45.63	≈45.70*	44.88	44.77	45.18	≈46.00
Al_2O_3	27.14	29.00	27.60	28.48	26.65	13.90
CaO	15.44	12.45	15.81	16.87	15.35	10.90
FeO	5.44	4.53	5.03	4.17	5.48	15.40
MgO	5.52	7.30	5.35	4.92	6.28	11.20
TiO_2	0.59	0.60	0.55	0.44	0.58	2.80
Petrology	% in A60501[2]	% in A63340[4]	% in A64421[6]	% in A67701[4]	% in A68501[4]	
Agglutinates	32.00	40.00	52.60	15.60	38.60	
Breccia		35.50		50.60	38.50	
Feldspar		12.60	13.60	21.00	12.30	
Anorthosite		5.90		3.30	1.90	
Pyroxenes		1.70	1.10	4.00	1.60	
Glasses		2.00	10.60	3.20	4.90	
I_s/FeO[10]	80	54	83	39	85	
^{21}Ne age(Myr)[11-15]	168	63	190	49	105	

Table 5.1. Major element chemistry and mineralogy of A60501, A63340, A64421, A67701 and A68501 compared to A12023.
* = amount of SiO_2 is unmeasured but has been approximated by mass balance calculations.
References: (1) Duncan *et al.* (1973), (2) Kerridge *et al.* (1975b), (3) Brunfelt *et al.* (1973), (4) Heiken *et al.* (1973), (5) LSPET (1972), (6) Butler *et al.* (1973), (7) Compston *et al.* (1973), (8) Bansal *et al.* (1973), (9) Woodcock and Pillinger (1978), (10) Morris (1976), (11) Bogard and Nyquist (1973), (12) Eberhardt *et al.* (1976), (13) Hintenberger and Weber (1973), (14) Kirsten *et al.* (1973), (15) Walton *et al.* (1973).

Lunar soil, A60501, is the <1 mm fraction of a mature soil (I_s/FeO = 80.0) collected from the surface of the regolith at station 10, approximately 100 m southwest of the lunar module. Soil A63340 was collected as a "shadow" soil from underneath the overhang of a 5 x 4 m breccia boulder at Station 13 (North Ray Crater). Lunar soil A64421 is the <1 mm fraction of a brownish-grey soil collected from station 4 near Cinco B crater close to Stone Mountain and South Ray crater. The sample was located on the base of a 15 m crater at the bottom of a 15 cm deep trench. Soil A67701 is a medium light grey soil (<1 mm fraction) collected from station 11 along the southwestern rim of North Ray crater. There is some doubt as to whether this sample is a typical soil as it was collected as a rake sample, from the top of a friable white rock. The lunar sampling rake was initially devised to collect regolith samples of >1 cm diameter whilst leaving samples of a smaller diameter. However, it was

decided during the mission that several scoops of local regolith were to be included with the sample. The analysis of the <10 μm fraction should limit any heterogeneity this sampling method may have created. The "soil" has been classified as sub-mature with I_s/FeO = 39 and an agglutinate content of only 15.6%. The soil consists of a significant proportion of breccia fragments (~50%), 21% feldspar and 4% pyroxenes (Heiken *et al.*, 1973). The major element chemistry is similar to the other soils analysed in this work but A67701 contains lower amounts of FeO, MgO and TiO_2 (Compston *et al.*, 1973). Soil A68501 was collected in conjunction with a rake sample at station 8 near Stone Mountain and South Ray crater (approximately 3 km south-southwest of the landing site) and has been classified as a mature soil (I_s/FeO = 85.0), medium light grey in colour. The station was located midway between two 15 m diameter craters.

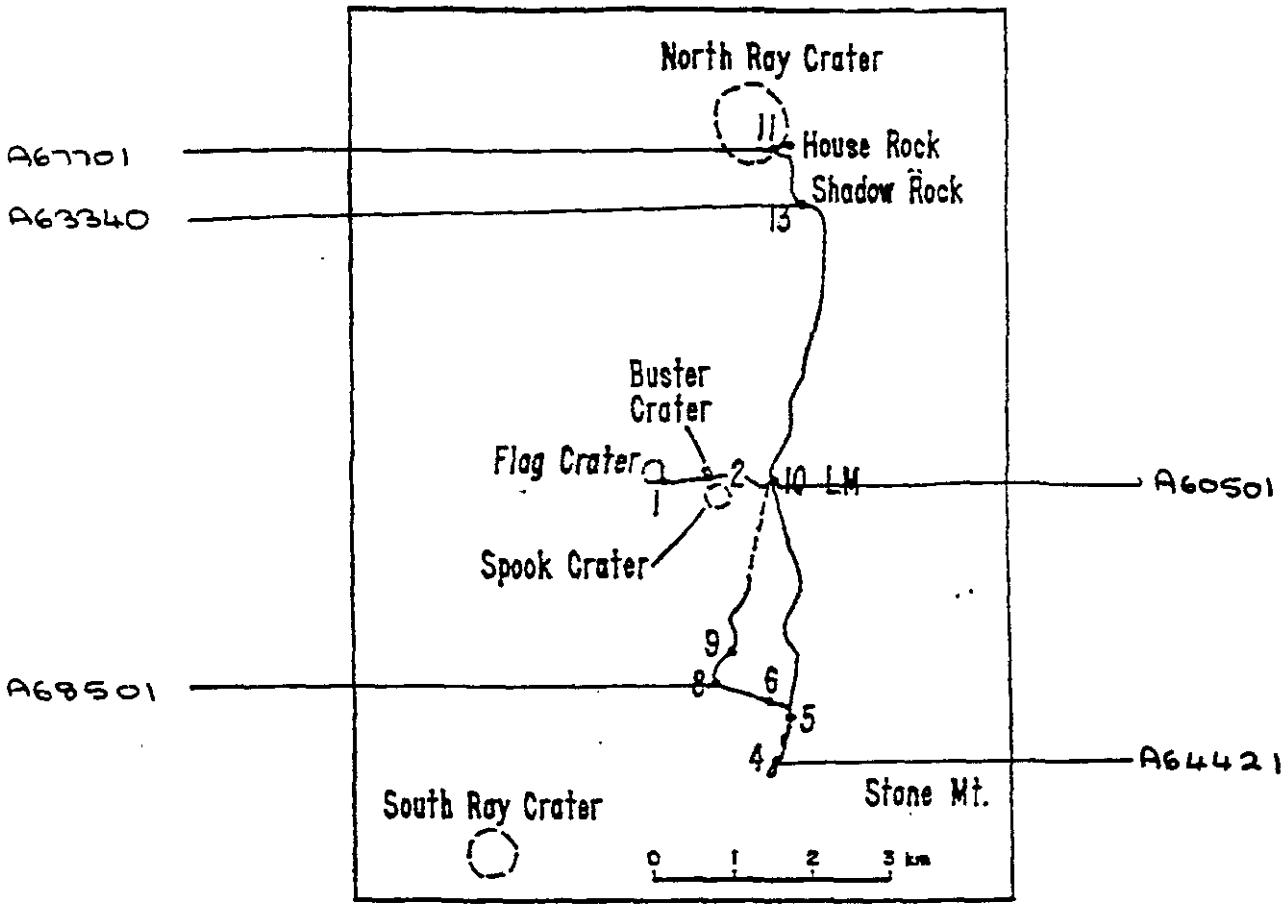

Figure 5.1. Geology of the Apollo 16 landing site (after Kerridge *et al.*, 1975b).

The lunar highland soils contain a higher proportion of CaO and Al_2O_3 (15% and 28% respectively) compared to A12023 (11% and 14% respectively). In addition, the highland soils contain less FeO (5%), MgO (6%) and TiO_2 (0.6%) than A12023 (FeO = 15%, MgO = 11% and TiO_2 = 3%). This reflects the mineralogical differences between the two landing sites.

5.3. Stepped heating extraction of the <10 μm grain size fraction from Apollo 16 soils

5.3.1. Nitrogen abundance and isotopic composition of the <10 μm fraction from Apollo 16 soils

The <10 μm grain size fraction of the Apollo 16 soils have been analysed by stepped combustion and stepped pyrolysis extraction using 50°C temperature resolution. The use of uniform temperature increments minimises the potential for any artefacts in the release or isotopic profile, and permits direct comparison between samples. The nitrogen data are given in Appendix D1 and the ΣN (ppm) and $\Sigma\delta^{15}N$ (‰) for each extraction are given in Table 5.2. Note that the $\delta^{15}N$ values at a temperature of ≤600°C for the pyrolysis extractions of A64421 (FIN220) and A68501 (FIN220) are not blank corrected, due to the low yields of nitrogen extracted for these steps (section 2.10).

Sample	Combustion			Pyrolysis		
	Extraction	ΣN (ppm)	$\Sigma\delta^{15}N$ (‰)	Extraction	ΣN (ppm)	$\Sigma\delta^{15}N$ (‰)
A60501<10 μm	FIN224	299.2	+25.6	FIN225	330.2*	+28.4*
A63340<10 μm	FIN208	265.0	+22.0	FIN209	285.0	+29.6
A64421<10 μm	FIN217	294.3	+14.7	FIN218	310.5	+16.6
A67701<10 μm	FIN222	150.3	+43.2	FIN223	201.2	+44.9
A68501<10 μm	FIN202	238.0	+21.0	FIN220	260.4	+26.5

Table 5.2. The ΣN (ppm) and $\Sigma\delta^{15}N$ values (‰) for the combustion and pyrolysis extraction of the <10 μm size fraction of A60501, A63340, A64421, A67701 and A68501.
* = excluding combustion steps at 400°C.

Table 5.2 shows that with the exception of A67701, there is reasonable agreement for ΣN and $\Sigma\delta^{15}N$ between the two extraction methods. In general, the combustion extractions liberate between 238 ppm (FIN202) and 299 ppm (FIN224) nitrogen with $\Sigma\delta^{15}N$ values ranging from +14.7‰ (FIN217) to +25.6‰ (FIN224). The pyrolysis extractions liberate consistently higher amounts of nitrogen (ranging from 260 ppm for FIN220 to 330 ppm for FIN225) and slightly higher $\Sigma\delta^{15}N$ values (from +16.6‰ for FIN218 to +29.6‰ for FIN209). The discrepancy of the yields may, in part, be due to consistent over-estimation of the blank during combustion, as the blank for the CuO decreases during the extraction. The more complete removal of low temperature contamination for the pyrolysis extractions using on-line pre-combustion (section 2.8.2) may account for the slightly higher $\Sigma\delta^{15}N$ values. No attempt was made to remove contamination for the combustion analyses. A further explanation for the yield discrpancy is preferential sorting of the sample during the weighing procedure, as in all cases, the combustion extraction for each sample was performed prior to the pyrolysis, and hence the sample analysed by combustion may consist of a larger grain size (and hence liberate less nitrogen) compared to that analysed by pyrolysis. However, the use of a stainless steel spatula to remove a representative sample from the storage bottle was believed to minimise these effects, and it seems unlikely that this would have occurred for five different samples.

The A67701 soil is clearly different from the other four samples; the nitrogen yield for the combustion (FIN217) and pyrolysis (FIN218) extraction is considerably lower (150 ppm and 201 ppm respectively) with $\Sigma\delta^{15}N$ values (+43.2‰ and +44.9‰ respectively) that are approximately 20‰ heavier. This may be due to the differences in maturity and exposure history of the sample, as A67701 is less mature (I_s/FeO = 39 and agglutinate content of 16%) than A60501, A64421 and A68501 ($I_s/FeO \approx 80$ and agglutinate content of 32-53%). Furthermore, the location of the collection site for A67701 has suggested that it may not be a typical lunar soil (section 5.2.2). Lunar rocks typically contain <1 ppm of nitrogen and high $\Sigma\delta^{15}N$ values, due to spallogenic nitrogen released upon melting, *e.g.* $\Sigma\delta^{15}N$ = +193‰ for A12063 (Becker & Clayton, 1975). The low nitrogen abundances and high $\Sigma\delta^{15}N$ for A67701 may suggest that the collection of this sample could have incorporated some fragments of the surrounding rocks (section 5.2.2), which, if sufficiently

fine-grained, could have been separated together with the soil, at the Lunar Curatorial Facility.

Sample	ΣN (ppm)	$\Sigma\delta^{15}N$ (‰)	Technique	Reference
A60501	109	+44	Pyrolysis/Combustion	(1)
	81		Kjeldahl method	(2)
A63340	52	+81	Pyrolysis/Combustion	(1)
	65		Pyrolysis	(3)
	91		Neutron activation	(4)
A67701	47	+96	Pyrolysis/Combustion	(1)
<4 μm[1]	407	+33	Pyrolysis/Combustion	(5)
A68501	83	+39	Pyrolysis/Combustion	(1)

Table 5.3. The ΣN (ppm) and $\Sigma\delta^{15}N$ values (‰) for the analyses of Apollo 16 soils by other workers.
[1] = Analysis of a <4 μm fraction of A67701 by Frick *et al.* (1988)
References: (1) Kerridge *et al.* (1975b), (2) Müller (1973), (3) Wszolek *et al.* (1973), (4) Kothari and Goel (1973), (5) Frick *et al.* (1988).

Table 5.3 displays the ΣN and $\Sigma\delta^{15}N$ data for the extractions of the five Apollo 16 soils by previous workers (Kothari and Goel, 1973; Müller, 1973; Wszolek *et al.*, 1973; Kerridge *et al.*, 1975b) using a variety of extraction techniques. It should be noted that the majority of analyses were performed using the whole-soil, as opposed to grain size fractions, hence this is by no means a good comparison, particularly in the case of the yield data. An exception to this is a single analysis of a <4 μm fraction of A67701 (Frick *et al.*, 1988) which liberated 407 ppm. This is consistent with the expected nitrogen concentration of 376-503 ppm using the nitrogen yields for FIN222 and FIN223 (150.3 and 201.2 ppm respectively) and the correlation between nitrogen yield and r^{-1} (Eberhardt *et al.*, 1970), where r = grain size (μm). The calculations are based on a grain size of 4 μm for the data obtained by Frick *et al.* (1988). Furthermore, the low ΣN (47 ppm) and high $\Sigma\delta^{15}N$

(+96‰) obtained by Kerridge *et al.* (1975b) for the whole-soil A67701, supports the conclusions in this work that A67701 may not be a typical soil.

The <10 μm fraction of the Apollo 16 samples from this study (Table 5.2) liberate between 3 and 5.5 times more nitrogen than the whole rock analyses by other workers (Table 5.3). Such an increase is not unexpected given the increased surface area per gram of the <10 μm fraction, compared with the whole-soil. A similar comparison for A12023 (Table 3.5 and Table 3.2 respectively) yields a ratio of ~2.2. It is likely that this discrepancy reflects the greater penetration depth of solar wind into plagioclase type minerals (Figure 1 in Jull and Pillinger, 1977) which are more dominant in highland soils. According to their sputter implantation model, lunar grains containing a low abundance of Fe-minerals would display high saturation contents. However, it does not imply that the Apollo 16 soils have greater exposure ages as it may be that the soil has remained buried in the highland regolith for long periods of time. The observed differences in nitrogen abundances are almost certainly linked to the differing mineralogy for the two sites.

Figure 5.2a to 5.2e illustrates the nitrogen release and isotopic profile for the combustion of the <10 μm fraction of the five Apollo 16 soils, and the equivalent pyrolysis extractions are displayed in Figure 5.3a to 5.3e. Note that to aid comparison between the two extraction techniques and individual samples, the graphs are plotted on identical axes. The peak isotopic composition and release temperatures for the heavy and light nitrogen components are given in Table 5.4.

For the majority of analyses in Figures 5.2 and 5.3, >70% of the total nitrogen is released as a single peak between 600 and 900°C. This release is directly comparable to the release of LTN in A12023 (section 3.3.1.2). There is evidence for a small release peak at a temperature of ≤400°C during the combustion extractions (Figures 5.2) which is attributed to terrestrial contamination. An exception is the combustion and pyrolysis extraction of the <10 μm fraction from A63340 (Figure 5.2b and 5.3b) which liberated an unusually high amount of nitrogen (58% and 53% respectively of the total) at a temperature of <600°C. The low temperature contamination may possibly have been introduced into the <10 μm fraction during grain size separation (section 2.7.2) as the Apollo 16 soils were one of the first group of samples to be processed. This explanation would account for the high C/N ratios in the initial few steps of the combustion extraction (Appendix D1).

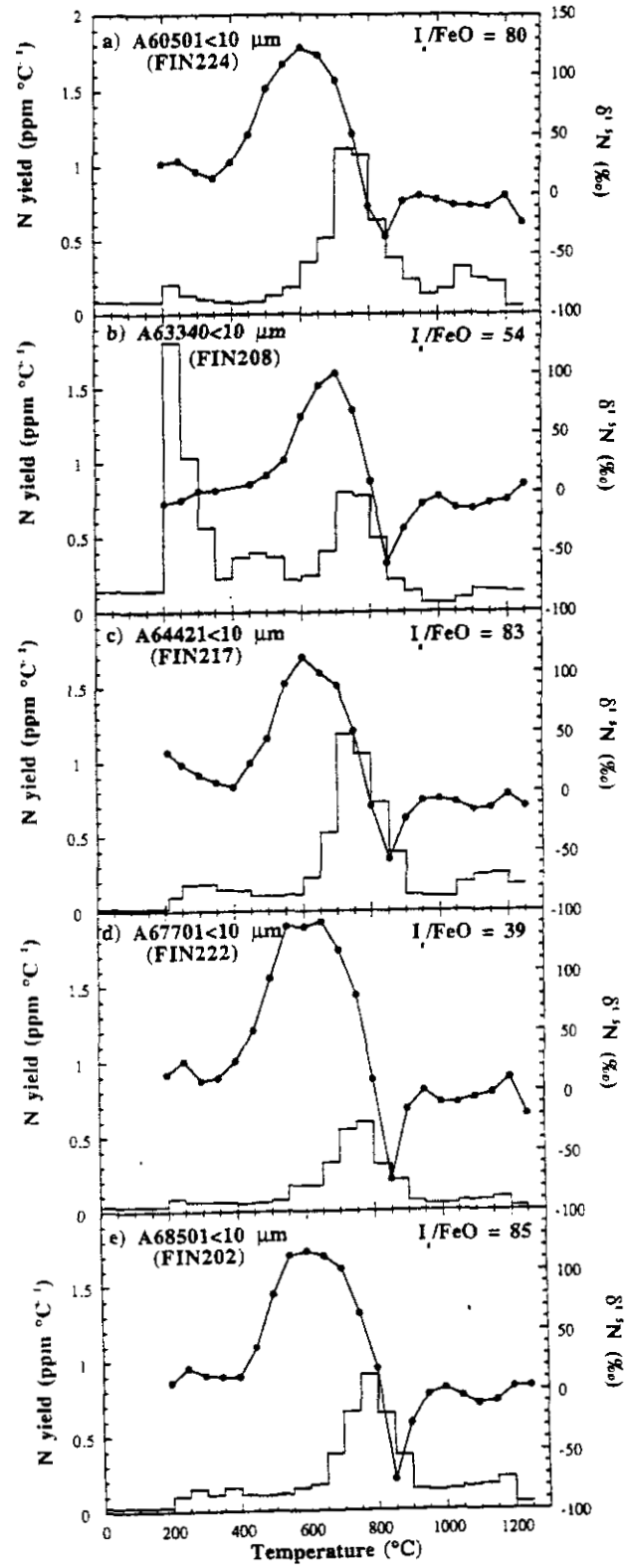

Figure 5.2. Nitrogen yields (ppm $°C^{-1}$) and isotopic compositions (‰) for the stepped combustion of the <10 µm fractions from Apollo 16 soils. The plots are as follows: a) A60501, b) A63340, c) A64421, d) A67701, e) A68501.

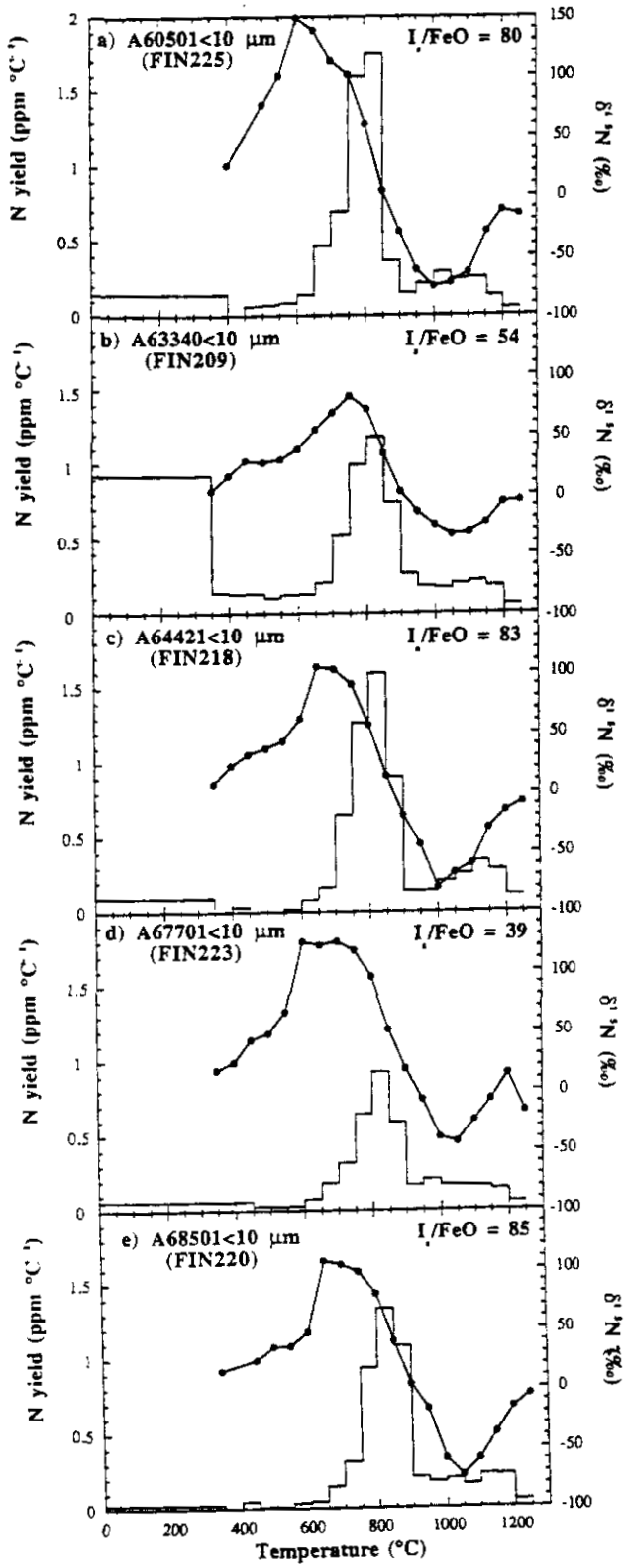

Figure 5.3. Nitrogen yields (ppm $°C^{-1}$) and isotopic compositions (‰) for the stepped pyrolysis of the <10 µm fractions from Apollo 16 soils. The plots are as follows: a) A60501, b) A63340, c) A64421, d) A67701, e) A68501.

All the extractions reveal the presence of a minor nitrogen component at a temperature of ≥1000°C, which constituted 12-21% of the total nitrogen. This component is equivalent to HTN as observed in the <10 μm grain size fraction of A12023 (section 3.4.1), although it should be noted that for A12023, the HTN component accounts for <10% of the total nitrogen. Interestingly, the soils which release a higher proportion of nitrogen at temperatures of ≥1000°C (18-21%) are A60501, A64421 and A68501 (Figures 5.2a, c, e, and Figures 5.3a, c, e) which are more mature, with I_s/FeO values of 80, 83 and 85 respectively. In comparison, soil A12023 is less mature with I_s/FeO = 55 (section 3.2.2). This substantiates the theory that the release of HTN is attributed to nitrogen trapped within complex secondary particles, such as agglutinates (section 3.4.1 and Brilliant *et al.*, 1994).

Sample	N_{LT} component		N_{MT} component		N_{HT} component	
<10 μm	$\delta^{15}N$ (‰)	Temp (°C)	$\delta^{15}N$ (‰)	Temp (°C)	$\delta^{15}N$ (‰)	Temp (°C)
A60501						
Comb (FIN224)	+122.6	600	-34.8	850		
Pyr (FIN225)	+149.5	600			-75.7	1000
A63340						
Comb (FIN208)	+100.4	700	-59.2	850		
Pyr (FIN209)	+82.7	750			-33.5	1050
A64421						
Comb (FIN217)	+113.0	600	-56.7	850		
Pyr (FIN218)	+105.2	650			-79.6	1000
A67701						
Comb (FIN222)	+138.6*	550-650	-73.7	850		
Pyr (FIN223)	+124.4*	600-700			-42.9	1050
A68501						
Comb (FIN202)	+116.6	600	-74.4	850		
Pyr (FIN220)	+107.6	650			-72.7	1050

Table 5.4. A comparison of the $\delta^{15}N$ values (‰) and release temperature (°C) of N_{LT}, N_{MT} and N_{HT} for the stepped combustion and pyrolysis extractions of the <10 μm fraction of A60501, A63340, A64421, A67701 and A68501.
* = weighted average $\delta^{15}N$ across the given temperature range.

The isotopic profile obtained for the Apollo 16 soils show some similarities with the <10 μm grain size fraction for A12023 (section 3.4.2.1). With the exception of A63340, all

the soils liberate an isotopically heavy component, comparable with N_{LT} for A12023, between 600-700°C with $\delta^{15}N$ values ranging from +105‰ to +150‰. The <10 μm fraction of A63340 also liberates N_{LT} at a higher release temperature (700°C for FIN208 and 750°C for FIN209) with $\delta^{15}N$ values of +100‰ and +83‰ respectively. The light isotopic composition for N_{LT} and the high release temperature, especially during the pyrolysis extraction, is due to significant amounts of contamination in the sample. Despite the use of multiple combustion steps at 350°C it appears that some contamination remained in the sample until higher temperatures and hence affected both the release temperature and isotopic composition of N_{LT}.

The combustion extractions liberate a single isotopically light nitrogen component at a temperature of 800-850°C with $\delta^{15}N$ values ranging from -35‰ (A60501) to -74‰ (A68501). This is consistent with N_{MT} as observed for the <10 μm fraction of A12023 (FIN62) with $\delta^{15}N$ = -44.7‰ (Table 3.6). However, the pyrolysis extractions of the soils liberate only a single light nitrogen component at a temperature of 1000-1050°C with $\delta^{15}N$ values ranging from -34‰ (A63340) to -80‰ (A64421). This component is termed N_{HT} in this study, despite the absence of N_{MT}, due to the high temperature of its release. The observation of a single light nitrogen component during pyrolysis is in contrast with the pyrolysis extraction of A12023 <10 μm (FIN73), which revealed two light nitrogen components (N_{MT} and N_{HT}) with $\delta^{15}N$ values of -28.4 and -92.7‰ (Table 3.6) at a temperature of 840°C and 1050°C respectively. Note that this is also in contrast with the observation of the W-shaped profile for all the lunar soils and breccias in the current study.

For the majority of the Apollo 16 soils (with the exception of A63340) analysed in this study, the release of N_{LT} is shifted to a lower temperature, during combustion when compared to its release temperature during pyrolysis (Table 5.4). An equivalent temperature shift (56 ± 4°C) was also observed for the <10 μm fraction of A12023 (section 3.4.2.1). In order to determine the magnitude of the temperature shift, the best fit lines for the isotopic profiles of the combustion and pyrolysis of A60501 are compared (Figure 5.4a), in a plot similar to Figure 3.12a for A12023. Soil A60501 is used as the most representative sample in this study, although similar features have been observed in the other Apollo 16 soils. Note that N_{LT} is used as the upper limit for both the combution and pyrolysis extraction, with N_{MT} as the lower limit for the combustion and N_{HT} as the lower limit for the pyrolysis.

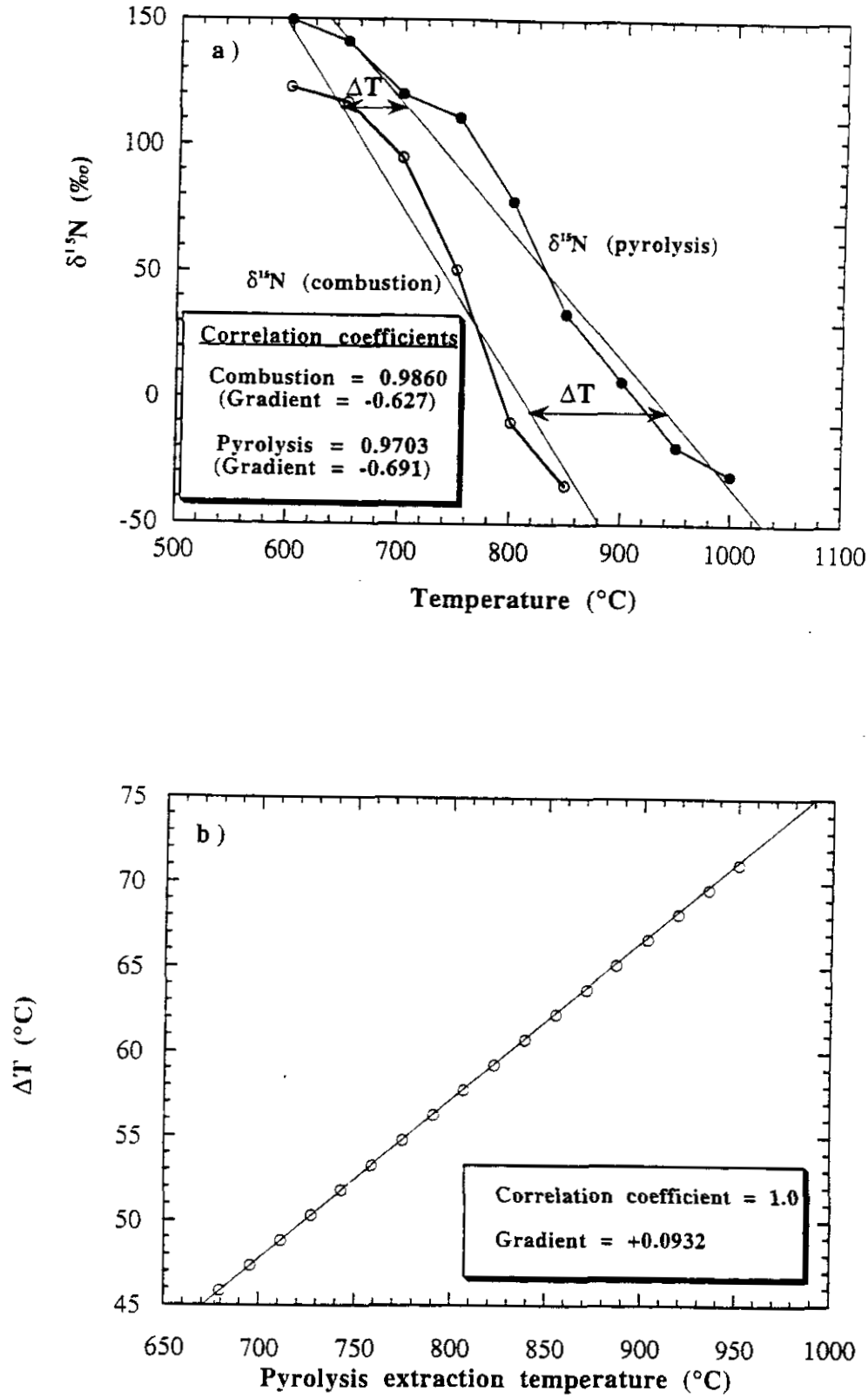

Figure 5.4. Isotopic mixing between N_{LT} and N_{MT} (or N_{HT}) for the combustion and pyrolysis of the <10 μm fraction from A60501. The plots are as follows: a) comparison of the $\delta^{15}N$ values against temperature for the combustion and pyrolysis extractions. The equations for the best fit lines for each isotopic trend are as follows: $\delta^{15}N_{comb} = 558.22 - 0.692T$ and $\delta^{15}N_{pyr} = 546.16 - 0.627T$, where T is extraction temperature (°C), b) plot of ΔT, *i.e.* $T_{pyr} - T_{comb}$, against pyrolysis extraction temperature (°C).

The equations for the best fit lines are given in the caption for Figure 5.4a. The equations are used to determine the release temperature for a range of $\delta^{15}N$ values (+120 to -50‰) for both the stepped combustion (T_{comb}) and pyrolysis (T_{pyr}), and the magnitude of the temperature shift, ΔT (defined as $T_{pyr} - T_{comb}$). The calculated ΔT are given in Table 5.5 (similar to Table 3.7), and are plotted against pyrolysis extraction temperature in Figure 5.4b (similar to Figure 3.12b).

$\delta^{15}N$ (‰)	T_{pyr} (°C)	T_{comb} (°C)	ΔT (°C)
+120	679.48	633.60	45.87
+110	695.42	648.06	47.36
+100	711.36	662.52	48.84
+90	727.31	676.98	50.33
+80	743.25	691.44	51.81
+70	759.20	705.90	53.30
+60	775.14	720.36	54.78
+50	791.08	734.81	56.27
+40	807.02	749.27	57.75
+30	822.97	763.73	59.24
+20	838.92	778.19	60.73
+10	854.86	792.65	62.21
0	870.80	807.11	63.70
-10	886.75	821.57	65.18
-20	902.69	836.03	66.67
-30	918.64	850.48	68.15
-40	934.58	864.94	69.64
-50	950.53	879.40	71.12

Table 5.5. Calculation of ΔT for $\delta^{15}N$ values (from +120‰ to -50‰) for the stepped combustion and pyrolysis of the <10 µm fraction from A60501.
ΔT defined in the figure caption for Figure 5.4b.

The comparison of the offset for the heavy-light trend indicates that there is a clear temperature shift of 58 ± 8°C towards lower temperatures in the presence of oxygen over the temperature range 650-900°C. This compares favourably with the mean offset of 56 ± 4°C over the same region for the <10 µm fraction from A12023 (section 3.4.2.1). However, the mixing trends for A12023 have been shown to converge at ~1850°C, in the absence of any other components, whereas the gradients of the mixing trends for A60501 show that will converge at ~190°C (Figure 5.4a). This is illustrated in Figure 5.4b, which displays a positive gradient, and can be compared to the equivalent plot for A12023 (Figure 3.12b) which displays a negative gradient.

The divergence of the two gradients for A60501 is due to the absence of N_{MT} in the pyrolysis extractions which implies several possibilities about the mineralogy and petrology of the Apollo 16 soils. Given that N_{MT} was only well defined using temperature increments of ≤25°C for A12023, it is not possible to determine whether it is absent from the Apollo 16 soil or not resolved due to the relatively low temperature resolution that was employed. However, it seems likely that if N_{MT} is present in Apollo 16 soils, its abundance is lower than in the mare soils and therefore masked by the more dominant nitrogen components. This suggestion may be linked to the differing major element chemistry of the highland and mare sites (Table 5.1 and 3.1 respectively). The highland samples with ^{21}Ne exposure ages = 49-190 Myr (Table 5.1) contain a greater proportion of plagioclase, compared to the mare samples which contain greater proportions of pyroxene, ilmenite and olivines with higher exposure ages, *e.g.* ^{21}Ne-age = ~250 Myr for A12042 and A12044 (Kerridge *et al.*, 1978). This implies that N_{MT} may be associated with nitrogen contained in pyroxene, olivine and ilmenite grains, which are less dominant in the highland soils, than in the mare soils.

As with the <10 μm fraction of A12023 (section 3.4.2.1), the difference in the isotopic profiles for the stepped combustion and pyrolysis extraction of the Apollo 16 soils is further investigated by determining the variation in $\delta^{15}N$, *i.e.* $\delta^{15}N_{pyr} - \delta^{15}N_{comb}$, across the temperature range 550-900°C. The data obtained are given in Table 5.6 (equivalent to Table 3.8) and the plot of $\delta^{15}N$ variation against extraction temperature (equivalent to Figure 3.13) is displayed in Figure 5.5.

Temperature (°C)	$\delta^{15}N_{pyr}$ (‰)	$\delta^{15}N_{comb}$ (‰)	Variation $\delta^{15}N$ (‰)
550	+100.4	+108.8	-8.4
600	+149.5	+122.6	+26.9
650	+138.6	+116.6	+22.0
700	+112.5	+95.1	+17.4
750	+100.9	+50.9	+50.0
800	+60.1	-9.7	+69.8
850	+4.5	-34.8	+39.3
900	-29.3	-5.5	-23.8

Table 5.6. Variation in $\delta^{15}N$ (‰) for common extraction temperatures (°C) between 550-900°C for the combustion and pyrolysis of the <10 μm fraction from A60501.
Variation in $\delta^{15}N$ is defined as $\delta^{15}N_{pyr} - \delta^{15}N_{comb}$.

Figure 5.5 does not reveal a similar trend to that displayed for A12023, which showed that the difference in the measured isotopic compositions between the two extraction techniques decreases with increasing temperature across the release of LTN. In addition, A12023 showed a decrease in the magnitude of the temperature shift with increasing temperature (Table 3.7 and Figure 3.12). The observations for A12023 were attributed to the decreasing effect of the presence of oxygen on the nitrogen release during extraction at higher temperature. However, an equivalent phenomenon is not observed for A60501, or any of the Apollo 16 soils in this study. Interestingly, the variation in $\delta^{15}N$ for the 600, 650 and 700°C temperature steps, do reveal a linear trend with a correlation coefficient r = 0.9998. Note that the slope of the best fit line for this trend is -0.095, which is similar to the equivalent best fit line for A12023 (Figure 3.13) with a slope of -0.1014. This suggests that the decreasing effect of the presence of oxygen with increasing temperature is observed for the Apollo 16 soils (albeit in only three temperature steps) and the difference in the isotopic profile is due to the absence or masking of N_{MT} during the pyrolysis extractions.

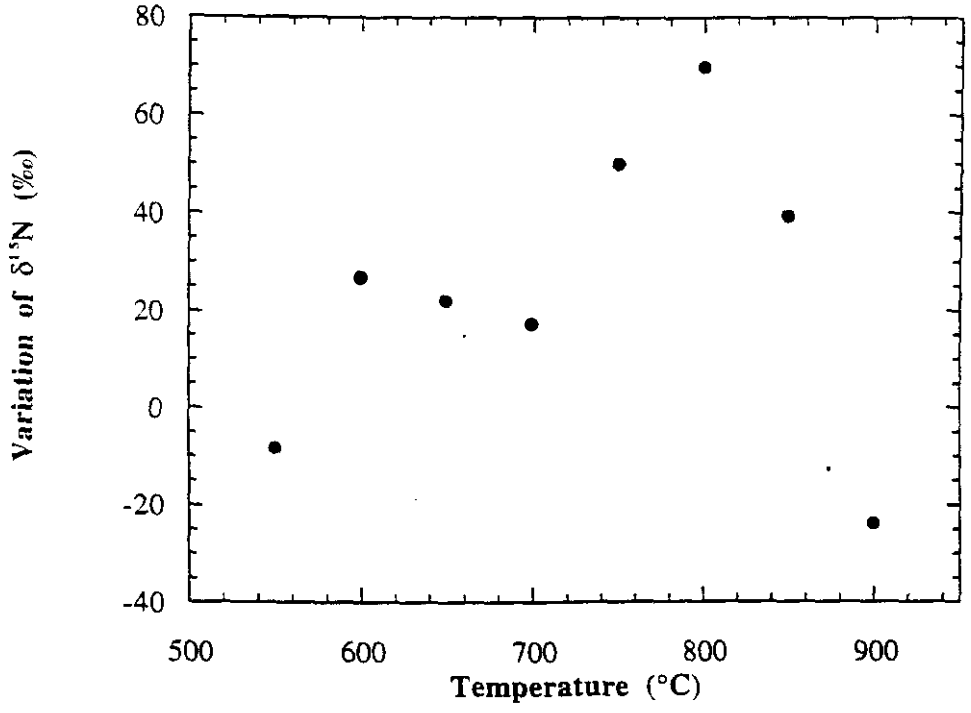

Figure 5.5. Variation in $\delta^{15}N$ (‰) against extraction temperature (°C) for the combustion and pyrolysis of the <10 μm fraction from A60501.

Variation in $\delta^{15}N$ is defined in the caption for Table 3.8.

5.3.2. Nitrogen yields and isotopic compositions: their relationship to exposure history

In order to determine a possible origin for the light nitrogen in the highland soils, it is useful to compare the nitrogen abundance and isotopic compositions with accepted parameters of surface exposure. The two most commonly used parameters are the intensity of ferromagnetic resonance (I_s) normalized to FeO (section 1.5.4.2), and cosmic-ray exposure ages calculated from the abundance of ^{21}Ne (section 1.5.4.3). Previous nitrogen analyses of Apollo 16 soils have revealed a strong positive correlation between nitrogen abundance (ppm) and I_s/FeO and a negative correlation between $\delta^{15}N$ and ^{21}Ne-exposure ages (Figures 1 & 2 in Kerridge *et al.*, 1977). Although this work utilised a larger number of samples, the extractions were performed using a mixture of whole-rock and <1 mm sieve fractions leading to a certain amount of scatter. By using only the finest fractions, it was hoped to remove any variation due to sample grain size effects.

The plots of ΣN (ppm) against I_s/FeO and $\Sigma\delta^{15}N$ (‰) against ^{21}Ne-exposure age (Myr) for the pyrolysis data obtained for the current investigation, are given in Figures 5.6a and 5.6b respectively. The pyrolysis data were chosen for this study in preference to the combustion data, as there appears to be better resolution of the isotopic maxima and minima during pyrolysis, in addition to the removal of low temperature contamination components. Note that the current data also include error bars for the measurement of nitrogen abundances and isotopic compositions. For this work, the errors for the nitrogen yield data has been estimated as 5% of the total abundance. The $\Sigma\delta^{15}N$ values plotted are the mean of the blank corrected $\Sigma\delta^{15}N$ (Table 5.2) and the uncorrected $\Sigma\delta^{15}N$ with the two extremes as outliers for the error bars. The errors for $\Sigma\delta^{15}N$ are given in the caption for Figure 5.6, but are generally within the size of the data points. Also shown on these figures for comparison are the equivalent data from a variety of Apollo 16 soils (adapted from Kerridge *et al.*, 1977). The references for this work are given in the figure captions. Although Figure 5.6a reveals a correlation for ΣN with I_s/FeO for this work, the correlation is weaker (correlation coefficient r = 0.71) compared to previous work (correlation coefficient r = 0.92). The trend for $\Sigma\delta^{15}N$ against ^{21}Ne-exposure age (Figure 5.6b) for this study is also less obvious than previous work (correlation coefficient r = 0.78 compared to 0.95).

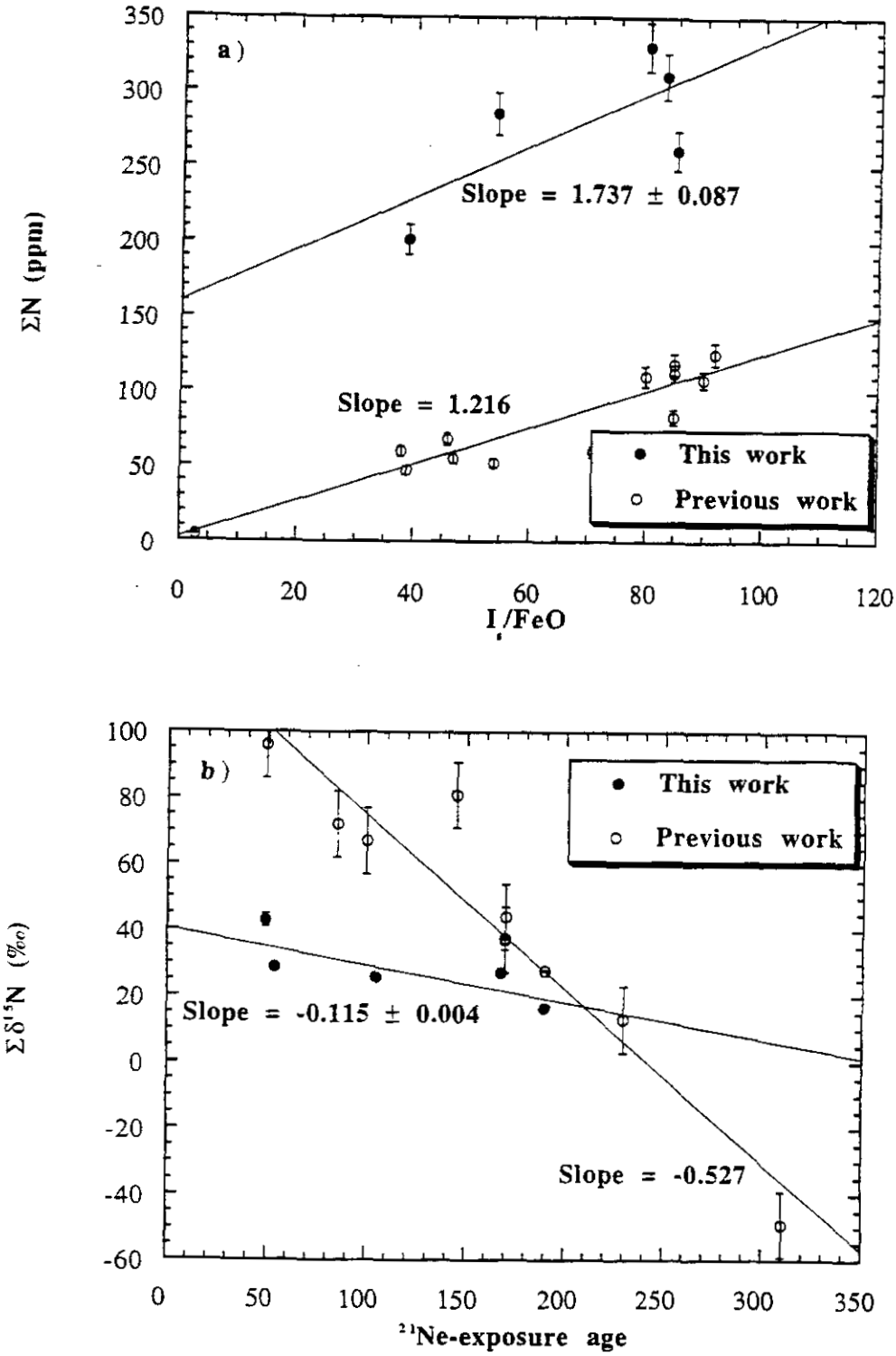

Figure 5.6. Nitrogen trends with surface exposure parameter for Apollo 16 soils for this work and previous work. The plots are as follows: a) N yield (ppm) against I_s/FeO, b) $\Sigma\delta^{15}N$ (‰) against ^{21}Ne-exposure age (Myr).

The I_s/FeO data are from Morris (1976). The ^{21}Ne data are from Bogard and Nyquist (1973), Hintenberger and Weber (1973), Kirsten *et al.* (1973), Walton *et al.* (1973), Eberhardt *et al.* (1976). The N data are from Müller (1973, 1974), Chang *et al.* (1974b), Petrowski *et al.* (1974), Becker and Clayton (1975), Kerridge *et al.* (1975b).

The errors for $\Sigma\delta^{15}N$ are as follows: 1.3‰ (A60501), 0.3‰ (A63340), 0.2‰ (A64421), 2.1‰ (A67701), and 0.9‰ (A68501).

The errors associated with the best fit lines for Figure 5.6a and 5.6b account, in part, for the discrepancy between the slopes obtained for this work and previous studies. However, it is more likely that the stronger correlation in earlier work is due to the greater number of samples which were analysed, compared to only five in this study. The analysis of <10 μm fractions account for the increased nitrogen yields in this study compared to previous work, although it should be noted that the sieving procedure (section 2.7.2.1) is not a well constrained technique and could result in <10 μm fractions of varying size distribution.

From Figures 5.6a and 5.6b, it can be reasoned that a mature lunar soil would contain a higher concentration of nitrogen with a lighter $\Sigma\delta^{15}N$ than a soil recently exposed on the lunar surface. The study of magnetic and density separates from A12023 (section 3.5) has shown that agglutinates are not the host of the isotopically light nitrogen component (N_{HT}). Furthemore, the absence of HTN in the <10 μm fraction of lunar soils (section 3.4.1), has led to the conclusion that HTN is attributed to the nitrogen liberated from complex secondary particles such as coarse-grained agglutinates (Brilliant *et al.*, 1994). As a continuation of the study of light nitrogen in A12023 (section 3.4.2.2), the data obtained in this work from the Apollo 16 soils are re-examined to determine any correlation between N_{HT} and I_s/FeO (Figure 5.7a) and ^{21}Ne-exposure age (Figure 5.8a). The errors for N_{HT} are calculated using the blank corrected $\delta^{15}N$ and uncorrected $\delta^{15}N$ as outliers, with the data points as the mean of the two extremes and are given in the figure caption for Figure 5.7. Figures 5.7a and 5.8a show that there is a correlation (correlation coefficient r=90%) between $\delta^{15}N$ of N_{HT} in Apollo 16 soils, with increasing maturity (I_s/FeO and ^{21}Ne-exposure age). The correlation is weak as not all the data points lie on the best fit line. However, the trends indicate that the isotopic composition of the light nitrogen in the lunar regolith is dependent on the length of time the soil was exposed to solar wind and solar and galactic cosmic-ray radiation. Interestingly, no such correlation has been observed between N_{LT} and the maturity parameters I_s/FeO and ^{21}Ne-exposure age and these plots are shown for comparison purposes in Figures 5.7b and 5.8b.

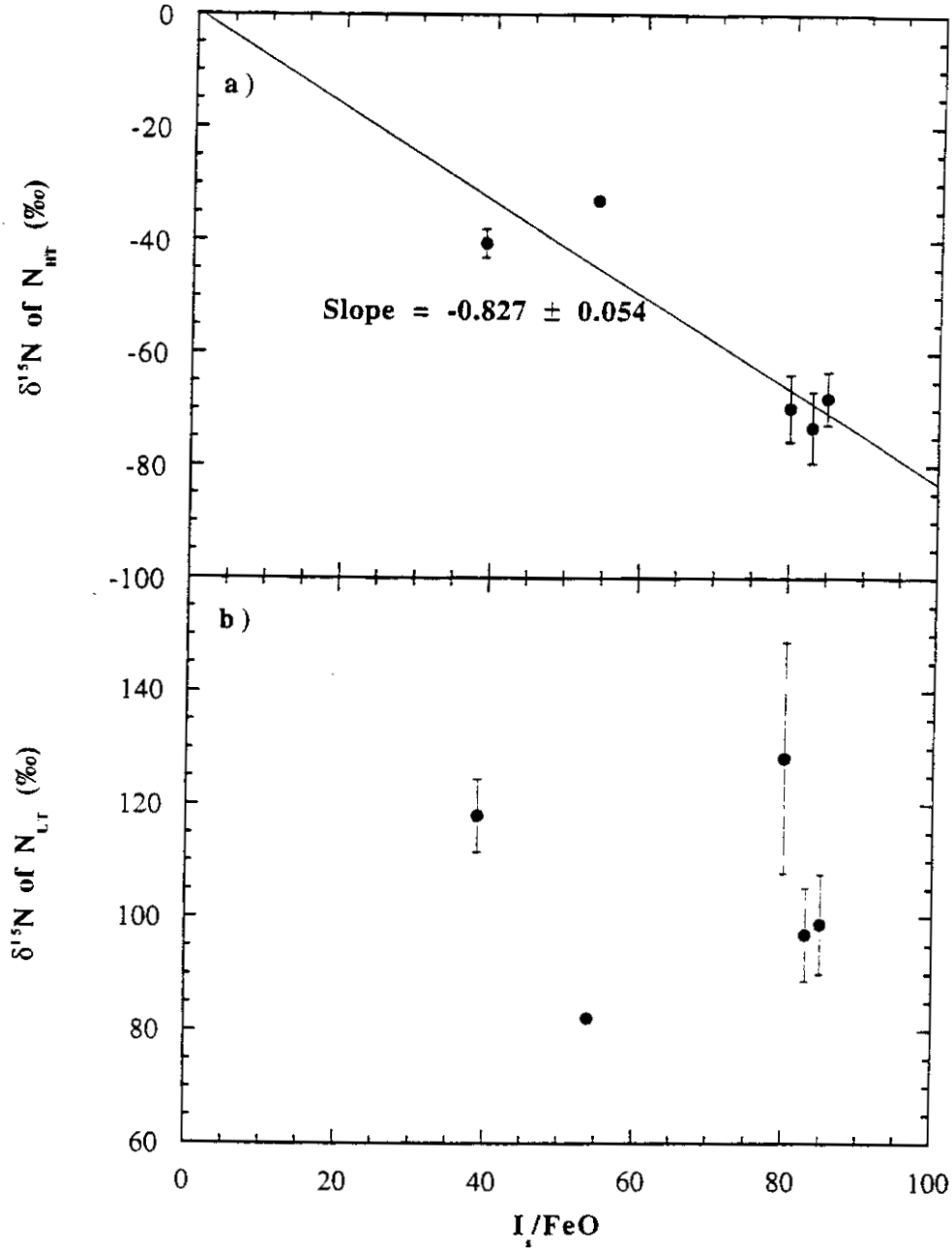

Figure 5.7. Plot of $\delta^{15}N$ (‰) for N_{HT} (Figure 5.7a) and N_{LT} (Figure 5.7b) against I_s/FeO for the pyrolysis extractions of <10 μm grain size fraction from Apollo 16 soils. I_s/FeO data are from Morris (1976).
The errors for the $\delta^{15}N$ of N_{HT} are as follows: 6.0‰ (A60501), 0.6‰ (A63340), 6.4‰ (A64421), 2.5‰ (A67701) and 4.7‰ (A68501), and for N_{LT} are 20.5‰ (A60501), 0.5‰ (A63340), 8.3‰ (A64421), 6.5‰ (A67701) and 8.8‰ (A68501).

Kerridge *et al.* (1975b) has shown that the lowest $\Sigma\delta^{15}N$ for Apollo 16 soils were obtained from the samples with the highest content of metallic iron (Figure 5.9a). These workers have suggested that Fe^0 in the lunar regolith originates from two main sources: an

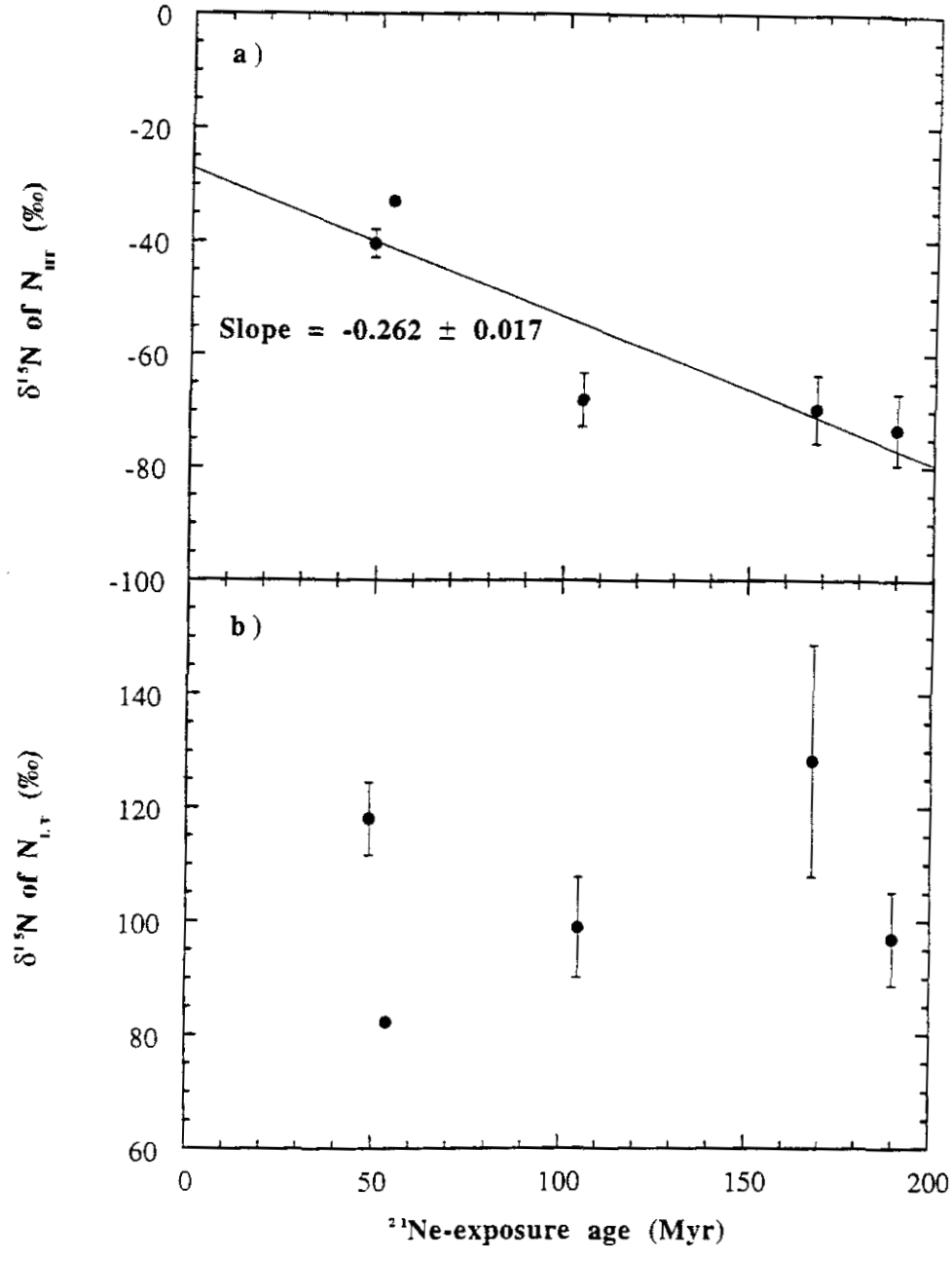

Figure 5.8. Plot of $\delta^{15}N$ (‰) for N_{HT} (Figure 5.8a) and N_{LT} (Figure 5.8b) against ^{21}Ne-exposure age (Myr) for the pyrolysis extractions of <10 μm grain size fraction from Apollo 16 soils.

The ^{21}Ne data are from Bogard and Nyquist (1973), Hintenberger and Weber (1973), Kirsten *et al.* (1973), Walton *et al.* (1973) and Eberhardt *et al.* (1976).

The errors for N_{LT} and N_{HT} are given in the caption for Figure 5.7.

ancient meteoritic component, containing 5.5 wt.% Ni (section 1.6.4), and the reduction of indigenous Fe^{2+} by preferential sputtering of solar wind hydrogen (section 1.6.1.1). The latter has been termed as the "excess" metal components by Kerridge *et al.* (1975b). Given

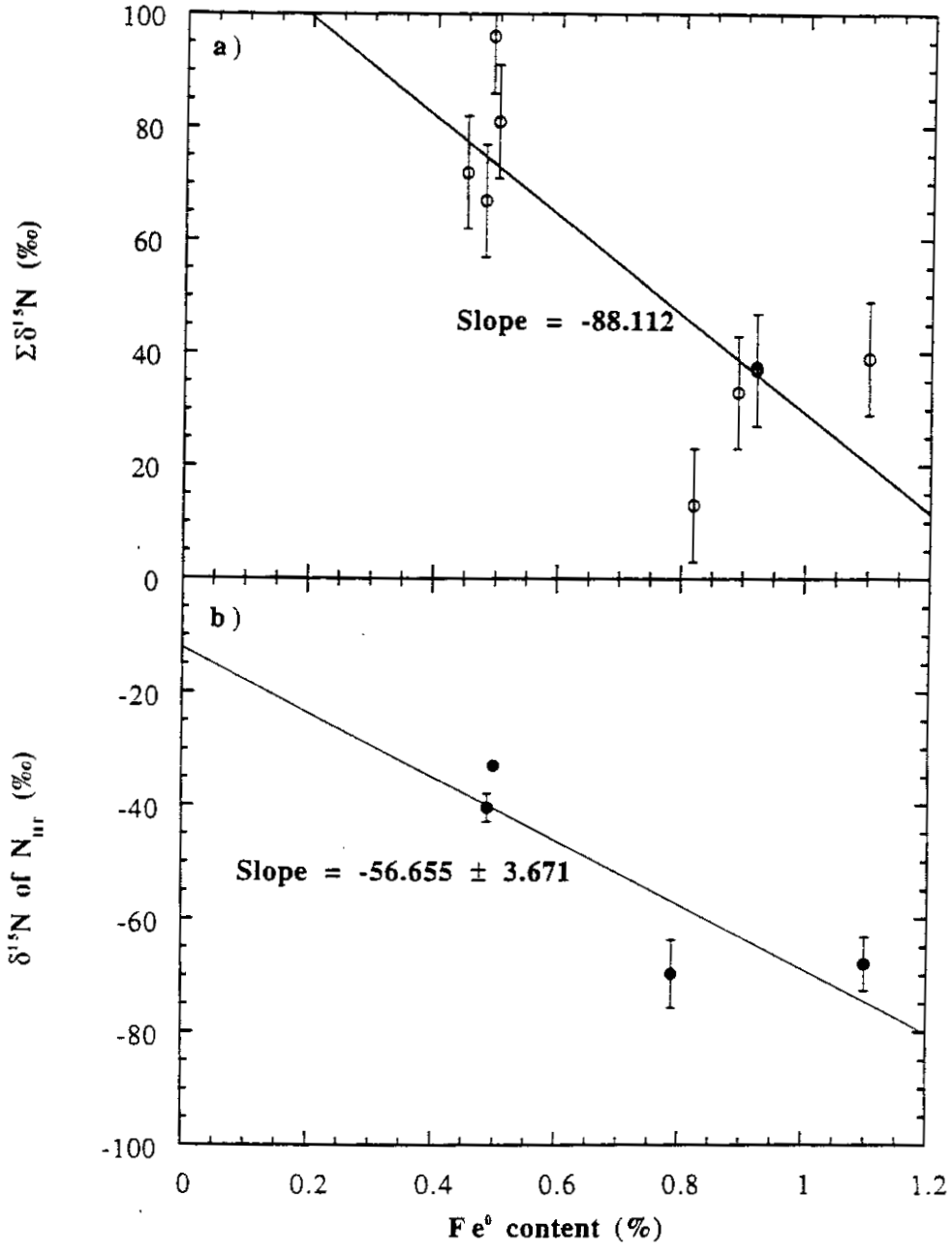

Figure 5.9. Plot of $\delta^{15}N$ (‰) against Fe^0 content (%). The plots are as follows: a) $\Sigma\delta^{15}N$ (‰) against Fe^0 content for the data obtained by Kerridge *et al.* (1975b), b) $\delta^{15}N$ of N_{HT} (‰) against Fe^0 content for the pyrolysis extractions of <10 μm grain size fraction from Apollo 16 soils.
The Fe^0 content data are from Kerridge *et al.* (1975b).
The errors for N_{HT} are given in the caption for Figure 5.7.

that there was a slight similarity between the trends of $\Sigma\delta^{15}N$ against I_s/FeO (Figure 5.6a) and $\delta^{15}N$ of N_{HT} against I_s/FeO (Figure 5.7a), it is necessary to determine whether there is a correlation between N_{HT} and the Fe^0 content of the Apollo 16 soils. This is shown in

Figure 5.9b for all soils in this work except A64421, as no value could be found in the literature for the Fe^0 content of the soil. Figure 5.9b displays a weak correlation (correlation coefficient r = 0.87) between N_{HT} and Fe^0 content, as the error bars for the majority of points do not intersect the best fit line. The discrepancy in the slopes of the best fit line is likely to be due to limited data set (only four samples) in this work and hence may not be truly represented of Apollo 16 soils. However, these results tentatively suggest that the origin of N_{HT} may be related to the Fe^0 content of the soils, possibly incorporated during the reduction of Fe^{2+} to Fe^0.

5.3.3. Argon analysis of the <10 μm fraction from Apollo 16 soils

Noble gas abundances, $^{36}Ar/^{38}Ar$ and $^{40}Ar/^{36}Ar$ ratios have been measured by previous workers (Bogard and Nyquist, 1973; Hintenberger and Weber, 1973; Walton *et al.*, 1973) for the five Apollo 16 soils analysed in this study. The $^{36}Ar/^{38}Ar$ ratios obtained by these workers range from 5.19 to 5.35, with a range of $^{40}Ar/^{36}Ar$ ratios from 0.966 to 1.61.

The $^{36}Ar/^{38}Ar$, $^{40}Ar/^{36}Ar$ and $N/^{36}Ar$ ratios have been measured (as detailed in section 3.3.2) for the stepped combustion and pyrolysis extractions of the <10 μm fractions of the five Apollo 16 soils, using the procedure detailed in section 3.3.2. The argon data are given in Appendix D1. As the $^{36}Ar/^{38}Ar$, $^{40}Ar/^{36}Ar$ and $N/^{36}Ar$ profiles are similar for all the combustion (and pyrolysis) extractions of the <10 μm grain size fraction of the Apollo 16 soils, A60501 is chosen as a representative sample. Figure 5.10a and 5.10b illustrates the $N/^{36}Ar$ (plot (i)), $^{40}Ar/^{36}Ar$ and $^{36}Ar/^{38}Ar$ (plot (ii)), and the nitrogen and ^{36}Ar yields (plot (iii)) for the stepped combustion (Figure 5.10a) and pyrolysis (Figure 5.10b) respectively of the <10 μm grain size fraction of A60501.

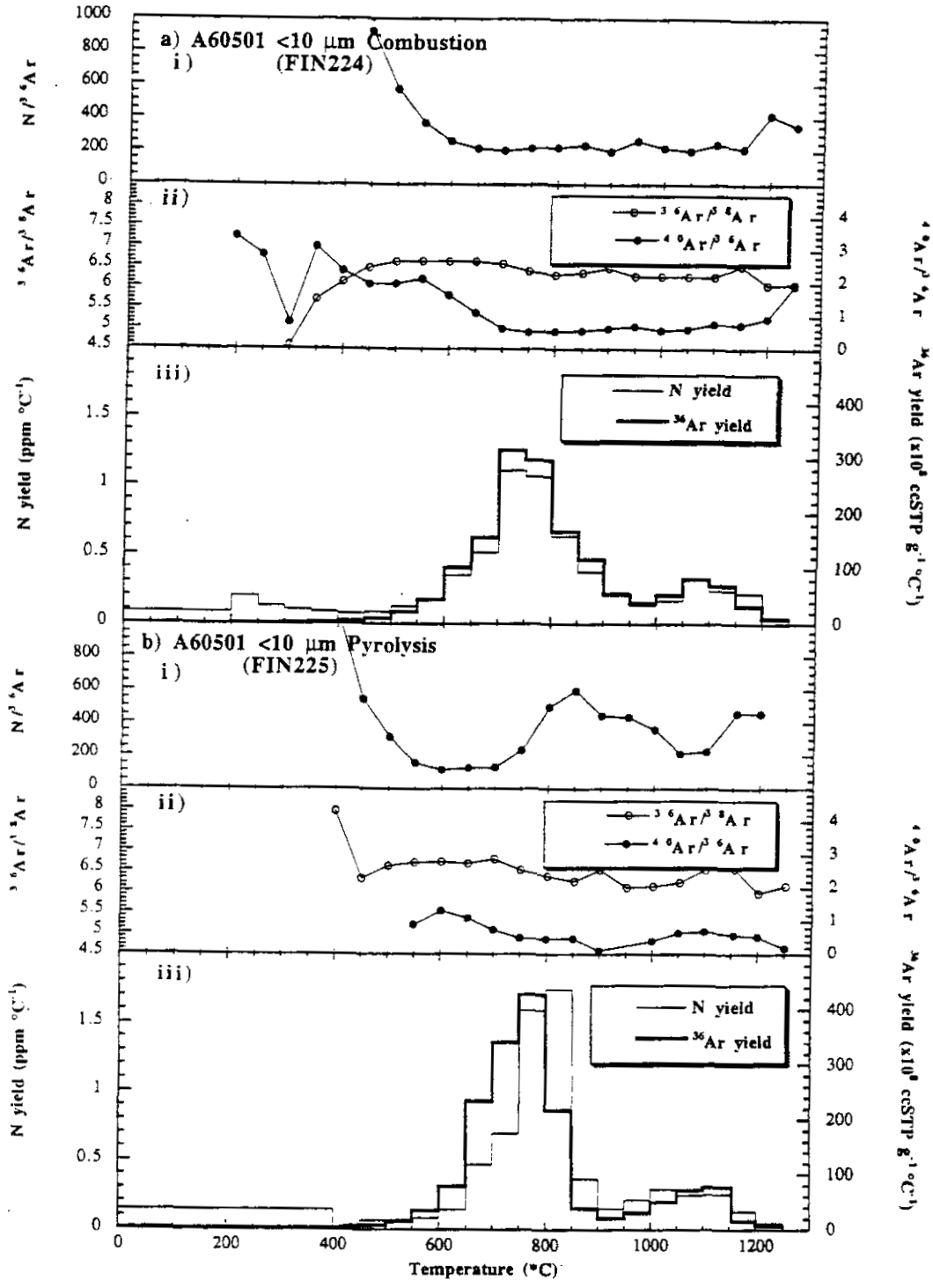

Figure 5.10. Conjoint nitrogen and ^{36}Ar data, and argon isotopic ratios against temperature for the stepped combustion (Figures 5.10a) and stepped pyrolysis (Figures 5.10b) of the <10 µm fraction from A60501. The plots are as follows: (i) $N/^{36}Ar$, (ii) $^{36}Ar/^{38}Ar$ (left ordinate) and $^{40}Ar/^{36}Ar$ (right ordinate), (iii) N yield in units of ppm $°C^{-1}$ (left ordinate) and ^{36}Ar in units of ccSTP g^{-1} $°C^{-1}$ (right ordinate).

The $^{36}Ar/^{38}Ar$ ratios obtained for A60501 in this study (Figure 5.10a (ii) and Figure 5.10b (ii)) decrease slightly throughout the extractions from a value of 6.6 to 6.0 for the

combustion and from 6.8 and 6.0 for the pyrolysis extractions. Note that the sharp decrease of the $^{36}Ar/^{38}Ar$ ratios at temperatures of ≥1150°C, due to the liberation of cosmogenic ^{38}Ar, was less than observed for the bulk soils and breccias in this work, *e.g.* section 3.3.2 (A12023), section 4.3.2 (A79035) and section 4.6.2 (A75080), but similar to that observed for the <10 μm grain size fraction of A12023 (section 3.4.2.2). Due to the semi-quantitative nature of the argon data in this work, these ratios can be taken as comparable to the solar $^{36}Ar/^{38}Ar$ ratios of previous workers (section 1.7.5.1 and 1.7.5.2).

The $^{40}Ar/^{36}Ar$ ratios (Figure 5.10a (ii) and Figure 5.10b (ii)) remain essentially constant throughout the extractions with a mean value of 1.13 and 0.61 for the combustion and pyrolysis respectively. The higher mean value for the combustion extraction is due to the liberation of re-implanted atmospheric ^{40}Ar (section 1.6.1.3) in the inital few steps, whereas this was removed for the pyrolysis extraction by pre-combusing the soil at 400°C (section 2.8.1). Note that the $^{40}Ar/^{36}Ar$ ratio for all the Apollo 16 soils in this investigation varies from 0.61 to 1.77, which compares reasonably well with the ratios obtained for these soils by previous workers, *e.g.* Bogard and Nyquist (1973). As with all the soils and breccias studied in this work (sections 3.3.2, 4.3.2 and 4.6.2), the constant $^{40}Ar/^{36}Ar$ ratios contadict the theory that the surface location of nitrogen in the lunar regolith is proof of its solar origin (section 1.7.2.1).

As with the other lunar soils and breccias in this work (refer to the aforementioned sections), nitrogen and ^{36}Ar are liberated conjointly during stepped combustion extraction (Figure 5.10a (iii)). Hence, the $N/^{36}Ar$ ratio remains constant across the release of LTN and HTN (Figure 5.10a (i)) with a mean value of 424. However, as has been shown with ^{40}Ar, a surface location for the nitrogen, as suggested by the constant $N/^{36}Ar$ ratios, is not conclusive proof of a solar origin for the nitrogen. Furthermore, the $N/^{36}Ar$ ratio for the combustion extraction is 11.5 times higher than the solar value of ~37 (Cameron, 1982; Anders and Grevesse, 1989). During stepped pyrolysis extraction, the nitrogen is preferentially retained in the soil to a higher temperature (~50°C), compared to ^{36}Ar (Figure 5.10b (iii)), hence the $N/^{36}Ar$ ratio varies from a minimum value of 114 at 650°C to a maximum value of 598 at 900°C, followed by a second minimum of 214 at 1100°C (Figure 5.10b (i). This is consistent with the pyrolysis extractions of other lunar soils and breccias in this work, and is attributed to the preferential retention of nitrogen when diffusion is the

sole release mechanism. With exception of the combustion and pyrolysis extractions of A63340 (due to high amounts of low temperature contamination), the Apollo 16 soils display $N/^{36}Ar$ ratios which vary from 332 to 934, equivalent to a factor of 9 and 25 times the solar value respectively.

5.3.4. Carbon abundances and C/N ratios for the <10 μm fractions of Apollo 16 soils

The carbon abundances and C/N ratios for the analysis of the <10 μm grain size fractions from the Apollo 16 soils are given in Appendix D1. The carbon release profile and C/N ratios for the stepped combustion of a representative sample, A60501, is illustrated in Figure 5.11, with errors of ±15% for the C/N ratios. The explanation for the use of the combustion data in preference to the pyrolysis data has been given in section 3.3.3.

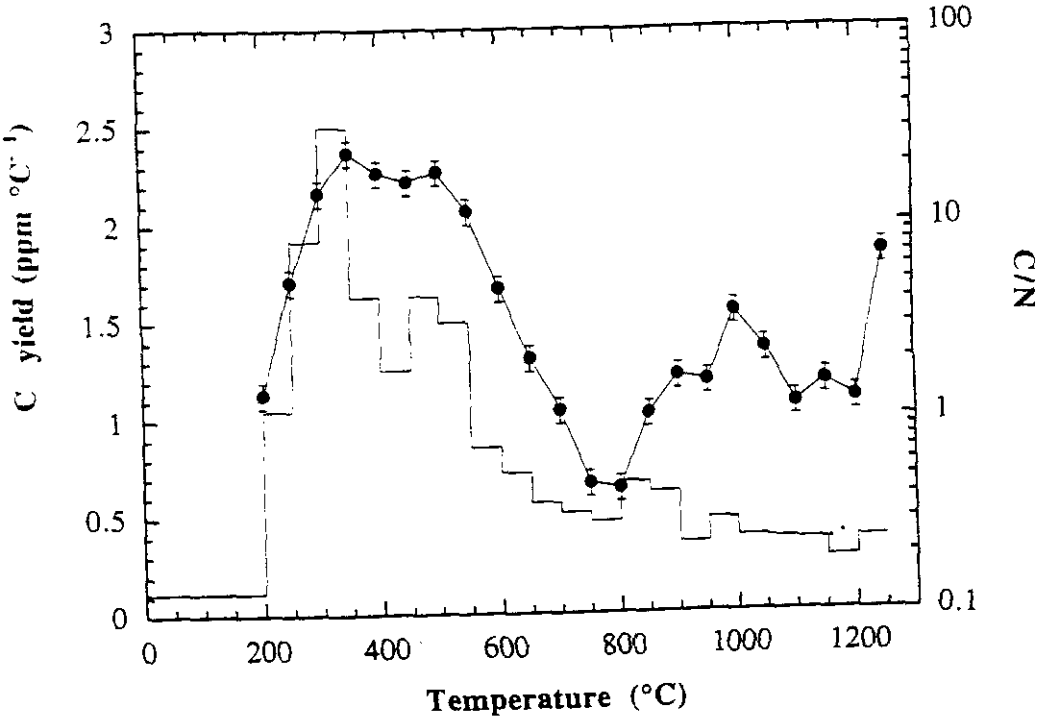

Figure 5.11. C/N ratios and carbon yields (ppm $°C^{-1}$) for the stepped combustion extraction of the <10 μm fraction from A60501.

The stepped combustion extraction of the <10 μm fractions of A60501 (FIN224) liberates 654 ppm of carbon as three release peaks: 200-400°C, 450-750°C and 800-900°C. The former of these peaks (and possibly the second) is attributed to low temperature

contamination as the C/N ratio decreases from ~24 at 350°C to 2.1 at 650°C. None of these peaks can be identified as equivalent to LTN as this is expected to be released between 600-900°C. The C/N ratios also shows considerably more variation than exhibited for the combustion extractions of other lunar soils and breccias in this work (section 3.3.3, 4.3.3 and 4.6.3). However the mean C/N ratio (between 600-1200°C) is 1.75 which is consistent with C/N ratios of 1-2 for other lunar soils and breccias, *e.g.* Holland *et al.* (1972b), and slightly higher than solar photospheric values of 1.1 (Anders and Grevesse, 1989). Note that the pyrolysis extraction of the <10 μm grain size fraction of A60501 liberates 236 ppm carbon with a mean C/N ratio of 1.77. This is due to the removal of low temperature contamination using on-line pre-combustion.

The carbon abundances and C/N ratios compare well with the other Apollo 16 soils analysed in this work. For the stepped combustion extractions, the amount of carbon liberated from the soil ranges from 360 (FIN222) to 2772 ppm (FIN208), although the latter is due to the high amount of contamination for A63340 which accounts for ~80% of the total carbon. The mean C/N ratios from 600-1200°C range from 2.1 (FIN222) to 4.0 (FIN208), although the latter value is due to low temperature contamination, and hence the true upper limit may be 2.8 (FIN202). Note that the C/N ratios from the Apollo 16 soils are intermediate to the solar photospheric ratio of 1.1 and solar system value of ~3.2 (Anders and Grevesse, 1989) and cannot be used to conclusively determine a solar or non-solar origin for the nitrogen.

Comparison of the carbon yields for the <10 μm grain size fractions of A60501 and A12023 (data are given in Appendix B2) reveal that the highland soil liberates a factor of ~2.2 more carbon than the mare soil, with a higher proportion of the total carbon liberated at a temperature of ≤600°C (53% for A60501 compared to 45% for A12023). The mean C/N ratios from 600-1200°C for A60501 are slightly higher than for A12023 with values of 1.75 and 1.1 respectively. Although, the magnitude of the ratios may vary with the other Apollo 16 soils in this study, the general trend is the same. This may be linked to the complex exposure history of A12023 (Becker and Clayton, 1978) compared to the Apollo 16 soils.

5.4. Potassium permanganate pre-combustion as a means of removing low temperature contamination

The potassium permanganate ($KMnO_4$) pre-combustion technique has been described in section 2.8.2, as a means of removing low temperature contamination from a sample, prior to stepped combustion or pyrolysis extraction. The <10 μm grain size fraction of A63340 was selected as a suitable test sample for this technique, as it has been shown (section 5.3.1) to liberate 50-60% of its total nitrogen at a temperature of ≤350°C.

The <10 μm grain size fraction of A63340 (weight = 1.05 mg), was pre-combusted off-line using 0.25 mg of $KMnO_4$, at a temperature of 350°C for 12 days. The pre-combusted sample was then transferred to the extraction system (Figure 2.2) and analysed by stepped combustion using 50°C resolution (FIN250). Extraction by stepped combustion is preferred as it allows a comparison of N_{LT} and ΣN, both with and without the $KMnO_4$ treatment. During the course of the extraction (at a temperature of 650°C), the glass loading section cracked, resulting in vacuum failure, and the experiment had to be aborted. The nitrogen, argon and carbon data obtained up to this temperature are given in Appendix D2 and the nitrogen release and isotopic profile in Figure 5.12a.

	Combustion (≤350°C) (FIN208)	Combustion ($KMnO_4$ @ 350°C) (FIN250)
N (ppm)	200.2	2.11
C (ppm)	1806.0	15.00

Table 5.7. A comparison of the nitrogen and carbon yields (ppm) at a temperature of ≤350°C for the pre-combustion (FIN250) and "ordinary" combustion (FIN208) of the <10 μm fraction of A63340.

Table 5.7 shows that the $KMnO_4$ pre-combustion technique removes 98.9% of the nitrogen and 99.2% of the carbon at a temperature ≤350°C from the sample. However, due to the incomplete extraction there is limited data on the effect (if any) this treatment would have on ΣN, $\Sigma\delta^{15}N$ or the isotopic composition of N_{LT} and N_{MT}. The data are compared to the "ordinary" combustion of the <10 μm fraction of A63340 (Figure 5.12b). Note that

Figure 5.12a and 5.12b are shown on identical axes with the nitrogen yield data plotted on a logarithmic axis to aid comparison.

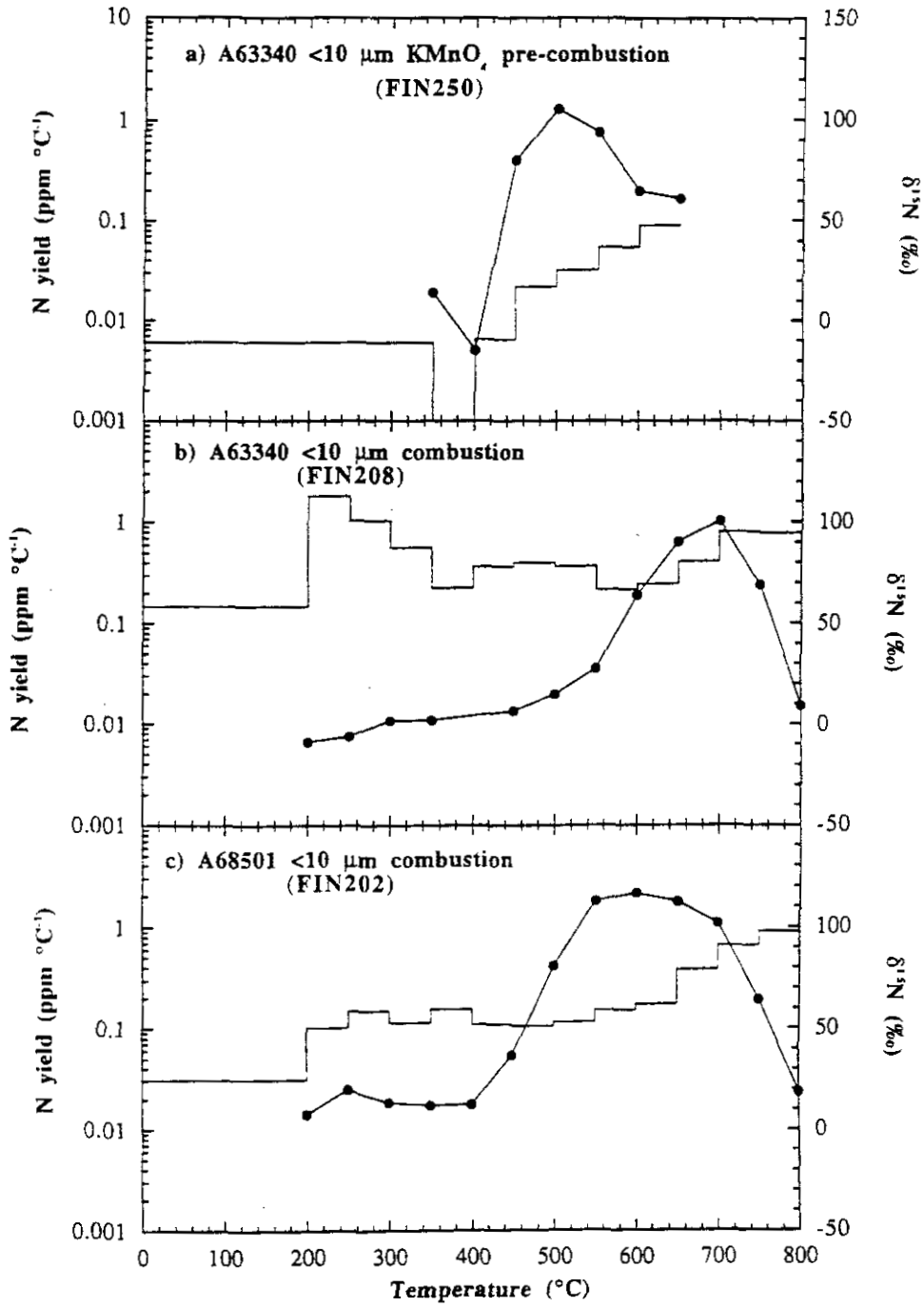

Figure 5.12. Nitrogen yield (ppm $°C^{-1}$) and isotopic compositions (‰) for the $KMnO_4$ pre-combustion (Figure 5.12a) compared to the "ordinary" combustion (Figure 5.12b) of the <10 µm fraction of A63340, and the combustion of the <10 µm fraction of A68501 (Figure 5.12c).

Figure 5.12 (a and b) and Table 5.6 shows that $KMnO_4$ pre-combustion of the soil is an effective means of removing low temperature atmospheric or organic contamination.

Despite the termination of the extraction, prior to the release of the majority of the nitrogen, it can be seen that the LTN release peak would be more pronounced in the pre-combustion (FIN250) compared to the "ordinary" combustion (FIN208). Furthermore the release of N_{LT} is shifted to lower temperature as a result of removal of the contamination and is liberated at a temperature of 500°C for the pre-combustion, compared to a temperature of 700°C for the "ordinary" combustion. However, it should be noted that the isotopic compositions of N_{LT} for *FIN250 and FIN208 are similar with* $\delta^{15}N$ *values of +105.5‰* and +100.4‰ respectively. This suggests that $\delta^{15}N$ value of ~+100‰ may be the true isotopic composition of N_{LT} for A63340. However, during the "ordinary" combustion it is admixed with the low temperature contamination and hence is not liberated until higher temperature. During the $KMnO_4$ pre-combustion, the contamination does not inhibit the release of N_{LT} and hence the latter is liberated at lower temperatures.

A similar temperature effect is observed if the $KMnO_4$ pre-combustion of the <10 μm fraction of A63340 is compared to the combustion extraction of a "cleaner" Apollo 16 soil. The sample chosen for this purpose is the <10 μm fraction of A68501 (FIN202) as it has similar major element chemistry to A63340, and the yield and isotopic profile is shown in Figure 5.12c. The release of N_{LT} for this extraction occurs at a temperature of 600°C, compared to the temperature of 500°C for the pre-combusted sample. This implies that the temperature shift between the treated and untreated sample is still present, but is reduced in magnitude when the comparison sample does not contain excessive amounts of contamination. In addition, the isotopic composition for N_{LT} for FIN202 is $\delta^{15}N$ = +116.6‰, compared to +105.5‰ for the pre-combusted sample but this can be attributed the differing maturity of the two soils, *i.e.* I_s/FeO = 85 (A68501) compared to 80 (A60501). An interesting feature is the rapid decrease of $\delta^{15}N$ for the $KMnO_4$ pre-combustion after the release of N_{LT}. For example, at a temperature of 650°C the $\delta^{15}N$ for the pre-combusted sample has decreased to +61‰, whereas $\delta^{15}N$ = +112‰ for A68501. This suggests that the removal of low temperature contamination may have resulted in an enhancement of the liberation of N_{MT}. Unfortunately, due to the vacuum failure during the extraction it was not possible to determine whether this was the case and extraction was unable to be repeated due to sample availablility.

From the data obtained from the <10 μm fraction of A63340, it appears that $KMnO_4$ pre-combustion is a valid technique which can be used to remove low temperature contamination from a variety of samples. This technique has also been used on an HF/HCl residue from lunar breccia A79035 and the results are discussed in section 4.4.3. It should be stated that at present no tests have been carried out as to the optimum amount of $KMnO_4$ that should be used, the appropriate extraction temperature or the length of time that pre-combustion should be performed. These parameters are likely to vary between different types of lunar samples, depending on the low temperature carbon content and the ease of extraction of the component from the sample. Preliminary results obtained in this work suggest that a lower pre-combustion temperature and a shorter pre-combustion period may be preferable for the analysis of some lunar soils and breccias. In addition, further tests should be performed to determine the effects of pre-combustion on the abundance, isotopic composition and release temperature of nitrogen components in lunar soils, rocks and breccias.

5.5. Discussions of results

The <10 μm grain size fractions from four Apollo 16 highland soils (A60501, A63340, A64421 and A68501) in this work exhibit similar ΣN and $\Sigma\delta^{15}N$ values. In general, the samples contain between 238 and 330 ppm nitrogen with a range of $\Sigma\delta^{15}N$ from +14.7 to +29.6‰. The range of abundances and isotopic compositions is believed to be associated with minor differences in the major element chemistry and petrology and the differing exposure histories of the samples (Table 5.1).

One exception to the results summarised above is the <10 μm fraction of A67701, which contains significantly less nitrogen than the other extractions (150-201 ppm) with $\Sigma\delta^{15}N \approx +44$‰, approximately 20‰ higher than the other extractions. Despite the possibility that the sample may have incorporated lunar rock material when collected, it appears that the low nitrogen content and high $\Sigma\delta^{15}N$ is due to its low maturity (I_s/FeO = 39) and ^{21}Ne-exposure age (49 Myr) compared to the other Apollo 16 soils ($I_s/FeO \approx 80$ and ^{21}Ne-exposure age ≈ 100 Myr). Note that this is also reflected in the low agglutinate content of A67701 (16%) compared to typical Apollo 16 soils (40-50%).

The nitrogen abundances and isotopic compositions obtained for the combustion and pyrolysis extractions of the <10 μm fraction from Apollo 16 soils have shown some similarities with the equivalent fraction from A12023 (section 3.4.2.2). The majority (>70%) of the nitrogen and argon is liberated as a single release (LTN) across a temperature range of 600-900°C. However, the <10 μm fraction of A12023 liberated >90% of the total as LTN. The $^{36}Ar/^{38}Ar$ ratios for all analyses display a similar trend to that observed for noble gas studies of lunar soils (section 1.7.5.2) consistent with a solar origin for ^{36}Ar. During combustion extractions, the $N/^{36}Ar$ ratio remains constant with mean values ranging from 424 to 1444 (although the latter is due to a large amount of low temperature contamination). This is equivalent to 11.5 to 39 times the solar value of 37 (Anders and Grevesse, 1989). Comparison of the nitrogen and ^{36}Ar yield profiles during pyrolysis extractions suggest that the nitrogen is preferentially retained when diffusion is the sole release mechanism. A similar phenomenon has been observed for all soils and breccias in this investigation. Furthermore the $^{40}Ar/^{36}Ar$ ratios in all extractions of the Apollo 16 soils are essentially constant across the release of LTN with a mean value ranging from 0.61 to 1.77. An exception to this is the initial few steps of the extraction where the $^{40}Ar/^{36}Ar$ are higher due to the re-implantation of atmospheric ^{40}Ar. However, the surface location of non-solar ^{40}Ar places a major constraint when invoking a recent solar wind origin for N_{LT} as postulated by the secular variation model for the $\delta^{15}N$ variation in the lunar regolith (section 1.7.4.1).

The mean C/N ratios for the Apollo 16 soils range from 2.1 to 2.8 across a temperature range of 600-1200°C. This is intermediate to the solar photospheric and solar system values of ~1.1 and ~3.2 respectively (Anders and Grevesse, 1989) and hence do not conclusively confirm a solar or non-solar origin for the carbon or nitrogen.

Analysis of the <10 μm fractions from Apollo 16 soils have shown that HTN is essentially absent in the finest grain sizes of lunar highland soils. This confirms the data obtained from a similar grain size study from lunar soil A12023 (section 3.4.2.2) that HTN is released from complex secondary particles at a temperature of ≥1050°C. In addition, it detracts from the suggestion (Becker & Clayton, 1975) that the isotopically light nitrogen is attributed to the ancient solar wind and liberated from the fossil surfaces of the sample. Recent observations (Kerridge *et al.*, 1993; Norris *et al.*, 1983) and the current study

(section 3.5) also show that agglutinates and complex particles are not the host of the isotopically light nitrogen.

The low temperature, isotopically heavy nitrogen component, N_{LT}, is released in all samples at a temperature of 550-700°C (with the exception of A63340), regardless of extraction method used. The isotopic composition of this component ranges from +105‰ to +150‰. For A63340, N_{LT} is liberated at a temperature of 700°C for the combustion and 750°C for the pyrolysis extractions with $\delta^{15}N$ values of +100‰ and +82.7‰ respectively. The high temperature of the release and the low $\delta^{15}N$ value (especially for the pyrolysis) is indicative of the presence of a significant (~50%) amount of low temperature contamination in the sample. In general, the combustion extractions reveal a 50°C shift to lower temperature for N_{LT} compared with the pyrolysis extractions. This substantiates the observations for A12023, whereby the release temperature of N_{LT} during combustion was up to 150°C lower than during pyrolysis, although part of this may have been due to inappropriate blank corrections. The shift to lower temperature does not appear to be linked to the variety of temperature increments utilised in the extractions of A12023. It should also be noted that N_{LT} in Apollo 16 soils does not exhibit any correlation with accepted parameters of exposure, *e.g.* I_s/FeO or ^{21}Ne exposure age (Figure 5.7b abd 5.8b), and is indicative of a uniform, non-exposure related origin. This component is not related to the solar wind exposure history of the samples, but may be linked to the initial regolith formation ages at the two Apollo sites.

The combustion analyses of the <10 μm fraction from Apollo 16 soils liberate the light nitrogen component (N_{MT}) at a temperature of 800-850°C, which is consistent with the soil and breccia samples from other sites. In contrast to other analyses in this work, the pyrolysis extractions reveal only a single nitrogen $\delta^{15}N$ minimum, which is released at a temperature of 1000-1050°C (equivalent to N_{HT}). The proportion of the light nitrogen, observed as N_{MT} in pyrolysis extractions of other lunar soils and breccias, is not present. It may be that 50°C temperature resolution in these extractions is not sufficient to reveal the presence of N_{MT}, if it is a minor component, hence it may have been masked by the higher temperature release of N_{HT}. This indicates that the carrier of N_{MT} may be constituent minerals such as ilmenite, olivine or pyroxene, which are depleted in highland soils relative to mare soils. These minerals, especially ilmenite, has been shown to retain nitrogen and

noble gases with the highest efficiency (Signer *et al.*, 1977; Frick *et al.*, 1988; Kerridge *et al.*, 1991b

Previous workers (Kerridge *et al.*, 1977) have shown that there is a positive trend between nitrogen abundance and I_s/FeO and an inverse correlation between $\Sigma\delta^{15}N$ and ^{21}Ne-exposure age in Apollo 16 soils. However, due to the limited number of data points a similar correlation cannot be conclusively confirmed for this study. A weak correlation does exist for nitrogen content against I_s/FeO, and for $\delta^{15}N$ of N_{HT} against maturity parameters. In addition, an inverse correlation had also been observed (Kerridge *et al.*, 1975b) between $\Sigma\delta^{15}N$ and Fe^0 content of the sample. The Fe^0 content is in excess of that expected from the ancient meteorite contribution of 5.5 wt.% Ni (section 1.6.4) and has been attributed to the reduction of indigenous Fe^{2+} by solar wind hydrogen, hence is related to the maturity of the soil. The investigation into the relationship between N_{HT} and Fe^0 content tentatively confirm the trends observed by Kerridge *et al.* (1975b). Initial results indicate a weak trend between $\delta^{15}N$ of N_{HT} against the Fe-metal content of the Apollo 16 soils, despite the fined grained nature of the samples. However, the data cannot be taken as conclusive due to the limited number of data points obtained in this study. A more extensive investigation will need to be carried out to determine whether this component can be fully attributed to fine grained Fe-metal.

Finally, the pre-combustion technique using potassium permanganate as the provider of oxygen has proved a valuable method for removing significant amounts of low temperature contamination from a lunar soil. However, the rapid decrease in the $\delta^{15}N$ values, after the liberation of N_{LT} has indicated that this treatment may also have removed a proportion of the indigenous nitrogen from the sample. Unfortunately, this was not proved conclusively in this study due to a vacuum failure during the extraction. Further tests still need to be performed to determine optimum parameters, but preliminary results show that this technique will not affect the isotopic composition of the nitrogen components within the soils.

5.6. Conclusions

The data obtained in this study have shown some similarities and differences between the <10 μm grain size fractions from Apollo 12 and Apollo 16 soils. The bulk of the nitrogen is released as LTN (80-85% of the total), across a temperature range of 600-900°C and the $^{36}Ar/^{38}Ar$ and C/N ratios may indicate a solar wind origin for the nitrogen. However, the $N/^{36}Ar$ ratios exceed by a factor of at least 12 the solar value of 37 (Anders and Grevesse, 1989). Despite the constant $N/^{36}Ar$ ratios during stepped combustion extraction, a solar origin cannot be invoked for all the nitrogen as the $^{40}Ar/^{36}Ar$ ratios are also constant across a similar temperature range. The Apollo 16 soils also reveal that, during pyrolysis extraction, the nitrogen is preferentially retained compared to ^{36}Ar, by approximately 50°C, although during combustion, both are liberated conjointly. The observation of this phenomena during pyrolysis at three Apollo sites in this work confirms that this is an artefact of the extraction procedure. The results are comparable with the results obtained from all other soils and breccias in this study. In addition, as with the <10 μm fraction from A12023, the HTN component is missing, which confirms the conclusions from this work that this component is associated with the nitrogen contained within complex particles, such as agglutinates. These results detract from the secular variation of $^{15}N/^{14}N$ in the solar convective zone as proposed to explain the isotopic variation observed in lunar soils and breccias (section 1.7.4.1).

The liberation of N_{LT} is shifted to lower temperature by ~50°C during combustion extraction of the <10 μm fraction of Apollo 16 soils. This is less than the temperature shift of ≈150°C for the equivalent fraction from A12023 (section 3.4.2.2), although the latter may be due to inappropriate blank corrections. The temperature shift for N_{LT} indicates that a proportion of this component may be in chemically bound form, but the mechanism for this has not yet been identified. The isotopic composition of N_{LT} for the Apollo 16 soils is not dependent on the maturity of the sample or its exposure to the solar wind

The pyrolysis extractions of the <10 μm fractions from Apollo 16 soils liberated a single light nitrogen (N_{HT}) component at a temperature of 1050°C. The absence of N_{MT} in the pyrolysis extraction has been attributed to the depletion of minerals, such as ilmenite and pyroxene, in the highland soils and hence the masking of N_{MT} by the liberation of N_{HT}.

There is a weak correlation between $\delta^{15}N$ of N_{HT} with known maturity parameters, such as I_s/FeO and ^{21}Ne exposure age, which substantiates the trends of nitrogen abundance and isotopic composition with maturity observed by previous workers, *e.g.* Kerridge *et al.* (1977). A weak correlation has also been observed in the current study between $\delta^{15}N$ of N_{HT} and content of metallic iron (Fe^0) for the Apollo 16 soils, which is similar to nthat observed for $\Sigma\delta^{15}N$ and Fe^0-content (Kerridge *et al.*, 1977). This may imply that N_{HT} is due to the reduction of Fe^{2+} to metallic iron by solar wind hydrogen. However, the data set used in this work is limited and hence the suggestion is tentative.

The data obtained from the <10 μm fraction of Apollo 16 soils have shown that there are many similarities in the nitrogen abundance and isotopic composition with the equivalent fraction for lunar soil A12023. The differences in the isotopic profile and composition of nitrogen within the Apollo 12 and 16 soils are primarily due to the differing mineralogy and petrology at the two sites, and the contrasting exposure histories of the soils.

Chapter 6

Discussion of lunar nitrogen components and isotopic variation in the lunar regolith.

6.1. Introduction

Although all workers agree that the majority of noble gases (with the exception of ^{40}Ar) in the lunar regolith originates from the solar wind, there is still much dispute over the origin of the nitrogen and the explanation for the observed nitrogen isotopic variation. The lunar soils and breccias analysed in this study liberate between 30 to 330 ppm nitrogen with $\Sigma\delta^{15}N$ values ranging from -185 to +45‰, constituting an isotopic variation of 23%. The isotopically heaviest ($\delta^{15}N$ = +160‰) and lightest nitrogen ($\delta^{15}N$ = -228‰) components observed in this work, constitute an isotopic variation of ~38%. Both of these values lie within the range of 20-50% observed by previous workers (section 1.7.4.1). However, the major problem encountered when attempting to interpret the observed isotopic variation is that no equivalent magnitude of variation is observed for any other solar wind isotopic ratio, *e.g.* only a 3% variation is exhibited for $^{20}Ne/^{22}Ne$ (Benkert *et al.*, 1993). This implies that any process(es) undergone by nitrogen to cause the observed variation does not appear to have affected other solar wind compositions to the same degree.

Two models have been invoked by previous workers to explain the variation in nitrogen isotopic compositions. The solar wind variation model advocates a secular increase of $^{15}N/^{14}N$ of 20-50% in the solar convective zone over the lifetime of the regolith. Using this model, the individual nitrogen isotopic components in lunar soils and breccias represent different generations of solar wind implantation (section 1.7.4.1). The second model invokes isotopic mixing between the solar wind and one (or more) non-solar components (section 1.7.4.2). This has been derived from the observation of "excess" nitrogen in the regolith (section 1.7.2.2), with $N/^{36}Ar$ ratios a factor of 10 higher than the solar value of 37 (Anders and Grevesse, 1989). Possible candidates for the non-solar component(s) are indigenous lunar nitrogen (Becker and Clayton, 1975), a fractionated lunar atmosphere (Ray

and Heymann, 1982), primitive meteoritic nitrogen (Norris *et al.*, 1983) and terrestrial atmospheric nitrogen implanted into the regolith by acceleration in the magnetosphere (Geiss and Bochsler, 1991). However, there is much dispute as to the number of components which have combined to produce the isotopic variation, and the proportion of the total nitrogen which is of a non-solar origin (Kerridge *et al.*, 1992a; Bochsler, 1994; Wieler *et al.*, 1999). Recent estimates (Wieler *et al.*, 1999) have suggested that ~90% of regolith nitrogen is of non-solar origin.

It should be noted that the advocators of each model have more convincing arguments against the opposing hypothesis, than in defence of their own theories. On these grounds no model can be said to have survived criticism and the current dispute remains unresolved. One of the major obstructions in resolving this problem is the absence of spacecraft measurement of the $^{15}N/^{14}N$ ratio in the recent solar wind and the large uncertainties associated with this ratio for solar flares (Mewaldt and Stone, 1989). This implies that the composition of the recent solar wind has to be inferred from a correlation of sample isotopic composition with surface exposure age and hence is subject to significant errors.

It should be noted that all workers agree on the origin of the low temperature (<600°C) nitrogen and high temperature, isotopically heavy nitrogen (>1100°C) component, liberated by stepped heating extractions of lunar soils and breccias. The former is attributed by all workers to the presence of terrestrial contamination with a "normal" isotopic composition, *i.e.* ~0‰. The latter is attributed to the liberation of spallogenic nitrogen, produced from cosmic-ray interaction with oxygen and which is enriched in ^{15}N. The former is omitted from this discussion, whereas the spallogenic nitrogen component (section 6.3.3) is discussed with reference to the data obtained in this work.

This chapter discusses the data obtained in this study in the light of the current theories surrounding the origin and isotopic variation of nitrogen in the lunar regolith. Several comparisons are made between this work and those of previous workers in an attempt to determine the cause of the isotopic variation. The differences observed in the isotopic profiles between the two extraction techniques are detailed as a means to constraining the location of nitrogen within the regolith.

6.2. The origin of the nitrogen in the lunar regolith

The data obtained in this work suggests that the solar wind is a significant contributor to the nitrogen inventory in the lunar regolith. However, on the basis of this investigation, the solar wind (SW) or higher energy solar energetic particles (SEP) are unable to account for all of the nitrogen in the regolith.

6.2.1. Evidence for a solar origin for the nitrogen in the lunar regolith

The main arguments in favour of a solar origin for the nitrogen are as follows:

1). The relatively high abundance of nitrogen in lunar soils and breccias (typically 100-150 ppm), compared to lunar rocks (typically <1 ppm) suggest that the majority of nitrogen is not indigenous to the Moon (Müller, 1974; Becker and Clayton, 1975). In addition to meteorite bombardment (section 1.6.4), sputtering, due to the interaction between solar wind ions and target elements in the regolith, is one of the major causes of erosion on the lunar surface (section 1.6.1.1). Furthermore, the observation of amorphous rims around soils grains has also confirmed the contribution of the solar wind to the lunar surface (section 1.6.1.2). The observation of solar noble gases, *i.e.* H, He, Ne and ^{36}Ar, in the lunar atmosphere (section 1.5.1), and the depletion of many of these elements in lunar rocks, suggests that a similar origin may be likely for at least some of the nitrogen.

2). A significant proportion, ranging from 58% to 92% of the total nitrogen is released across a temperature range of 600-900°C (LTN) for the stepped combustion and pyrolysis extractions, indicative of a surface location for this component. Furthermore, a suite of grain size separates from a typical lunar soil, A12023 (section 3.4.1), verified the grain size correlation with nitrogen content, with the highest yields obtained for the finest (<10 μm) size fraction. However, a plot of log ΣN (ppm) against log r^{-1} (μm), where r = grain size, displays a gradient of -0.6 (Figure 3.8 and section 3.4.1), compared to a gradient of -1 if all the nitrogen was surface correlated. This implies that approximately 60% of the nitrogen is surface correlated, with the remainder located within composite particles. However as will

be discussed in section 6.2.2, the surface siting of the nitrogen does not conclusively confirm a solar origin. Across the release of LTN, the C/N ratios typically remain constant, with mean values ranging from 0.7 to 3.7. The upper limit of this range has been observed in regolith breccia A79035, and for agglutinate breccia A70019, whereas lunar soils typically reveal an upper limit of ~2.5. The C/N ratios (across the release of LTN) are similar to the values of ~1.1 for the solar photosphere and corona (section 1.7.6.2).

3). Previous workers (Kerridge *et al.*, 1977) have shown a correlation between nitrogen abundances and isotopic composition, with maturity parameters, such as I_s/FeO and ^{21}Ne-exposure age, for Apollo 16 soils (section 5.3.2). Furthermore, they have shown a correlation between $\Sigma\delta^{15}N$ and Fe^0-content of the sample (Figure 5.9a). The latter is due to the reduction of indigenous Fe^{2+} by solar wind hydrogen, and hence confirms that the nitrogen inventory in the regolith is dependent on the solar wind exposure history. However, the current study has only revealed a weak correlation between $\delta^{15}N$ of N_{HT} with Fe^0, due to the limited number of samples analysed (Figure 5.9b), and cannot substantiate the conclusions of Kerridge *et al.* (1977). This is discussed further in section 6.2.2.

4). Nitrogen and ^{36}Ar in lunar soils and breccias are liberated conjointly during stepped combustion extraction, and hence the N/^{36}Ar ratios remain constant. This suggests that the nitrogen originates from the same source as ^{36}Ar, *i.e.* the solar wind. The variation in the N/^{36}Ar ratios during stepped pyrolysis extractions has been interpreted as due to the preferential retention of chemically bound nitrogen (to higher temperature by ~50°C) during pyrolysis extraction, where diffusion is the sole release mechanism. Note that this does not account for the "excess" nitrogen in the regolith (section 1.7.2.2) which is discussed in section 6.2.2. Interestingly at high temperatures (>1000°C) the N/^{36}Ar profiles are similar for both extraction techniques, which may signify the less pronounced effect of oxygen with increasing temperature (section 3.4.2.1).

6.2.2. Evidence for a non-solar origin for the nitrogen in the lunar regolith

There are several problems associated with the arguments discussed in section 6.2.1, which suggest that the solar wind is not the sole contributor of nitrogen to the lunar regolith.

The major problem when advocating a solar origin for lunar regolith nitrogen is that the $N/^{36}Ar$ in lunar soils and breccias exceed by a factor of ~10 the solar value of 37 (section 1.7.2.2). The mean $N/^{36}Ar$ ratios in all analyses in this investigation vary from 173 to 1444, equivalent to a range of 5 to 39 times the solar value, consistent with a range of 4 to 440 for single ilmenite grains from lunar soil A71501 (Humbert *et al.*, 1997). A recent suggestion (Becker and Pepin, 1994) was that the solar $N/^{36}Ar$ value had been underestimated by a factor of 10, although measurements of the $N/^{36}Ar$ ratio in solar energetic particles of 45 ± 8 (Brenemann and Stone, 1985) suggest that this is not the case (section 1.7.2.1). This implies that either non-solar nitrogen has been added to the lunar regolith, or ^{36}Ar has been lost (section 1.7.2.1). In the former suggestion at least 90-95% of nitrogen must be of a non-solar origin to produce the observed excess. In the latter, 90% of ^{36}Ar and heavier noble gases would have to be lost by diffusion. Furthermore, the similarity of the mean C/N ratios across LTN in the current study, with the solar photospheric and coronal values (point 2 in section 6.2.1) suggests that the latter may be correct. However, the variation of the C/N ratios in single extraction steps may be indicative of the contribution of non-solar nitrogen (or carbon) into the soil or breccia grains. Although the explanation for the "excess" nitrogen in the regolith is not clear from this study, with the assumption of a solar $N/^{36}Ar$ value, it seems unlikely that either of the two explanations, *i.e.* addition of 90% non-solar nitrogen or loss of 90% of ^{36}Ar, can exclusively account for the observed $N/^{36}Ar$ ratios in lunar soils and breccias.

A further problem is that the surface location of the nitrogen in lunar soil grains is not conclusive proof of a solar wind origin. This has been confirmed in this work by the conjoint liberation of nitrogen, ^{36}Ar and ^{40}Ar, and the constant $^{40}Ar/^{36}Ar$ ratios in stepped combustion and pyrolysis extractions of both lunar soils and breccias (section 3.3.2, 4.3.2, 4.6.2 and 5.3.3). The mean $^{40}Ar/^{36}Ar$ ratios in this study ranges from 0.7 to 3.3, within the range of 0.4 to 14 for lunar soils and breccias (Kirsten *et al.*, 1973; Reynolds *et al.*, 1974). The ^{40}Ar is clearly surface correlated, but has been shown to be re-implanted into the regolith from the lunar atmosphere, by solar wind ionisation (section 1.6.1.3). As the ^{40}Ar originates from the radioactive decay of ^{40}K, it is not of a solar origin. The constant $^{40}Ar/^{36}Ar$ ratios implies that a solar origin for the nitrogen cannot be invoked solely on the basis of the constant $N/^{36}Ar$ ratios. However, both the $^{40}Ar/^{36}Ar$ and $N/^{36}Ar$ ratios are

higher than the mean in the initial few steps of each extraction in this study. For the $^{40}Ar/^{36}Ar$ ratios, this has been interpreted as re-implanted atmospheric ^{40}Ar, and it may be possible that similar processing has occurred for nitrogen. The current investigation suggests that the initial release of $^{40}Ar/^{36}Ar$ and $N/^{36}Ar$, may be due to recently re-implanted atmospheric species, which have not yet diffused into the soil grains. At progressively higher temperature, the recently re-implanted ^{40}Ar mixes with earlier re-implanted ^{40}Ar, or indigenous ^{40}Ar (possibly diffusing towards the surfaces of soil grains following radioactive decay of ^{40}K) to produce the observed trends. A similar effect may be occurring for nitrogen, with mixing between recently re-implanted atmospheric nitrogen and nitrogen previously implanted (either from the solar wind or non-solar sources, or both) into soil grains. An interesting observation is that for regolith breccia A79035, the $^{40}Ar/^{36}Ar$ and $N/^{36}Ar$ ratios show little mixing in the initial few steps of the extraction, compared to lunar soils. This is believed to be due to the exposure history of the breccia, and hence the nitrogen residing on the grain surface represents implanted gases since consolidation. The possibility of re-implanted atmospheric nitrogen in the lunar regolith is discussed further in section 6.4.4, in conjunction with the isotopic composition of N_{LT}.

Further evidence for non-solar nitrogen in the lunar regolith is the Fe^0-content of lunar soils. Although the aforementioned discussion (point 3 in section 6.2.1) has revealed a correlation between $\delta^{15}N$ and Fe^0-content, it has been shown that a proportion of the Fe^0 (~5.5 wt.% Ni), is due to meteorite impacts on the lunar surface (Goldstein and Axon, 1973). Furthermore, studies of siderophile elements has shown that meteorites contribute 1-2% carbonaceous chondrite material into the lunar regolith (Ganapathy *et al.*, 1970; Wasson and Baedecker, 1970). These observations have been discussed in section 1.6.4, and a search for presolar diamond in lunar breccia A79035 in the current study is summarised in section 6.4.2, in conjunction with the isotopically light nitrogen component.

An additional problem with invoking a solar origin for lunar nitrogen is that the magnitude of $\delta^{15}N$ variation (38% in this work), both between individual samples and within a single analysis, significantly exceeds the variation exhibited by solar noble gases, *e.g.* $^{20}Ne/^{22}Ne$. If a solar origin for the nitrogen is to be invoked, this implies that either the magnitude of the nitrogen variation is incorrect, or a mechanism is required which affect the

nitrogen isotopic composition without affecting the noble gases. Furthermore, the variation of $\delta^{15}N$ in the regolith cannot be accounted for by current solar models (section 1.7.6.2).

In conclusion, from the data obtained in this investigation, the nitrogen in the lunar regolith cannot be exclusively attributed to a solar or non-solar origin. The observations suggest that both sources are likely to have played a significant role in producing the familiar nitrogen release and isotopic profile in lunar soils and breccias, although the proportion of solar and non-solar nitrogen is not clear. It should be noted that determining the origin and location of implanted nitrogen (and other elements) components in the lunar regolith is extremely difficult due to the constant modification of the regolith by gardening processes. This has resulted in the masking, if not obliteration, of many of the effects of surface exposure, and complicated the lunar nitrogen inventory due to diffusion of the implanted gases into or out of constituent soil grains.

6.3. Secular variation of the solar wind

Advocators of a solar origin for the nitrogen in the lunar regolith, have suggested that the $\delta^{15}N$ variation is due to a secular increase in $^{15}N/^{14}N$ of 20-50% in the solar convective zone over the lifetime of the regolith (section 1.7.4.1). These workers have attributed the low temperature (600-900°C), isotopically heavy nitrogen to implanted recent solar wind, located on the grain surfaces of lunar minerals, and the higher temperature (900-1000°C), isotopically light nitrogen component to the ancient solar wind, previously implanted on the surface of soil grains but since incorporated into complex particles, such as agglutinates and microbreccias, due to regolith gardening processes.

This investigation shows unambiguously that LTN (constituting 58 to 92% of the total nitrogen) in lunar soils is a mixture between two components: an isotopically heavy component N_{LT}, and isotopically light nitrogen N_{MT}. The isotopic compositions of these components are not well constrained, and no release peaks can be identified to correspond to the end-member compositions. The observation of N_{LT} and N_{MT} in the finest grain size fraction of A12023 are the closest that this investigation has come to resolving the two components and the absence of complex secondary particles (although fine-grained

agglutinates may be present) in this size fraction suggests that both components are surface-correlated.

6.3.1. Nitrogen isotopic composition of the recent solar wind

The nitrogen isotopic composition of the recent solar wind has been estimated as $\delta^{15}N \approx +110‰$ from the low temperature, isotopically heavy component in lunar soils by stepped pyrolysis (Becker and Clayton, 1977) and BrF_5 etching (Becker *et al.*, 1976). However, Kerridge (1993) acknowledges the difficulty of accurately constraining the composition of the recent solar wind without the aid of spacecraft measurements. Recent studies of a plagioclase separate from immature soil A67601 (exposure age = 49 Myr) and lunar rock A68815 (exposure age = 2 Myr) have led to an estimate of $\delta^{15}N = +38 \pm 6‰$ for the recent solar wind (Kim *et al.*, 1995). These workers have suggested that the solar wind has undergone two isotopic extremes: the first to a minimum of <-280‰ (~2-2.5 Gyr ago) followed by a maximum of >+160‰ (~1 Gyr ago) and is currently ~+40‰.

The variety of lunar soils analysed in this work display $\delta^{15}N$ values for N_{LT} which range from +37 to +229‰, although the latter is subject to significant blank corrections (section 3.3.1.2). A more realistic upper limit from this study may be +160‰. The whole-soils and <10 μm grain size fractions display a range of $\delta^{15}N$ values for N_{LT} typically from +100 to +140‰, which is liberated at a temperature of 500-650°C. The composition of N_{LT} compares well with previous estimates, *e.g.* Becker and Clayton (1977). However, the similarity of $\delta^{15}N$ for N_{LT} from the whole-soils and <10 μm fractions from three sites in this work suggests that there may be a common origin for N_{LT} in the lunar regolith. In addition there is no correlation between $\delta^{15}N$ for N_{LT} and maturity parameters (section 5.3.2), which implies that the isotopic composition of this component is independent of solar wind exposure history, and may be linked to the formation ages of the regolith at the various landing sites.

As has previously been discussed (section 6.2.2), there is no observed nitrogen release associated with N_{LT}, and both N_{LT} and N_{MT} appear to be end-member components for isotopic mixing across LTN. With the assumption that LTN is solar in origin and surface-correlated, the weighted average $\delta^{15}N$ across this component can be determined as

an estimate of the present-day solar wind. This calculation has been undertaken for all pyrolysis extractions of the whole-soil and <10 μm grain size fractions in this work (as these liberate >70% of the total nitrogen as LTN). The pyrolysis extractions are used in preference to the combustions, as the release of N_{LT} occurs at the start of the liberation of LTN. This study suggests that the isotopic composition of the recent solar wind is $\delta^{15}N$ = +35.1 ± 13.6‰, which is similar to the estimate of +38 ± 6 by Kim *et al.* (1995b). However, this implies that an alternative explanation is required to account for the $\delta^{15}N$ of of N_{LT} of +100 to +140‰, as observed for whole-soil and <10 μm fraction studies in this work (section 6.4.4 and section 6.4.5).

6.3.2. Composition of the ancient solar wind

The workers who advocate a secular variation of the solar wind have suggested that the isotopically light nitrogen in the lunar regolith is attributed to implanted ancient solar wind, which resides in complex particles such as agglutinates and microbreccias. Early stepped heating extractions (Becker and Clayton, 1975, 1977; Becker *et al.*, 1976) of lunar soils estimated that this component has a $\delta^{15}N$ value of -105‰. In accordance with this model, an agglutinate or microbreccia fraction would be expected to liberate isotopically light nitrogen with a minimal contribution of isotopically heavy nitrogen. Conversely, a pure mineral fraction of a lunar soil, *i.e.* plagioclase, would be expected to reveal low temperature, isotopically heavy nitrogen but little of the light component as the nitrogen would primarily reside on grain surfaces.

6.3.2.1. The mineral and density separates data

The data obtained in this work from the study of density and magnetic separates of the 106-152 μm grain size fraction from soil A12023 (section 3.5) do not correlate with the expected results from the secular variation model. The isotopically heaviest $\delta^{15}N$ value for N_{LT} was observed for the agglutinate (ρ<2.96, M3.5) and microbreccia (2.96<ρ<3.3, M2.0) fractions, with measured $\delta^{15}N$ values of +91 and +58‰ respectively. In addition, no significant isotopically light nitrogen (N_{MT} and N_{HT}) was observed in these fractions

with $\delta^{15}N$ values of +2 and -17‰ obtained for the agglutinate and microbreccia fraction respectively. Furthermore, the pure mineral fractions ($\rho<2.96$ NM) and ($2.96<\rho<3.3$ NM) did not reveal the presence of N_{LT}, comparable with postulated recent solar wind estimates (~+110‰), with $\delta^{15}N$ values of +37 and +46‰ obtained for the plagioclase and interwoven plagioclase/pyroxene grains respectively. Interestingly, the isotopically lightest nitrogen obtained for the magnetic and density separates in this work, were obtained for N_{MT} in the plagioclase fraction with $\delta^{15}N$ = -76‰. However, as discussed in section 3.5, the isotopic measurements for the pure mineral, non-magnetic fractions are subject to large blank corrections due the low yields of nitrogen (7-15 ppm) liberated from these separates.

Despite these uncertainties, the analyses of the magnetic and density separates clearly illustrate that the complex particles are not the host of the isotopically light nitrogen in lunar soils and breccias. The samples studied in this investigation suggest that, at the temperature at which complex grains are melted and release the nitrogen trapped within composite particles, the isotopic composition is always higher than lightest isotopic composition, *i.e.* N_{HT}. The conclusion must be that the lowest $\delta^{15}N$ are located somewhere at the surfaces of grains. This result has been confirmed independently (Norris *et al.*, 1983), from the study of agglutinates from A12023 which showed that the nitrogen was not isotopically lighter than the parent sample from which it was separated. The $\delta^{15}N$ for the agglutinate fraction varied from +30 to +64‰ throughout the extraction, compared to +13 to +83‰ for the bulk sample. In addition, a study of agglutinates separated from lunar breccia, A79035, yielded light nitrogen with $\delta^{15}N$ = ~-180‰, compared to the bulk sample $\delta^{15}N$ of -243‰ (Kerridge *et al.*, 1993). These results contradict the secular variation model and indicate that the complex particles are not the host for the isotopically light nitrogen.

6.3.2.2. The grain size separates data

The study of a suite of grain size separates from A12023 in this study have confirmed the trends observed by previous workers (Goel and Kothari, 1972; Holland *et al.*, 1972a; Müller, 1974) who postulated an increase in ΣN and a decrease in $\Sigma\delta^{15}N$ with decreasing grain size. This implies that the finest grain sizes would be expected to contain the highest abundance of nitrogen and the lowest $\Sigma\delta^{15}N$.

The data obtained in this work (section 3.4.1) indicates a clear inverse correlation between nitrogen content and grain size, with an estimated mean grain size for whole-soil A12023 of 10-40 μm. The variation of $\Sigma\delta^{15}N$ with grain size is less obviously systematic. In addition the proportion of nitrogen liberated as LTN shows an inverse correlation with grain size, such that the finest fractions yield >90% of the total nitrogen across this release, and an increasing proportion of the total nitrogen liberated as HTN (with increasing grain size). The minimal contribution of HTN in the <10 μm fraction has also been confirmed by the study of five Apollo soils (section 5.3.1). This implies that the liberation of LTN and HTN is linked to the relative surface:volume ratio of the soil. Hence, the <10 μm fraction would be expected to contain significantly less of the volume-correlated component than the >1 mm fraction. The logical extension of this argument results in the conclusion that HTN predominantly consists of the volume-correlated component, such as glass-welded agglutinates or microbreccia. This can only be liberated from the sample during melting at temperatures of >1050°C, equivalent to that for glass of similar composition to Apollo 12 basalts. This work has observed in lunar soil A12023 (section 3.3.2.1 and 3.4.1) that across the release of HTN, the $\delta^{15}N$ value increases rapidly to higher values. Prior to this increase, the $\delta^{15}N$ values reach a plateau, *e.g.* Figure 3.3a (1100-1200°C), with $\delta^{15}N$ values similar to the $\Sigma\delta^{15}N$ for the whole-soil (Brilliant *et al.*, 1994). Table 3.11 has compared the weighted average $\delta^{15}N$ across the release of HTN, with the $\Sigma\delta^{15}N$ for the agglutinate separate and estimated that the $\delta^{15}N$ of the ancient solar wind is +27.0 ± 6.0‰. The ancient solar wind component constitutes >80% of the total nitrogen liberated at a temperature of >1050°C. Hence, the current observations further contradicts the isotopically light nature of the ancient solar wind as proposed by the secular variation model.

6.3.3. Spallogenic nitrogen

It should be noted that the conclusion discussed in section 6.3.2, does not contradict the spallogenic origin of the very high temperature (>1200°C) nitrogen. Spallogenic ^{15}N is produced from cosmic-ray interaction with oxygen and is characterised by $^{15}N/^{14}N$ ratio ≈ 1, and an increase in spallogenic ^{38}Ar. If HTN was indicative of "pure" spallogenic

nitrogen, it would reveal $\delta^{15}N$ values significantly in excess of +277‰ (the highest observed in this study), and significantly lower $^{36}Ar/^{38}Ar$ ratios.

The conclusion is that HTN consists of a minor contribution (<20%) of spallogenic nitrogen which increases the $\delta^{15}N$ to heavier values and results in a rapid decrease, at high temperature or at depth within the soil, of $^{36}Ar/^{38}Ar$ ratios (Benkert *et al.*, 1993). This decrease can be distinguished from the gradual decrease in $^{36}Ar/^{38}Ar$ due to the liberation of SEP radiation (Wieler *et al.*, 1986; Frick *et al.*, 1988; Benkert *et al.*, 1993).

6.3.4. Temporal variation of the solar wind

The data obtained in this study has shown that the major release of nitrogen between 600-900°C (LTN) is likely to be predominantly of solar wind origin and exhibits $^{36}Ar/^{38}Ar$ ratios which display a similar trend as observed in noble gas studies (section 1.7.5.2). However, although the current study has shown that LTN is surface-correlated, a non-solar origin for a proportion of LTN cannot be ruled out.

The secular variation model suggests that there has been a secular increase of 20-50% for $^{15}N/^{14}N$ in the solar convective zone over the lifetime of the lunar regolith (section 1.7.4.1). However, the current study has shown that the isotopic extremes attributed to the recent and ancient solar wind may have revised compositions. Although the current study does not deny that a secular variation has occurred, its magnitude is significantly lower than that invoked by advocators of a solar origin for regolith nitrogen. Assuming that LTN is due to surface-correlated solar gases, and HTN is the equivalent release from agglutinates, the mean $\delta^{15}N$ across these releases can be used as estimates of the recent and ancient solar wind (section 6.3.1 and 6.3.2 respectively). For the data obtained in this work, the composition of the ancient solar wind is estimated as $\delta^{15}N = +27.0 \pm 6.0$‰, and the recent solar wind is $\delta^{15}N = +35.3 \pm 13.6$‰. Hence the maximum $\delta^{15}N$ variation is ~2.8%, which is comparable with the observed increase of 3% for $^{20}Ne/^{22}Ne$ (Becker and Pepin, 1989; Pepin, 1989) and is a more plausible estimate of changes within the solar convective zone. Interestingly, if the upper and lower limits from this investigation for the isotopic composition of the recent and ancient solar wind are used, the proportion of nitrogen in the lunar regolith which is of a solar origin is ~30%.

The absence of isotopically light nitrogen in agglutinates separated from lunar soils (Norris *et al.*, 1983; Kerridge *et al.*, 1993) and the similarity of the release pattern for all lunar samples, irrespective of origin or agglutinate content, has led Kerridge *et al.* (1992b) to suggest that the observed variation represents a difference in the implantation energy of the component. In their work, the isotopically heavy nitrogen has been attributed to the implantation of low energy solar wind particles, whereas the isotopically light component is attributed to higher energy, and hence more deeply sited solar energetic particles. The implantation energy theory has not yet been verified experimentally but is believed by the aforementioned workers to be analogous to the SW and SEP components observed from noble gas analysis (section 1.7.5.2) which may sample different source regions in the Sun. The isotopic mixing trends in this work (Figure 3.12) for the <10 μm fraction of A12023, confirms that the ratio of SW/SEP is proportional to ΔT (the temperature shift between the combustion and pyrolysis extractions) for a given $\delta^{15}N$. Therefore the SW contribution is higher (relative to SEP) for N_{LT}, where the temperature shift is greatest, whereas for N_{MT}, the SW/SEP ratio is lower. It should be noted that SEP radiation, although implanted with higher energy than SW, are solar-correlated, as they have been identified using $^{36}Ar/^{38}Ar$ ratios in <10 μm grain size fractions of A12023 (section 3.4.2.2) and by previous workers (section 1.7.5.2). Although SEP's are not easily recognised in agglutinates, they should be present due to agglutinate formation processes. It is likely that SEP radiation has been masked by other components in agglutinates. Furthermore, the isotopic composition of SW and SEP nitrogen is not known and at the present time it cannot be confirmed from this investigation whether the isotopically heavy and light nitrogen components can be attributed to SW/SEP variation. If this suggestion is correct it further contradicts the model which invokes secular variation of the solar wind. In addition, the deconvolution of N_{LT} and N_{MT} for the <10 μm fraction of A12023 (Figure 3.11) has suggested that the isotopically heavy and light nitrogen is present in approximately equal proportions, whereas the current model postulates that SEP is far less abundant than the solar wind. However, noble gas studies (section 1.7.5.2) has suggested that SEP noble gases are more abundant than anticipated, and are believed to constitute ~30% of the total gas. Hence it may be possible that SW and SEP are present in equal proportions, which would account for the observed correlation

(although tentative) between N_{HT} and maturity parameters (Figures 5.7a and 5.8a). This is an issue which remains a problem and requires further investigation.

6.4. Isotopic mixing with non-solar nitrogen

The above discussion concludes that lunar soils consist of a significant contribution of solar wind nitrogen, together with a proportion of non-solar nitrogen (section 6.2.1 and 6.2.2). The amount of non-solar nitrogen in the lunar regolith is unknown but is believed to be an significant component. Preliminary calculations estimate ~30% of the total nitrogen is solar in origin. Furthermore the data obtained in this study has suggested that a secular increase of $^{15}N/^{14}N$ has occurred over the lifetime of the regolith, although this increase is estimated as ~3% (section 6.3.1 and 6.3.2), similar to the increase observed for $^{20}Ne/^{22}Ne$ in noble gas studies (section 1.7.5.2). However, the observation in this work of $\delta^{15}N$ variations of up to 38% cannot be explained using the secular variation model, and hence an alternative explanation is required. Furthermore, the $N/^{36}Ar$ ratios in lunar soils and breccias in this study, exceed by a factor of 5 to 39 times the solar value of 37 (Anders and Grevesse, 1989).

The observation of "excess" nitrogen in the lunar regolith (section led some workers to advocate non-solar nitrogen as the source of a proportion of the isotopically light nitrogen in lunar soils and breccias (section 1.7.4.2). However, many workers argue that if only the isotopically light nitrogen is non-solar in origin, it would not be sufficient to account for the observed nitrogen excess (Wieler, *pers. comm.*). In this section, several possible sources of non-solar nitrogen are discussed, in order to account for the isotopically heaviest and lightest nitrogen components observed in this study of lunar soils and breccias.

6.4.1. Combustible and non-combustible light nitrogen

For all the lunar soils analysed by both stepped combustion and pyrolysis extraction in the current study (section 3.3.1.2, 3.4.2.1, 4.6.1 and 5.3.1), the release of N_{LT} is shifted to lower temperatures by 50-75°C in the presence of oxygen. A similar effect has also been observed for the isotopically light nitrogen component, N_{HT}, whereby during combustion

the liberation of this component is enhanced by up to 200°C. This has been confirmed by a conjoint pyrolysis and combustion extraction, which liberated N_{HT} with $\delta^{15}N$ = -186‰, at a temperature of ~750°C, following the removal of N_{MT} (section 3.4.2.2). The significance of the isotopic composition for this component is discussed in section 6.4.2. Furthermore, during pyrolysis extractions in this work, the isotopic profile has been shown to resemble a W-shape, with the observation of two isotopic light components, N_{MT} and N_{HT} (at temperatures of ~850 and ~1050°C respectively), previously only observed for stepped pyrolyses of lunar breccias (section 1.7.3.1). However, during combustion extractions, the isotopic profile resembles a V-shape with the liberation of a single light nitrogen component, N_{MT}, at temperature of ~850°C. The conclusion from this investigation is that the liberation of N_{HT} is shifted to lower temperature during combustion, and hence is liberated across a similar temperature range as N_{MT}. This implies that the isotopically light nitrogen, N_{HT}, is combustible, *i.e.* its release is affected by the presence of oxygen during extraction, whereas the majority of light nitrogen, N_{MT}, is relatively unaffected. Several possible sources for N_{HT} are considered in this work: these are discussed in sections 6.4.2 and 6.4.3.

One exception to the observation of N_{MT} and N_{HT} in lunar soils was the <10 μm grain size fractions of five Apollo 16 soils (section 5.3.1). These soils liberated N_{MT} at a temperature of 800-850°C for the combustion extractions, but liberated only a single light nitrogen component, N_{HT}, at a temperature of 1050°C during pyrolysis extractions. This work has shown that N_{MT} is a minor component in Apollo 16 soils, and hence is masked during pyrolysis extractions by the liberation of N_{HT}. N_{MT} is therefore likely to be associated with the nitrogen within pure mineral grains, such as ilmenite and pyroxene, which are depleted in Apollo 16 soils relative to Apollo 12 soils.

6.4.2. Primitive meteoritic nitrogen in the lunar regolith

Trace element studies have shown that the regolith contains a contribution (1-2 wt.%) of carbonaceous chondrite debris (section 1.6.4). Studies of these meteorites (section 4.1.2.2) have led to the identification of presolar diamond with $\delta^{15}N$ values of ~-350‰. Furthermore, the isotopically light nitrogen component ($\delta^{15}N$ = ~-210‰) in breccia A79035 could not be accounted for by analysis of individual mineral separates, *e.g.* Kerridge *et al.*,

1993, and hence a further carrier was required. In addition, the conjoint study of <10 μm fraction of A12023 (section 3.4.2.2) yielded $\delta^{15}N$ = -186‰ for N_{HT} (following the removal of N_{HT}). This constitutes the lowest $\delta^{15}N$ observed for a lunar soil and was similar to the $\delta^{15}N$ values obtained for breccia A79035. The $^{40}Ar/^{36}Ar$ ratio for the N_{HT} component in A12023 was 1.17, less than the mean $^{40}Ar/^{36}Ar$ of 1.73 for a temperature range of 690-925°C (where $\delta^{15}N$ < -200‰) for A79035. This may suggest that a proportion of the light nitrogen in lunar breccias (incorporated prior to breccia consolidation) may still be present in lunar soils, but has been masked in the latter by mixing with isotopically heavier nitrogen. For lunar breccias, the absence of N_{LT} implies that the isotopically light nitrogen is not masked by a heavy component. It should also be noted that the conjoint pyrolysis and combustion extraction did not fully resolve N_{HT}, and hence this component is likely to contribute more than the calculated 3% of the total light nitrogen, and have a $\delta^{15}N$ value which is lower than -186‰.

In the light of observations in this work and previous studies discussed above, an approximate mass balance calculation in this work has resulted in the suggestion of one (or more) unknown component(s) with $\Sigma\delta^{15}N$ = ~-323‰ (section 4.4), similar to that obtained for presolar grains. Hence, the possibility of a presolar origin for the light nitrogen in breccia A79035 was investigated (section 4.4 and Brilliant *et al.*, 1992).

This study of the HF/HCl and $HClO_4$ residues of A79035 (section 4.4.1 and 4.4.2) did not liberate sufficiently light nitrogen, comparable to that observed in carbonaceous chondrites, despite an equivalent release temperature for the nitrogen, *i.e.* ~500°C during combustion and ~1000°C during pyrolysis. No evidence of pristine presolar diamond could be identified either from the nitrogen isotopic compositions or from a TEM study of the residues. The C/N ratios for these analyses were significantly higher than typical solar wind values, with ratios of between 30-40 obtained for the HF/HCl residue, although were lower than the typical values associated with presolar diamond (section 4.4.1).

The absence of pristine presolar diamond in A79035 may suggest the absence of this component in the lunar regolith. However, this seems unlikely as erosion and deposition by meteorite impacts are an important factor in both the modification of the lunar regolith and the formation of breccias. Furthermore, the high C/N ratios obtained in this work, compared to solar wind values, indicate that a meteoritic component may be present in the

form of amorphous carbon, possibly diamond, which has been modified by interaction with the solar wind and solar and cosmic-rays. Such a component would be weakly bound to the breccia and hence could plausibly be removed during harsh chemical treatments. It, however, cannot be a major contributor otherwise the C/N ratio would be much higher than the typical values of 0.7 to 2.5 observed for the lunar soils in this study. There does not appear to be any plausible way of decoupling isotopically light interstellar nitrogen from diamond carbon during impact or sputter erosion.

6.4.3. Fine grained Fe-metal (Fe^0) in the lunar regolith

In addition to the known concentration of Fe^0 (~5.5 wt.% Ni) in the lunar regolith due to the contribution of impacting meteorites (section 1.6.4), an "excess" component of finely divided metallic iron (0.5-0.9 wt.%) has also been identified. This component is due to the reduction of Fe^{2+} to Fe^0 by reactions with implanted solar wind hydrogen (section 1.6.1.1). Kerridge *et al.* (1977) has shown a correlation between nitrogen content and isotopic composition, and maturity parameters, *i.e.* I_s/FeO and ^{21}Ne (section 5.3.2), for a suite of Apollo 16 soils. Further, these workers have observed a correlation between $\Sigma\delta^{15}N$ and the Fe^0-content the soils.

In addition to verifying previous trends (although tentatively as a limited number of samples were analysed), the current study has also revealed a weak correlation between N_{HT} and maturity parameters, although no equivalent correlation is observed for N_{LT}. These results imply that the isotopic composition of N_{HT} is dependent on the exposure of the soil to the solar wind or solar cosmic-rays, whereas N_{LT} does not appear to be exposure dependent. This indicates that a proportion of the light nitrogen may be associated with the reduction of Fe^{2+} to Fe^0 by solar wind hydrogen in the lunar regolith. In addition, N_{HT} may be due to the meteorite contribution into the lunar regolith, as suggested by the possible presence of amorphous carbon (section 6.4.2) and the correlation between Fe^0-content (of which impacting meteorites constitute ~5.5 wt.% Ni) and N_{HT}.

6.4.4. Re-implantation of atmospheric nitrogen into the lunar regolith

In the current work, the conjoint nitrogen and argon abundance measurements have shown that nitrogen, ^{40}Ar and ^{36}Ar are liberated at the same temperature during stepped combustion extractions, and hence the $N/^{36}Ar$ and $^{40}Ar/^{36}Ar$ are constant in all but the initial and final steps of the extractions (section 3.3.2, 4.3.2, 4.6.2 and 5.3.3). The surface location of ^{40}Ar has been attributed to the liberation of re-implanted atmospheric ^{40}Ar (section 1.6.1.3), and the constant $^{40}Ar/^{36}Ar$ ratios have detracted from the model which invokes a secular variation of the solar wind, as this necessitates that surface-correlated gases originate from the solar wind. The $N/^{36}Ar$ ratio in lunar soils and breccias displays a similar trend to $^{40}Ar/^{36}Ar$ and hence it may be possible that N_{LT} is due to re-implanted atmospheric nitrogen. In order for this process to occur, the nitrogen would initially need to be loosely bound on the surface of soil grains, such that diffusion can occur. It would then require loss of ^{14}N, relative to ^{15}N and subsequent re-implantation into the lunar regolith. This is a possible mechanism to account for N_{LT} in lunar soils, although it is unresolved whether it is sufficient to account for the $\delta^{15}N$ values obtained in this study for N_{LT}.

6.4.5. Fractionation effects on the lunar surface and in the laboratory

The role of isotopic fractionation on the lunar surface was originally believed to be of minor importance (Kerridge, 1975, 1980). However, the vast array of regolith and implantation processes which have occurred on the lunar surface during the last 4 Gyr implies that fractionation is a major factor in constraining the isotopic compositions of the nitrogen components in the regolith. The question remains as to whether the fractionation processes can account for the variation in $\delta^{15}N$ observed in lunar soils and breccias, and whether addition laboratory induced fractionation has occurred. The latter is discussed in sections 2.5.1 and 3.4.2.1, in conjunction with the analysis of small aliquots of reference gas and the expected effect of fractionation on the isotopic profile in lunar samples.

There are several mechanisms which can cause isotopic fractionation in the lunar regolith and these are primarily associated with mass-dependent implantation, *i.e.* increased implantation depth for heavier isotopes relative to lighter isotopes.

1). Thermal diffusion or diffusive loss of ^{14}N from the soil results in a relative increase of ^{15}N, due to the faster diffusion rates of the former and higher implantation depth of the latter. Solar wind elements, such as He and Ne have undergone substantial diffusive loss from the regolith, whereas Kr and Xe are relatively well retained, due to the increased depth of implantation and lower diffusion rates of these species.

2). Sputtering processes would preferentially remove ^{14}N relative to ^{15}N once equilibrium with solar wind implanted gases had been reached, due to the lower implantation depth of ^{14}N (section 1.6.1.1).

3). The combination of processes 1) and 2) above results in the accumulation of these gases in the tenuous lunar atmosphere. The high-energy species can escape from the atmosphere, whereas the low-energy species are accelerated by the solar wind and re-implanted into the regolith, together with some atmospheric species (section 1.6.1.3). The re-implanted species would have a lower energy than the solar wind gases and hence would have a lower implantation depth, resulting in further isotopic fractionation.

4). The agglutination process is believed to increase ^{15}N relative to ^{14}N during maturation of the regolith. A comprehensive study of magnetic and density separates (Norris, 1987 *unpublished data*) has estimated this fractionation to be ~20‰.

In addition to the shift to lower temperature of N_{HT} during combustion extractions (section 6.4.1), a minor temperature shift was also observed for N_{LT} (50-75°C) in the presence of oxygen. This may indicate that the nitrogen is chemically bound within the sample and hence will be liberated at a slightly higher temperature when diffusion is the sole release mechanism. A possible candidate for the origin of the chemically bound nitrogen may be the amorphous rims around many soil grains (section 1.6.1.2). The observation of isotopically heavy nitrogen with $\delta^{15}N$ values from +100 to +140‰ in this work may be due to fractionation of solar wind gases during the formation of the amorphous rims. The fractionation process would account for preferential loss of ^{14}N, and hence the increase to higher $\delta^{15}N$ values, *i.e.* ^{15}N-rich. Whether such a mechanism would be able to account for the observed increase in $\delta^{15}N$ (from ~+40 to ~+100‰) is not well understood.

Chapter 7
Conclusions and further work

7.1. Appraisal of instrumentation

The static-vacuum, mass spectrometer used in this study has been shown to operate with sufficient precision and sensitivity to enable high-resolution stepped heating extractions of lunar soils and breccias. The mass spectrometer is capable of measuring picogram quantities of nitrogen, although is regularly employed to measure nanogram abundances of nitrogen, with a $\delta^{15}N$ precision of $\pm 0.5‰$. The high sensitivity ensures that small amounts of material are required for an analysis, typically 1 mg for a 20 step extraction using a sample containing ~100-150 ppm nitrogen. This is crucial for the analysis of samples such as lunar soils and breccias which are often in limited supply.

The high-resolution temperature steps (10°C) used for some extractions in this work, constitute the highest resolution studies of lunar soils and breccias performed to date. The results act as further confirmation of the validity of the stepped extraction technique as a tool to resolve individual components within the samples, and to eliminate the effects of contamination on the indigenous nitrogen components. The use of conjoint argon (although semi-quantitative) and carbon measurements, together with the nitrogen analyses, have provided a valuable aid in constraining the location and origin of solar wind nitrogen in the lunar regolith.

7.2. Nitrogen isotopic variation in the lunar regolith: summary of results and conclusions.

The data obtained in this work has revealed some new and interesting observations regarding the location and isotopic variation of nitrogen within the lunar regolith. The data do not comprehensively confirm either of the postulated models by previous work, but instead suggests a variation which is based on both models, with the solar wind and non-

solar nitrogen as significant contributors to the nitrogen inventory. This chapter details the main conclusions from this work and suggests some further work which is required to continue the recent advances made in this area.

The following conclusions can be drawn from the study of nitrogen abundances and isotopic compositions in lunar soils and breccias:

1). The nitrogen is liberated from lunar soils (except the <10 μm grain size fractions) and lunar breccias as two components: LTN (600-1000°C) and HTN (1000-1200°C). The absence of HTN in the <10 μm fractions, suggests that LTN is surface-correlated, and a mixture of two isotopic components, N_{LT} and N_{MT}. The C/N ratios across LTN are similar to the solar photospheric and coronal ratios of ~1.1 (section 1.7.6.2), indicative of a solar wind origin. However, the $N/^{36}Ar$ ratios, although essentially constant across LTN for the combustion extractions, are between 5 and 39 times the solar value of 37 (section 1.7.2.2), suggesting the presence of a significant proportion of non-solar nitrogen. The relative proportion of the solar and non-solar contribution to the lunar regolith has not been accurately determined, but preliminary calculation suggest that ~30% of the nitrogen originates from the solar wind.

2). The proportion of nitrogen liberated as HTN is greater for coarser grain sizes, than for the finer grain size fractions. The converse has been observed for LTN. This suggests that the majority of HTN (>80%) represents the nitrogen located within composite particles, such as coarse-grained agglutinates and microbreccia. These are essentially absent in the finest grain size fractions. Also associated with the release of HTN, is a minor component (<20%) of spallogenic ^{15}N, which increases the $\delta^{15}N$ to higher values (>100‰) at temperatures of ≥1200°C.

3). This work has confirmed the presence of both the V-shaped and W-shaped isotopic profiles in lunar soils and breccias, with the former observed only in the combustion extractions and the latter restricted to the pyrolysis extractions. The maximum isotopic variation between the isotopically heavy nitrogen component, N_{LT}, and light nitrogen components, N_{MT} and N_{HT}, is ~38%. The observation of the V-shaped profile for the pyrolysis extractions of Apollo 16 soils is associated with the relatively small amounts of

ilmenite and pyroxene in highland soils compared to mare soils. The light nitrogen component, N_{MT}, is believed to be masked, by the more dominant N_{HT} component.

4). This work has estimated the isotopic composition of the recent solar wind as $\delta^{15}N$ = +35.3 ± 13.6‰. This estimate is calculated from the mean $\delta^{15}N$ across the release of LTN. Furthermore, the conclusion in 2) above, and the absence of isotopically light nitrogen in agglutinate fractions of lunar soils (section 3.5), suggests that the ancient solar wind is the mean $\delta^{15}N$ across the release of HTN (prior to the liberation of spallogenic ^{15}N). The ancient solar wind composition has been estimated in this work as $\delta^{15}N$ = +27.0 ± 6.0‰. Hence this investigation has shown that the secular variation of the solar wind is a maximum of ~2.8‰, significantly less than the maximum $\delta^{15}N$ variation of 38% observed in this work.

4). The low-temperature, isotopically heavy component, N_{LT}, displays a mean $\delta^{15}N$ of between +100 to +140‰, a proportion of which appears to be chemically bound. An explanation for the isotopic composition of this component, when compared to the recent solar wind ($\delta^{15}N$ = ~+35‰) is not clearly understood. The chemically bound nitrogen may be linked to solar wind which was fractionated during the formation of amorphous rims around the soil grains. The loosely bound nitrogen may be attributed to re-implantation of atmospheric nitrogen, in a similar manner to ^{40}Ar. A sufficient investigation was not undertaken to confirm recent suggestions that the isotopically heavy and light nitrogen components are associated with the implantation energy of solar particles, *i.e.* SW and SEP implantation.

5). The isotopically light nitrogen component, N_{HT}, is not attributed to the ancient solar wind as it is absent in agglutinate fractions. The liberation of N_{HT} is shifted to lower temperature during conjoint pyrolysis and combustion extractions, by ~200°C and has been shown to display a minimum $\delta^{15}N$ = -186‰, the lowest observed in lunar soils to date. The isotopic composition of this component is similar to that observed in lunar breccias. Calculations in this work estimate that ~3% of N_{HT} may be of a non-solar origin. This minor component may be of a carbonaceous origin but if this is the case, it is present as amorphous carbon. A further possibility is that N_{HT} can be attributed to Fe^0, from the reduction of Fe^{2+} by solar wind hydrogen, as it has been observed to correlate with maturity parameters, *i.e.* I_s/FeO and ^{21}Ne exposure age, and the Fe^0-content of the soil.

The implantation of solar wind and solar and cosmic-ray radiation into the lunar regolith is a continuous and gradual process, and the major problem encountered when investigating the magnitude of nitrogen isotopic variation, is the significantly lower variation observed for other solar species. However, by careful selection of the lunar soils and breccias to be analysed (include grain size and magnetic separates), this investigation has revealed a secular variation of $^{15}N/^{14}N$ of ~3, similar to that observed for $^{20}Ne/^{22}Ne$. However, the secular increase does not account for the magnitude of $\delta^{15}N$ variation displayed for lunar soils and breccias in this work (~38‰). The explanation for the magnitude of variation has not been conclusively confirmed in this work, however, some constraints as to the nature of the isotopically lightest nitrogen in the regolith have been made. The origin of the isotopically heavy nitrogen is currently unknown and requires further study.

7.3. Further work

This study has re-evaluated the current theories regarding the isotopic variation in the lunar regolith and has resulted in some new and interesting observations. In order to confirm these observations, further specific experiments should be performed.

To fully constrain the isotopic variation in the lunar regolith, a comprehensive study should be made of a variety of soils and breccias with known surface-exposure histories. A recent study of lunar meteorites (Thalmann *et al.*, 1996) has revealed a strong correlation between concentration of cosmic-ray produced noble gases and trapped solar species, *e.g.* ^{36}Ar. This has resulted in an estimation of the exposure periods for many of the lunar meteorites. The use of a similar technique for lunar soils could prove valuable in determining their exposure histories, and hence constraining the isotopic compositions of individual components in the regolith. This would enable identification of the end-members for the isotopic variation and hence aid in identifying the origin for the nitrogen. These samples should be analysed by stepped combustion and pyrolysis techniques using minimum temperature resolution of 50°C, to ensure elimination of the masking of individual components.

Furthermore, a study is required of a suite of density, magnetic and metal separates from a lunar soil, with sufficient material to ensure accurate and reliable isotope measurements at low temperatures. This would confirm whether the pure mineral fractions are enriched in ^{15}N, as inferred by the secular variation model and could examine the effect of the agglutination process on the isotopic composition of HTN. In addition, the preliminary work of Humbert *et al.* (1997) should be continued for conjoint nitrogen, argon and neon isotopic measurements on a number of individual soil grains. This would enable investigation of the real excess nitrogen component and could potentially determine a non-solar or implantation origin for this component.

A valuable extension of this work would be the ability to obtain conjoint nitrogen, argon and carbon measurements on a single sample. This would be dependent on the calibration of the instrument to obtain quantitative argon measurements, which would also allow comparison of this data with previous and current observations by other workers. Furthermore, accurate carbon abundance measurements, with a low blank contribution, would be a valuable aid in resolving terrestrial contamination and indigenous carbon components in the lunar regolith.

The use of joint combustion and pyrolysis extractions should be continued to attempt to fully resolve N_{HT} and to determine its isotopic composition. This would determine the link between the lightest nitrogen in both lunar soils and breccias and may confirm or refute a presolar origin for the nitrogen.

However, the most useful advance in this area would be a spacecraft measurement of the isotopic composition of the current solar wind radiation. This would provide a useful reference point, to which samples of a variety of exposure ages could be compared. The Genesis - Discovery 5 mission has been accepted for this purpose.

Appendix A
Blank measurements

As the following extractions were all performed to obtain a measurement of the blank for the empty extraction section and empty platinum buckets, the nitrogen and carbon yields are given in nanograms of nitrogen, as opposed to the conventionally used ppm. This enables a direct measurement of the blank at each temperature step.

A1. Stepped combustion on an empty extraction section

Temp (°C)	N (ng)	$\delta^{15}N$ (‰)	Error	C (ng)
100	0.61	-6.6	2.0	2.09
200	0.58	-5.2	2.4	2.09
300	0.61	-4.0	2.8	2.09
400	0.46	+5.1	2.4	2.25
500	0.49	-11.1	6.3	1.92
600	0.41	-5.8	2.3	2.09
700	0.43	-17.0	7.9	1.92
800	0.45	-14.3	2.4	2.09
900	0.59	-2.6	7.4	2.73
1000	0.75	-1.7	3.7	2.41
1110	0.75	-7.0	1.9	1.92
1200	0.86	-13.6	1.8	2.09
Total	6.98	-6.9	3.4	25.68

A2. Platinum bucket blanks

Platinum bucket combustion (**FIN110**)
Bucket weight = 16.357 mg

Temp (°C)	N (ng)	$\delta^{15}N$ (‰)	Error	C (ng)
200	2.06	-15.6	0.1	5.37
250	1.09	-14.1	0.1	5.37
300	1.23	-14.5	0.3	6.02
350	0.85	-12.9	0.2	4.17
402	0.61	-12.4	0.1	3.98
450	0.54	-8.7	0.6	2.41
502	0.50	-8.6	0.3	4.54
550	0.48	-9.8	0.6	2.04
600	0.48	-10.6	0.4	0.83
650	0.55	-5.7	0.5	5.56
700	0.60	nm	nm	0.28
750	0.73	-6.0	0.5	1.76
800	0.60	-10.8	0.5	4.82
850	0.59	-10.4	0.3	1.48
900	0.63	-12.0	0.6	2.41
950	0.63	-12.3	0.0	2.13
1000	0.63	-13.4	0.3	0.46
1050	0.65	-15.5	0.4	1.30
1100	0.73	-15.8	0.5	1.48
1150	0.74	-16.5	0.2	0.74
1200	0.84	-20.3	0.5	2.22
Total	15.75	-12.5	0.3	59.38

Platinum bucket pyrolysis (**FIN111**)
Bucket weight = 19.217 mg

Temp (°C)	N (ng)	$\delta^{15}N$ (‰)	Error	C (ng)
350(C)	2.74	-7.2	0.9	11.48
400	0.78	-9.4	0.1	5.19
450	0.49	-10.5	0.4	2.78
500	0.41	-9.4	0.2	3.24
550	0.41	-10.0	0.2	2.04
600	0.36	-9.6	0.2	0.93
650	0.34	-8.8	0.3	2.04
700	0.48	-8.9	0.8	1.02
750	0.55	-9.8	0.2	0.46
800	0.56	-8.2	0.2	2.96
850	0.46	-7.3	0.2	0.83
900	0.43	-12.9	0.3	1.67
950	0.39	-9.8	0.8	0.74
1000	0.41	-13.0	0.4	0.19
1052	0.58	-14.4	0.5	1.48
1100	0.74	-15.1	0.6	3.06
1150	0.99	-10.9	0.1	3.06
1200	1.20	-14.2	0.5	nm
Total	12.32	-10.2	0.5	43.15

Appendix B

Stepped extraction data from lunar soil A12023

The data obtained from the stepped combustion and pyrolysis of a variety of lunar soils and breccias are given in Appendices B, C and D. The nitrogen and carbon yields, $\delta^{15}N$ and 1σ errors are given for each temperature step, and as a total at the end of each table. The nitrogen and carbon yields are given in parts per million (ppm); the former measured by the major intercept value (t=0) of the m/z = 28 peak, and the latter using a capacitance manometer. Where an aliquot of sample gas was lost, or was too small to allow accurate abundance or isotopic composition measurement, "nm" is displayed in the table.

The argon isotopic ratios, *i.e.* $^{36}Ar/^{38}Ar$ and $^{40}Ar/^{36}Ar$, are semi-quantitative and, although internally consistent during a single extraction, cannot be compared between extractions in this work or with data obtained by other workers. No attempt has been made to calibrate the mass spectrometer for the measurement of argon abundances or isotopic composition. The calculation of the $N/^{36}Ar$ ratio is achieved by converting the mean ratios of the respective peak heights for all the analyses in this study, to the mean of the literature $N/^{36}Ar$ value of 380. The calculated multiplication factor is used to convert the individual $N/^{36}Ar$ measurements. The mean C/N, $^{36}Ar/^{38}Ar$, $N/^{36}Ar$ and $^{40}Ar/^{36}Ar$ values are quoted with the totals for the nitrogen data at the end of each data table.

For the analyses of HF/HCl and $HClO_4$ residues for lunar breccia, A79035, *i.e.* Appendix C4.2 to C4.4 inclusive, the nitrogen and carbon yields are also expressed as ppm for the whole-rock. These are given in the columns N (ppmOP) and C (ppmOP) respectively.

Note that for the majority of the pyrolysis extractions, a series of pre-combustion steps were performed at 350°C prior to the commencement of the pyrolysis. This is displayed in the table as 350(C), although it should be noted that the data obtained from these steps are not included in the Totals.

B1. Bulk soil combustion and pyrolysis extractions

A12023 Combustion (**FIN7**)
Sample weight = 1.158 mg

Temp (°C)	N (ppm)	$\delta^{15}N$ (‰)	Error
400	0.24	nm	nm
450	0.37	+96.8	0.3
500	1.09	+98.8	0.1
550	0.77	+107.5	0.2
600	1.15	+69.5	0.0
650	2.64	+47.0	0.4
700	3.03	+21.2	0.1
725	3.37	+17.0	0.0
750	2.51	+2.7	0.1
775	2.21	-9.8	0.1
800	1.93	-13.1	0.2
850	2.84	-2.9	0.1
900	2.96	+11.2	0.1
950	1.68	+19.2	0.1
1000	1.58	+30.6	0.1
1050	2.40	+38.7	0.1
1100	2.48	+52.1	0.1
1150	6.66	+48.5	0.0
1200	4.84	+87.4	0.2
1250	2.01	+78.6	0.5
Total	46.76	+37.3	0.1

A12023 Pyrolysis (**FIN9**)
Sample weight = 1.133 mg

Temp (°C)	N (ppm)	$\delta^{15}N$ (‰)	Error
400	0.06	+17.0	0.7
500	0.01	+45.4	0.7
550	0.26	+48.9	0.7
600	0.87	+66.3	0.5
650	1.36	+108.0	0.4
700	3.21	+79.0	0.5
750	7.50	+39.2	0.6
775	8.13	+22.4	0.4
810	11.53	+19.5	0.4
850	9.33	+13.6	0.5
875	6.96	+10.7	0.4
900	4.03	+18.8	0.5
950	3.81	+18.3	0.4
1000	2.71	+0.1	0.4
1050	2.42	-17.0	0.5
1100	3.81	+7.1	0.4
1150	9.74	+43.0	0.6
1200	8.12	+82.7	0.4
1250	1.33	+94.5	0.6
Total	85.20	+31.9	0.5

A12023 Combustion (**FIN23**)
Sample weight = 0.863 mg

Temp (°C)	N (ppm)	$\delta^{15}N$ (‰)	Error
400	0.34	+21.5	1.5
500	2.63	+72.5	0.8
550	2.49	+75.1	0.8
600	3.05	+60.3	0.6
625	2.32	+47.0	0.8
650	2.96	+34.3	0.7
675	3.67	+26.7	0.7
700	4.81	+19.1	0.8
725	5.27	+11.4	0.8
760	6.26	-0.8	0.7
780	3.88	-6.1	0.9
800	4.40	-16.7	0.7
850	6.43	-7.9	0.8
900	5.89	+2.9	0.8
950	4.87	+7.2	0.8
1000	4.07	+15.8	0.8
1050	4.47	+19.6	0.8
1100	5.64	+36.0	0.8
1150	14.21	+31.1	0.7
1200	3.26	+75.3	0.9
1250	1.23	+90.6	1.6
Total	92.18	+22.6	0.8

A12023 Combustion **(FIN10)**
Sample weight = 1.539 mg

Temp (°C)	N (ppm)	$\delta^{15}N$ (‰)	Error
400	1.05	+16.0	0.5
500	0.60	+73.9	0.5
550	1.88	+98.9	0.5
600	2.24	+80.8	0.4
625	1.96	+64.6	0.4
650	2.19	+49.8	0.4
675	2.89	+37.1	0.4
700	3.59	+26.7	0.4
725	4.36	+13.2	0.4
750	5.67	+0.9	0.4
775	5.07	-9.1	0.5
800	4.54	-17.7	0.4
850	8.27	-18.9	0.5
900	7.10	-4.7	0.4
950	4.67	+3.2	0.4
1000	4.10	+14.3	1.0
1050	4.32	+18.6	0.4
1100	4.29	+19.5	0.4
1150	17.03	+24.5	0.4
1200	4.82	+47.8	0.5
1250	1.62	+96.9	0.6
Total	92.26	+17.9	0.5

A12023 Pyrolysis **(FIN27)**
Sample weight = 0.816 mg

Temp (°C)	N (ppm)	$\delta^{15}N$ (‰)	Error
400	nm	+10.0	0.8
500	nm	+14.2	0.8
550	nm	+20.4	0.8
600	0.86	+30.1	0.8
650	0.92	+36.4	0.6
700	2.87	+55.9	0.6
725	3.38	+35.7	0.6
750	3.03	+24.7	0.6
780	4.40	+21.4	0.6
800	4.39	+18.7	0.5
825	4.55	+12.7	0.6
850	4.40	+9.9	0.7
875	2.72	+12.5	0.6
900	2.75	+14.0	0.6
950	1.63	+5.6	0.7
1000	2.77	-4.3	0.6
1050	3.21	-2.3	0.6
1100	4.40	+13.8	0.5
1130	8.40	+26.3	0.6
1150	6.23	+28.9	0.6
1175	3.99	+26.9	0.6
1200	1.65	+32.9	0.7
1250	7.38	+15.4	0.6
Total	73.93	+20.2	0.6

A12023 High Resolution Combustion (**FIN37**)
Sample weight = 3.315 mg

Temp (°C)	N (ppm)	$\delta^{15}N$ (‰)	Error	C (ppm)	C/N	$^{36}Ar/^{38}Ar$	$N/^{36}Ar$	$^{40}Ar/^{36}Ar$
400	0.68	+130.7	0.4	14.15	20.79	nm	1824.7	13.54
450	0.79	+156.2	0.5	5.70	7.23	6.29	892.0	6.51
475	0.74	+159.8	0.5	5.73	7.77	6.22	550.0	4.34
500	0.86	+152.5	0.6	6.54	7.59	6.39	389.3	3.10
525	1.14	+138.1	0.6	9.08	7.93	6.45	332.2	2.34
550	1.24	+129.5	0.5	6.65	5.34	6.37	273.0	1.87
575	1.49	+117.2	0.4	8.13	5.46	6.36	213.0	1.41
600	1.56	+102.0	0.5	5.61	3.60	6.35	188.9	1.16
610	1.54	+90.8	0.5	5.67	3.67	6.29	181.5	1.01
620	1.37	+83.2	0.5	4.05	2.96	6.31	188.5	0.96
630	1.37	+76.1	0.4	4.05	2.95	nm	190.7	0.93
640	1.51	+67.1	0.5	2.43	1.61	6.10	193.0	0.88
650	1.75	+59.8	0.5	2.85	1.62	6.15	196.0	0.80
660	1.90	+54.0	0.4	3.30	1.73	6.14	185.3	0.71
670	2.21	+48.0	0.5	3.49	1.58	6.07	196.3	0.68
680	2.46	+41.6	0.4	2.60	1.06	6.07	184.3	0.62
690	2.58	+37.0	0.5	3.30	1.28	5.99	166.4	0.59
700	2.85	+31.2	0.5	3.63	1.27	6.07	191.9	0.58
710	2.89	+24.7	0.5	3.72	1.29	6.05	197.1	0.59
720	2.96	+19.3	0.4	3.04	1.03	6.05	208.0	0.60
730	3.04	+12.8	0.6	1.34	0.44	6.02	225.5	0.61
740	3.00	+7.3	0.6	2.18	0.73	6.03	218.3	0.61
750	3.28	+2.2	0.5	1.68	0.51	6.02	227.7	0.59
760	3.24	-3.4	0.6	4.02	1.24	6.02	223.4	0.62
770	3.36	-7.7	0.6	4.27	1.27	6.03	236.2	0.60
780	2.88	-13.2	0.5	2.71	0.94	6.00	232.8	0.66
790	2.57	-17.6	0.5	3.69	1.43	5.95	235.6	0.69
800	2.67	-22.7	0.5	3.13	1.17	6.00	249.8	0.71
810	2.67	-30.3	0.5	2.82	1.06	5.95	284.0	0.78
820	2.68	-35.0	0.5	1.26	0.47	5.96	245.2	0.73
830	2.69	-36.6	0.5	0.89	0.33	5.99	252.6	0.72
840	2.94	-24.1	0.5	5.95	2.02	5.96	245.6	0.71
850	2.81	-15.8	0.4	3.44	1.22	5.99	239.6	0.71
875	3.67	-11.1	0.6	5.67	1.54	6.01	250.7	0.63
900	4.39	-6.7	0.6	1.15	0.26	6.01	263.9	0.62
950	4.56	-2.6	0.5	3.49	0.77	6.06	219.0	0.56
1000	4.79	+5.0	0.5	1.20	0.25	6.03	210.5	0.55
1050	4.85	+15.8	0.5	3.41	0.70	6.01	231.2	0.56
1100	5.23	+25.1	0.5	1.87	0.36	6.01	228.4	0.55
1125	4.25	+30.1	0.6	5.67	1.33	5.91	255.4	0.66
1150	7.80	+35.3	0.6	9.64	1.24	6.08	368.6	0.63
1175	3.49	+62.6	0.6	nm	nm	5.74	291.3	0.91
1200	0.81	+128.8	0.7	2.63	3.26	5.47	257.2	2.09
1250	0.36	+102.9	0.8	3.91	10.74	5.03	621.7	6.89
Total	115.95	+23.4	0.5	179.72	2.76	6.05	301.3	1.51

A12023 High Resolution Pyrolysis (**FIN44**)
Sample weight = 2.791 mg

Temp (°C)	N (ppm)	$\delta^{15}N$ (‰)	Error	C (ppm)	C/N	$^{36}Ar/^{38}Ar$	$N/^{36}Ar$	$^{40}Ar/^{36}Ar$
350(C)	2.70	+29.9	0.4	54.35	20.14	nm	6354.8	41.06
400	0.60	+55.7	0.3	2.46	4.10	nm	3371.9	15.34
450	0.33	+187.2	0.4	1.43	4.34	nm	795.2	7.17
500	0.41	+216.5	0.5	3.32	8.16	6.34	328.3	3.11
525	0.28	+228.6	0.5	0.33	1.19	6.41	218.8	2.51
550	0.41	+186.0	0.6	2.36	5.81	6.47	184.7	2.05
578	0.51	+168.0	0.6	2.62	5.15	6.57	142.7	1.66
600	0.67	+151.7	0.5	2.69	4.04	6.62	116.2	1.37
625	1.07	+137.1	0.4	1.23	1.15	6.52	99.0	1.04
650	1.62	+118.6	0.5	1.82	1.13	6.54	93.4	0.77
662	1.50	+105.5	0.5	1.86	1.16	6.32	88.7	0.65
670	1.63	+96.3	0.5	1.79	1.19	6.69	95.3	0.58
680	1.85	+83.8	0.4	4.51	2.45	6.47	108.0	0.52
700	3.28	+68.8	0.5	5.11	1.56	6.48	122.5	0.41
720	5.49	+47.7	0.5	1.00	0.18	6.57	134.4	0.32
742	7.88	+31.1	0.4	4.88	0.62	6.47	157.9	0.29
750	6.82	+20.5	0.5	2.75	0.40	6.35	188.7	0.34
760	6.60	+13.6	0.4	1.16	0.18	6.30	228.5	0.38
770	6.00	+9.8	0.5	3.19	0.53	6.29	264.2	0.47
780	5.63	+6.1	0.5	0.83	0.15	6.25	306.6	0.52
790	4.73	+3.3	0.5	0.56	0.12	6.28	349.1	0.60
800	5.29	-2.4	0.4	0.27	0.05	6.22	417.9	0.67
820	6.04	-7.4	0.6	3.65	0.60	6.29	462.4	0.70
840	6.37	-11.3	0.6	1.26	0.20	6.33	523.4	0.76
860	5.24	-8.5	0.5	1.53	0.29	6.31	511.6	0.88
880	4.14	-3.1	0.6	2.95	0.71	6.34	467.2	0.94
900	2.83	-1.6	0.6	2.06	0.73	6.31	427.7	0.98
925	2.69	-6.7	0.5	3.02	1.12	6.31	424.2	0.98
950	2.39	-15.8	0.5	1.63	0.68	6.39	419.5	1.30
962	1.79	-21.5	0.5	5.41	3.03	6.31	428.4	1.24
970	1.25	-24.4	0.5	2.36	1.88	6.24	446.8	1.50
980	1.11	-24.9	0.5	5.01	4.50	6.42	483.3	1.79
990	1.18	-26.1	0.5	0.13	0.11	6.67	479.5	1.74
1000	1.15	-25.4	0.5	5.04	4.40	6.53	481.9	1.71
1025	1.41	-31.9	0.4	4.55	3.23	6.70	396.9	1.32
1075	3.59	-29.6	0.6	6.04	1.68	6.97	285.7	0.71
1100	4.11	+3.4	0.6	7.67	1.87	7.03	310.6	0.73
1125	6.05	+26.6	0.5	6.87	1.13	7.13	326.5	0.70
1150	6.36	+46.3	0.5	8.36	1.32	7.00	422.3	0.81
1179	2.32	+109.2	0.5	15.36	6.61	6.64	372.0	1.40
1200	0.23	+270.1	0.5	6.84	29.92	nm	509.0	7.42
Total	122.83	+21.9	0.5	135.89	2.69	6.49	400.0	1.93

B2. Grain size separates study

B2.1. <10 μm size fraction

A12023 <10 μm Combustion (**FIN29**)
Sample weight = 0.544 mg

Temp (°C)	N (ppm)	$\delta^{15}N$ (‰)	Error
400	2.03	+84.7	0.6
500	4.39	+127.0	0.6
550	3.83	+120.8	0.7
600	5.44	+109.0	0.6
625	2.52	+109.1	0.8
650	3.91	+88.0	0.5
675	4.92	+61.0	0.7
700	6.70	+63.7	0.6
725	10.81	+43.3	0.6
750	10.88	+26.7	0.6
775	13.91	+4.2	0.6
800	16.28	-13.2	0.7
825	10.93	-32.4	0.7
850	9.27	-48.1	0.7
900	13.17	-36.6	0.7
950	12.41	-22.6	0.7
1000	5.54	-18.0	0.8
1050	3.09	-14.6	0.8
1100	2.20	-27.8	0.9
1150	1.11	-20.8	0.9
1200	1.25	-14.2	0.8
1250	0.29	-6.9	1.2
Total	144.89	+13.3	0.7

A12023 <10 μm High Resolution Combustion **(FIN62)**
Sample weight = 1.641 mg

Temp (°C)	N (ppm)	$\delta^{15}N$ (‰)	Error	C (ppm)	C/N	$^{36}Ar/^{38}Ar$	$N/^{36}Ar$	$^{40}Ar/^{36}Ar$
400	2.84	+86.3	0.3	42.37	14.94		3043.2	6.99
425	1.59	+141.2	0.2	24.99	15.69		1020.2	3.96
450	1.69	+137.6	0.4	14.22	8.43		776.0	3.36
475	2.21	+135.1	0.4	15.34	6.95		675.6	2.71
500	2.71	+134.6	1.2	11.96	4.42		606.3	2.23
525	3.00	+138.7	0.2	8.63	2.88		441.5	1.80
550	3.54	+126.1	0.4	6.54	1.85		382.2	1.43
575	3.90	+114.7	0.4	0.01	0.00		326.3	1.07
600	4.68	+99.7	0.4	5.81	1.24		289.7	0.81
612	4.89	+87.2	0.4	4.40	0.90		273.7	0.68
620	4.73	+78.7	0.3	3.89	0.83		273.6	0.62
630	4.86	+73.8	0.4	4.06	0.84		265.8	0.56
640	5.06	+66.4	0.4	0.17	0.03		255.9	0.52
651	5.72	+58.4	0.5	5.19	0.91		262.3	0.49
660	6.83	+53.6	0.3	1.35	0.20		268.4	0.46
670	6.40	+45.4	0.4	4.12	0.64		274.0	0.46
680	5.83	+35.0	0.5	3.89	0.67		271.2	0.45
690	7.07	+29.0	0.4	1.52	0.22		291.5	0.44
700	6.99	+19.4	0.5	2.43	0.35		302.9	0.45
710	6.88	+11.0	0.5	0.90	0.13		301.6	0.44
720	7.30	+3.1	0.5	5.08	0.70		307.6	0.43
730	7.75	-4.1	0.4	3.55	0.46		309.8	0.43
740	8.00	-12.4	0.4	4.63	0.58		306.4	0.42
750	8.62	-21.1	0.5	4.80	0.56		312.3	0.41
760	8.05	-28.4	0.4	3.89	0.48		308.3	0.42
770	6.89	-33.6	0.5	3.78	0.55		304.5	0.44
780	6.35	-36.2	0.5	4.34	0.68		304.0	0.46
790	6.80	-40.4	0.5	9.59	1.41		316.7	0.46
800	6.72	-44.7	0.5	4.29	0.64		321.8	0.47
810	6.48	-43.2	0.6	2.09	0.32		317.6	0.48
820	6.00	-35.2	0.5	7.45	1.24		314.6	0.51
830	5.80	-27.4	0.6	8.12	1.40		306.4	0.53
850	8.34	-23.1	0.4	11.79	1.41		317.0	0.47
900	10.20	-19.2	0.5	14.56	1.43		306.1	0.46
950	9.69	-21.7	0.6	8.69	0.90		303.0	0.48
1000	5.86	-15.5	0.5	6.38	1.09		279.8	0.49
1050	3.76	-20.5	0.5	5.59	1.49		234.6	0.51
1100	3.02	-28.5	0.6	9.99	3.31		244.4	0.59
1150	3.49	-14.2	0.5	5.87	1.68		274.1	0.68
1200	0.62	-21.2	0.7	5.13	8.34		151.4	1.81
Total	221.19	+14.1	0.5	291.40	2.27		411.1	1.02

Note: Due to an error with the ^{38}Ar measurements, no $^{36}Ar/^{38}Ar$ data is calculated for this extraction.

A12023 <10 µm High Resolution Pyrolysis (**FIN73**)
Sample weight = 1.492 mg

Temp(°C)	N (ppm)	$\delta^{15}N$ (‰)	Error	C (ppm)	C/N	$^{36}Ar/^{38}Ar$	$N/^{36}Ar$	$^{40}Ar/^{36}Ar$
350(C)	14.18	+20.9	0.3	287.69	20.30	9.58	9231.1	19.36
400	1.73	+24.1	0.4	9.93	5.74	5.13	2913.0	13.82
450	0.98	+87.1	0.3	14.40	14.72	5.87	515.5	3.83
500	0.84	+100.7	0.3	5.21	6.22	5.93	209.8	2.12
550	1.54	+103.7	0.3	9.49	6.15	6.00	178.1	1.59
576	1.98	+135.7	0.4	8.31	4.20	6.04	128.6	1.20
601	1.82	+134.4	0.5	4.65	2.56	6.02	106.1	1.00
625	2.89	+123.7	0.5	6.08	2.10	6.04	114.1	0.79
651	5.28	+104.5	0.3	4.84	0.92	6.00	127.1	0.58
660	4.41	+97.5	0.5	5.21	1.18	5.98	121.1	0.48
670	5.04	+88.0	0.4	8.81	1.75	5.95	136.8	0.42
680	5.48	+80.1	0.5	3.85	0.70	5.90	151.1	0.37
690	6.66	+75.2	0.4	3.66	0.55	5.85	171.7	0.35
700	8.32	+63.5	0.5	3.10	0.37	5.83	195.5	0.32
710	9.31	+52.9	0.4	5.59	0.60	5.83	217.6	0.30
720	8.61	+45.8	0.4	3.85	0.45	5.78	217.5	0.28
730	9.45	+35.7	0.5	4.72	0.50	5.75	253.9	0.28
740	9.98	+25.0	0.3	5.77	0.58	5.74	288.1	0.30
750	9.29	+17.0	0.5	nm	nm	5.69	304.0	0.32
761	13.11	+9.3	0.5	13.47	1.03	5.63	413.1	0.37
770	10.47	+3.7	0.5	7.38	0.71	5.63	474.8	0.43
780	11.02	-2.2	0.5	9.31	0.84	5.66	568.4	0.48
790	9.92	-9.3	0.3	4.41	0.44	5.63	646.7	0.58
800	9.15	-16.7	0.5	8.50	0.93	5.57	742.8	0.60
820	11.49	-23.8	0.4	11.29	0.98	5.73	892.8	0.62
842	10.13	-28.4	0.4	12.04	1.19	5.47	925.9	0.71
860	7.33	-27.1	0.4	9.93	1.35	5.60	910.3	0.82
880	4.72	-25.7	0.4	7.63	1.62	5.74	789.2	0.84
900	3.81	-27.2	0.4	6.76	1.77	5.72	746.8	0.87
925	3.84	-39.2	0.3	7.01	1.82	5.76	675.2	0.78
950	3.69	-55.6	0.5	5.96	1.62	5.70	573.7	0.69
975	3.39	-71.5	0.5	6.27	1.85	5.73	481.2	0.65
1000	3.33	-79.5	0.5	8.63	2.59	5.69	422.4	0.64
1050	5.58	-92.7	0.5	8.26	1.48	5.69	340.9	0.47
1103	8.11	-76.4	0.5	13.90	1.71	5.61	265.6	0.37
1155	3.31	-26.9	0.5	23.08	6.97	5.47	279.7	0.56
1200	1.20	-2.4	0.6	22.40	18.61	5.40	341.4	1.96
Total	217.22	+11.9	0.4	293.70	2.77	5.74	467.8	1.13

A12023 <10μm Pyrolysis (to 890°C)
Combustion (350-1200°C) **(FIN115)**
Sample weight = 0.886 mg

Temp (°C)	N (ppm)	$\delta^{15}N$ (‰)	Error	C (ppm)	C/N	$^{36}Ar/^{38}Ar$	$N/^{36}Ar$	$^{40}Ar/^{36}Ar$
350(C)	17.49	+37.4	0.1	433.50	24.78	15.17	4934.1	34.13
400	1.23	+52.9	0.2	17.66	14.39	6.81	1320.0	12.19
460	1.64	+99.5	0.2	17.87	10.87	6.12	425.0	3.65
500	0.98	+96.9	0.1	6.37	6.52	6.29	150.1	2.36
550	2.10	+103.6	0.2	18.08	8.61	6.29	139.1	1.54
603	3.46	+144.1	0.2	17.76	5.13	6.33	107.0	1.09
625	3.87	+131.6	0.1	12.02	3.11	6.46	71.2	0.77
650	5.87	+111.8	0.1	9.09	1.55	6.33	82.5	0.55
675	10.95	+93.0	0.2	13.69	1.25	6.30	103.5	0.40
703	18.97	+75.4	0.2	11.60	0.61	6.30	132.5	0.30
725	22.26	+50.6	0.2	12.54	0.56	6.05	144.6	0.27
750	25.01	+27.7	0.1	14.84	0.59	6.00	190.5	0.26
775	32.70	+10.5	0.2	18.39	0.56	5.94	280.5	0.31
801	26.90	-5.1	0.2	25.71	0.96	6.01	395.2	0.40
820	19.94	-19.3	0.2	7.63	0.38	6.02	535.9	0.54
830	18.16	-18.4	0.3	25.39	1.40	6.04	901.5	2.36
840	6.03	-28.0	0.2	14.94	2.48	6.11	590.6	1.03
850	3.90	-29.1	0.2	17.35	4.45	6.03	540.8	1.21
860	2.51	-31.9	0.2	18.91	7.54	5.28	462.0	1.43
871	1.95	-34.9	0.2	18.81	9.64	6.17	421.2	1.57
880	1.56	-40.8	0.3	10.76	6.90	6.12	374.0	1.63
890	0.70	-52.9	0.3	18.60	26.75	6.06	363.8	1.95
Total	210.69	+25.8	0.2	328.02	5.44	6.15	368.2	1.71
355(C)	1.12	-0.3	0.4	25.51	22.79	nm	nm	nm
505(C)	0.00	+1.6	0.1	3.55	nm	nm	nm	nm
600(C)	0.15	+26.0	1.2	3.44	22.97	nm	nm	nm
650(C)	0.35	-61.5	0.4	2.19	6.23	6.15	245.2	4.23
700(C)	0.87	-139.9	0.2	nm	nm	5.98	222.7	1.60
725(C)	1.02	-168.6	0.4	5.22	5.13	6.04	188.2	1.22
750(C)	0.81	-185.4	0.2	4.49	5.51	6.22	137.6	1.08
775(C)	0.77	-185.8	0.3	1.46	1.90	6.12	136.0	1.17
800(C)	0.71	-162.9	0.3	2.09	2.93	5.84	194.2	1.75
825(C)	0.77	-134.6	0.4	2.09	2.72	5.91	240.8	2.22
850(C)	0.81	-122.8	0.2	6.17	7.57	6.19	213.3	1.91
875(C)	1.13	-89.0	0.4	4.08	3.60	6.07	213.6	1.59
900(C)	0.94	-86.1	0.3	5.12	5.45	5.74	175.8	1.42
950(C)	2.03	-79.0	0.5	5.85	2.88	6.00	169.4	0.89
1000(C)	2.81	-77.9	0.2	7.94	2.82	5.97	153.5	0.66
1050(C)	2.70	-91.9	0.2	4.28	1.59	5.90	126.5	0.59
1100(C)	2.59	-80.8	0.2	5.85	2.26	5.91	139.3	0.65
1150(C)	2.54	-64.9	0.3	11.08	4.36	5.77	151.6	0.76
1200(C)	1.20	-14.4	0.2	10.45	8.72	5.51	443.7	4.61
1250(C)	1.94	-15.4	0.3	18.91	9.73	nm	8320.2	64.33
Total	25.27	-85.3	0.3	129.69	6.27	5.96	674.8	5.33

B2.2. 40-53 µm size fraction

A12023 40-53 µm Pyrolysis **(FIN189)**
Sample weight = 0.941 mg

Temp (°C)	N (ppm)	$\delta^{15}N$ (‰)	Error
350(C)	6.08	+5.1	1.0
400	0.75	+3.4	0.6
450	1.75	+27.9	0.7
500	1.44	+43.7	0.6
550	1.39	+32.6	0.6
600	1.62	+56.2	0.7
650	1.77	+69.1	0.6
700	3.06	+58.2	0.6
750	4.36	+36.3	0.7
800	7.14	+8.9	0.9
850	8.64	+5.3	1.7
900	6.08	+1.2	0.7
950	5.93	+8.8	0.7
1000	3.96	-5.5	0.7
1050	3.04	-14.4	0.6
1100	4.03	+11.2	0.6
1150	5.68	+29.7	0.5
1200	5.30	+52.1	0.5
1250	1.61	+157.7	0.7
Total	67.55	+23.0	0.8

B2.3. 106-152 µm size fraction

A12023 106-152 µm Pyrolysis **(FIN188)**
Sample weight = 0.742 mg

Temp (°C)	N (ppm)	$\delta^{15}N$ (‰)	Error
350(C)	13.89	+4.8	1.3
400	1.52	+6.1	1.8
450	1.13	+14.4	2.0
500	1.19	+14.1	1.3
550	1.40	+15.2	1.1
600	1.43	+20.1	1.0
650	1.75	+35.8	1.1
700	1.43	+52.7	0.8
750	4.40	+26.6	0.9
800	5.88	+9.3	0.8
850	3.75	-5.2	1.2
900	3.98	+5.8	0.9
950	2.05	+2.0	1.0
1000	1.32	-15.0	0.9
1050	1.36	+5.8	0.9
1100	4.01	+28.9	1.0
1150	6.25	+48.6	0.9
1200	2.03	+124.1	0.8
1250	0.42	+88.5	1.9
Total	45.30	+24.4	1.0

B2.4. >1 mm size fraction

A12023 >1 mm Combustion **(FIN63)**
Sample weight = 0.866 mg

Temp (°C)	N (ppm)	$\delta^{15}N$ (‰)	Error
400	0.14	+17.7	0.5
425	0.32	+22.8	0.7
453	0.22	+34.9	0.5
475	0.10	+39.4	0.4
500	0.24	+36.7	0.3
525	0.43	+46.4	0.6
550	0.43	+51.0	0.7
575	0.62	+49.5	0.6
600	0.77	+41.4	0.6
625	0.93	+41.1	0.4
650	1.19	+37.9	0.4
700	2.74	+42.7	0.5
750	5.90	+22.2	0.4
775	4.57	+6.3	0.5
800	4.93	-3.1	0.5
825	4.37	-6.4	0.5
852	4.69	-8.0	0.4
900	7.41	-4.7	0.4
953	5.77	-1.7	0.5
1050	6.27	+5.8	0.4
1100	3.89	+14.8	0.3
1125	3.64	+18.6	0.5
1152	3.07	+20.1	0.4
1175	4.33	+20.7	0.4
1203	4.73	+24.7	0.5
1250	3.96	+50.4	0.3
Total	75.67	+13.2	0.4

A12023 >1 mm Pyrolyis **(FIN151)**
Sample weight = 0.910 mg

Temp (°C)	N (ppm)	$\delta^{15}N$ (‰)	Error
350(C)	2.31	+5.6	0.1
400	0.00	+4.0	0.2
500	0.08	+39.8	0.5
550	0.06	+38.1	0.1
600	0.12	+49.1	0.3
625	0.09	+39.3	0.1
650	0.31	+37.8	0.1
675	0.41	+41.0	0.4
700	0.80	+69.5	0.1
725	1.45	+39.6	0.1
750	2.33	+15.9	0.1
775	3.05	+0.4	0.1
800	3.62	-6.4	0.2
825	3.89	-13.6	0.1
850	3.80	-21.0	0.2
875	2.89	-16.3	0.2
900	1.72	-8.8	0.1
950	1.65	-14.0	0.1
1000	1.33	-34.8	0.2
1050	1.31	-57.3	0.1
1100	1.42	-4.4	0.1
1150	2.90	+14.0	0.1
1200	2.47	+70.0	0.1
1250	2.18	+26.8	0.1
Total	37.85	+2.6	0.1

B3. Magnetic/density separates

B3.1. 106-152 μm ρ<2.96

A12023 ρ<2.96 NM Pyrolysis (**FIN239**)
Sample weight = 0.514 mg

Temp (°C)	N (ppm)	$\delta^{15}N$ (‰)	Error
350(C)	6.38	-10.8	0.8
400	0.10	nm	nm
450	0.15	nm	nm
500	0.51	-35.6	0.9
550	0.86	-21.2	1.3
600	0.85	+2.5	0.8
650	0.98	+26.0	0.8
700	1.74	+36.9	1.0
750	1.99	+3.2	0.9
800	1.49	-48.5	0.8
850	0.63	-75.9	0.9
900	0.28	-56.0	1.1
950	0.86	-25.4	0.9
1000	0.55	-35.2	0.9
1050	0.17	nm	0.9
1100	0.64	+14.9	1.1
1150	0.63	+47.9	1.1
1200	1.19	+64.3	0.1
1255	1.84	+30.6	0.1
Total	15.44	+3.7	0.9

A12023 ρ<2.96 M3.5 Pyrolysis (**FIN248**)
Sample weight = 0.850 mg

Temp (°C)	N (ppm)	$\delta^{15}N$ (‰)	Error
350(C)	5.57	+10.1	0.7
400	nm	nm	nm
450	0.74	+44.5	0.8
500	0.95	+56.2	0.8
550	1.03	+91.0	0.7
600	0.97	+86.4	0.7
650	2.50	+81.6	0.6
700	7.02	+41.8	0.5
750	8.86	+17.1	0.6
800	10.75	+9.4	0.5
850	6.32	+19.4	1.4
900	6.13	+12.6	0.5
950	3.26	+3.3	0.4
1000	3.38	+1.8	0.5
1050	9.70	+25.7	0.5
1100	11.44	+37.0	0.6
1150	2.42	+62.1	0.7
1200	0.69	+102.7	0.8
1250	0.58	-8.1	1.0
Total	76.74	+27.6	0.6

B3.2. 106-152 μm 2.96<ρ<3.3

A12023 2.96<ρ<3.3 NM Pyrolysis (**FIN259**)
Sample weight = 1.048 mg

Temp (°C)	N (ppm)	$\delta^{15}N$ (‰)	Error
350(C)	6.33	-3.5	0.6
400	0.14	+30.2	1.9
450	0.16	+29.3	2.2
500	0.17	+23.9	1.7
550	0.18	+37.5	1.5
600	0.23	+43.4	1.2
650	0.44	+46.4	0.8
700	0.71	+37.0	2.8
750	0.93	+3.6	0.4
800	0.74	-27.0	0.5
850	0.54	-25.5	0.9
900	0.33	+4.4	1.1
950	0.36	+17.5	0.8
1000	0.39	+15.8	0.8
1050	0.35	+38.4	0.9
1100	0.34	+161.9	0.8
1150	0.35	+276.8	0.8
1200	0.37	+245.7	0.8
1250	0.42	+25.8	0.8
Total	7.15	+45.8	1.0

A12023 2.96<ρ<3.3 M2.0 Pyrolysis (**FIN227**)
Sample weight = 0.321 mg

Temp (°C)	N (ppm)	$\delta^{15}N$ (‰)	Error
350(C)	2.63	+1.6	0.7
400	1.58	+9.5	0.8
450	1.30	+20.8	0.8
500	1.32	+27.6	0.8
550	1.33	+34.8	0.8
600	1.40	+44.4	1.2
650	1.84	+58.1	1.1
700	4.73	+55.5	0.8
750	12.86	+19.7	0.7
800	14.61	+8.1	0.7
850	12.56	+16.6	0.8
900	5.75	+23.4	0.6
950	3.68	+18.0	0.8
1000	2.33	+2.9	1.2
1050	2.18	-16.9	0.8
1100	7.34	+12.4	0.7
1150	12.94	+23.0	0.7
1200	2.85	+80.5	0.7
1250	3.35	+33.2	1.1
Total	93.96	+21.7	1.1

Appendix C

Stepped extraction data from the Apollo 17 site

C1. A70019 Whole-rock

A70019 WR Combustion (**FIN35**)
Sample weight = 3.077 mg

Temp (°C)	N (ppm)	$\delta^{15}N$ (‰)	Error	C (ppm)	C/N	$^{36}Ar/^{38}Ar$	$N/^{36}Ar$	$^{40}Ar/^{36}Ar$
400	0.55	+95.5	0.4	38.64	70.48	nm	1175.1	7.13
500	1.63	+125.7	0.7	30.25	18.55	9.30	646.9	2.42
550	1.86	+114.1	0.5	19.12	10.27	8.87	426.4	1.76
600	2.11	+92.2	0.5	17.07	8.08	8.46	320.6	1.27
625	1.89	+76.9	0.5	13.79	7.31	7.86	287.7	1.05
650	2.67	+61.2	0.5	11.68	4.38	7.46	313.4	0.80
675	3.01	+49.5	0.5	10.72	3.56	7.16	285.9	0.68
700	3.63	+38.7	0.5	7.20	1.98	6.94	315.8	0.62
725	3.82	+29.8	0.5	8.97	2.35	6.82	337.7	0.62
750	4.45	+16.2	0.5	7.50	1.69	6.71	369.6	0.63
778	4.31	+1.7	0.5	4.73	1.10	6.69	382.7	0.66
800	3.75	-12.3	0.6	4.34	1.16	6.62	367.7	0.71
825	3.74	-31.5	0.6	8.52	2.28	6.61	385.3	0.75
855	3.92	-37.9	0.6	8.34	2.13	6.57	429.2	0.80
900	5.40	-13.3	0.6	6.69	1.24	6.45	424.5	0.80
950	4.36	-6.5	0.6	8.64	1.98	6.42	361.7	0.86
1000	3.13	-0.4	0.6	5.81	1.86	6.35	343.7	0.87
1050	2.70	+10.0	0.6	8.94	3.32	6.27	371.6	0.95
1100	2.46	+12.2	0.6	6.17	2.50	6.20	397.9	1.01
1150	4.00	+18.0	0.5	6.30	1.58	6.13	469.6	1.03
1200	8.17	+36.2	0.6	7.17	0.88	6.30	614.3	1.04
1250	1.90	+82.8	0.6	11.04	5.83	6.06	457.0	2.97
Total	73.44	+22.1	0.6	251.64	7.02	6.96	395.7	1.34

A70019 WR High Resolution Combustion to 600°C (**FIN247**)
Sample weight = 9.325 mg

Temp (°C)	N (ppm)	$\delta^{15}N$ (‰)	Error	C (ppm)	C/N	$^{36}Ar/^{38}Ar$	$N/^{36}Ar$	$^{40}Ar/^{36}Ar$
200	1.74	+8.0	0.9	37.60	21.65	6.37	1791.0	8.54
250	0.06	+18.7	0.6	12.30	217.74	5.92	292.4	0.90
300	0.10	+39.0	0.5	16.10	166.82	6.04	285.9	0.89
325	0.06	+78.4	0.4	9.24	153.87	6.21	158.6	nm
350	0.10	+75.6	0.4	7.20	73.24	6.24	209.6	0.74
375	0.10	+109.4	0.4	7.61	74.23	6.34	144.8	0.32
400	0.13	+115.7	0.4	5.80	45.00	6.33	118.3	0.57
410	0.14	+110.8	0.6	4.46	31.03	6.39	113.6	0.69
420	0.15	+112.2	0.4	3.84	26.30	6.04	113.0	0.71
430	0.14	+120.8	1.2	2.16	14.95	6.04	103.4	0.70
440	0.15	+124.4	1.9	2.07	13.70	6.09	94.9	0.80
450	0.20	+108.9	0.3	1.64	8.11	6.26	104.4	0.94
460	0.18	+121.5	0.3	1.76	9.72	6.25	83.4	0.96
470	0.19	+120.2	0.5	2.14	11.35	6.35	76.9	1.00
480	0.19	+121.8	0.3	1.40	7.36	6.57	74.9	0.78
490	0.20	+122.9	0.3	1.78	8.73	6.59	67.2	0.80
500	0.22	+115.4	0.4	1.23	5.51	6.64	59.7	0.80
525	0.62	+100.8	0.4	2.70	4.34	6.62	68.7	0.80
600	1.47	+76.0	0.6	1.07	0.73	6.64	60.8	0.66
Total	6.14	+71.7	0.6	122.18	47.07	6.31	211.7	1.13

A70019 WR Pyrolysis **(FIN143)**
Sample weight = 1.587 mg

Temp (°C)	N (ppm)	$\delta^{15}N$ (‰)	Error	C (ppm)	C/N	$^{36}Ar/^{38}Ar$	$N/^{36}Ar$	$^{40}Ar/^{36}Ar$
350 (C)	2.00	+14.7	0.2	161.76	80.81	nm	3024.0	18.29
400	nm	-32.2	0.6	8.93	nm	nm	nm	15.02
500	0.43	+147.2	0.1	11.96	27.79	5.97	344.4	2.36
550	0.37	+158.5	0.2	13.77	36.75	5.89	262.5	2.37
602	0.55	+139.3	0.3	8.05	14.77	6.17	220.3	1.85
625	0.47	+139.3	0.2	9.92	21.24	6.27	153.1	1.57
650	0.58	+138.6	0.1	5.60	9.73	6.17	140.1	1.26
675	0.93	+117.8	0.1	4.43	4.77	6.20	151.2	0.97
700	1.42	+99.1	0.2	6.36	4.47	5.92	172.7	0.80
728	3.12	+77.6	0.2	4.96	1.59	6.31	201.1	0.53
750	4.36	+55.1	0.2	7.76	1.78	6.39	233.8	0.44
775	6.75	+35.7	0.2	8.46	1.25	6.27	306.6	0.46
800	7.67	+23.0	0.2	8.58	1.12	6.19	419.1	0.54
830	8.03	+10.2	0.2	8.29	1.03	6.24	542.9	0.64
850	5.32	+0.6	0.3	8.87	1.67	6.31	653.8	0.73
877	4.02	+0.0	0.2	6.89	1.71	6.27	697.5	0.84
900	2.14	+5.2	0.3	5.31	2.49	6.07	622.6	1.06
950	2.27	-4.0	0.2	7.00	3.08	6.13	639.1	1.01
1000	1.96	-30.0	0.3	8.75	4.46	6.10	535.7	0.97
1050	2.15	-42.4	0.2	8.11	3.78	6.17	441.2	0.89
1100	2.87	-27.0	0.3	8.05	2.81	6.16	433.5	0.87
1150	4.66	+3.5	0.2	12.49	2.68	6.25	465.8	0.76
1200	3.02	+55.1	0.3	13.25	4.38	5.76	411.3	0.86
1250	0.57	-6.3	0.1	15.58	27.53	nm	2556.9	13.67
Total	63.65	+24.1	0.2	201.38	8.22	6.15	461.1	2.19

C2. A73221 Whole-rock

A73221 WR Combustion **(FIN107)**
Sample weight = 1.664 mg

Temp (°C)	N (ppm)	$\delta^{15}N$ (‰)	Error	C (ppm)	C/N	$^{36}Ar/^{38}Ar$	$N/^{36}Ar$	$^{40}Ar/^{36}Ar$
400	0.94	-5.7	0.3	12.80	13.56	nm	4636.4	18.73
450	0.31	+36.0	0.1	6.62	21.15	5.39	784.8	11.42
500	0.42	+74.9	0.1	7.40	17.59	5.79	348.1	6.59
550	0.70	+131.2	0.2	4.51	6.42	6.16	246.7	4.42
602	1.38	+107.0	0.1	2.56	1.85	6.07	213.4	2.98
625	1.13	+89.3	0.2	2.11	1.87	6.19	178.8	2.50
650	1.18	+82.2	0.2	2.11	1.80	5.98	165.7	1.74
675	1.25	+70.5	0.1	1.67	1.33	5.93	160.7	1.43
700	1.54	+55.4	0.2	2.73	1.78	5.90	173.2	1.29
727	1.70	+36.3	0.3	3.34	1.97	5.79	202.0	1.28
750	1.75	+13.7	0.3	1.28	0.73	5.77	222.1	1.37
775	1.99	-16.1	0.4	1.39	0.70	5.76	259.2	1.48
800	1.81	-51.8	0.3	1.67	0.92	5.81	283.8	1.68
825	1.54	-63.6	0.4	1.06	0.69	5.85	262.5	1.74
850	1.13	-35.1	0.3	2.56	2.26	5.81	238.2	1.92
900	1.40	-15.1	0.4	1.11	0.79	5.88	241.8	1.88
950	1.01	+1.1	0.3	1.11	1.10	5.78	245.1	2.23
1000	0.76	+11.8	0.3	1.17	1.53	5.75	217.6	2.37
1050	0.88	+18.4	0.2	1.39	1.58	5.86	225.7	2.35
1100	1.41	+26.0	0.3	1.28	0.91	5.73	259.1	2.14
1125	1.37	+34.7	0.1	1.11	0.81	5.79	302.0	2.11
1150	1.26	+43.3	0.2	1.11	0.88	5.69	327.6	2.20
1175	1.57	+62.0	0.3	1.22	0.78	5.71	418.5	2.37
1200	0.91	+89.0	0.4	0.95	1.04	5.42	489.9	3.99
1250	0.28	+36.0	0.4	0.78	2.76	3.42	645.7	12.53
Total	29.79	+27.0	0.3	65.06	3.47	5.72	296.3	3.79

A73221 WR Pyrolysis **(FIN146)**
Sample weight = 1.531 mg

Temp (°C)	N (ppm)	$\delta^{15}N$ (‰)	Error	C (ppm)	C/N	$^{36}Ar/^{38}Ar$	$N/^{36}Ar$	$^{40}Ar/^{36}Ar$
350(C)	1.72	+6.3	0.1	229.59	133.30	nm	nm	nm
400	0.13	+17.1	0.4	12.70	97.23	nm	nm	nm
500	0.45	+84.4	0.1	10.46	23.46	nm	843.8	8.05
550	0.33	+106.0	0.1	10.77	32.77	6.04	341.8	6.14
600	0.37	+113.0	0.2	8.77	23.72	6.27	187.4	4.61
625	0.32	+133.5	0.3	7.26	22.45	6.32	106.6	3.57
650	0.34	+136.3	0.2	6.23	18.31	6.27	89.5	2.79
675	0.58	+124.5	0.0	6.59	11.28	6.20	104.1	2.07
700	0.95	+104.0	0.1	5.26	5.52	6.28	129.4	1.63
725	1.74	+91.5	0.2	7.08	4.07	6.16	167.8	1.23
750	2.76	+71.6	0.1	7.38	2.67	6.22	204.2	0.97
775	3.45	+53.0	0.1	6.41	1.86	6.16	256.3	0.88
800	3.84	+34.8	0.1	7.26	1.89	6.15	328.6	0.94
825	5.14	+16.0	0.2	7.98	1.55	6.08	499.2	1.07
850	4.08	-1.7	0.2	7.32	1.79	6.20	727.3	1.25
875	2.29	-15.7	0.1	5.99	2.62	5.99	777.7	1.81
900	1.07	-16.5	0.2	6.05	5.68	5.82	616.4	2.40
950	1.19	-19.2	0.2	9.86	8.31	5.86	615.2	2.20
1000	1.26	-31.5	0.1	6.47	5.15	5.82	554.9	2.06
1050	1.60	-40.2	0.2	7.26	4.53	6.00	518.8	1.94
1100	2.12	-31.8	0.2	8.95	4.22	5.89	445.9	1.73
1150	5.63	+7.8	0.2	13.25	2.35	6.18	456.2	1.28
1200	4.06	+38.3	0.2	15.48	3.82	6.12	507.4	1.32
1250	1.19	+65.3	0.2	12.04	10.09	5.87	539.3	3.25
Total	44.89	+25.7	0.2	196.81	12.84	6.09	389.2	2.42

C3. A75080 Whole-rock

A75080 WR Combustion **(FIN104)**
Sample weight = 1.923 mg

Temp (°C)	N (ppm)	$\delta^{15}N$ (‰)	Error	C (ppm)	C/N	$^{36}Ar/^{38}Ar$	$N/^{36}Ar$	$^{40}Ar/^{36}Ar$
400	0.53	+48.3	0.3	12.04	22.73	nm	2942.0	4.58
450	0.59	+100.0	0.2	9.73	16.44	5.90	895.9	2.35
500	0.83	+121.5	0.1	6.26	7.56	6.03	507.0	1.81
550	1.23	+98.3	0.3	4.09	3.33	6.21	370.3	1.31
600	1.60	+77.3	0.2	3.61	2.25	6.04	297.9	0.79
626	1.55	+54.6	0.3	2.41	1.55	6.01	261.5	0.52
650	1.71	+34.1	0.3	0.39	0.23	5.93	270.6	0.49
675	1.72	+20.1	0.3	1.93	1.12	5.85	279.6	0.44
700	1.59	+6.9	0.2	2.79	1.75	5.81	313.4	0.43
726	1.69	-9.6	0.2	1.83	1.08	5.81	320.4	0.44
750	1.58	-21.2	0.4	1.78	1.13	5.77	302.4	0.50
776	1.59	-23.7	0.3	2.55	1.60	5.73	293.1	0.53
801	1.37	-21.8	0.3	1.44	1.05	5.83	271.6	0.57
827	1.69	-12.7	0.2	2.26	1.34	5.75	320.2	0.63
850	1.29	-9.0	0.3	1.30	1.00	5.82	306.9	0.64
902	1.35	-8.5	0.4	1.30	0.96	5.84	295.3	0.67
950	1.31	-2.0	0.3	0.96	0.73	5.82	304.3	0.67
1000	1.25	+9.6	0.4	0.53	0.42	5.82	310.1	0.67
1050	1.51	+17.5	0.3	2.70	1.78	5.79	345.2	0.63
1100	1.93	+20.4	0.3	1.20	0.62	5.73	367.7	0.73
1125	2.46	+30.8	0.2	2.60	1.06	5.57	454.9	0.82
1150	3.29	+41.3	0.3	1.78	0.54	5.66	573.1	0.89
1175	1.68	+90.2	0.3	1.30	0.77	5.38	550.8	1.09
1200	0.24	+101.1	0.5	1.64	6.96	5.15	826.8	5.16
Total	35.60	+25.8	0.3	68.42	3.25	5.79	499.2	1.14

A75080 WR Pyrolysis (**FIN150**)
Sample weight = 2.087 mg

Temp (°C)	N (ppm)	$\delta^{15}N$ (‰)	Error	C (ppm)	C/N	$^{36}Ar/^{38}Ar$	$N/^{36}Ar$	$^{40}Ar/^{36}Ar$
350(C)	6.33	+25.9	0.2	120.47	19.03	nm	nm	nm
400	0.46	+27.1	0.1	6.61	14.36	nm	4349.4	17.48
500	0.60	+87.1	0.2	4.97	8.33	6.45	881.3	3.15
550	0.53	+82.9	0.3	4.84	9.15	6.12	584.1	2.47
600	0.67	+90.3	0.3	3.73	5.60	6.20	390.0	1.92
625	0.68	+87.6	0.3	3.64	5.39	6.34	287.2	1.58
650	0.84	+87.7	0.2	2.93	3.50	6.38	248.1	1.20
675	1.30	+87.8	0.1	3.99	3.07	6.37	253.5	0.90
700	2.09	+81.3	0.1	2.48	1.19	6.47	269.9	0.65
725	3.22	+66.4	0.1	4.48	1.39	6.56	319.0	0.49
750	4.24	+43.8	0.2	4.17	0.98	6.60	369.5	0.40
778	5.24	+21.2	0.2	5.90	1.13	6.28	441.8	0.41
800	4.93	+3.2	0.2	6.66	1.35	6.46	529.9	0.48
825	4.51	-12.3	0.2	5.99	1.33	6.32	620.5	0.57
850	3.77	-26.7	0.3	6.83	1.81	6.39	803.4	0.72
875	2.55	-22.2	0.3	3.68	1.45	6.25	799.5	0.93
900	1.65	-8.2	0.2	4.57	2.77	6.21	760.8	1.09
950	1.83	-20.9	0.2	4.26	2.33	6.14	660.9	0.98
1000	1.60	-41.4	0.3	4.53	2.82	6.15	679.3	0.96
1050	1.92	-51.0	0.2	6.26	3.26	6.22	616.4	0.84
1100	2.46	-36.5	0.3	8.61	3.50	6.23	569.8	0.81
1150	3.59	-10.9	0.3	10.12	2.81	6.34	458.2	0.70
1200	4.17	+31.9	0.2	6.92	1.66	6.28	545.4	0.76
1250	0.94	+168.5	0.3	7.37	7.86	5.45	645.3	1.85
Total	53.76	+15.7	0.2	123.54	3.79	6.28	699.3	1.80

C4. Apollo 17 regolith breccia, A79035

C4.1. Whole-rock analyses of A79035

A79035 High Resolution Combustion **(FIN100)**
Sample weight = 1.868 mg

Temp (°C)	N (ppm)	$\delta^{15}N$ (‰)	Error	C (ppm)	C/N	$^{36}Ar/^{38}Ar$	$N/^{36}Ar$	$^{40}Ar/^{36}Ar$
413	0.70	-12.1	0.6	15.57	22.25	5.67	403.4	22.80
450	0.73	-39.2	0.7	17.35	23.65	5.88	178.9	6.78
500	1.16	-96.0	0.7	11.55	9.95	6.15	170.5	7.49
525	0.96	-116.0	0.9	6.69	6.95	6.03	137.8	7.33
550	0.97	-136.0	0.6	7.04	7.26	6.11	122.1	6.13
575	1.09	-152.0	0.7	7.09	6.52	6.17	124.6	5.07
600	0.99	-163.2	0.6	8.38	8.45	6.09	128.3	4.28
627	1.52	-168.3	0.5	11.10	7.29	5.98	143.5	3.71
650	1.95	-187.1	0.6	2.97	1.53	6.05	130.5	2.87
660	1.94	nm	nm	8.48	4.36	6.00	124.9	2.50
670	1.64	-197.0	0.6	6.84	4.16	5.93	122.0	2.46
680	1.63	-199.1	0.5	7.04	4.32	5.92	122.5	2.23
690	1.59	-204.9	0.6	5.40	3.39	5.88	117.7	2.30
700	1.84	-206.7	0.5	3.12	1.70	5.90	122.8	2.24
710	2.06	-211.3	0.7	6.84	3.32	5.86	120.8	1.99
721	2.31	-212.9	0.7	4.91	2.13	5.86	125.0	2.23
731	2.64	-211.3	0.6	9.12	3.46	5.89	131.5	2.18
740	2.75	-219.7	0.6	6.79	2.47	5.87	127.1	1.79
751	2.93	-224.9	0.6	4.36	1.49	5.83	127.6	1.68
760	2.90	-225.8	0.6	6.94	2.39	5.81	131.6	1.68
770	2.95	-224.0	0.7	6.00	2.03	5.78	139.9	1.97
781	3.06	-227.9	0.7	6.79	2.22	5.80	139.3	1.60
790	3.61	-226.1	0.6	5.35	1.48	5.82	144.0	1.73
800	3.06	-227.8	1.1	7.83	2.56	5.93	125.1	1.42
810	4.38	-224.8	0.6	3.57	0.82	5.80	139.2	1.48
821	4.67	-220.2	0.7	6.59	1.41	5.79	144.6	1.37
830	4.39	-218.4	0.7	6.89	1.57	5.70	147.4	1.36
840	4.36	-214.9	0.6	5.16	1.18	5.76	149.9	1.50
850	3.88	-213.1	0.5	6.94	1.79	5.81	144.6	1.43
875	4.95	-209.8	0.6	5.70	1.15	5.79	156.2	1.49
900	4.72	-204.2	0.6	6.74	1.43	5.76	161.4	1.61
925	3.97	-200.0	0.7	5.85	1.47	5.79	167.4	1.61
953	3.12	-196.4	0.7	8.58	2.75	5.74	166.9	1.66
1000	4.38	-190.9	0.6	7.29	1.66	5.75	168.5	1.54
1053	4.81	-180.7	0.6	6.64	1.38	5.72	174.7	1.57
1108	6.49	-173.4	0.6	8.48	1.31	5.71	182.2	1.55
1125	5.29	-154.4	0.6	19.19	3.63	5.67	197.1	1.72
1150	6.78	-143.8	0.6	9.12	1.34	5.60	240.1	1.77
1175	5.11	-98.6	0.5	7.59	1.48	5.47	273.2	1.87
1200	1.69	-36.4	0.5	nm	nm	nm	286.3	2.63
1250	0.43	-5.3	0.42	9.37	22.04	5.10	724.3	13.59
Total	120.44	-185.2	0.6	307.27	4.54	5.81	172.8	3.32

A79035 High Resolution Pyrolysis (**FIN125**)
Sample weight = 2.108 mg

Temp (°C)	N (ppm)	$\delta^{15}N$ (‰)	Error	C (ppm)	C/N	$^{36}Ar/^{38}Ar$	$N/^{36}Ar$	$^{40}Ar/^{36}Ar$
350(C)	0.79	-4.2	0.3	76.70	97.63	10.45	965.9	31.80
400	nm	nm	nm	6.02	nm	5.32	nm	12.27
450	0.04	-25.0	0.8	6.41	157.2	6.91	28.5	6.82
500	0.11	-34.9	0.8	7.95	69.26	6.16	51.3	5.94
550	0.25	-43.6	0.7	6.15	24.65	6.08	72.7	5.92
575	0.23	-43.9	0.7	4.88	21.19	6.16	63.2	6.37
601	0.35	-51.9	0.6	6.59	19.03	6.31	71.8	5.99
625	0.55	-117.5	0.5	6.72	12.21	6.39	76.1	5.04
650	0.92	-124.2	0.5	8.13	8.84	6.33	90.1	4.00
675	1.74	-137.5	0.5	7.47	4.29	6.43	110.8	2.94
700	3.16	-160.7	0.5	7.25	2.29	6.54	134.6	2.07
710	3.72	-174.0	0.6	8.17	2.20	6.36	156.2	1.67
720	4.02	-185.8	0.6	7.25	1.80	6.34	170.6	1.34
730	4.15	-196.7	0.6	9.05	2.18	6.32	180.9	1.15
740	4.35	-203.7	0.5	8.30	1.91	6.28	185.4	1.01
750	4.31	-208.3	0.6	8.79	2.04	6.23	187.8	0.96
760	4.22	-211.4	0.6	7.99	1.90	6.22	190.5	0.93
770	3.90	-214.5	0.6	7.16	1.84	6.16	189.3	0.93
780	3.72	-212.9	0.6	11.20	2.74	6.15	200.0	0.86
790	2.85	nm	nm	22.40	7.85	nm	228.0	1.34
800	2.35	-208.6	0.8	8.21	3.50	6.14	114.5	0.97
811	2.71	-214.1	0.6	9.09	3.35	6.13	241.1	1.00
820	2.49	-211.2	0.6	8.74	3.51	6.12	286.6	1.08
830	2.33	-209.3	0.5	11.47	4.92	6.11	314.7	1.14
840	2.00	-208.2	0.5	8.79	4.40	6.09	339.7	1.28
850	1.76	-206.5	0.6	6.85	3.88	6.13	361.2	1.39
875	2.08	-197.0	0.5	10.06	4.85	6.19	404.4	1.41
900	1.95	-177.5	0.6	7.99	4.09	6.20	414.0	1.48
925	1.77	-167.1	0.5	12.70	7.16	6.05	429.2	1.52
950	1.77	-158.3	0.4	11.07	6.24	6.05	452.9	1.46
975	1.76	-158.7	0.5	12.08	6.88	6.08	417.1	1.33
1000	2.12	-151.7	0.4	15.86	7.47	6.08	421.1	1.22
1025	2.48	-159.6	0.4	12.61	5.07	6.08	353.6	1.09
1050	3.34	-151.6	0.4	22.98	6.87	6.04	347.9	1.09
1075	4.23	-140.3	0.4	23.90	5.64	6.08	354.7	1.09
1100	4.29	-135.0	0.5	28.69	6.69	6.08	331.7	1.16
1127	4.54	-118.9	0.5	26.67	5.87	5.85	310.9	1.38
1150	5.09	-100.0	0.4	29.92	5.87	5.96	347.2	1.48
1177	3.40	-29.2	0.4	38.35	11.28	5.60	437.2	1.50
1200	1.98	+26.3	0.4	33.69	17.04	5.25	685.2	1.84
Total	97.05	-159.3	0.5	506.55	5.75	6.13	250.1	2.40

C4.2. HF/HCl residue from A79035

A79035 HF/HCl High Resolution Combustion (**FIN196**)
Sample weight = 0.229 mg

Temp (°C)	N (ppm)	N (ppmOP)	$\delta^{15}N$ (‰)	Error	C (ppm)	C (ppmOP)	C/N
350	22.58	0.010	-15.9	1.2	1105.96	0.498	48.96
375	17.28	0.008	-28.6	1.0	1454.30	0.654	84.15
400	23.94	0.011	-31.0	1.1	1310.63	0.590	54.76
425	21.52	0.010	-36.1	1.2	1569.26	0.706	72.94
450	26.33	0.012	-38.0	1.4	1792.80	0.807	68.09
460	23.97	0.011	-49.9	1.0	1719.92	0.774	71.75
470	28.38	0.013	-51.2	1.0	1657.56	0.746	58.42
480	32.30	0.015	-54.5	1.0	1679.28	0.756	51.99
490	32.63	0.015	-59.9	0.9	1778.07	0.800	54.49
500	34.04	0.015	-71.9	1.1	1616.88	0.728	47.49
510	34.07	0.015	-73.8	0.9	1041.47	0.469	30.57
520	39.57	0.018	-80.2	0.9	1157.13	0.521	29.24
530	32.36	0.015	-85.8	1.0	990.34	0.446	30.60
540	25.56	0.012	-82.2	1.0	604.87	0.272	23.66
550	27.86	0.013	-83.5	0.9	530.54	0.239	19.04
575	23.38	0.011	-85.9	0.9	596.43	0.268	25.51
600	18.06	0.008	-92.5	0.8	353.23	0.159	19.56
625	13.20	0.006	-78.6	0.9	482.19	0.217	36.54
650	6.43	0.003	-74.4	0.9	442.24	0.199	68.76
700	4.31	0.002	-72.6	0.9	201.15	0.091	46.64
800	4.20	0.002	-49.7	1.0	182.92	0.082	43.51
900	4.83	0.002	-24.0	0.8	144.38	0.065	29.92
1000	4.05	0.002	-8.1	0.9	147.88	0.067	36.55
1100	4.09	0.002	-7.7	1.0	75.69	0.034	18.53
1200	4.51	0.002	-0.6	1.1	60.26	0.027	13.36
Total	509.50	0.230	-60.8	1.0	22695.50	10.213	43.40

A79035 HF/HCl High Resolution Pyrolysis (**FIN231**)
Sample weight = 0.214 mg

Temp (°C)	N (ppm)	N (ppmOP)	$\delta^{15}N$ (‰)	Error	C (ppm)	C (ppmOP)	C/N
350(C)	58.13	0.026	-51.0	1.0	8073.67	3.633	138.90
400	0.80	0.000	nm	nm	125.08	0.056	157.19
450	3.08	0.001	-67.1	1.1	182.89	0.082	59.45
500	3.19	0.001	-79.5	0.9	291.75	0.131	91.45
550	3.61	0.002	-83.9	0.7	264.72	0.119	73.37
600	5.75	0.003	-87.8	0.7	289.49	0.130	50.37
650	8.54	0.004	-90.0	0.7	195.65	0.088	22.92
675	6.55	0.003	-90.7	0.8	222.68	0.100	33.98
700	6.40	0.003	-97.5	0.6	133.33	0.060	20.82
725	6.54	0.003	-96.3	0.7	116.82	0.053	17.87
750	8.64	0.004	-102.5	0.7	185.14	0.083	21.42
775	9.31	0.004	-103.2	1.3	134.09	0.060	14.41
800	16.43	0.007	-109.5	0.6	113.06	0.051	6.88
825	21.21	0.010	-103.7	0.7	177.63	0.080	8.37
850	26.50	0.012	-106.1	0.9	203.91	0.092	7.70
875	33.37	0.015	-108.8	0.6	224.18	0.101	6.72
900	29.23	0.013	-109.1	0.8	197.15	0.089	6.74
925	46.49	0.021	-109.7	0.7	340.54	0.153	7.33
950	47.16	0.021	-105.2	1.0	457.66	0.206	9.70
975	32.91	0.015	-97.4	0.6	848.39	0.382	25.78
1000	23.64	0.011	-93.8	0.9	417.88	0.188	17.68
1050	33.14	0.015	-89.1	0.8	537.24	0.242	16.21
1100	37.30	0.017	-89.7	0.8	824.78	0.371	22.11
1150	46.78	0.021	-83.8	0.8	1118.75	0.503	23.91
1200	40.49	0.018	-77.0	0.7	1480.20	0.666	36.56
1250	23.85	0.011	-68.9	1.1	1494.46	0.673	62.67
Total	520.90	0.234	-95.6	0.8	10577.50	4.760	32.87

A12023 HF/HCl Combusion (**FIN26**)
Sample weight = 0.570 mg

Temp (°C)	N (ppm)	N (ppmOP)	$\delta^{15}N$ (‰)	Error	C (ppm)	C (ppmOP)	C/N
350	0.92	0.001	-0.1	0.6	75.25	0.111	81.99
400	0.76	0.001	-5.1	0.7	75.73	0.111	100.35
430	0.58	0.001	+5.9	1.1	64.85	0.096	111.97
450	0.34	0.000	+7.3	1.2	37.71	0.056	111.32
460	0.38	0.001	+7.3	1.2	34.13	0.050	89.75
470	0.39	0.001	-3.3	1.2	49.90	0.073	129.23
480	0.37	0.001	+8.5	1.2	42.54	0.063	113.80
490	0.26	0.000	-0.0	1.2	26.33	0.039	100.00
500	0.37	0.001	-4.3	1.0	19.18	0.028	51.31
525	0.30	0.001	-3.0	1.0	5.69	0.008	18.73
550	0.48	0.001	-4.7	1.4	57.69	0.085	120.40
600	2.01	0.003	+7.8	0.8	93.12	0.137	46.26
650	2.46	0.004	+15.1	0.8	95.40	0.140	38.75
700	1.04	0.002	-6.1	1.2	34.29	0.051	33.12
800	0.46	0.001	-9.3	1.4	25.03	0.037	54.85
900	0.39	0.001	-9.6	1.5	17.72	0.026	45.89
1000	0.60	0.001	-3.3	1.0	8.94	0.013	14.99
1100	0.30	0.000	-0.1	1.4	5.20	0.077	17.14
1200	0.31	0.001	+0.8	1.1	3.09	0.005	9.94
Total	12.71	0.019	+3.0	1.0	771.80	1.136	67.88

C4.3. $HClO_4$ residue from A79035

A79035 $HClO_4$ Combustion (**FIN6**)
Sample weight = 0.097 mg

Temp (°C)	N (ppm)	N (ppmOP)	$\delta^{15}N$ (‰)	Error
350	3.83	0.002	-3.2	0.0
375	4.86	0.002	+3.8	0.2
400	2.48	0.001	-1.8	0.2
425	3.90	0.002	+3.3	0.2
450	1.64	0.001	+6.5	0.2
460	4.76	0.002	+5.6	0.1
470	6.62	0.003	+6.7	0.1
482	0.41	0.000	+10.4	0.2
490	1.28	0.001	-1.3	0.3
500	3.00	0.001	+4.1	0.1
513	0.83	0.000	+4.0	0.1
525	2.90	0.001	+6.4	0.1
550	2.17	0.001	+5.0	0.1
610	3.21	0.002	+10.1	0.1
700	3.21	0.002	+5.3	0.2
800	4.86	0.002	+5.8	0.1
900	4.96	0.002	+12.6	0.2
1000	1.02	0.001	+11.8	0.3
1100	5.27	0.003	+8.3	0.1
1200	6.20	0.003	+8.2	0.1
1250	12.30	0.006	+5.5	0.1
Total	79.71	0.040	+5.7	0.1

C4.4. $KMnO_4$ treatment of A79035

A79035 $KMnO_4$ Combustion (**FIN261**)
Sample weight = 0.44 mg

Temp (°C)	N (ppm)	N (ppmOP)	$\delta^{15}N$ (‰)	Error	C (ppm)	C (ppmOP)	C/N
350	4.21	0.002	+11.7	1.0	10.90	0.005	2.59
375	1.01	0.001	-14.0	0.9	3.46	0.002	3.42
400	1.08	0.001	-10.4	1.0	5.32	0.002	4.93
425	0.96	0.001	-11.1	0.8	4.28	0.002	4.47
450	1.12	0.001	-14.1	1.0	5.04	0.002	4.51
475	1.39	0.001	-14.8	0.8	11.10	0.005	7.96
500	1.76	0.001	-25.2	0.6	19.70	0.009	11.18
510	1.71	0.001	-11.2	0.8	34.62	0.016	20.30
520	1.68	0.001	-11.9	0.7	28.04	0.013	16.71
530	1.64	0.001	-9.2	0.8	26.12	0.012	15.95
540	1.79	0.001	-9.4	0.7	31.54	0.014	17.59
550	1.53	0.001	-10.2	1.2	27.34	0.012	17.92
560	1.58	0.001	-8.5	1.5	24.54	0.011	15.54
570	1.75	0.001	-11.8	1.0	20.36	0.009	11.65
580	1.97	0.001	-7.4	0.7	20.82	0.009	10.55
590	2.10	0.001	-6.9	1.2	33.48	0.015	15.91
600	2.04	0.001	-6.3	0.7	29.18	0.013	14.27
625	2.31	0.001	-14.4	0.8	25.02	0.011	10.81
650	2.02	0.001	-8.1	0.9	15.74	0.007	7.80
700	2.27	0.001	-12.5	0.7	27.68	0.012	12.20
750	2.13	0.001	-11.2	0.9	14.08	0.006	6.62
800	2.41	0.001	-14.5	2.4	9.60	0.004	3.99
850	2.34	0.001	-1.1	1.8	6.14	0.003	2.63
900	1.80	0.001	+1.0	1.4	4.60	0.002	2.55
950	1.78	0.001	+10.3	0.8	4.34	0.002	2.44
1000	1.55	0.001	+0.8	0.9	2.62	0.001	1.69
1100	1.67	0.001	+19.1	0.8	5.50	0.002	3.29
1200	2.23	0.001	+9.6	0.8	10.92	0.005	4.90
Total	51.84	0.023	-5.7	1.0	462.03	0.208	9.08

Appendix D

Stepped extraction data from the Apollo 16 site

D1. <10 μm grain size fraction of Apollo 16 soils

A60501 <10 μm Combustion **(FIN224)**
Sample weight = 0.314 mg

Temp (°C)	N (ppm)	$\delta^{15}N$ (‰)	Error	C (ppm)	C/N	$^{36}Ar/^{38}Ar$	$N/^{36}Ar$	$^{40}Ar/^{36}Ar$
400	4.40	+28.1	0.7	81.64	18.57	6.15	2308.2	2.39
450	3.77	+50.8	1.1	62.75	16.64	6.49	920.7	1.98
500	4.36	+88.5	0.8	81.64	18.71	6.62	573.7	1.98
550	6.40	+108.8	0.8	75.00	11.71	6.63	368.4	2.13
600	9.11	+122.6	0.6	42.84	4.70	6.64	257.6	1.63
650	17.58	+116.6	0.7	36.20	2.06	6.62	214.3	1.10
700	25.70	+95.1	0.7	28.54	1.11	6.58	204.1	0.62
750	55.42	+50.9	0.6	25.99	0.47	6.39	217.8	0.51
800	53.33	-9.7	0.6	23.44	0.44	6.30	222.2	0.55
850	31.67	-34.8	0.7	33.65	1.06	6.35	234.2	0.55
900	18.83	-5.5	0.7	31.09	1.65	6.47	199.0	0.63
950	11.52	-0.5	0.7	17.82	1.55	6.28	263.3	0.70
1000	6.84	-4.0	0.6	23.95	3.50	6.27	218.2	0.58
1050	8.61	-8.6	0.6	19.35	2.25	6.27	201.0	0.61
1100	15.93	-9.6	0.7	18.84	1.18	6.26	242.7	0.76
1150	12.02	-10.0	0.8	18.33	1.53	6.53	213.9	0.75
1200	11.06	-0.6	0.6	13.73	1.24	6.06	417.3	0.93
1250	2.67	-23.4	0.8	18.84	7.02	6.08	349.1	1.93
Total	299.24	+25.6	0.7	653.65	5.30	6.39	423.6	1.13

A60501 <10 μm Pyrolysis **(FIN225)**
Sample weight = 0.323 mg

Temp (°C)	N (ppm)	$\delta^{15}N$ (‰)	Error	C (ppm)	C/N	$^{36}Ar/^{38}Ar$	$N/^{36}Ar$	$^{40}Ar/^{36}Ar$
400(C)	57.50	+25.9	0.6	402.26	6.99	7.94	5361.3	8.76
450	nm	nm	nm	5.01	nm	6.32	nm	nm
500	3.28	+76.4	0.7	9.97	3.04	6.63	545.8	nm
550	3.62	+100.4	0.8	15.92	4.39	6.70	316.7	0.88
600	4.25	+149.5	0.8	10.96	2.58	6.73	155.1	1.31
650	7.16	+138.6	1.0	10.46	1.46	6.69	113.8	1.08
700	23.48	+112.5	0.6	11.45	0.49	6.80	124.8	0.73
750	34.80	+100.9	0.7	13.44	0.39	6.53	126.3	0.48
800	79.74	+60.1	1.2	10.96	0.14	6.38	230.7	0.47
850	87.19	+4.5	1.1	18.89	0.22	6.26	497.7	0.47
900	18.42	-29.3	0.8	19.39	1.05	6.54	598.3	0.10
950	7.61	-61.5	1.7	11.45	1.50	6.11	446.8	nm
1000	10.82	-75.7	0.8	14.43	1.33	6.15	438.9	0.40
1050	14.72	-72.4	0.5	9.97	0.68	6.23	361.2	0.65
1100	12.42	-63.8	1.0	16.41	1.32	6.54	214.1	0.69
1150	14.15	-29.7	0.9	26.83	1.90	6.56	226.8	0.59
1200	6.03	-12.0	0.7	18.40	3.05	5.99	459.7	0.54
1250	2.52	-15.5	1.3	11.95	4.74	6.15	458.8	0.18
Total	320.23	+28.4	1.0	235.90	1.77	6.43	332.2	0.61

A63340 <10 µm Combustion (**FIN208**)
Sample weight = 0.809 mg

Temp (°C)	N (ppm)	$\delta^{15}N$ (‰)	Error	C (ppm)	C/N	$^{36}Ar/^{38}Ar$	$N/^{36}Ar$	$^{40}Ar/^{36}Ar$
400	11.35	nm	nm	732.38	64.50	6.15	13675.4	4.29
450	18.37	+6.6	0.6	655.81	35.71	6.76	4795.3	5.27
500	19.89	+14.8	0.6	473.68	23.81	6.46	2661.4	4.12
550	18.46	+27.3	0.6	271.32	14.69	6.77	1125.7	3.20
600	10.83	+64.1	1.3	153.28	14.16	6.80	367.1	2.31
650	12.24	+90.2	0.7	66.78	5.46	6.75	213.7	1.37
700	20.37	+100.4	0.7	70.15	3.44	6.49	181.9	0.83
750	40.04	+69.1	0.8	51.30	1.28	6.32	230.6	0.71
800	38.84	+9.0	0.7	42.58	1.10	6.24	289.3	0.85
850	24.78	-59.2	1.0	36.23	1.46	6.25	291.0	0.92
900	10.73	-30.2	0.8	43.37	4.04	6.41	250.5	0.94
950	7.06	-9.9	0.6	42.38	6.01	6.23	278.3	1.05
1000	3.10	-3.7	0.6	26.50	8.54	6.24	225.2	0.95
1050	2.95	-13.5	0.7	13.81	4.67	6.23	216.1	0.97
1100	4.69	-14.4	0.6	16.98	3.62	6.25	220.8	0.97
1150	7.47	-9.0	0.7	35.83	4.79	5.97	250.6	1.04
1200	7.25	-6.4	0.9	24.72	3.41	6.50	268.3	0.97
1250	6.60	+6.2	0.6	14.40	2.18	6.12	444.9	1.06
Total	265.02	+22.0	0.7	2771.50	11.27	6.39	1443.7	1.77

A63340 <10 µm Pyrolysis (**FIN209**)
Sample weight = 0.903 mg

Temp (°C)	N (ppm)	$\delta^{15}N$ (‰)	Error	C (ppm)	C/N	$^{36}Ar/^{38}Ar$	$N/^{36}Ar$	$^{40}Ar/^{36}Ar$
350(C)	323.82	+2.9	0.6	3386.66	10.46	17.63	97860.9	10.03
400	6.97	+15.8	0.5	39.31	5.64	0.64	6886.5	5.24
450	6.43	+28.6	0.6	49.08	7.63	6.59	2021.3	4.68
500	6.72	+26.7	0.6	48.01	7.15	6.92	981.1	3.61
550	5.41	+29.2	0.6	36.47	6.74	6.66	410.7	2.83
600	6.34	+37.8	0.6	37.35	5.89	6.69	196.5	2.26
650	6.39	+54.2	0.8	44.46	6.96	6.97	110.3	1.50
700	10.30	+68.8	0.6	37.00	3.59	6.64	94.9	1.09
750	26.38	+82.7	0.8	34.33	1.30	6.56	150.5	0.80
800	49.83	+71.6	0.6	49.43	0.99	6.34	265.2	0.78
850	59.21	+34.4	0.8	60.27	1.02	6.57	645.8	0.69
900	37.23	+2.1	0.8	73.59	1.98	6.34	1444.2	0.69
950	13.20	-14.5	0.6	76.79	5.82	6.31	1193.6	0.75
1000	9.02	-25.8	1.7	63.47	7.03	6.49	853.2	0.89
1050	8.39	-33.5	1.3	81.76	9.74	6.56	620.4	1.05
1100	10.10	-31.8	0.7	96.33	9.54	6.42	438.4	1.05
1150	10.91	-23.8	2.1	157.61	14.44	6.33	378.1	0.91
1200	9.12	-6.7	3.0	106.81	11.71	6.23	409.2	0.83
1250	3.02	-5.3	0.8	59.03	19.52	6.19	430.5	0.85
Total	284.98	+29.6	0.9	1151.10	7.04	6.19	973.9	1.69

A64421 <10 μm Combustion **(FIN217)**
Sample weight = 0.836 mg

Temp (°C)	N (ppm)	$\delta^{15}N$ (‰)	Error	C (ppm)	C/N	$^{36}Ar/^{38}Ar$	$N/^{36}Ar$	$^{40}Ar/^{36}Ar$
400	7.26	+4.6	0.8	250.47	34.48	7.02	4323.3	0.77
450	6.99	+24.6	1.0	177.92	25.44	6.61	1609.0	1.66
500	5.28	+45.1	0.8	124.37	23.58	6.96	725.0	1.71
550	5.23	+90.8	1.0	81.95	15.66	7.10	341.0	1.65
600	5.55	+113.0	1.0	33.59	6.04	7.06	191.6	1.50
650	11.30	+99.5	0.8	35.31	3.13	7.07	194.0	1.07
700	26.32	+88.9	1.8	30.13	1.14	6.53	214.0	0.77
750	59.42	+51.0	0.6	35.70	0.60	6.39	270.5	0.69
800	52.87	-12.1	0.7	39.54	0.75	6.35	257.2	0.68
850	36.51	-56.7	0.7	35.70	0.98	6.68	251.8	0.66
900	19.70	-22.5	1.0	30.32	1.54	6.30	214.0	0.74
950	5.42	-7.6	0.8	17.08	3.15	6.69	216.5	0.63
1000	4.87	-6.1	0.8	22.26	4.57	6.28	218.7	0.62
1050	4.60	-9.1	1.4	15.74	3.42	6.68	198.8	0.56
1100	9.64	-15.5	0.9	22.65	2.35	6.41	234.4	0.76
1150	11.97	-13.5	0.7	13.43	1.12	6.25	259.8	0.87
1200	12.64	-2.4	0.8	13.63	1.08	6.25	308.2	0.94
1250	8.75	-13.2	1.0	4.80	0.55	6.44	732.5	0.88
Total	294.31	+14.7	0.9	984.60	7.20	6.61	597.8	0.95

A64421 <10 μm Pyrolysis **(FIN218)**
Sample weight = 0.901 mg

Temp (°C)	N (ppm)	$\delta^{15}N$ (‰)	Error	C (ppm)	C/N	$^{36}Ar/^{38}Ar$	$N/^{36}Ar$	$^{40}Ar/^{36}Ar$
350(C)	33.71	+7.6	0.8	933.15	27.69	5.83	10465.9	3.79
400	0.23	+23.1	0.9	18.41	79.35	6.80	347.5	2.35
450	1.77	+57.2	0.8	16.09	9.08	6.67	626.2	2.17
500	0.18	+37.7	0.9	15.38	84.50	6.80	34.9	1.91
550	0.16	+43.8	0.7	17.69	108.46	6.88	13.2	1.78
600	1.08	+62.5	0.7	8.08	7.51	6.91	38.5	1.63
650	4.13	+105.2	1.3	12.35	2.99	6.88	60.5	1.33
700	8.30	+103.0	0.9	20.01	2.41	6.76	65.3	0.93
750	32.51	+90.6	0.6	20.36	0.63	6.55	128.7	0.71
800	63.42	+56.8	0.8	31.76	0.50	6.59	245.4	0.65
850	79.84	+13.9	0.9	64.51	0.81	6.44	525.0	0.65
900	45.17	-18.9	0.8	47.78	1.06	6.19	1043.3	0.70
950	6.96	-43.6	0.7	26.77	3.85	6.43	592.1	0.62
1000	7.00	-79.6	1.1	24.64	3.52	6.44	523.2	0.76
1050	10.30	-67.2	1.1	20.72	2.01	6.39	505.0	0.96
1100	12.77	-59.6	0.8	21.85	1.71	6.26	344.7	1.09
1150	16.91	-30.0	0.7	25.70	1.52	6.31	351.4	1.04
1200	14.15	-15.6	1.3	14.13	1.00	6.31	739.9	0.93
1250	5.55	-8.1	0.9	11.46	2.07	6.36	1088.8	0.57
Total	310.45	+16.6	0.9	417.71	17.39	6.55	404.1	1.15

A67701<10 µm Combustion **(FIN222)**
Sample weight = 0.498 mg

Temp (°C)	N (ppm)	$\delta^{15}N$ (‰)	Error	C (ppm)	C/N	$^{36}Ar/^{38}Ar$	$N/^{36}Ar$	$^{40}Ar/^{36}Ar$
400	3.31	+25.7	0.6	85.32	25.80	6.01	2747.9	nm
450	2.74	+51.0	0.7	45.09	16.43	6.32	1020.5	1.08
500	3.08	+94.4	0.7	31.57	10.26	6.58	512.9	1.42
550	4.03	+137.5	0.8	20.95	5.20	6.65	305.2	1.20
600	8.60	+136.6	0.6	18.70	2.17	6.72	263.5	1.00
650	8.66	+141.2	0.9	19.67	2.27	6.98	166.5	0.52
700	16.24	+117.2	0.7	8.08	0.50	6.68	150.1	0.32
750	27.26	+79.8	0.9	9.69	0.36	6.39	178.0	0.25
800	29.78	+10.0	1.6	19.99	0.67	6.31	240.6	0.32
850	15.58	-73.7	1.0	18.06	1.16	6.39	307.5	0.36
900	10.37	-15.1	0.7	15.80	1.52	6.25	289.3	0.53
950	3.34	+0.3	1.7	12.91	3.86	6.24	232.3	0.28
1000	2.30	-9.6	0.8	13.55	5.90	6.18	203.8	0.23
1050	2.26	-9.9	0.8	7.11	3.15	6.22	168.7	0.28
1100	3.28	-5.2	0.7	6.79	2.07	6.16	191.9	0.42
1150	3.56	-2.0	1.0	7.11	2.00	6.06	206.8	0.52
1200	4.52	+10.8	0.7	8.08	1.79	6.31	283.7	0.65
1250	1.42	-19.8	1.1	10.98	7.73	6.70	578.7	2.07
Total	150.31	+43.2	1.0	359.45	5.16	6.40	447.1	0.67

A67701 <10 µm Pyrolysis **(FIN223)**
Sample weight = 0.598 mg

Temp (°C)	N (ppm)	$\delta^{15}N$ (‰)	Error	C (ppm)	C/N	$^{36}Ar/^{38}Ar$	$N/^{36}Ar$	$^{40}Ar/^{36}Ar$
350(C)	22.25	+17.7	1.0	356.49	16.02	0.78	124220.3	68.52
400	2.93	+24.5	0.8	16.07	5.49	5.30	6355.5	nm
450	3.12	+43.4	1.4	16.61	5.32	7.03	1922.4	0.52
500	1.52	+48.4	1.0	10.71	7.03	6.73	447.6	1.00
550	1.31	+66.7	1.1	18.49	14.13	6.81	168.1	1.23
600	1.55	+125.4	0.8	9.37	6.04	6.81	81.3	1.10
650	3.81	+122.1	1.2	12.32	3.23	6.83	83.4	0.82
700	9.20	+125.1	0.6	8.56	0.93	7.33	77.9	0.48
750	15.97	+117.6	1.0	10.71	0.67	6.52	98.0	0.33
800	32.35	+95.6	0.8	11.24	0.35	6.26	191.7	0.34
850	46.46	+51.3	0.9	19.56	0.42	5.97	615.9	0.36
900	29.60	+18.4	0.7	17.68	0.60	6.20	1684.6	0.28
950	8.39	-7.3	2.0	9.63	1.15	5.75	1213.1	nm
1000	10.43	-38.9	0.9	13.66	1.31	6.12	979.5	0.47
1050	8.46	-42.9	0.7	10.44	1.23	6.11	657.8	0.60
1100	8.20	-24.9	0.8	12.59	1.54	6.21	473.3	0.65
1150	8.13	-7.3	0.6	12.32	1.52	6.19	354.2	0.64
1200	7.07	+13.8	0.8	12.85	1.82	6.07	447.1	0.69
1250	2.69	-17.2	0.7	7.49	2.78	5.99	951.6	1.43
Total	201.19	+44.9	0.9	230.29	3.09	6.35	933.5	0.68

A68501<10 μm Combustion (**FIN202**)
Sample weight = 0.831 mg

Temp (°C)	N (ppm)	$\delta^{15}N$ (‰)	Error	C (ppm)	C/N	$^{36}Ar/^{38}Ar$	$N/^{36}Ar$	$^{40}Ar/^{36}Ar$
400	7.78	+12.3	0.5	214.01	27.51	6.90	3843.6	2.24
450	5.50	+36.7	0.7	136.79	24.89	7.24	1356.7	2.03
500	5.27	+80.9	0.7	114.57	21.75	7.16	592.2	1.86
550	5.76	+112.8	1.3	73.06	12.69	7.15	325.6	1.57
600	7.55	+116.6	0.9	51.44	6.81	7.18	232.2	1.30
650	8.63	+112.4	0.9	52.21	6.05	7.33	171.7	0.83
700	18.84	+101.9	0.7	41.40	2.20	7.08	176.7	0.53
750	32.95	+64.3	1.1	33.48	1.02	7.11	217.0	0.42
800	45.32	+18.4	0.9	47.57	1.05	7.00	269.8	0.42
850	32.26	-74.4	0.8	36.38	1.13	6.81	307.1	0.48
900	18.28	-27.7	0.6	54.91	3.00	6.71	279.2	0.53
950	6.95	-3.6	1.9	19.00	2.73	6.94	234.7	0.54
1000	6.50	+1.4	1.0	21.32	3.28	6.73	256.2	0.54
1050	6.86	-5.5	0.9	20.16	2.94	6.71	243.7	0.54
1100	7.80	-11.7	0.8	18.81	2.41	6.94	227.4	0.53
1150	8.33	-9.3	0.7	18.42	2.21	6.86	233.1	0.60
1200	10.93	+2.4	0.8	21.12	1.93	6.82	308.4	0.84
1250	2.53	+2.8	0.8	12.24	4.83	6.51	310.9	1.54
Total	238.03	+21.0	0.9	986.85	7.13	6.95	532.6	0.96

A68501 <10 μm Pyrolysis (**FIN220**)
Sample weight = 0.597 mg

Temp (°C)	N (ppm)	$\delta^{15}N$ (‰)	Error	C (ppm)	C/N	$^{36}Ar/^{38}Ar$	$N/^{36}Ar$	$^{40}Ar/^{36}Ar$
350(C)	9.23	+15.5	1.0	711.26	77.07	5.18	3581.4	4.03
400	nm	nm	nm	33.46	nm	6.78	nm	2.89
450	2.43	+24.2	0.7	38.84	15.98	6.48	1081.9	2.48
500	0.64	+35.5	nm	30.34	47.66	6.67	153.5	2.22
555	0.44	+36.1	nm	22.71	46.90	6.78	54.2	2.04
600	1.72	+47.8	0.5	16.26	10.52	6.84	79.2	1.75
650	2.37	+107.6	0.6	32.93	13.89	6.85	48.0	1.35
700	7.44	+104.5	0.7	31.04	4.17	7.39	64.7	0.82
750	15.72	+98.3	0.7	24.06	1.53	6.58	92.3	0.61
800	46.95	+79.6	0.9	42.33	0.90	6.36	185.7	0.53
850	66.87	+39.8	0.6	33.19	0.50	6.23	380.8	0.54
900	54.27	+3.7	0.8	67.33	1.24	6.20	856.4	0.58
950	10.51	-16.8	0.8	38.57	3.67	6.46	744.8	0.87
1000	8.65	-58.7	1.1	40.99	4.74	6.13	601.2	0.77
1050	9.80	-72.7	1.2	25.13	2.56	6.19	466.4	0.89
1100	7.88	-59.2	1.0	35.88	4.55	6.62	305.6	0.90
1150	11.34	-37.4	1.6	47.71	4.21	6.42	276.0	0.90
1200	10.95	-15.6	0.9	34.00	3.10	6.15	318.2	0.85
1250	2.42	-5.4	0.7	28.63	11.83	6.00	284.2	0.70
Total	260.39	+26.5	0.8	623.40	10.47	6.51	350.7	1.19

D2. Potassium permanganate treatment of <10 μm fraction of A63340

A63340 <10 μm Combustion (**FIN250**)
Sample weight = 1.048 mg

Temp (°C)	N (ppm)	$\delta^{15}N$ (‰)	Error	C (ppm)	C/N	$^{36}Ar/^{38}Ar$	$N/^{36}Ar$	$^{40}Ar/^{36}Ar$
350	2.11	+14.1	0.5	15.01	7.12	18.63	6363.2	155.20
400	0.02	-14.8	0.9	0.92	40.10	6.21	95.2	0.32
450	0.32	+80.3	0.7	nm	nm	6.64	143.6	1.47
500	1.10	+105.5	0.6	3.06	2.79	6.52	108.6	0.94
550	1.61	+93.9	0.6	0.31	0.19	6.54	58.8	1.10
600	2.72	+64.8	1.9	nm	nm	6.45	37.2	1.16
650	4.49	+60.9	0.6	nm	nm	6.50	24.3	0.91
Total	12.37	+62.4	0.9	19.30	7.17	8.21	975.9	23.01

References

Abell P.I., Eglinton G., Maxwell J.R. and Pillinger C.T. (1970) Indigenous lunar methane and ethane. *Nature*, **226**, 251-252.

Abell P.I., Cadogan P.H., Eglinton G., Maxwell J.R. and Pillinger C.T. (1971) Survey of lunar carbon compounds. I: The presence of indigenous gases and hydrolysable carbon compounds in Apollo 11 and Apollo 12 samples. *Proc. 2nd Lunar Sci. Conf.*, 1843-1863.

Alexander C.M.O'D., Arden J.W., Ash R.D. and Pillinger C.T. (1990) Presolar components in the ordinary chondrites. *Earth Planet. Sci. Lett.*, **99**, 220-229.

Amari S., Anders E., Virag A. and Zinner E. (1990) Interstellar graphite in meteorites. *Nature*, **345**, 238-240.

Anders E and Grevesse N. (1989) Abundances of the elements: Meteoritic and solar. *Geochim. Cosmochim. Acta*, **53**, 197-214.

Apollo 17 Preliminary Examination Team (1973) Apollo 17 Lunar Samples: Chemical and petrographic description. *Science*, **182**, 659-672.

Ash R.D. (1990) A carbon and nitrogen study of interstellar grains. *Unpublished PhD thesis, Open University*.

Ash R.D., Arden J.W., Grady M.M., Wright I.P. and Pillinger C.T. (1989a) Recondrite interstellar carbon components in the Allende meteorite revealed by preparative precombustion. *Geochim. Cosmochim. Acta*, **54**, 455-468.

Ash R.D., Arden J.W. and Pillinger C.T. (1989b) Light nitrogen associated with SiC in Cold Bokkeveld (abstract). *Meteoritics*, **24**, 248.

Aston F.W. (1919) A positive ray spectrograph. *Phil. Mag.*, **38**, 707-714.

Baldwin R.R. (1973) Mission description. *Apollo 17 Prelim. Sci. Report*, **NASA SP-330**, 2-1 to 2-10.

Balogh A., Smith E.J., Tsurutani B.T., Southwood D.J., Forsyth R.J. and Horbury T.S. (1995) The heliospheric magnetic field over the south polar region of the Sun. *Science*, **268**, 1007-1010.

Bame S.J., Hundhausen A.J., Ashbridge J.R. and Strong I.B. (1968) Solar wind ion composition. *Phys. Rev. Lett.*, **20**, 393-395.

Bame S.J., Ashbridge J.R., Hundhausen A.J. and Montgomery M.D. (1970) Solar wind ions: $^{56}Fe^{+8}$ to $^{56}Fe^{+12}$, $^{28}Si^{+7}$, $^{28}Si^{+8}$, $^{28}Si^{+9}$ and $^{16}O^{+6}$. *J. Geophys. Res.*, **75**, 6360-6365.

Bansal B.M., Church S.E., Gast P.W., Hubbard N.J., Rhodes J.M. and Wiesmann H. (1973) Chemical compositions of soil from the Apollo 16 and Luna-20 sites. *Earth Planet. Sci. Letts.*, **17**, 29.

Basu A., DesMarais D.J., Hayes J.M. and Meinschein W.G. (1975) Integrated investigation of the mixed origin of lunar sample 72161, 11. *The Moon*, **14**, 129-138.

Baur H., Frick U., Funk H., Schultz L. and Singer P. (1972) Thermal release of helium, neon and argon from lunar fines and minerals. *Proc. 3rd Lunar Sci. Conf.*, 1947-1966.

Becker R.H. (1980a) Light elements in lunar soils revisited: Carbon, nitrogen, hydrogen and helium. *Proc. 11th Lunar Planet. Sci. Conf.*, 1743-1761.

Becker R.H. (1980b) Evidence for secular variation in the $^{13}C/^{12}C$ ratio of carbon implanted into lunar soils. *Earth Planet. Sci. Letts.*, **50**, 189-196.

Becker R.H. (1995) An evaluation of possible explanations for "excess" nitrogen in the lunar regolith (abstract). *Lunar Planet. Sci. Conf.*, **XXVI**, 89-90.

Becker R.H. and Clayton R.N. (1975) Nitrogen abundances and isotopic compositions in lunar samples. *Proc. 6th Lunar Sci. Conf.*, 2131-2149.

Becker R.H., Clayton R.H. and Mayeda T.K. (1976) Characterisation of lunar nitrogen components. *Proc. 7th Lunar Sci. Conf.*, 441-458.

Becker R.H. and Clayton R.N. (1977) Nitrogen isotopes in lunar soils as a measure of cosmic-ray exposure and regolith history. *Proc. 8th Lunar Sci. Conf.*, 3685-3704.

Becker R.H. and Clayton R.N. (1978) Nitrogen isotope systematics of two Apollo 12 soils. *Proc. 9th Lunar Planet. Sci. Conf.*, 1619-1627.

Becker R.H. and Epstein S. (1981) Carbon isotope ratios in some low-$\delta^{15}N$ lunar breccias. *Lunar Planet. Sci. Conf.*, **XII**, 289-293.

Becker R.H. and Pepin R.O. (1989) Long term changes in solar wind elemental and isotopic ratios: A comparison of two lunar ilmenites of different antiquities. *Geochim. Cosmochim. Acta*, **53**, 1135-1146.

Becker R.H. and Pepin R.O. (1994) Solar wind noble gases and nitrogen in metal from lunar soil A68501. *Meteoritics*, **29**, 724-738.

Behrmann C., Crozaz G., Drozd R., Hohenberg C., Ralston C., Walker R. and Yuhas D. (1973) Cosmic-ray exposure history of North Ray and South Ray material. *Proc. 4th Lunar Sci. Conf.*, 1957-1974.

Benkert J.P., Baur H., Signer P. and Wieler R. (1993) He, Ne and Ar from the solar wind and solar energetic particles in lunar ilmenites and pyroxenes. *J. Geophys. Res (Planets)*, **98**, 13147-13162.

Bibring J.P., Burlingame A.L., Langevin Y., Maurette M. and Wszolek P.C. (1974) Simulation of lunar carbon chemistry: II. Lunar winds contribution. *Proc. 5th Lunar Sci. Conf.*, 1763-1784.

Bibring J.P., Burlingame A.L., Langevin Y., Maurette M. and Vassent B. (1975) Solar wind and solar flare maturation of the lunar regolith. *Proc. 6th Lunar Sci. Conf.*, 3471-3493.

Black D.C. (1972) On the origins of trapped helium, neon and argon isotopic variations in meteorites - II. Carbonaceous meteorites. *Geochim. Cosmochim. Acta*, **36**, 377-394.

Black D.C. and Pepin R.O. (1969) Trapped neon in meteorites II. *Earth Planet. Sci. Lett.*, **6**, 395-405.

Bochsler P. (1994) Solar wind composition from the moon. *Adv. Space Research*, **14**, 161-173.

Bogard D.D. and Nyquist L.E. (1973) $^{40}Ar/^{36}Ar$ variations in Apollo 15 and 16 regolith. *Proc. 4th Lunar Sci. Conf.*, 1975-1985.

Bogard D.D., Hirsch W.C. and Nyquist L.E. (1974) Noble gases in Apollo 17 fines. Mass fractionation effects in trapped Xe and Kr. *Proc. 5th Lunar Sci. Conf.*, 1975-2003.

Boyd S.R. and Pillinger C.T. (1991) Rubidium Sulfate - Ammonium Sulfate solid solution: A standard for use during the determination of nitrogen abundance and isotopic composition at the ppm level by static vacuum mass spectrometry. *Analytical Chemistry*, **63**, 1332-1335.

Boyd S.R., Wright I.P., Franchi I.A. and Pillinger C.T. (1988) Preparation of sub-nanomole quantities of nitrogen gas for stable isotope analysis. *J. Phys. E. Sci. Instrum.*, **21**, 876-885.

Bradley J.P., Dukes C., Baragiola R., McFadden L., Johnson R.E. and Brownlee D.E. (1996) Radiation processing and the origins of interplanetary dust (abstract). *Lunar Planet. Sci. Conf.*, **XXVII**, 149-150.

Brenemann H.H. and Stone E.C. (1985) Solar coronal and photospheric abundances from solar energetic particles. *Astrophys. J.*, **299**, L57-L61.

Brilliant D.R., Franchi I.A., Arden J.W. and Pillinger C.T. (1992) An interstellar component in the lunar regolith (abstract). *Meteoritics*, **27**, 206-207.

Brilliant D.R., Franchi I.A. and Pillinger C.T. (1994) Nitrogen components in lunar soil 12023: Complex grains are not the carrier of isotopically light nitrogen. *Meteoritics*, **29**, 718-723.

Brown P.W. and Pillinger C.T. (1981) Nitrogen concentrations and isotopic ratios from separated lunar soils (abstract). *Meteoritics*, **16**, 298.

Brunfelt A.O., Heier K.S., Nilssen B., Steinnes E. and Sundvoll B. (1973) Elemental composition of Apollo 15 and 16 rocks, fines and minerals. *Lunar Science*, **IV**, 100-102. Lunar Science Institute, Houston.

Bühler F., Geiss J., Meister J., Eberhardt P., Huneke J.C. and Signer P. (1966) Trapping of the solar wind in solids. Part 1. Trapping probability of low energy He, Ne and Ar ions. *Earth Planet. Sci. Letts.*, **1**, 249-255.

Butler J.C., Greene G.M. and King E.A.Jr. (1973) Grain size frequency distributions and modal analyses of Apollo 16 fines. *Proc. 4th Lunar Sci. Conf.* 267-278.

Cadogan P.H., Eglinton G., Maxwell J.R. and Pillinger C.T. (1971) Carbon chemistry of the lunar surface. *Nature*, **231**, 29-31.

Cadogan P.H., Eglinton G., Firth J.N.M., Maxwell J.R., Mays B.T. and Pillinger C.T. (1972) Survey of lunar carbon compounds: II. The carbon chemistry of Apollo 11, 12, 14 and 15 samples. *Proc. 3rd Lunar Sci. Conf.* 2069-2090.

Cadogan P.H., Eglinton G., Gowar A.P., Jull A.J.T., Maxwell J.R. and Pillinger C.T. (1973) Location of methane and carbide in Apollo 11 and 16 lunar fines. *Proc. 4th Lunar Sci. Conf.* 1493-1508.

Cameron A.G.W. (1962) The formation of the sun and planets. *Icarus*, **1**, 13-69.

Cameron A.G.W. (1982) Elemental and nuclidic abundances in the solar system. *In: Essays in Nuclear Astrophysics (eds C.A.Barnes, D.D.Clayton and D.N.Schramm), Cambridge University Press, New York*, 23-43.

Cameron A.G.W. and Ward W.R. (1976) The origin of the Moon (abstract). In: *Lunar Science*, **VII**, 120-122. The Lunar Science Institute, Houston.

Carr L.P., Wright I.P. and Pillinger C.T. (1985a) Nitrogen content and isotopic composition of lunar breccia 79035: A high resolution study (abstract). *Meteoritics*, **20**, 622-623.

Carr L.P., Wright I.P. and Pillinger C.T. (1985b) Nitrogen abundance and isotopes in lunar breccias - A progress report. *Lunar Planet. Sci. Conf.*, **XVI**, 115.

Carr R.H., Wright I.P., Joines A.W. and Pillinger C.T. (1986) Measurement of carbon stable isotopes at the nanaomole level: a static mass spectrometer and sample preparation technique. *J. Phys. E. Sci. Instrum.*, **19**, 798-808.

Carrier W.D.III. (1973) Lunar soil grain size distribution. *The Moon*, **6**, 250-263.

Carter G. and Colligon J.S. (1968) Ion bombardment of solids. *Heinemann Educational Books Ltd., London*, 446pp.

Carter G., Baruah J.N. and Grant W.A. (1972) The collection of ions in semiconductors. II. Range distributions derived from collection and sputter-etch curves. *Rad. Effects*, **16**, 107-114.

Cerutti H. (1974) Die Bestimmung des Argons im Sonnenwind aus Messungen an den Apollo-SWC-folien. *PhD thesis, Univ. Bern.*

Chang S., Lawless J., Romiez M., Kaplan I.R., Petrowski C., Sakai H. and Smith J.W. (1974a) Carbon, nitrogen and sulfur in lunar fines 15012 and 15013, abundances, distributions and isotopic compositions. *Geochim. Cosmochim. Acta*, **38**, 853-872.

Chang S., Lennon K. and Gibson E.K.Jr. (1974b) Abundances of C, N, H, He and S in Apollo 17 soils from Stations 3 and 4 : Implications for solar wind exposure ages and regolith evolution. *Proc. 5th Lunar Sci. Conf.*, 1785-1800.

Charette M.P. and Adams J.B. (1975) Agglutinates as indicators of lunar soil maturity: The rare gas evidence at Apollo 16. *Proc. 6th Lunar Sci. Conf.*, 2281-2289.

Clayton D.D. and Ward R.A. (1968) Principles of stellar evolution and nucleosynthesis. *McGraw-Hill, New York*, 612pp.

Clayton D.D. and Ward R.A. (1978) s-Process studies: xenon and krypton isotopic abundances. *Astrophys. J.*, **224**, 1000-1006.

Clayton R.N., Grossman L. and Mayeda T.K. (1973) A component of primitive nuclear composition in carbonaceous chondrites. *Science*, **182**, 485-488.

Clayton R.N. and Thiemens M.H. (1980) Lunar nitrogen: Evidence for a secular change in the solar wind. *In: Proc. Conf. Ancient Sun (eds R.O.Pepin, J.A.Eddy and R.B.Merril), Pergamon.*, 463-473.

Compston W., Vernon M.J., Chappell B.W. and Freeman R. (1973) Rb-Sr model ages and chemical compositions of nine Apollo 16 soils. *Lunar Science*, **IV**, 158-160. Lunar Science Institute, Houston.

Cook W.R., Stone E.C. and Vogt R.E. (1980) Elemental composition of solar energetic nuclei. *Astrophys. J.*, **238**, L97 59-F8.

Crozaz G., Haack U., Hair M., Maurette M., Walker R. and Woolum D. (1970) Nuclear track studies of ancient solar radiation and dynamic lunar surface processes. *Proc. Apollo 11 Lunar Sci. Conf.*, 2051-2080.

Crozaz G., Walker R. and Woolum D. (1971) Nuclear track studies of dynamic surface processes on the moon and the constancy of solar activity. *Proc. 2nd Lunar Sci. Conf.*, 2543-2558.

Crozaz G., Drozd R., Hohenberg C., Morgan C., Ralston C., Walker R. and Yuhas D. (1974) Lunar surface dynamics - some general conclusions and new results from Apollo 16 and 17. *Proc. 5th Lunar Sci. Conf.*, 2475-2499.

Cuttitta F., Rose H.J., Annell C.S., Carron M.K., Christian R.P., Dwornik E.J., Greenland L.P., Helz A.W. and Ligon D.T. (1971) Elemental composition of some Apollo 12 lunar rocks and soils. *Proc. 2nd Lunar Sci. Conf.*, 1217-1229.

Delano J.W. (1986) Pristine lunar glasses: Criteria, data and implications. *Proc. 16th Lunar Planet. Sci. Conf. (J. Geophys. Res. supplement)*, 91, D201-D213.

DesMarais D.J. (1978) Carbon, nitrogen and sulfur in Apollo 15,16 and 17 rocks. *Proc. 9th Lunar Sci. Conf.*, 2451-2467.

DesMarais D.J. (1983) Light element geochemistry and spallogenesis in lunar rocks. *Geochim. Cosmochim. Acta*, **47**, 1769-1781.

DesMarais D.J., Hayes J.M. and Meinschein W.G. (1973) The distribution in lunar soils of carbon released by pyrolysis. *Proc. 4th Lunar Sci. Conf.*, 1543-1558.

DesMarais D.J., Hayes J.M. and Meinschein W.G. (1974a) Retention of solar wind implanted elements in lunar soils (abstract). *Lunar Science*, V, 168-170.

DesMarais D.J., Hayes J.M. and Meinschein W.G. (1974b) The distribution in lunar soil of hydrogen released by pyrolysis. *Proc. 5th Lunar Sci. Conf.*, 1811-1822.

DesMarais D.J., Basu A., Hayes J.M and Meinschein W.G. (1975) Evolution of carbon isotopes, agglutinates and the lunar regolith. *Proc. 6th Lunar Sci. Conf.*, 2353-2373.

Dran J.C., Durrieu L., Jouret C. and Maurette M. (1970) Habit and texture studies of lunar and meteoritic material with the 1 MeV electron microscope. *Earth Planet. Sci. Letts.*, **9**, 391-400.

Duncan A.R., Erlank A.J., Willis J.P. and Ahrens L.H. (1973) Composition and inter relationships of some Apollo 16 samples. *Proc. 4th Lunar Sci. Conf.*, 1097-1113.

Eberhardt P., Geiss J., Graf H., Gröglerr N., Krähenbühl U., Schwaller H., Schwarzmüller J. and Stettler A. (1970) Trapped solar wind noble gases, exposure age and K/Ar age in Apollo 11 lunar fine material. *Proc. Apollo 11 Lunar Sci. Conf.*, 1037-1070.

Eberhardt P., Geiss J., Graf H., Grögler M., Mendia D., Mörgeli M., Schwaller H., Stettler A., Krähenbühl U. and Gunten H.R.von. (1972) Trapped solar wind noble gases in Apollo 12 lunar fines 12001 and Apollo 11 breccia 10046. *Proc. 3rd Lunar Sci. Conf.*, 1821-1856.

Eberhardt P., Eugster O., Geiss J., Grögler N., Guggisberg S. and Mörgeli M. (1976) Noble gases in the Apollo 16 special soils from the East-West split and the permanently shadowed area. *Proc. 7th Lunar Sci. Conf.*, 561-585.

Eberhardt P., Jungck M.H.A., Meier F.O. and Niederer F.R. (1981) A neon-E rich phase in Orgeil: results obtained from density separates. *Geochim. Cosmochim. Acta*, **45**, 1515-1528.

Epstein S. and Taylor H.P.Jr. (1970) The concentration and isotopic composition of hydrogen, carbon and silicon in Apollo 11 lunar rocks and minerals. *Proc. Apollo 11 Lunar Sci. Conf.*, 1085-1096.

Epstein S. and Taylor H.P.Jr. (1971) $^{18}O/^{16}O$, $^{30}Si/^{28}Si$, D/H and $^{13}C/^{12}C$ ratios in lunar samples. *Proc. 2nd Lunar Sci. Conf.*, 1421-1441.

Epstein S. and Taylor H.P.Jr. (1972) $^{18}O/^{16}O$, $^{30}Si/^{28}Si$, $^{13}C/^{12}C$ and D/H studies of Apollo 14 and 15 samples. *Proc. 3rd Lunar Sci. Conf.*, 1429-1454.

Epstein S. and Taylor H.P.Jr. (1973) The isotopic composition and concentration of water, hydrogen and carbon in some Apollo 15 and 16 soils and in the Apollo 17 orange soil. *Proc. 4th Lunar Sci. Conf.*, 1559-1575.

Epstein S. and Taylor H.P.Jr. (1975) Investigation of the carbon, hydrogen, oxygen and silicon isotope and concentration relationships on the grain surfaces of a variety of lunar soils and in some Apollo 15 and 16 core samples. *Proc. 6th Lunar Sci. Conf.*, 1771-1798.

Etique P. (1981) L'utilisation des plagioclases du regolith lunaire comme detecteurs des gaz rares provant des rayonnements corpusculaires solaires. *Unpublished PhD thesis, ETH Zürich.*.

Eugster O., Geiss J. and Grögler N. (1983) Dating of early regolith exposure and the evolution of trapped $^{40}Ar/^{36}Ar$ with time. *Lunar Planet. Sci. Conf.*, **XIV**, 177-178.

Exley R.A., Boyd S.R., Mattey D.P. and Pillinger C.T. (1987) Nitrogen isotope geochemistry of basaltic glasses: implications for mantle degassing and structure? *Earth Planet. Sci. Letts.*, **81**, 163-174.

Fallick A.E., Gardiner L.R., Jull A.J.T. and Pillinger C.T. (1980) Instrumental effects in the application of static mass spectrometry to high sensitivity carbon isotope measurements. *Adv. Mass Spectum. A*, **8**, 309-317.

Filleux C., Spear R.H., Tombrello T.A. and Burnett D.S. (1978) Direct measurement of surface carbon concentrations for lunar soil breccias. *Proc. 9th Lunar Sci. Conf.*, 1385-1398.

Foukal P. (1990) Chapter 12. The solar wind and heliosphere. In: *Solar Astrophysics*, 397-430. John Wiley & Sons Inc., New York.

Franchi I.A. (1988) Nitrogen isotopic variations in Irons and other Fe-Ni metal rich meteorites. *Unpublished PhD thesis, Open University.*

Frick U. and Pepin R.O. (1981) Fractionation in solar system krypton and xenon, and their isotopic compositions in the solar wind (abstract). *Meteoritics*, **16**, 316-317.

Frick U., Baur H., Ducati H., Funk H., Phinney D. and Signer P. (1975) On the origin of helium, neon and argon isotopes in sieved mineral separates from an Apollo 15 soil. *Proc. 6th Lunar Sci. Conf.*, 2097-2129.

Frick U., Becker R.H. and Pepin R.O. (1988) Solar wind record in the lunar regolith: Nitrogen and noble gases. *Proc. 18th Lunar Sci. Conf.*, 87-120.

Friedman I., Gleason J.D. and Hardcastle K.G. (1970) Water, hydrogen, deuterium, carbon and ^{13}C content of selected lunar material. *Proc. Apollo 11 Lunar Sci. Conf.*, 1103-1109.

Friedman I., O'Neil J.R., Gleason J.D. and Hardcastle K. (1971) The carbon and hydrogen content and isotopic composition of some Apollo 12 materials. *Proc. 2nd Lunar Sci. Conf.*, 1407-1415.

Frondel C., Klein C.J. and Ito J. (1971) Mineralogical and chemical data on Apollo 12 lunar fines. *Proc. 2nd Lunar Sci. Conf.*, 719-726.

Ganapathy R., Keays R.R., Laul J.C. and Anders E. (1970) Trace elements in Apollo 11 lunar rocks : Implications for meteorite influx and origin of the Moon. *Proc. Apollo 11 Lunar Sci. Conf.*, 1117-1142.

Gardiner L.R. and Pillinger C.T. (1979) Static vacuum mass spectrometry for the determination of active gases. *Anal. Chem.*, **51**, 1230-1236.

Gardiner L.R., Woodcock M.R., Pillinger C.T. and Stephenson A. (1977) Carbon chemistry and magnetic properties of bulk and agglutinate size fractions from soil 15601. Proc. 8th Lunar Sci. Conf., 2817-2839.

Geiss J. (1973) Solar wind composition and implications about the history of the solar system. *Proc. 13th Int. Cosmic Ray Conf.*, 3375-3398.

Geiss J. and Bochsler P. (1982) Nitrogen isotopes in the solar system. *Geochim. Cosmochim. Acta*, **46**, 529-548.

Geiss J. and Bochsler P. (1991) Long time variations in solar wind properties: Possible causes versus observations. *In: The Sun In Time (eds C.P.Sonnett, M.S.Giampapa and M.S.Matthews), University of Arizona Press*, 98-117.

Geiss J., Eberhardt P., Bühler F., Meister J. and Signer P. (1970) Apollo 11 and 12 Solar Wind Composition Experiments: Fluxes of He and Ne isotopes. *J. Geophys. Res.*, **75**, 5972-5979.

Geiss J., Bühler F., Cerutti H., Eberhardt P. and Meister J. (1971) The Solar Wind Composition Experiment. *Apollo 14 Prelim. Sci. Report*, **NASA SP-272**, 221-226.

Geiss J., Bühler F., Cerutti H.and Eberhardt P. (1972a) Solar wind composition experiment. *Apollo 15 Prelim. Sci. Report*, **NASA SP-289**, 15.1-15.7.

Geiss J., Bühler F., Cerutti H., Eberhardt P. and Filleux Ch. (1972b) Solar wind composition experiment. *Apollo 16 Prelim. Sci. Report*, **NASA SP-315**, 14.1-14.10.

Geiss J., Gloeckler G., von Steiger R., Balsiger H., Fisk L.A., Galvin A.B., Ipavich F.M., Livi S., McKenzie J.F., Ogilvie K.W. and Wilken B. (1995) The southern high-speed stream: Results from the SWICS instrument on Ulysses. *Science*, **268**, 1033-1036.

Gibson E.G. (1973) *The Quiet Sun*. **NASA SP-303**.

Gibson E.K.Jr. and Moore G.W. (1972) Inorganic gas release and thermal analysis study of Apollo 14 and 15 soils. *Proc. 3rd Lunar Sci. Conf.*, 2029-2040.

Gibson E.K.Jr. and Moore G.W. (1973) Carbon and sulfur distributions and abundances in lunar fines. *Proc. 4th Lunar Sci. Conf.*, 1577-1586.

Goel P.S. and Kothari B.K. (1972) Total nitrogen contents of some Apollo 14 lunar samples by neutron activation analysis. *Proc. 3rd Lunar Sci. Conf.*, 2041-2050.

Goldstein J.I. and Axon H.J. (1973) Composition, structure and thermal history of metal particles in Apollo 16 rake samples. *Proc. 4th Lunar Sci. Conf.*, 751-775.

Goldstein J.I. and Yakowitz H. (1971) Metallic inclusions and metal particles in the Apollo 12 lunar soil. *Proc. 2nd Lunar Sci. Conf.*, 177-191.

Grady M.M. (1983) The content and isotopic composition of carbon in stony meteorites. *Unpublished PhD thesis, University of Cambridge.*

Graf J.C. (1993) Lunar soils Grain Size Catalog. **NASA Reference Publication 1265**.

Greenwood N.N. and Howe A.T. (1970) Mossbauer studies of Apollo 11 lunar samples. *Proc. Apollo 11 Lunar Sci. Conf.*, 2163-2169.

Halstead R.E. and Nier A.O. (1950) Gas flow through the mass spectrometer viscous leak. *Rev. Sci. Instrum.*, **21**, 1019-1021.

Hartmann W.K. (1968) Lunar crater counts. VI. The young craters Tycho, Aristarchus and Copernicus. *Comm. Lunar Planet. Lab.*, **7**, 145-156.

Hartmann W.K. and Davis D.R. (1975) Satellite-sized planetesimals and lunar origin. *Icarus*, **24**, 504-515.

Heiken G. and McKay D.S. (1974) Petrography of Apollo 17 soils. *Proc. 5th Lunar Sci. Conf.*, 843-860.

Heiken G.H., McKay D.S. and Fruland R.M. (1973) Apollo 16 soils: grain size analysis and petrography. *Proc. 4th Lunar Sci. Conf.*, 251-265.

Heymann D., Yaniv A., Adams J.A.S. and Fryer G.E. (1970) Inert gases in lunar samples. *Science*, **167**, 555-558.

Hinners N.W. (1973) Apollo 17 site selection. *Apollo 17 Prelim. Sci. Report.* **NASA SP-330**, 1-1 to 1-5.

Hintenberger H. and Weber H.W. (1973) Trapped rare gases in lunar fines and breccias. *Proc. 4th Lunar Sci. Conf.*, 2003-2019.

Hintenberger H., Weber H.W., Voshage H., Wänke H., Begemann F. and Wlotzka F. (1970) Concentrations and isotopic abundances of the rare gases, hydrogen and nitrogen in Apollo 11 lunar matter. *Proc. Apollo 11 Lunar Sci. Conf.*, 1269-1282.

Hintenberger H., Weber H.W. and Takaoka N. (1971) Concentration and isotopic abundances of the rare gases in lunar matter. *Proc. 2nd Lunar Sci. Conf.*, 1607-1625.

Hintenberger H., Weber H.W. and Schultz L. (1974) Solar, spallogenic and radiogenic rare gases in Apollo 17 soils and breccias. *Proc. 5th Lunar Sci. Conf.*, 2005-2022.

Hodges R.R.Jr. (1975) Formation of the lunar atmosphere. *The Moon*, **14**, 139-157.

Hohenberg C.M., Davis P.K., Kaiser W.A., Lewis R.S. and Reynold J.H. (1970) Trapped and cosmogenic rare gases from stepwise heating of Apollo 11 samples. *Proc. Apollo 11 Lunar Sci. Conf.*, 1283-1309.

Holland P.T., Simoneit B.R., Wszolek P.C. and Burlingame A.L. (1972a) Compounds of carbon and other volatile elements in Apollo 14 and 15 samples. *Proc. 3rd Lunar Sci. Conf.*, 2131-2147.

Holland P.T., Simoneit B.R., Wszolek P.C., McFadden W.H. and Burlingame A.L. (1972b) Carbon chemistry of Apollo 14 size fractionated fines. *Nature Phys. Sci.*, **235**, 106-108.

Housley R.M., Blander M., Abel-Gaward M., Grant R.W. and Muir A.H. (1970) Mossbauer spectroscopy of Apollo 11 samples. *Proc. Apollo 11 Lunar Sci. Conf.*, 2251-2268.

Housley R.M., Grant R.W. and Abdel-Gawad M. (1972) Study of excess Fe-metal in the lunar fines by magnetic separation. Mössbauer spectroscopy and microscopic examination. *Proc. 3rd Lunar Sci. Conf.*, 1065-1076.

Housley R.M., Cirlin E.H. and Grant R.W. (1973a) Characterization of fines from the Apollo 16 site. *Proc. 4th Lunar Sci. Conf.*, 2729-2735.

Housley R.M., Grant R.W. and Paton N.E. (1973b) Origin and characteristics of excess Fe metal in lunar glass welded aggregates. *Proc. 4th Lunar Sci. Conf.*, 2737-2749.

Hübner W., Kirsten T. and Kiko J. (1975) Rare gases in Apollo 17 soils with emphasis on analysis of size and mineral fractions of soil 74241. *Proc. 6th Lunar Sci. Conf.*, 2009-2026.

Humbert F., Marty B. and Wieler R. (1997) Nitrogen and argon in individual lunar soils grains. *Meteoritics and Planetary Science*, **32**, A62-A63.

Hundhausen A.J. (1970) Composition and dynamics of the solar wind plasma. *Rev. Geophys. Space Phys.*, **8**, 729-811.

Huss G.R. and Lewis R.S. (1994) Noble gases in presolar diamonds. I: Three distinct components and their implications for diamond origins. *Meteoritics*, **29**, 791-916.

Huss G.R., Lewis R.S. and Hemkin S. (1996) The "normal planetary" noble gas component in primitive chondrites: compositions, carrier and metamorphic history. *Geochim. Cosmochim. Acta.*, **60**, 3311-3340.

Irako M., Oguri T. and Kanomata I. (1975) The static operation mass spectrometer. *Japan. J. Appl. Phys.*, **14**, 523-543.

James O.B. (1981) Petrologic and age relations in Apollo 16 rocks: Implications for subsurface geology and the age of the Nectaris basin. *Proc. 12B Lunar Planet. Sci. Conf.*, 209-233.

Javoy M. and Pineau F. (1986) Nitrogen isotopes in mantle materials Terra Cognita. *IGOG*, **VI**, 6, 103.

Javoy M., Pineau F. and Demaiffe D. (1984) Nitrogen and carbon isotopic composition in the diamonds of Mbuji Mayi (Zaire). *Earth Planet. Sci. Letts.*, **68**, 399-412.

Jull A.J.T. and Pillinger C.T. (1977) Effects of sputtering on solar wind element accumulation. *Proc. 8th Lunar Sci. Conf.*, 3817-3833.

Kaplan I.R. (1975) Stable isotopes as a guide to biochemical processes. *Proc. R. Soc. Lond. B.*, **189**, 183-211.

Kaplan I.R., Smith J.W. and Ruth E. (1970) Carbon and sulfur concentration and isotopic composition in Apollo 11 lunar samples. *Proc. Apollo 11 Lunar Sci. Conf.*, 1317-1329.

Kaplan I.R., Kerridge J.F. and Petrowski C. (1976) Light element geochemistry of the Apollo 15 site. *Proc. 7th Lunar Sci. Conf.*, 481-492.

Keller L.P. and McKay D.S. (1997) The nature and origin of rims on lunar soil grains. *Geochim. Cosmochim. Acta.*, **61**, 2331-2341.

Kerridge J.F. (1975) Solar nitrogen: Evidence for a secular increase in the ratio of N-15 to N-14. *Science*, **188**, 162-164.

Kerridge J.F. (1980) Secular variations in compositions of the solar wind: Evidence and causes. *In: Proc. Conf. Ancient Sun (eds R.O.Pepin, J.A.Eddy and R.B.Merrill), Pergamon*, 475-489.

Kerridge J.F. (1989) What has caused the secular increase in solar nitrogen-15? *Science*, **245**, 480-486.

Kerridge J.F. (1993) Long-term compositional variation in solar corpuscular radiation: Evidence from nitrogen isotopes in the lunar regolith. *Reviews of Geophysics*, **31**, 423-437.

Kerridge J.F. and Matthews M.S. (Eds) (1988) Meteorites and the early solar system. University of Arizona Press, Tuscon, Arizona, 1269pp.

Kerridge J.F., Kaplan I.R. and Lesley F.D. (1974) Accumulation and isotopic evolution of carbon on the lunar surface. *Proc. 5th Lunar Sci. Conf.*, 1855-1868.

Kerridge J.F., Kaplan I.R.and Petrowski C. (1975a) Nitrogen in the lunar regolith: Solar origin and effects. *Lunar Science*, **VI**, 469-471.

Kerridge J.F., Kaplan I.R., Petrowski C. and Chang S. (1975b) Light element geochemistry of the Apollo 16 site. *Geochim. Cosmochim. Acta*, **39**, 137-162.

Kerridge J.F., Kaplan I.R., Lingenfelter R.E. and Boynton W.V. (1977) Solar wind nitrogen: Mechanisms for isotopic evolution. *Proc. 8th Lunar Sci. Conf.*, 3773-3789.

Kerridge J.F., Kaplan I.R., Kung C.C., Winter D.A., Friedman D.L. and DesMarais D.J. (1978) Light element geochemistry of the Apollo 12 site. *Geochim. Cosmochim. Acta*, **42**, 391-402.

Kerridge J.F., Eugster O., Kim J.S. and Marti K. (1991a) Nitrogen isotopes in the 74001/74002 double-drive tube from Shorty crater, Apollo 17. *Lunar Planet. Sci. Conf.*, **XXI**, 291-299.

Kerridge J.F., Signer P., Wieler R., Becker R.H. and Pepin R.O. (1991b) Long term changes in composition of solar particles implanted in extra-terrestrial materials. In: *The Sun In Time (eds C.P.Sonnett, M.S.Giampapa and M.S.Matthews), University of Arizona Press*, 389-412.

Kerridge J.F., Bochsler P., Eugster O. and Geiss J. (1992a) Modelling the evolution of N and $^{15}N/^{14}N$ in the lunar regolith: Mixing models involving two components. *Proc. Lunar Planet. Science*, **22**, 239-248.

Kerridge J.F., Kim J.S., Kim Y. and Marti K. (1992b) Evolution of isotopic signatures in lunar-regolith nitrogen: noble gases and nitrogen in grain-size fractions from regolith breccia 79035. *Proc. Lunar Planet. Science*, **22**, 215-224.

Kerridge J.F., Kim Y., Kim J.S. and Marti K. (1993) Nitrogen isotopic signatures in agglutinates from breccia 79035 (abstract). *Lunar Planet. Sci. Conf.*, **XXIV**, 795-796.

Kim J.S., Kim Y., Marti K. and Kerridge J.F. (1995a) The isotopic signature of recently implanted solar nitrogen in 68815. *Lunar Planet. Sci. Conf.*, **XXVI**, 749-750.

Kim J.S., Kim Y., Marti K. and Kerridge J.F. (1995b) Nitrogen isotope abundances in the recent solar wind. *Nature*, **375**, 383-385.

King A.S. and Birge R.T. (1929) An isotope of carbon, mass 13. *Nature*, **124**, 127.

Kirsten T., Müller O., Steinbrunn F. and Zähringer J. (1970) Study of distribution and variation of rare gases in lunar material by a microprobe technique. *Proc. Apollo 11 Lunar Sci. Conf.*, 1331-1345.

Kirsten T., Deubner J., Horn P., Kaneoka I., Kiko J., Schaeffer O.A. and Thio S.K. (1972) The rare gas record of Apollo 14 and 15 samples. *Proc. 3rd Lunar Sci. Conf.*, 1865-1889.

Kirsten T., Horn P. and Kiko J. (1973) ^{39}Ar-^{40}Ar dating and rare gas analysis of Apollo 16 rocks and soils. *Proc. 4th Lunar Sci. Conf.*, 1757-1784.

Kothari B.K. and Goel P.S. (1973) Nitrogen in lunar samples. *Proc. 4th Lunar Sci. Conf.*, 1587-1596.

Langevin Y. and Arnold J.R. (1977) The evolution of the lunar regolith. *Annu. Rev. Earth Planet. Sci.*, 5, 449-489.

Laul J.C. and Papike J.J. (1980) The lunar regolith: Comparative chemistry of the Apollo sites. *Proc. 11th Lunar Planet. Sci. Conf.*, 1307-1340.

Lewis R.S. and Anders E. (1983) Interstellar matter in meteorites. *Sci. Am.*, **249**, 54-66.

Lewis R.S., Srinivasan B. and Anders E. (1975) Host phase of a strange xenon component in Allende. *Science*, **190**, 1251-1262.

Lewis R.S., Anders E., Wright I.P., Norris S.J. and Pillinger C.T. (1983) Isotopically anomalous nitrogen in primitive meteorites. *Nature*, **305**, 767-771.

Lewis R.S., Tang M., Wacker J.F., Anders E. and Steel E. (1987) Interstellar diamonds in meteorites. *Nature*, **326**, 160-162.

Lewis R.S., Anders E. and Draine B.T. (1989) Interstellar diamonds in meteorites: properties, detectability and origin. *Nature*, **339**, 117-121.

Lingenfelter R.E., Canfield E.H. and Hampel V.E. (1972) The neutron flux revisited. *Earth Planet. Sci. Letts.*, **16**, 355-369.

LSPET (1970) Preliminary examination of Apollo 12 lunar samples. *Science*, **167**, 1325-1339.

LSPET (1972) Preliminary examination of lunar samples. *Apollo 16 Preliminary Science Report*, **NASA SP-315**.

LSPET (1973) Apollo 17 preliminary science report. *NASA SP-330*, 7-1 to 7-46.

McDonnell J.A.M. and Ashworth D.G. (1972) Erosion phenomena on the lunar surface and meteorites. In: *Space Research*, **XII**, 333-347, Akademi-Verlag, Berlin.

McDonnell J.A.M. and Flavill R.P. (1974) Solar wind sputtering on the lunar surface: equilibrium crater densities related to past and present microparticle influx rates. *Proc. 5th Lunar Sci. Conf.*, 2441-2449.

McDonnell J.A.M., Ashworth D.G., Flavill R.P. and Jennison R.C. (1972) Simulated microscale erosion on the lunar surface by hypervelocity impact, solar wind sputtering and thermal cycling. *Proc. 3rd Lunar Sci. Conf.*, 2755-2765.

McEwen A.S., Robinson M.S., Eliason E.M., Lucey P.G., Duxbury T.C. and Spudis P.D. (1994) Clementine observations of the Aristarchus region of the Moon. *Science*, **266**, 1858-1862.

McKay D.S., Basu A. and Nace G. (1980) Lunar core 15010/11: Grain size, petrology and implications for regolith dynamics. *Proc. 11th Lunar Planet. Sci. Conf.*, 1531-1550.

McGuire R.E., von Rosenvinge T.T. and McDonald F.B. (1986) The composition of solar energetic particles. *Astrophys. J.*, **301**, 938-961.

McKay D.S., Fruland R.M. and Heiken G.H. (1974) Grain size and the evolution of lunar soils. *Proc. 5th Lunar Sci. Conf.*, 887-906.

McKay D.S., Bogard D.D., Morris R.V., Korotev R.L., Johnson D. and Wentworth S.J. (1986) Apollo 16 regolith breccias: Characterization and evidence for early formation in the megaregolith. *Proc. 16th Lunar Planet. Sci. Conf. (J. Geophys. Res. supplement)*, **91**, D277-D303.

McKay D.S., Heiken G., Basu A., Blanford G., Simon S., Reedy R., French B.M. and Papike J. (1991). Chapter 7: The lunar regolith. In: *Lunar Sourcebook - a user's guide to the Moon (eds G.H.Heiken, D.T.Vaniman and B.M.French)*, University of Cambridge Press, 285-356.

Manka R.H. and Michel F.C. (1971) Lunar atmosphere as a source of lunar surface elements. *Proc. 2nd Lunar Sci. Conf.*, 1717-1728.

Marti K., Lightner B.D., Lugmair G.W., Osborn T.W. and Scheinin N. (1973) On the early lunar history: evidence from 244Pu and 314Nd. II. The age of North Ray crater. *Lunar Science*, **IV**, 502-504. Lunar Science Institute, Houston.

Mewaldt R.A. and Stone E.C. (1989) Isotopic abundances of solar coronal material derived from solar energetic particle measurements. *Astrophys. J.*, **337**, 959-963.

Meyer J.P. (1985) The baseline composition of solar energetic particles. *Astrophys. J. suppl.*, **57**, 151-171.

Misra K.C. and Taylor L.A. (1975) Characteristics of metal particles in Apollo 16 rocks. *Proc. 6th Lunar Sci. Conf.*, 615-639.

Moore C.B., Gibson E.K.Jr., Larimer J.W., Lewis C.F. and Nichiporuk W. (1970) Total carbon and nitrogen abundances in Apollo 11 lunar samples and selected achondrites and basalts. *Proc. Apollo 11 Lunar Sci. Conf.*, 1375-1382.

Moore C.B., Lewis C.F., Larimer J.W., Delles F.M., Gooley R.C., Nichiporuk W. and Gibson E.K.Jr. (1971) Total carbon and nitrogen abundances in Apollo 12 lunar samples. *Proc. 2nd Lunar Sci. Conf.*, 1343-1350.

Moore C.B., Lewis C.F., Cripe J., Delles F.M., Kelly W.R. and Gibson E.K.Jr. (1972) Total carbon, nitrogen and sulfur in Apollo 14 lunar samples. *Proc. 3rd Lunar Sci. Conf.*, 2051-2058.

Moore C.B., Lewis C.F. and Gibson E.K.Jr. (1973) Total carbon contents of Apollo 15 and 16 lunar samples. *Proc. 4th Lunar Sci. Conf.*, 1613-1623.

Morris R.V. (1976) Surface exposure indices of lunar soils: A comparative FMR study. *Proc. 7th Lunar Sci. Conf.*, 315-335.

Müller H.W., Jordan J., Kalbitzer S., Kiko J. and Kirsten T. (1976) Rare gas ion probe analysis of helium profiles in individual lunar soil particles. *Proc. 7th Lunar Sci. Conf.*, 937-951.

Müller O. (1973) Chemically bound nitrogen contents of Apollo 16 and Apollo 15 lunar fines. *Lunar Science*, **IV**, 546-548. Lunar Science Institute, Houston.

Müller O. (1974) Solar wind nitrogen and indigenous nitrogen in Apollo 17 lunar samples. *Proc. 5th Lunar Sci. Conf.*, 1907-1918.

Murer C.A., Baur H., Signer P and Wieler R. (1997) Helium, neon and argon abundances in the solar wind. *Geochim. Cosmochim. Acta*, **61**, 1303-1314.

Neugebauer M. (1981) Observations of solar-wind He. *Fundamentals of cosmic physics*, **7**, 131-199.

Neugebauer M. and Snyder C.W. (1966) Mariner 2 observations of the solar wind. *J. Geophys. Res.*, **71**, 4469-4484.

Newton J. (1994). A carbon and nitrogen isotope study of CO3 chondrites. *Unpublished PhD thesis, Open University.*

Newton J., Bischoff A., Arden J.W., Franchi I.A., Geiger T., Greshake A. and Pillinger C.T. (1995) Acfer 094, a uniquely primitive carbonaceous chondrite from the Sahara. *Meteoritics*, **30**, 47-56.

Nichols R.H.Jr., Hohenberg C.M. and Olinger C.T. (1994) Implanted solar helium, neon and argon in individual lunar ilmenite grains: Surface effects and a temporal variation on the solar wind composition. *Geochim. Cosmochim. Acta*, **58**, 1031-1042.

Nier A.O. (1947) A mass spectrometer for isotope and gas analysis. *Rev. Sci. Instrum.*, **18**, 398-411.

Norris S.J. (1987) A high sensitivity mass spectrometric study of the nitrogen released from lunar samples. *Unpublished PhD thesis, Open University.*

Norris S.J., Swart P.K., Wright I.P., Grady M.M. and Pillinger C.T. (1983) A search for correlatable, isotopically light carbon and nitrogen components in lunar soils and breccias. *Proc. 14th Lunar Planet. Sci. Conf.(J. Geophys. Res supple)* **88**, B200-B210.

Nozette S., Rustan P., Pleasance L.P., Horan D.M., Regeon P., Shoemaker E.M., Spudis P.D., Acton C.H., Baker D.N., Blamont J.E., Buratti B.J., Corson M.P., Davies M.E., Duxbury T.C., Eliason E.M., Jakosky B.M., Kordas J.F., Lewis T., Lichtenberg C.L., Lucey P.G., Malaret E., Massie M.A., Resnich J.H., Rollins C.J., Parks H.S., McEwen A.S., Priest R.E., Pieters C.M., Reisse R.A., Robinson M.S., Simpson R.A., Smith D.E., Sorenson T.C., Vorder Breugge R.W. and Zuber M.T. (1994) The Clementine mission to the Moon : Scientific overview. *Science*, **266**, 1835-1839.

Ogilvie K.W. and Wilkerson T.D. (1969) Helium abundance in the solar wind. *Solar Physics*, **8**, 435-449.

Papike J.J. and Vaniman D.T. (1978) Luna 24 ferrobasalts and the mare basalt suite: Comparative chemistry, mineralogy and petrology. In *Mare Crisium: The View from Luna 24 (J.J. Papike and R.B. Merrill, eds)*, 371-401, Pergamon, New York.

Papike J.J., Hodges F.N., Bence A.E., Cameron M. and Rhodes J.M. (1976) Mare basalts: Crystal chemistry, mineralogy and petrology. *Rev. Geophys. Space Phys.*, **14**, 475-540.

Parker E.N. (1958) *Astrophys. J.*, **128**, 664-676.

Pedroni A. and Begemann F. (1994) On unfractionated solar noble gases in the H3-6 meteorites Acfer 111. *Meteoritics*, **29**, 632-642.

Pedroni A., Baur H., Signer P. and Wieler R. (1991) Solar Ne and Ar in Kapoeta plagioclase: SW and SEP components identical to those in minerals from the lunar regolith. *Lunar Planet. Sci.*, **XXII**, 1049-1050.

Pepin R.O. (1980) Rare gases in the past and present solar wind. *In: Proc. Conf. Ancient Sun (eds R.O.Pepin, J.A.Eddy and R.B.Merrill)*, Pergamon, 411-421.

Pepin R.O. (1989) On the relationship between early solar activity and the evolution of the terrestrial planetary atmospheres. In: *The Formation and Evolution of Planetary Systems (eds. H.Weaver, F.Paresce and L.Danly)*. *Cambridge University Press, New York*, 55-70.

Pepin R.O. and Becker R.H. (1990) Isotopic compositions of solar wind neon, argon and krypton. *Meteoritics*, **25**, 398.

Pepin R.O., Nyquist L.E., Phinney D and Black D.C. (1970) Rare gases in Apollo 11 lunar material. *Proc. Apollo 11 Lunar Sci. Conf.*, 1435-1454.

Petrowski C., Kerridge J.F. and Kaplan I.R. (1974) Light element geochemistry of the Apollo 17 site. *Proc. 5th Lunar Sci. Conf.*, 1939-1948.

Phillips J.L., Bame S.J., Feldman W.C., Goldstein B.E., Gosling J.T., Hammond C.M., McComas D.J., Neugebauer M., Scime E.E. and Suess S.T. (1995) Ulysses solar wind plasma observations at high southerly latitudes. *Science*, **268**, 1030-1033.

Pieters C.M., Staid M.I., Fischer E.M., Tompkins S. and He G. (1994) A sharper view of impact craters from Clementine data. *Science*, **266**, 1844-1848.

Pillinger C.T. (1979) Solar wind exposure effects in the lunar soil. *Rep. Prog. Phys.*, **42**, 899-961.

Pillinger C.T., Cadogan P.H., Eglinton G., Maxwell J.R., Mays B.J., Grant W.A. and Nobes M.J. (1972) Simulation of lunar carbon chemistry. *Nature*, **235**, 108-109.

Pillinger C.T., Batts B.D., Eglinton G., Gowar A.P., Jull A.J.T. and Maxwell J.R. (1973) Formation of lunar carbide from lunar iron silicates. *Nature Phys. Sci.*, **245**, 3-5.

Pillinger C.T., Davis P.R., Eglinton G., Gowar A.P., Jull A.J.T., Maxwell J.R., Housley R.M. and Cirlin E.H. (1974) The association between carbide and finely divided metallic iron in lunar fines. *Proc. 5th Lunar Sci. Conf.*, 1949-1961.

Pillinger C.T., Gardiner L.R. and Jull A.J.T. (1976) Preferential sputtering as a method of producing metallic iron, inducing major element fractionation and trace element enrichment. *Earth Planet. Sci. Letts.*, **33**, 289-299.

Pillinger C.T., Jull A.J.T., Woodcock M.R. and Stephenson A. (1978) Maturation of the lunar regolith: Some implications from magnetic measurements and hydrolysable carbon data on bulk soils and particle separates from 12023 and 15601. *Proc. 9th Lunar Sci. Conf.*, 2167-2193.

Price P.B. and O'Sullivan D. (1970) Lunar erosion rate and solar flare paleontology. *Proc. Apollo 11 Lunar Sci. Conf.*, 2351-2359.

Prombo C.A. and Clayton R.N. (1985) A striking nitrogen isotope anomaly in the Bencubbin and Weatherford meteorites. *Science*, **230**, 935-937.

Ray J. and Heymann D. (1980) A model for nitrogen variations in the lunar regolith: Possible solar system contributions from a nearby planetary nebula. *In: Proc. Conf. Ancient Sun (eds R.O.Pepin, J.A.Eddy and R.B.Merrill)*, *Pergamon*, 491-512.

Ray J. and Heymann D. (1982) Long-term solar wind activity as inferred from lunar regolith samples (abstract). *Lunar Planet. Sci.*, **XIII**, 640-641.

Reed S.J.B. and Taylor S.R. (1974) Meteoritic metal in Apollo 16 samples. *Meteoritics*, **9**, 23-34.

Reedy R.C., Arnold J.R. and Lal D. (1983) Cosmic ray record in solar system matter. *Science*, **219**, 127-135.

Reeves H. (1978) The origin of the Solar System. *In: The origin of the Solar system. Ed. S.F. Dermott. Wiley*.

Reynolds J.H. (1956) High sensitivity mass spectrometer for noble gas analysis. *Rev. Sci. Instrum.*, **27**, 928-934.

Reynolds J.H. and Turner G. (1964) Rare gases in the chondrite Renazzo. *J. Geophys. Res.*, **69**, 3262-3281.

Reynolds J.H., Hohenberg C.M., Lewis R.S., Davis P.K. and Kaiser W.A. (1970) Isotopic analysis of rare gases from stepwise heating of lunar fines and rocks. *Science*, **167**, 545-548.

Reynolds J.H., Alexander J.R., Davis P.K. and Srinivasan B. (1974) Studies of K-Ar dating and xenon from extinct radioactivities in breccia 14318: implications for early lunar history. *Geochim. Cosmochim. Acta.*, **38**, 401-417.

Rhodes J.M., Blanchard D.P., Dungan M.A., Brannon J.C. and Rodgers K.V. (1977) Chemistry of Apollo 12 mare basalts: Magma types and fractionation processes. *Proc. 8th Lunar Sci. Conf.*, 1305-1338.

Rose H.J.Jr., Cuttitta F., Berman S., Brown F.W., Carron M.K., Christian R.P., Dwornik E.J. and Greenland L.P. (1974) Chemical composition of rocks and soils at Taurus-Littrow. *Proc. 5th Lunar Sci. Conf.*, 1119-1133.

Runcorn S.K., Collinson D.W., O'Reilly W., Battey M.K., Stephenson A., Jones J.M., Manson A.J. and Readman P.W. (1970) Magnetic properties of Apollo 11 lunar samples. *Proc. Apollo 11 Lunar Sci. Conf.*, 2369-2387.

Runcorn S.K., Libby W.F. and Libby L.M. (1977) Primeval melting of the Moon. *Nature*, **270**, 676-681.

Russell S.S. (1992) A carbon and nitrogen isotope study of chondritic diamond and silicon carbide. *Unpublished PhD thesis, Open University*.

Russell S.S., Arden J.W. and Pillinger C.T. (1991) Evidence for multiple sources of diamond from primitive chondrites. *Science*, **254**, 1188-1191.

Schaeffer O. A. and Husain L. (1973) Isotopic ages of Apollo 17 lunar material. *EOS Trans. AGU*, **54**, 614.

Schaeffer O.A., Husain L. and Schaeffer G.A. (1976) Ages of highland rocks - the chronology of lunar basin formation revisited. *Proc. 7th Lunar Sci. Conf.*, 2067-2092.

Schmitt H.H. and Cernan E.A. (1973) A geological investigation of the Taurus-Littrow valley. *Apollo 17 Prelim. Sci. Report*, **NASA SP-330**, 5-1 to 5-21.

Selesnick R.S., Cummings A.C., Cummings J.R., Leske R.A., Mewaldt R.A. and Stone E.C. (1993) *Coronal abundances of neon and magnesium isotopes from solar energetic particles. Astrophys. J.*, **418**, L45-L48.

Shervais J.W., Taylor L.A., Laul J.C., Shih C-Y. and Nyquist L.E. (1985) Very high potassium (VHK) basalt: Complications on mare basalt petrogenesis. *Proc. 16th Lunar Planet. Sci. Conf. (J. Geophys. Res. supplement)*, **90**, D3-D18.

Shoemaker E.M., Bailey N.G., Batson R.M., Dahlem D.H., Foss T.H., Grolier M.J., Goddard E.M., Hait M.H., Holt H.E., Larson K.B., Rennilson J.J., Schaber G.G., Schleicher D.L., Schmitt H.H., Sutton R.L., Swann G.A., Waters A.C. and West M.N. (1970a) Geologic setting of the lunar samples returned by the Apollo 11 mission. *Apollo 11 Prelim. Sci. Report*, **NASA SP-214**, 41-84.

Shoemaker E.M., Batson R.M., Bean A.L., Conrad C. Jr., Dahlem D.H., Goddard E.M., Hait M.H., Larson K.B., Schaber G.G., Schleicher D.L., Sutton R.L., Swann G.A. and Waters A.C. (1970b) Preliminary geologic investigation of the Apollo 12 landing site. Part A. Geology of the Apollo 12 landing site. *Apollo 12 Prelim. Sci. Report*, **NASA SP-235**, 113-182.

Shoemaker E.M., Robinson M.S. and Eliason E.M. (1994) The South Pole region of the moon as seen by Clementine. *Science*, **266**, 1851-1854.

Signer P., Eberhardt P. and Geiss J. (1965) Possible determination of solar wind composition. *J. Geophys. Res.*, **70**, 2243-2244.

Signer P., Baur H., Derksen U., Etique P., Funk H., Horn P. and Wieler R. (1977) Helium, neon and argon records of lunar soil evolution. *Proc. 8th Lunar Sci. Conf.*, 3657-3683.

Signer P., Baur H., Etique Ph. and Wieler R. (1986) Nitrogen and noble gases in the 71501 bulk soil and ilmenites as records of the solar wind exposure: Which is correct? In: *Workshop on past and present solar radiation (edited by R.O.Pepin & D.S.McKay)*, 36-37, Lunar and Planetary Institute, Houston.

Signer P., Baur H. and Wieler R. (1993) Closed system stepped etching; an alternative to stepped heating. In: *Proc. Alfred O. Nier Symp. Inorganic Mass Spectrometry, Durango, New Mexico (ed. D.J.Rokop)*; Los Alamos Natl. Lab. Publ. LA-12522-C, 181-202.

Simoneit B.R., Christiansen P.C. and Burlingame A.L. (1973a) Volatile element chemistry of selected lunar, meteorite and terrestrial samples. *Proc. 4th Lunar Sci. Conf.*, 1635-1650.

Simoneit B.R., Wszolek P.C., Christiansen P., Jackson R.F. and Burlingame A.L. (1973b) Carbon chemistry of Luna 16 and Luna 20 samples. *Geochim. Cosmochim. Acta*, **37**, 1063-1074.

Simpson J.A. (1983) Elemental and isotopic composition of the galactic cosmic-rays. *Annu. Rev. Nucl. Part. Sci.*, **33**, 323-381.

Simpson J.A., Anglin J.D., Bothmer V., Connell J.J., Ferrando P., Heber B., Kunow H., Lopate C., Marsden R.G., McKibben R.B., Müller-Mellin R., Paizis C., Rastoin C., Raviart A., Sanderson T.R., Sierks H., Trattner K.J., Wenzel K-P., Wibberenz G. and Zhag M. (1995) Cosmic ray and solar particle investigations over the south polar regions of the Sun. *Science*, **268**, 1019-1023.

Smith E.J. (1991) The sun and interplanetary magnetic field. In: *The Sun In Time (eds C.P.Sonnett, M.S.Giampapa and M.S.Matthews)*, *University of Arizona Press*, 389-412.

Smith E.J., Marsden R.G. and Page D.E. (1995) Ulysses above the Sun's south pole: An Introduction. *Science*, **268**, 1005-1007.

Spudis P.D. (1984) Apollo 16 site geology and impact melts: Implications for the geologic history of the lunar highlands. *Proc. 15th Lunar Planet. Sci. Conf. (J. Geophys. Res. supplement)*, **89**, C95-C107.

Spudis P.D., Reisse R.A. and Gillis J.J. (1994) Ancient multiring basins on the Moon revealed by Clementine Laser Altimetry. *Science*, **266**, 1848-1851.

Srinivasan B. and Anders E. (1978) Noble gases in the Murchison meteorite: possible relics of s-process nucleosynthesis. *Science*, **201**, 51-56.

Stephenson A., Collinson D.W. and Runcorn R.K. (1974) Lunar magnetic field paleointensity determinations on Apollo 11, 16 and 17 rocks. *Proc. 5th Lunar Sci. Conf.*, 2859-2871.

Strong I.B., Ashbridge J.R., Bame S.J. and Hundhausen A.J. (1967) Zodiacal light and the Interplanetary medium (ed. J.L.Weinberg). **NASA SP-150**, 365-372.

Swann G.A., Bailey N.G., Batson R.M., Freeman V.L., Hait M.H., Head J.W., Holt H.E., Howard K.A., Irwin J.B., Larson K.B., Muehlberger W.R., Reed V.S., Rennilson J.J., Schaber G.G., Scott D.R., Silver L.T., Sutton R.L., Ulrich G.E., Wilshire H.G. and Wolfe E.W. (1972) Preliminary geologic investigations of the Apollo 15 landing site. *Apollo 15 Prelim. Sci. Report*, **NASA SP-289**, 5-1 to 5-112.

Swann G.A., Bailey N.G., Batson R.M., Eggleton R.E., Hait M.H., Holt H.E., Larson K.B., Reed V.S., Schaber G.G., Sutton R.L., Trask N.I., Ulrich G.E. and Wilshire H.G. (1977) Geology of the Apollo 14 landing site in the Fra Mauro highlands. *U.S. Geol. Surv. Prof. Pap.*, 800, 103pp.

Swart P.K., Grady M.M., Pillinger C.T., Lewis R.S. and Anders E. (1983) Interstellar carbon in meteorites. *Science*, **220**, 406-410.

Tang M. and Anders E. (1988) Isotopic anomalies of Ne, Xe and C in meteorites II. Interstellar diamond and SiC: carriers of exotic noble gases. *Geochim. Cosmochim. Acta*, **52**, 1235-1244.

Taylor G.J., Warren P., Ryder G., Delano J., Pieters C. and Lofgren G. (1991) Lunar rocks. *In: Lunar Sourcebook - a user's guide to the Moon (eds G.H.Heiken, D.T.Vaniman and B.M.French)*, Cambridge University Press, New York, 183-284.

Taylor S.R. (1975) Chapter 3: The surface of the Moon. *In: Lunar Science: A post Apollo view*, Pergamon Press, 55-119.

Taylor S.R. (1982) Planetary Science: A Lunar Perspective. Lunar and Planetary Institute, Houston, 481.

Tera F., Papanastassiou D.A. and Wasserburg G.J. (1974) Isotopic evidence for a terminal lunar cataclysm. *Earth Planet. Sci. Letts.*, **22**, 1-21.

Thalmann Ch., Eugster O., Herzog G.F., Klein J., Krähenbühl U., Vogt S. and Xue S. (1996) History of lunar meteorites Queen Alexandra Range 93069, Asuka 881757 and Yamato 793169 based on noble gas isotopic abundances, radionuclide concentrations and chemical composition. *Meteoritics and Planetary Science*, **31**, 857-868.

Thiemens M.H. and Clayton R.N. (1980) Ancient solar wind in lunar microbreccias. *Earth Planet. Sci. Lett.*, **47**, 34-42.

Tsay F.D., Chan S.I. and Mannett S.L. (1971) Magnetic resonance studies of Apollo 11 and Apollo 12 samples. *Proc. 2nd Lunar Sci. Conf.*, 2515-2528.

Urey H.C. (1948) Oxygen isotopes in nature and the laboratory. *Science*, **108**, 489-497.

Vaniman D., Dietrich J., Taylor G.J. and Heiken G. (1991) Exploration, samples and recent concepts of the Moon. *In: Lunar Sourcebook - a user's guide to the Moon (eds G.H.Heiken, D.T.Vaniman and B.M.French), Cambridge University Press, New York*, 5-26..

Verchovsky A.B. and Pillinger C.T. (1994) Chemical reactions occurring during pyrolysis of presolar diamonds and release patterns of light nitrogen and noble gases. *Meteoritics*, **29**, 543-544.

von Steiger R. and Geiss J. (1989) Supply of fractionated gases to the corona. *Astron. Astrophys.*, **225**, 222-238.

Walker R.M. (1975) Interaction of energetic nuclear particles in space with the lunar surface. *Ann. Rev. Earth Planet. Sci.*, **3**, 99-128.

Walker R.M. (1980) Nature of the fossil evidence: Moon and meteorites. *In: Proc. Conf. Ancient Sun (eds R.O.Pepin, J.A.Eddy and R.B.Merrill)*, Pergamon, 11-28.

Walton J.R., Lakatos S. and Heymann D. (1973) Distribution of inert gases in fines from the Cayley-Descartes region. *Proc. 4th Lunar Sci. Conf.*, 2079-2095.

Wänke H. (1965) Der Sonnenwind als quelle der Uredelgase in steinmeteorites. *Z. Natur.*, **20a**, 946-949.

Warasila R.L. and Schaeffer O.A. (1974) Trappped solar wind He, Ne and Ar and energetic He in Surveyor 3. *Earth Planet. Sci. Letts.*, **24**, 71-77.

Warren P.H. (1985) The magma ocean concept and lunar evolution. *Annu. Rev. Earth Planet. Sci.*, **13**, 201-240.

Warren P.H. and Kallemeyn G.W. (1991) The MacAlpine Hills lunar meteorite and implications of the lunar meteorites collectively for the composition and origin of the Moon. *Geochim. Cosmochim. Acta*, **55**, 3123-3138.

Warren P.H., Afiattalab F. and Wasson J.T. (1978) Investigation of unusual KREEPy samples: Pristine rock 15386, Cone Crater soil fragments 14143, and 12023, a *Typical* Apollo 12 soil. *Proc. 8th Lunar Planet. Sci. Conf.*, 653-660. **Warren P.H. and Kallemeyn G.W.** (1991) The MacAlpine Hills lunar meteorite and implications of the lunar meteorites collectively for the composition and origin of the Moon. *Geochim. Cosmochim. Acta*, **55**, 3123-3138.

Wasson J.T. and Baedecker P.A. (1970) Ga, Ge, In, Ir and Au in lunar, terrestrial and meteoritic basalts. *Proc. Apollo 11 Lunar Sci. Conf.*, 1741-1750.

Wetherill G.W. (1981) Nature and origin of basin-forming projectiles. In: *Multi-Ring Basins, Proc. Lunar Planet. Sci. Conf. 12A* (P.H.Schultz and R.B.Merrill, eds), 1-18, Pergamon, New York.

Wieler R. and Baur H. (1994) Krypton and xenon from the solar wind and solar energetic particles in two lunar ilmenites of different antiquities. *Meteoritics*, **29**, 570-580.

Wieler R. and Baur H. (1995) Fractionation of Xe, Kr and Ar in the solar corpuscular radiation deduced by closed system etching of lunar soils. *Astrophys. J.*, **453**, 987-997.

Wieler R., Etique Ph., Signer P. and Poupeau G. (1980) Record of the solar corpuscular radiation in minerals from lunar soils: A comparative study of noble gases and tracks. *Proc. 11th Lunar Sci. Conf.*, 1369-1393.

Wieler R., Etique Ph., Signer P. and Poupeau G. (1983) Decrease of the solar flare/solar wind flux ratio in the past several aeons deduced from solar flare neon and tracks in lunar soil plagioclases. *Proc. 13th Lunar Planet. Sci. Conf. (J. Geophys. Res. supplement)*, **88**, A713-A724.

Wieler R., Baur H. and Signer P. (1986) Noble gases from solar energetic particles revealed by closed system stepwise etching of lunar soils minerals. *Geochim. Cosmochim. Acta*, **50**, 1997-2017.

Wieler R., Baur H. and Signer P. (1993) A long-term change of the Ar/Kr/Xe fractionation in the solar corpuscular radiation (abstract). *Lunar Planet. Science*, **XXIV**, 1519-1520.

Wieler R., Kehm K., Meshik A.P. and Hohenberg C.M. (1996) Secular changes in the xenon and krypton abundances in the solar wind recorded in single lunar grains. *Nature*, **384**, 46-49.

Wieler R., Humbert F. and Marty B. (1999) Evidence for a predominantly non-solar origin of nitrogen in the lunar regolith revealed by single grain analysis. *Earth Planet. Sci. Letts.*, (in press).

Wilhelms D.E. (1984) The Moon. In: *The Geology of the Terrestrial Planets (eds M.Carr et al.)*, 107-205. **NASA SP-469**.

Wlotzka F., Spettel B. and Wänke H. (1973) On the composition of metal from Apollo 16 fines and the meteoritic component. *Proc. 4th Lunar Sci. Conf.*, 1483-1491.

Wood J.A., Dickey J.S., Marvin U.B. and Powell B.N. (1970) Lunar anorthosites and a geophysical model of the Moon. *Proc. Apollo 11 Lunar Sci. Conf.*, 965-988.

Woodcock M.R. and Pillinger C.T. (1978) Major element chemistry of agglutinate size fractions. *Proc. 9th Lunar Sci. Conf.*, 2195-2214.

Wright I.P. (1984) $\delta^{13}C$ measurements of smaller samples. *J. Trends Anal. Chem.*, **3**, 210-215.

Wright I.P., McNaughton N.J., Fallick A.E., Gardiner L.R. and Pillinger C.T. (1983) A high precision mass spectrometer for stable carbon isotope analysis at the nanogram level. *J. Phys. E. Sci. Instrum.*, **16**, 497-504.

Wright I.P., Ash R.D., Grady M.M., Pillinger C.T. and Tang M. (1988a) The carbon components in Murray residue CF. *Meteoritics*, **23**, 312-313.

Wright I.P., Boyd S.R., Franchi I.A. and Pillinger C.T. (1988b) High-precision determination of nitrogen stable isotope ratios at the sub-nanomole level. *J. Phys. E. Sci. Instrum.*, **21**, 865-875.
Wright I.P., McNaughton N.J., Fallick A.E., Gardiner L.R. and Pillinger C.T. (1983) A high precision mass spectrometer for stable carbon isotope analysis at the nanogram level. *J. Phys. E. Sci. Instrum.*, **16**, 497-504.

Wszolek P.C., Jackson R.F., Burlingame A.L. and Maurette M. (1973) Carbon chemistry of Apollo 15 and 16 samples and solar wind ion implantation studies. *Lunar Science*, **IV**, 801-803. Lunar Science Institute, Houston.

Yaniv A. and Heymann D. (1972) Atmospheric ^{40}Ar in lunar fines. *Proc. 3rd Lunar Sci. Conf.*, 1967-1980.

Yokoyama Y., Guichard F., Reyss J.L. and Sato J. (1976) Dating of fresh lunar craters by cosmogenic ^{22}Na-^{26}Al studies and a preliminary study on the ^{26}Al-^{53}Mn method (abstract). *Lunar Science*, **VII**, 956-958.

Zinner E. and Walker R.M. (1975) Ion probe studies of artificially implanted ions in lunar samples. *Proc. 6th Lunar Sci. Conf.*, 3601-3617.

Zinner E., Tang M. and Anders E. (1987) Large isotopic anomalies of Si, C, N and noble gases in interstellar silicon carbide from the Murray meteorite. *Nature*, **330**, 730-732

Zuber M.T., Smith D.E., Lemoine F.G. and Neumann G.A. (1994) The shape and internal structure of the Moon from the Clementine Mission. *Science*, **266**, 1839-1843.